Surface Modification of Copper by Electro-codeposition

Thesis submitted in partial fulfillment
of the requirements of the degree of

Doctor of Philosophy

in

Metallurgical and Materials Engineering

by

Himanshu Sekhar Maharana
(Roll No: 511MM608)

based on research carried out

Under the Supervision of

Prof. Anindya Basu

December, 2016

Department of Metallurgical and Materials Engineering
National Institute of Technology, Rourkela

Department of Metallurgical and Materials Engineering
National Institute of Technology Rourkela

December 15, 2016

Certificate of Examination

Roll Number: *511MM608*

Name: *Himanshu Sekhar Maharana*

Title of Dissertation: ***Surface Modification of Copper by Electro-codeposition***

The persons, mentioned below, after checking the dissertation mentioned above and official record book(s) of the student, here by, state their approval of the dissertation submitted in partial fulfillment of the requirements for the degree *of Doctor of Philosophy in Metallurgical and Materials Engineering* at the National Institute of Technology Rourkela. The persons are satisfied with the volume, quality, correctness, and originality of the work.

Subash Chandra Mishra
HOD and Chairman DSC

Anindya Basu
Supervisor

A Thirugnanam
Member, DSC

Debasis Chaira
Member, DSC

Mithilesh Kumar
Member, DSC

External Examiner

Department of Metallurgical & Materials Engineering
National Institute of Technology Rourkela

Prof. Anindya Basu
Associate professor

December15, 2016

Supervisors' Certificate

This is to certify that the thesis entitled, *"**Surface Modification of Copper by Electro-codeposition**"* submitted by Mr. *Himanshu Sekhar Maharana*, Roll no- 511MM608, in partial fulfillment of the requirements for the award of Doctor of Philosophy Degree in *Metallurgical and Materials Engineering* at the National Institute of Technology, Rourkela, is an authentic work carried out by him under my supervision and guidance. To the best of my knowledge, the matter embodied in the thesis has not been submitted to any other University/Institute for the award of any Degree or Diploma.

Prof. A. Basu
Metallurgical and Materials Engineering
NIT Rourkela

Dedicated

To

My parents

Declaration of Originality

I, *Himanshu Sekhar Maharana*, Roll Number *511MM608*, hereby declare that this dissertation entitled ***"Surface Modification of Copper by Electro-codeposition*** " represents my original work carried out as a doctoral student of NIT Rourkela and, to the best of my knowledge, it contains no material previously published or written by another person, nor any material presented for the award of any other degree or diploma of NIT Rourkela or any other institution. Any contribution made to this research by others, with whom I have worked at NIT Rourkela or elsewhere, is explicitly acknowledged in the dissertation. Works of other authors cited in this dissertation have been duly acknowledged under the section of "*References*". I have also submitted my original research records to the scrutiny committee for evaluation of my dissertation.

I am fully aware that in case of any non-compliance detected in future, the Senate of NIT Rourkela may withdraw the degree awarded to me on the basis of the present dissertation.

December 15, 2016

NIT Rourkela *Himanshu Sekhar Maharana*

Acknowledgment

During the writing of this thesis, I feel this thesis might be coalition of my works carried out during my PhD stay at NIT Rourkela, but actually this is a product of plentiful conscious and unconscious contributions from several people. If, I remember the support and encouragement of my well-wishers and my friends during my journey as a research scholar at Rourkela; making a written gratitude for all these people is actually a difficult assignment for me.

At this moment, it is with immense gratitude that, I acknowledge my supervisor **Dr. A. Basu**, Metallurgical and Materials Engineering department, NIT, Rourkela for the student teacher relationship which I will cherish forever. It gives me immense pleasure to acknowledge my supervisor for his guidance, support and encouragement. Without which this dissertation could not have been possible. I learned a lot, which may not be possible write in words during my tenure as a research scholar under his supervision. Despite of his demanding schedule, he used to correct my dissertation and review my progress from time to time and give his constructive suggestions. Personally, I cannot find any words to express my gratitude to Dr. A. Basu, a person I admire not only for his learning but also for his cordialness, simplicity and kind gesture, which makes him a complete teacher. I am really indebted to him and feel lucky to have the company to work with him.

I also express my sincere gratitude to **Dr. Sourav Chatarjee,** Professor of Chemistry Department, NIT Rourkela, for his valuable advice and constructive suggestions during my PhD work. I am also indebted to all the professors of Metallurgical and Materials Engineering Department, NIT Rourkela, for their timely suggestions and help during the course of my PhD work.

I would also like to extend my gratitude to **Mr. Subrat kumar Pradhan**, **Mr. Subhobrata Chakraborty** and **Mr. Shyamu Hemram**, **Mr. Rajesh Pattanaik**, and **Mr. Uday Sahoo**, all from NIT, Rourkela, for their technical support for the experimentation and characterization involved in this dissertation. I am also gratefully acknowledged to all staff members of Metallurgical and Materials Engineering Department for their kind cooperation.

Writing a few lines about my dearest friends since my NIT days, will simply very little to them for their inherent characteristics of unconditional help, which I always took as granted during my PhD work. I, therefore, simply thank my friends Ananta Prasad Chakraverty (C.V Raman college of Engineering, Bhubaneswar), Sushanta Kumar Swain (Hindalco Ltd.), Jagannath Panigrahi (NPL, Delhi), Narashima Chary (NIT, Rourkela), Lailesh Kumar (NIT, Rourkela), Bikash Ranjan Parhi (NIT, Rourkela), Deepankar Panda (NIT, Rourkela), Surjya Kanta Panda (NIT Rourkela), Sumanta Kumar Sahoo (NIT Rourkela).

Really, it is incomplete without saying something about my family. It is my pleasant duty to recall with gratitude for the eternal affection, unconditional love, encouragement and all sorts of supports, which I have been receiving from my father Mr Rama Chandra Maharana, my mother Mrs. Prativa Maharana, and younger brother Mr. Sudhanshu Sekhar Maharana during my PhD work as well as throughout my life.

Finally, I would like to thank God and all whose direct and indirect support has helped me in completing my thesis.

NIT, Rourkela — Himanshu Sekhar Maharana

December 15, 2016 — Roll No: 511MM608

Abstract

Copper has good electrical and thermal conductivity which makes it useful for engineering and thermal applications. But its poor mechanical property necessitates strengthening of the same without adversely affecting its electrical conductivity for its use in electrical applications. Surface engineering approach does not adversely affect the bulk properties and among various such techniques, electro-codeposition technique is considered cost effective due to its simple operation, high production rate and capability to handle complex geometry.

The objective of the dissertation is to improve the surface mechanical properties of Cu by electro-co-deposition of Cu based different oxide nanoparticles (Al_2O_3, SiO_2, Y_2O_3, ZrO_2 and graphene oxide (GO), reduced graphene oxide (RGO), thermally reduced graphene oxide (TRGO)) dispersed composite coating on it by direct current (DC) and pulse current (PC) mode without much deteriorating the electrical conductivity. Cu-Al_2O_3 composite coatings were prepared with varying current density (5, 8, 11 and 14 A/dm^2) and Al_2O_3 content, whereas, Cu-SiO_2/Y_2O_3 was prepared at different pulsing condition (1, 5 and 10 kHz frequency) and Cu-ZrO_2 were studied with different surfactant addition. Detailed texture study of Cu-SiO_2/Y_2O_3 coatings was also carried out along with oxidation behavior of Cu-Y_2O_3 coating. Cu-GO/RGO/TRGO coatings were also analyzed for the optimum coating parameters. Coatings were characterized by field emission scanning electron microscopy (FESEM), X-ray diffraction (XRD), microhardness testing, wear testing, electrical conductivity study etc.

When results of the each system was analyzed, it was observed that the better surface-mechanical property obtained was due to finer matrix, better dispersion and favorable crystallographic orientation. These were obtained with specific current density/ pulsing condition/ second phase amount. Electrical conductivity was found to be dependent mainly on matrix fineness and dispersion fraction. Better surface mechanical properties leads to marginal deterioration of electrical conductivity but the values obtained in the present study was in the acceptable range of commercial application.

Keywords: Copper, Surface modification, Nanotechnology, Electro-codeposition, Surface-mechanical properties, Electrical conductivity.

CONTENTS

List of Figures

List of Tables

Chapter 1

Introduction

1.1 Background and motivation

Ultrafine hard particle-reinforced metal matrix composites generally exhibit a wide range of applications due to their enhanced mechanical properties such as hardness, better wear, and corrosion resistance compared to parent metal [1]. The wide variety of surface coating techniques available are physical vapor deposition, chemical vapor deposition, thermal spraying, electrodeposition, electroless deposition, diffusion coatings and laser-based techniques, etc. Combining these two concepts lead to the concept of nanocomposite coating. Metal matrix nanocomposite coating containing dispersed second-phase particulates have various special properties such as self-lubricity, high temperature inertness, chemical and biological compatibility [2–7]. Electro-codeposition or composite electrodeposition process has been identified to be a technologically convenient and economically superior technique for the development of such composite coatings. Successful codeposition of ultrafine particles such as silicon carbides, oxides, titanium oxide, diamond and polymers with metal or alloy matrix has been reported, and their corresponding structures and properties were investigated by many researchers over the past decades [8–11]. The structure and properties of composite coatings not only depend on the concentration, size, distribution, and nature of the reinforced particles, but also indirectly on the type of electrolyte used and deposition parameters (current density, pulse parameters in case of pulsed deposition, temperature, pH value, etc.). It is worth mentioning that in case of pulsed deposition; the controlling parameters are more, leading to better control on the coating and its properties. Some researchers have also reported about the effect of various cationic and anionic surfactants on different mechanical and electrochemical properties of the composite coating [12–17].

Copper (Cu) is a cheap, easily available and environment friendly material that possesses a unique combination of high electrical (5.96×10^7 S/m) and thermal conductivity (394 W m^{-1} K^{-1}), excellent malleability, reasonably good corrosion resistance at ambient temperature [18] and recyclability. Owing to these excellent combinations of electrical and electrochemical

properties, Cu and its alloys are most widely used engineering materials for conduction of electricity (electrical conductors, wires, contacts, plugs) and heat (heat exchangers, linings, radiators, electrodes). However, poor mechanical property of the material is the major drawback for applicability in electrical contacts. For applicable in electrical contacts the material should have better mechanical properties as well as good electrical conductivity. Though Cu has very good electrical conductivity, but mechanical property necessitates strengthening without adversely affecting its electrical/thermal conductivity. Some applications like electrical contacts require mainly good surface mechanical properties like hardness, wear resistance due to frequent rubbing action during switching [19]. Bulk modification/alloying technique for fabrication of new material for applicable in electrical contacts increases the mechanical properties but decreases thermal and electrical conductivity of the material drastically, which is considered as negative for switching applications. Along with electrical conductivity, thermal conductivity is also important so that the contacts can quickly release the heat accumulated for resistance heating and rubbing action during switching.

In such components surface engineering approach for modification of surface to increase the mechanical properties is wise one as it does not adversely affect bulk properties like electrical and thermal conductivities compared to bulk modification. Among various surface engineering techniques electro-co-deposition technique is considered to be cost effective due to simple operation, high production rate, reduction of waste and capability to handle complex geometry. In view of the above, Cu-based composite coating on Cu substrate by electro-co-deposition was felt important as detailed study of such coating with processing-structure-property correlation was not plenty in existing literature.

1.2 Objectives and scope of the thesis

The main objective of the present work is to improve the surface-mechanical properties of Cu by electro-co-deposition process with dispersion of second phase ultra-fine ceramic oxide particles like Al_2O_3, SiO_2, Y_2O_3, ZrO_2 and graphene oxide (GO)/reduced graphene oxide (RGO) individually and manipulating the processing parameters for different composite coating systems to maximize the mechanical properties and to retain the electrical

conductivity of the copper as much as possible. Structural characterizations and brief study on orientation dependent mechanism of electrical and mechanical (microhardness) properties of some systems, like Cu-SiO_2 and Cu-Y_2O_3 has also been reported in the current dissertation.

Scope of the present work is to elaborately discuss about the effect of various second phase oxide particles, such as Al_2O_3, SiO_2, Y_2O_3, ZrO_2 and GO concentrations with different process parameters (current density and pulse frequency) on the microstructure, hardness, wear resistance, oxidation behavior, and electrical conductivity of electrodeposited Cu based composite coatings. Effects of different kind of surfactants (cationic, anionic and polymeric) on surface mechanical and electrical properties have also been studied for Cu-ZrO_2 composite coating system. Crystallographic orientation dependent mechanical and electrical properties of few systems (Cu-SiO_2 and Cu-Y_2O_3) have been explored.

Thus, overall purpose of this study is to improve the surface-mechanical properties of composite coating in comparison to pure copper without much deterioration of electrical conductivity.

1.3 Structure of the thesis

The thesis contains 9 chapters. The 1st chapter, 'Introduction' has been emphasized on an insight to the work under taken mentioning background, objective and thesis structure in brief. The 2nd chapter on 'Literature Review' is entirely dedicated to an extensive survey of the work carried out by other investigators or agencies in the same field. The work carried out by these researchers has been referred, wherever necessary, to explain and support the present experimental findings. This chapter has been dedicated to gather clear cut information regarding microstructural and mechanical properties of Cu based ceramic oxide composite by electro-co-deposition technique and effect of various process parameters and concentrations of different ceramic oxide particles on the said properties. The 3rd chapter, 'Materials and Methods' is dealt with details of the sample preparation, bath solution compositions, specifications with manufacturer name of the used chemicals, details of graphene oxide synthesis and clear cut description of accessed instruments. The 4th, 5th, 7th and 8th chapter

houses the results and discussions of different copper based systems, such as Cu/Al_2O_3, Cu/SiO_2, Cu/Y_2O_3, Cu/ZrO_2 and Cu/RGO in the form of tables, graphs, bar-diagrams, SEM and FESEM micrographs etc. which have been generated while carrying out various characterizations. Each of these chapters begins with a brief introduction and ends with observed conclusions. The introduction part deals with specific experiment related information. These chapters also explain the detailed discussion of the results made on the basis of the obtained experimental data. Brief study on structural characterization of Cu/SiO_2 and Cu/Y_2O_3 systems has also been discussed in 6^{th} chapter. Finally, on the basis of the experimental findings some useful conclusions have been provided in the 9^{th} chapter. Finally, the references used in the thesis are listed in last after 9^{th} chapter.

1.4 Novelty

Cu is used mainly in electrical and thermal applications due to superior electrical and thermal conductivity. In case of electrical switching applications, improved surface-mechanical property is a prime factor to retain its life. Thus, improvement of surface-mechanical properties of such Cu components is highly required without adversely affecting its electrical properties. Thus, electro-co-deposition of Cu-based composite coating on Cu is need of time due to its inherent cost effectiveness, but is less discussed by scientists. As per available literature, the present study is the first trial to investigate such in depth study on Cu-based electro-co-deposition.

Chapter 2

Literature review

2.1 Introduction

This current chapter starts with the brief presentation and discussion about the Cu, applications, properties of copper followed by description about different types and advantage of electrodeposition technique. Then, significant contributions of different copper based composite coatings, effect of process parameters on various properties, followed by the discussion on the characteristics of various ceramic oxide materials reinforced in copper matrix, and insights on their surface-mechanical, structural and electrical properties by various researchers was also discussed briefly. Elucidations of several deposition techniques are also presented to explain their differences in processing, advantages, and limitations in relation to coating preparation.

2.2 Copper

Copper (Cu) is a metal of reddish brown color having electrical conductivity just after Silver (Ag) and found as 15 different types of ores. Some of the important ores of copper is Chalcopyrite ($CuFeS_2$), Chalcocite (Cu_2S), Covellite (CuS), Cuprite (Cu_2O), Bornite ($2Cu_2S.CuS.FeS$). Out of these copper bearing minerals maximum pure copper can be extracted from cuprite followed by chalcocite and covellite. Around 80 percent of the extracted copper of the world basically oxide and sulphide ores, in which copper is bonded either with oxide or sulphide, which is considered an essential element for all living organisms in various ways [20, 21].

2.2.1 Properties and applications of Cu

Cu possesses various unique properties, which make it an invincible material for human beings [21], such as:

- High electrical conductivity (5.96×10^7 S/m)
- High thermal conductivity (394 W m−1 K−1)

- Reasonably good corrosion resistance at ambient temperatures
- Environmentally friendly and easily available material
- Excellent malleability

These unique combinations of properties of Cu make it an important material for various electrical applications [21], such as

- Electrical conductors
- Heat exchanger
- Electrical plugs
- Electrical wires
- Radiators
- Electrical busbars
- Use in transformer and motor winding

2.2.2 Limitations

Large amount of copper is used in different electrical applications as cable wires, busbars and transformer winding, other conductors, etc. [21]. Copper has numerous advantages as a contact material, and these advantages are the reason for its use in small wiring cables in preference to aluminium, which can give much more trouble through deteriorating contact. Presently copper is used in various electrical contact applications, either in the material of the contacts themselves, as a backing material, or in the construction of the contact carrier connections and terminals of the switch contact assembly. But poor mechanical properties [22] (hardness and wear resistance) weakens the applicability in specific electrical contacts such as electrical switching, because due to the ductility nature, and poor strength and frictional behavior Cu loses its material quickly by continuous sliding contacts of the electrical switch. Thus poor mechanical property of the Cu often necessitates strengthening without adversely affecting its electrical/ thermal conductivity. Some specific application like electrical switching require mainly good surface mechanical properties like hardness, wear resistance due to frequent rubbing action during switching.

2.2.3 Concept of bulk modification

Earlier many researchers have tried various bulk modification techniques to improve the mechanical properties of the Cu and Cu-based alloy and composites, because Cu has very poor mechanical properties (hardness and wear resistance). So, to enhance the mechanical properties of Cu, various bulk modification techniques can be used; such as solid solution strengthening (substitutional/interstitial), precipitation method (coherent/semi-coherent) and/or dispersion (externally added phases) strengthening mechanism [23].

(a) Solid solution Strengthening/Alloying

Solid solution strengthening [24] is one of the common phenomena to improve the strength of the pure metal. To strengthen the pure copper small amounts of an alloying element added to molten copper will completely dissolve and as a result form a uniform microstructure (a single phase). Normally alloying elements used for copper are Zn, Be, Cr, Sn, Ag, Al, Au, Ni, As, Fe, etc. For example bronze is an alloy of Cu formed by the addition of Sn to Cu, which is stronger and harder than pure Cu. Similarly by addition of Zn to pure Cu, another alloy is formed and known brass. Due to more strength of bronze than brass, tin is considered more effective in strengthening of copper than zinc, but is also consider as more expensive and has higher negative effect on the electrical and thermal conductivities than zinc. Other metals such as Aluminum (forming alloys known as aluminum bronzes), Nickel, Manganese, and Silicon can also be added to strengthen the Cu.

(b) Precipitation hardening and Dispersion Strengthening

Precipitation hardening and Dispersion Strengthening are other strengthening mechanisms [25]. Both the processes involve hindering or trapping the dislocation motion in matrix phase and strengthen the matrix. Precipitation process is often used for copper based alloys containing beryllium, nickel, chromium, or zirconium. The above process involves quenching of a supersaturated solid solution from an elevated temperature, then reheating at a lower temperature to allow the excess solute to precipitate and form a second phase. But in case of dispersion hardening mechanism, the strength of the primary metal such as copper (Cu) can

be increased by uniformly dispersing small, hard and inert particles in copper matrix. The dispersed ultrafine second phase particle obstructs the dislocation motions, which in turn densify the matrix and increase the strength. But this is not as effective as the precipitation method for increase the strength of the material, because in case of dispersion strengthening generally the size of dispersed particles are greater than 10 nm and the particles are not coherent with the matrix. But, the main advantage of dispersion hardening is that the dispersed foreign particles in the matrix neither grow in size nor dissolve at high temperatures unlike precipitation method. So, even in high temperature dispersion strengthened materials sustain their strength.

(c) Grain size refinement

Grain size strengthening mechanism [25] is a process to strengthen the materials by increasing the grain boundary area and decrease the grain sizes over the existing grain sizes. This mechanism basically established as Hall-Petch relation and it states that the strength of a particular material is inversely proportional to the square root of the average grain diameter of that material (i.e., $\sigma_y = \sigma_o + k\, d^{-1/2}$) where σ_y is the yield stress, σ_o is friction stress, k is the constant, and d is grain diameter.

Though, bulk modification method is widely studied for enhancement of mechanical properties of Cu and thereby refining the longevity of the Cu based electrical contacts. But, in case of bulk modification, there is a restriction on solubility limit, which indirectly affect the mechanical properties and also affecting in deterioration of electrical and thermal conductivities. Though, bulk modification of Cu with Zn, Sn Si, and Al is effective in improving mechanical properties by solid solution strengthening but proves detrimental in decreasing the mean free path of electrons, which in turn increase the electrical resistivity [26]. Moreover, it was reported that Cr and Be are the only alloying elements that improves mechanical properties of Cu without adversely affecting its original electrical/thermal conductivity [27]. However, addition of Cr improves the mechanical properties of Cu up to limited label due to their restriction of solid solubility in Cu (e.g. 0.89 at. % Cr in Cu at 1000

°C) and breathing of Cu-Be dust, as formed by machining or welding may cause serious lung damage due to the toxicity nature of Be [28].

Due to the requirement of high electrical conduction throughout the material, surface modification techniques can be considered as an alternative way to improve the mechanical properties of Cu without much deterioration of original electrical and thermal conductivity for applicable as electrical contacts. So by surface engineering techniques, hard coating on the copper surface to improve the mechanical properties without decrease in electrical properties can be considered as fruitful for desired application purpose.

2.2.4 Surface modification concept

Surface modification is a technique to modify the surface of a material by bringing physical, mechanical, chemical, electrochemical, electrical, tribological or biological characteristics of the material, which is different from the original characteristics found on the surface of a material for various application purposes such as automotive, aerospace, missile, power, electronic, biomedical, textile, petroleum, petrochemical, chemical, steel, power, cement, machine tools, and construction industries [29]. Virtually every type of materials including metals, polymers and ceramics can be coated on similar or dissimilar materials according to requirements.

There are wide variety of surface modification techniques used for modifying the surface of the materials such as thermochemical treatment (carburizing, nitriding etc.), Electrodeposition, Electroless deposition, Physical Vapor deposition, (Sputtering, Ion Plating, Ion Implantation etc.), Chemical Vapor deposition (Plasma Enhanced chemical vapor deposition etc.), Spray Coatings (thermal, Flame, Plasma), and Laser Cladding, etc. Some of the techniques are briefly discussed below.

(a) Electrodeposition

Electroplating is a plating process that uses electric current to reduce dissolved metal cations to form a coherent metal coating on an electrode (surface of conducting substrate). It is generally used to change the surface properties such as abrasion and wear resistance,

corrosion protection, and lubricity of the substrate material. The whole process of electroplating is often called as electrodeposition [30].

(b) Electroless plating

Electroless plating process is unlike electroplating process, in which no external current is required to reduce the metal cations into metal atoms. Metal coatings in this process are produced by chemical reduction with electrons supplied by a reducing agent present in the solution. The process was first reported by Brenner and Riddell [31] in 1946 for nickel and cobalt coatings and has been extended to electroless plating of copper, gold, palladium, platinum, silver and a variety of alloys involving one or more of these metals. Generally electroless deposition coatings are uniform and continuous, which makes this process very attractive for various applications. Applications of electroless deposition related to energy conversion, aerospace, electronics, biomedical and automotive industries.

(c) Physical Vapor Deposition

Physical vapor deposition (PVD) process are generally operated in vacuum conditions, in which the material is physically removed from a source material by sputtering, transported through vacuum and condensed as a film on the surface of the substrate [32]. The coating thickness of the specimens in these processes can vary from angstroms to millimeters. PVD coatings are generally used to improve different properties (hardness, wear resistance and oxidation resistance). Thus these types of coatings are useful in wide range of applications such as aerospace, automotive, medical/surgical cutting tools [33]. The advantages of PVD are excellent coating adhesion and easily tuning the microstructure by choosing the coating parameters. The main disadvantages of this technique are relatively low deposition rates and film thicknesses, technologically demanding processes (vacuum based) and coating of geometrically complex parts is difficult.

(d) Chemical Vapor Deposition

Chemical vapor deposition (CVD) is an extensively used materials-processing technology in the field of surface engineering field [34]. The most of its applications involve applying solid

thin or thick composite as well as single metal coatings on surfaces of the substrates. It can also be useful to produce high-purity bulk materials and powders, as well as fabricating composite materials through infiltration techniques. This process involves chemical reaction of one or more volatile precursor gases at the substrate and then reacts or decomposes forming a solid phase which is deposited onto the surface of the substrate. The important steps that occur during the CVD process can be summarized as [34, 35]:

- Transport of reacting gaseous molecules to the surface.
- Adsorption of the molecules on the surface.
- Heterogeneous surface reaction catalyzed by the surface.
- Surface diffusion of the gaseous molecules to growth sites.
- Nucleation and growth of the deposit.
- Desorption of gaseous reaction products and transport of reaction products away from the surface.

CVD is a complex method of producing coatings and thin films compared to PVD. CVD displays several advantages such as the ability to produce extremely pure and dense coatings or ultrafine particles at reasonably good deposition rates. The ability of coating complex-shaped components homogenously on the substrate due to its non-line-of-sight nature unlike thermal spray coating can be considered as another advantage. CVD is considered as useful technique for production of metallic, ceramic compound and semiconducting films, some of these coatings include elements, metals and alloys, oxides, carbides, borides, nitrides, etc. The deposition process can be categorized into laser-assisted, plasma-assisted, and thermally activated CVD depending on the sources used for the activation of chemical reactions. The main disadvantage of this technique is the related high temperature.

(e) Thermal Spray Coatings

Thermal spray coating is one of the techniques which used to form hard coatings on selected surface. The process involves heated or melted material to be mixed in a gaseous medium and projected at high speed onto a surface of the substrate to coat the molten droplets. Upon impacting the substrate surface, the droplets become compressed and transfer the heat to the

cold substrate and solidify rapidly to form a thin coating. Powders, rod and wires can be used as raw materials [36]. Numerous processing routes can be used depending on the materials and desired coating performances. These include plasma spraying, detonation flame spraying, high speed oxyfuel (HVOF) spraying, and flame spraying. Metals, ceramic, and polymers are the most commonly used coating materials. Typical deposit thickness of 50-300 μm can be achievable. There are some major advantages of the thermal spray coatings; (i) the extensive variety of materials that can be used for the coating process. Virtually any material can be used, which melts without decomposition, (ii) without significantly heating the substrate, most of the thermal spray processes able to apply a coating onto a substrate. (iii) Another advantage is the ability to strip and recoat damaged or worn coatings without changing the properties or dimensions of the substrate. One of the main disadvantages of the coating process is the line-of-sight nature of these deposition processes.

Out of all the above coating methods electrodeposition is the oldest and frequent using technique to produce thin and thick films for various application purposes. The reasons behind the abandon use of electrodeposition process will be explained in the next section.

2.3 Electrodeposition basics

2.3.1 Faraday's Law of Electrolysis

Faraday's laws of electrolysis define the connection between the amount of electricity passed through the electrolyte and the quantity of a substance liberated at the electrode [37].

First law:

First law states that the mass of a substance liberated at the electrode is directly proportional to the quantity of electricity passed through the electrolyte [37].

$$m \propto Q,\ m \propto I \times t,\ m = Z \times I \times t$$

Where Q = quantity of electricity, I = current in amperes, t = time in seconds, Z = constant of proportionality called electrochemical equivalent (ECE).

If I = 1 ampere and t = 1 second, then m = Z

Thus, electrochemical equivalent (ECE) of a substance is the amount of substance liberated at the electrode when current of one ampere is passed through the electrolyte for one second.

Second law:

The second law states that, the amounts of different substances liberated by the same quantity of electricity passing through their electrolyte solution are directly proportional to their chemical equivalent masses (chemical equivalent mass of metal can be obtained by dividing its atomic mass with number of electrons required to reduce its cation) [37].

For example:

If two electrolytic cells X and Y (containing $AgNO_3$ and $CuSO_4$ solution respectively) are connected in series and same quantity of electricity is passed through the cells. Weight of silver deposited μ Equivalent weight of silver and weight of copper deposited μ Equivalent weight of copper.

$$W (Ag) = E (Ag)$$

$$W (Cu) = E (Cu)$$

2.3.2 Electrodeposition, electrophoretic deposition, electro-codeposition

Electrodeposition for brief has been in practice around for a century, but serious scientists and engineers still get excited by it. Because there are quite a few answers. At first, electrodeposition is an interesting phenomenon; that means by donating electrons to ions in solution one can put a shiny coating of one metal on another. Electrodeposition is remarkably versatile for tailoring the properties for valuable application purposes. Now-a-days the feasibility of using the electrodeposition technique as a tool of material technology is attracting a lot of attention for obtaining thick and thin films of a wide variety of materials including metals, alloys, composites, polymer films, semiconductors, superconductors,

materials for bio stimulation, specific electronic device application materials and others. Some of the key advantages of the electrodeposition technique over other deposition techniques are [38]:

- By electrodeposition it is possible to produce films over large areas as well as irregularly shaped surfaces.
- Compositionally modulated structures or non-equilibrium alloys can be electroplated.
- Low cost, high throughput, scalability and industrial applicability
- Simple operation with easy to tailor the required properties
- High production rates
- Versatility as the deposition process can produce wide range of defect free coating
- Capability to handle complex geometry
- Precise control, and near room temperature operation
- Reduction of waste
- Room temperature operation

Electrodeposition in its simplest form consists of an electrolyte containing metal ions, two electrodes; one is an electrode (substrate) on which the deposition is desired, and a counter electrode. By applying current through the bath solution, the cations and anions migrate towards the cathode and anode electrodes, respectively, and get deposit on the electrode after undergoing a charge transfer phenomena.

Charged powder particles dispersed or suspended as second phase in electrolyte are attracted and deposited onto a conductive substrate of opposite charge is called electrophoretic deposition (EPD). The process of particle incorporation during the electrolytic deposition of metals, such as Cu, Ni, Co, Cr, Al, Zn and various alloys as Matrices. Particles of pure metals, ceramics and organic materials can be taken as dispersed second phase. Electrophoretic deposition is a process which involves depositing the charged powder particles dispersed or suspended in the electrolyte on the conducting substrate of opposite charge by the applying DC Electric field. This technique is regarded as versatile compared to other advanced coating techniques due to its capability of coating on any substrate shape for specific application. For

example, by electrophoretic technique coating can be made on flat, cylindrical or any other shaped substrate with only minor modification in design and positioning of electrode. It has many advantages such as short coating formation time, needs simple apparatus, very little restriction in shape of substrates [39].

The EPD process involves deposition of charged particles from the suspension onto the conducting substrate (cathode) by the applying the electric field. Therefore, two groups of parameters control the characteristics of this process.

(1) Parameters related to the suspension such as Particle size, conductivity, stability and viscosity of the suspension as well as Zeta potential. (2) Parameters related to the deposition process including the physical parameters such as electrical nature of the electrodes, applied current, deposition time, applied voltage, concentration of the solid particles in the suspension.

The electrophoretic deposition (EPD) has a wide range of novel applications in the fabrication of advanced ceramic materials and coatings, such as in the development of anti-oxidant and wear resistant ceramic coatings, fabrication of functional films for advanced microelectronic devices and solid oxide fuel cells as well as in the development of novel composites or bioactive coatings for medical implants. It has also been successfully used for thick film of silica, nanosize zeolite membrane, hydroxyapatite coating on metal substrate for biomedical applications, luminescent materials, high-Tc superconducting films, gas diffusion electrodes and sensors, multi-layer composites, glass and ceramic matrix composites by infiltration of ceramic particles onto fibre fabrics, oxide nanorods, carbon nanotube film, functionally graded ceramics, piezoelectric materials etc. [39-45].

The process of particle incorporation during the electrolytic deposition of metals is generally called as electro-codeposition or composite electrodeposition. By composite electrodeposition method Cu, Ni, Co, Cr, Al, Zn and various alloys as matrices can be deposited. Particles of pure metals, ceramics and organic materials–dispersed second phase particles can also be deposited by the composite electrodeposition method. Basically composite electrodeposition is method in which wide range of metals, alloys, ceramics and the combinations of these can

easily deposited. Electrophoretic deposition is generally considered as a sub part of electro-codeposition.

2.3.3 Types of electrodeposition

Electrodeposition technique can be classified according to the nature of the electric field applied across the electrolysis cell:

- Direct current (DC) deposition
- Periodic or pulse current (PC) deposition

DC electrodeposition (Fig.2.1) is a coating technique, in which voltage and current can be controlled during the deposition [46]. In case of DC plating current is constant and the movement of metal ions depends on their diffusion coefficient.

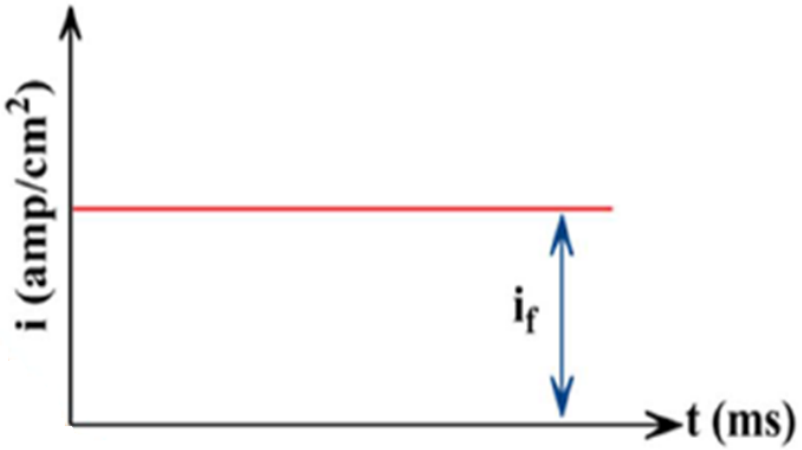

Fig. 2.1: Schematic representation of DC waveform

In pulse electrodeposition, between two given different values current and potential is varied to form a series of pulses with same amplitude, duration and polarity separated by zero current. Every pulse consists of an ON time (T_{ON}) and OFF time (T_{OFF}). During T_{ON} time current and/potential is applied and during T_{OFF} time current supply is aborted. In case of PC or pulse reverse current (PRC) deposition methods (Fig. 2.2) modulated current waveforms are used which helps in enabling to control the composition of deposited film and thickness of the film by varying the pulse amplitude and width. Pulse DC favor the initiation of grain

nuclei and hence increase the number of grains per unit area that result in finer grained deposit with better properties than DC plated coatings. Under the pulsed deposition condition the nearest diffusion layer gets splitted into two individual diffusion layers. Because of this thin nearest diffusion layer high current density can be applied with pulse DC. This enhances nucleation rate and hence finer depositions can be obtained.

Pulse current technique involves application of a forward current of certain time interval with a short, high energy reverse pulse periodically interposed. The main difference in pulse current deposition is that parameters such as ON time, OFF time and peak current density, duty cycle can be controlled independently unlike DC deposition. These variables are believed by many to create mass transport situation, an electro-crystallization conditions, and adsorption and desorption phenomena which are not otherwise possible.

The properties can be improved in case of pulse electrodeposition due to possibility of obtaining coherent and non-dendritic deposits at much higher current densities compared to direct current deposition [46, 47]. Formation of finer grain sizes in case of pulse electrodeposition due to higher nucleation resulted by high over potentials. Because of minimal chances of adsorbing foreign materials when current is off during pulse deposition [48, 49]. The mechanical properties, the structure and texture of the pulse electrodeposition coating can be different from those observed with direct current deposition.

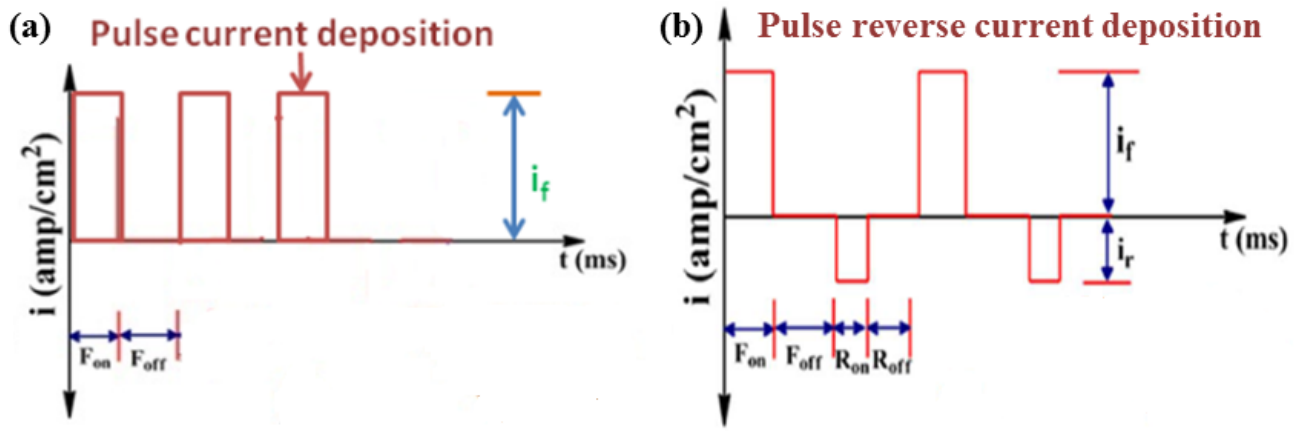

Fig. 2.2: Schematic representation of (a) PC and (b) PRC waveforms

The sum of the ON and OFF times constitutes one pulse cycle is called pulse frequency (*f*) and the duty cycle is defined as follows:

$$f = \frac{1}{(T_{ON} + T_{OFF})}, \text{ Duty Cycle} = \frac{T_{ON}}{T_{ON} + T_{OFF}} \times 100\%$$

A duty cycle of 100% means to conventional plating because OFF time is zero. In practice, pulse plating usually involves a duty cycle of 5% or greater according to the deposition requirements. The average current density (Ia) under pulse electrodeposition conditions is defined as

Average current density (Ia) = Peak current density × duty cycle

During the ON time the concentration of the metal ions to be deposited is reduced within a certain distance from the cathode surface. This so-called diffusion layer pulsates with the same frequency as the applied pulse current. Its thickness is also related to peak current but reaches a limiting value governed primarily by the diffusion coefficient of the metal ions. During the OFF time the concentration of the metal ions build up again by diffusion from the bulk electrolyte and will reach the equilibrium concentration of the bulk electrolyte if enough time is allowed.

Pulse electrodeposition has various advantages over conventional DC electrodeposition, viz., [50]

(i) Hard deposit, crack free, with better adhesion
(ii) Fine grained deposition with more homogeneity and less porosity
(iii) Faster coating rates due to increased allowable current densities
(iv) Less hydrogen entrapment
(v) Lesser impurity content

2.3.4 Electro-codeposition parameters and effects

Electrolyte used for codeposition of the metal matrix is not only defined by the chemical compositions and concentrations, but also by the second phase particle loading in suspension,

the *pH*, stirring rate, the temperature, and the surfactants used. For composite electrodeposition, number of deposition bath solutions have been used to coat the Cu based metal matrix. The bused bath for Cu deposition includes acid copper sulfate bath, alkaline pyrophosphate bath and copper cyanide bath [17, 51].

(a) Concentration of second phase particles in Suspension

Concentration of electrolyte used second phase particles or particle loading in the suspension are important factors which directly affect the amount of particle incorporation in the deposits. This also indirectly affects the various properties of the coating material. For example, at low loadings, codeposition of suspended particle is limited to the electrode surfaces (substrate) leads to lesser amount of particles in the deposition matrix. As the particle concentration increases in the suspension increases, migration of particles to the electrode increases as well as the incorporation level in the deposition matrix. But, beyond the certain loading level, the increase in incorporation of second phase particles is not quantitatively proportional to the increase in particle loading in the suspension [52-55]. The particle concentrations can have a dramatic effect on the amount of incorporation obtained for a particular bath composition. For example three times more TiO_2 compared to $A1_2O_3$ has reportedly [56] been incorporated into a Ni matrix, under the same deposition conditions with same concentration.

(b) Bath Agitation

Increase in the bath agitation or stirring rate before and during the deposition process in the parallel plate electrode setup has shown better incorporation of second phase particles in the deposited matrix, for example; Ni-TiO_2 and Ni-Al_2O_3 systems [57]. It has been well established that with increasing bath agitation higher amount of incorporated second phase particles in the matrix was observed. But, beyond certain agitation limit (if the agitation is too intense) the residency time for the particles at the electrode surface (substrate) is not sufficient enough to get deposited into the developing coating before they could sweep away. Similar observation was also observed in case of Cu-CrB_2 and Cu-SiC coating systems, in which the amount of codeposition decreased with increasing agitation [56].

(c) Surfactant

Surfactants have important role on the deposition of second phase particles in the coating matrix. Different surfactants have different role on the corresponding deposition system. It have been reported that for Ni-Al_2O_3 composite coating the codeposition of Al_2O_3 was increased with increasing concentration of cationic surfactant named as hexadecylpyridinium bromide (HPB) and also reported about better hardness and wear resistance at 150 mg/l of HPB [58]. Another literature reported about increasing amount of codeposited SiC in Ni-SiC composite matrix with increasing concentration of CTAB [59]. For similar composite coating (Ni-SiC), another report says that with increasing surfactant concertation SiC codeposition increases, but it is also reported that TMAH (Tetramethyl ammonium hydroxide) has better deposition rate for SiC than CTAB surfactant [60]. The increase in codeposition of second phase particles resulted with increase in concentration of surfactant in the solution, because the surface charge of the particles modified in the suspension by the absorbed molecules or ions, thus decreasing agglomeration of second phase particles and promoting the migration of the suspended particles towards the substrate. Thus higher amount of particle loading in the film with uniform distribution can be expected. Copper based composite coating such as Cu-Si_3N_4 assisted with SDS surfactant was reported, but no effect of surfactant on particle concentrations or any properties was discussed [17].

(d) Current Density

In the electrodeposition process current density plays an important role in the amount of second phase particles incorporation onto the matrix by controlling the deposition rate. This will directly affect the various properties of the developed coatings. It also affects the thickness of the composite films, in other words the current density is directly proportional to coating thickness of the composite coating. Few reports on Ni and Cu based composite coatings are available establishing the relationship between current density, the amount of particle incorporation in the deposits as well as its effect on various properties [56, 61, 62].

(e) Particle Characteristics

The particle size is also an important factor for deposition, such as the amount of particles incorporation in the deposited matrix is depend on the size of the particle. For example when the particle size in the electrolyte increases then amount of adsorbed ions on the surface increases, which leads to the increase in the migration velocity of the particles and also results in a higher columbic force of attraction, leads to increase in the amount of the particles. But the density of particles in the coating decreases as the particle size in the electrolyte increases. For instance increasing the particle size resulted in an increase in the amount of incorporation for Ni-$A1_2O_3$, Ni-SiC, Ni-Cr, Cu-P, and Cu-Al_2O_3 [63]. However, other investigators found particle size to have a insignificant effect on the amount of incorporation for Ni-$A1_2O_3$ and Sn-Ni-SiC [63]. A variety of second phase particle sizes ranging from 4 nm to 800 nm diameters, have been successfully incorporated into the developed metallic electrodeposits [5, 64-69]. By incorporating nanosized particles into deposit matrix, various properties of the coating such as hardness, wear resistance, high-temperature corrosion protection, oxidation resistance and self-lubrication, etc., are significantly improved [70, 71]. But, it has been also reported that the reduction of particle size decreased the amount of codeposited particles in the deposits [3, 8–9]. It was also reported that the smaller the particle size, the more difficult for particles to embedded in the deposition layer [65, 70, and 72].

(f) Zeta potential

All particles in suspension display a zeta potential, or surface charge, which at the interface between the particle surface and the stationary layer of the fluid attached to the particle. Zeta potential is one of the key factors in electrophoretic and electro-codeposition or composite electrodeposition techniques. The measurement and knowledge of zeta potential for composite electrodeposition is important for optimization of processing, predicting stability of the suspension and interactions as well as a simple method of quality control [73].

The zeta potential is crucial in determining the stability of a suspension. The particles with high negative or high positive zeta potential will repel each other, and consequently the suspension will be stable. Generally if the zeta potential with value more positive than +30

mV or more negative than -30 mV are usually considered stable [74]. If the zeta potential is low the tendency for flocculation is higher. Another important factor is *pH* when discussing zeta potential; in fact, mentioning a zeta potential without citing *pH* is almost meaningless. Because, for suspensions of most materials, a plot between zeta potential and *pH* displays an isoelectric point (shown in Fig. 2.3), a particular *pH* value of solution where the net charge on the particles is zero. At this point of *pH* value the suspension is highly unstable, and flocculation is at its most likely.

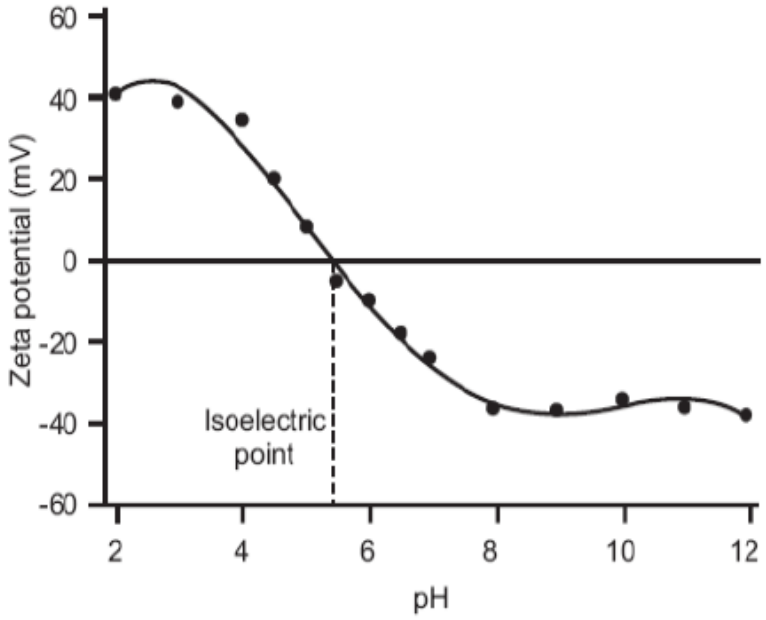

Fig. 2.3: Representative plot of *pH* versus zeta potential demonstrating the isoelectric point [74].

2.4 Different baths used for Copper Electroplating

Different types of electrolytes, which are most commonly used for copper electrodeposition for different application purpose, are copper sulfate bath, copper cyanide bath and copper pyrophosphate bath [75, 76]. Copper sulfate bath typically contain 200 to 250 g/l of copper sulfate and 10 to 75 g/l of sulfuric acid depending upon the requirement of the type of coatings. These types of electrolytes are generally considered more economical for synthesis and operate compared to copper pyrophosphate bath. Sulfate bath is basically used for plating of Cu-based electrical components such as, printed circuits, electrical busbars, electronics,

rotogravure, and plastics, and for electroforming and other various components. Other copper plating baths such as, copper cyanide plating baths typically contain 30 g/l of copper cyanide and either 59 g/l of potassium cyanide or 48 g/l of sodium cyanide. Cathode efficiencies of cyanide bath ranges from 30 to 60 percent. These baths mainly used widely in many plating operations as a strike. Copper pyrophosphate plating baths typically contain 53 to 84 g/l of copper pyrophosphate and 200 to 350 g/l of potassium pyrophosphate. These baths are used for plating on plastics and printed circuits and requires more control and maintenance of the plating bath than copper cyanide plating. However, copper pyrophosphate solutions are relatively nontoxic compared to other plating baths. But among the entire electrolyte used for copper plating sulfate bath is used more frequently than other baths due to its economic viability.

2.5 Electro-codeposition of copper based composite coatings

Though, there were enormous research on electrodeposition of metal matrix composite and effect of various process parameters on the composite coatings was available [77-81]. But, after extensive literatures searching, only few Cu based ceramic oxides composite coatings by composite electrodeposition was found. Brief reviews of the existing literatures are provided below.

Catalina et al. developed Cu-TiO_2 composite coating on a copper substrate using electro-codeposition method from acidic copper sulfate electrolyte. The effect of different current densities as well as the concentration of TiO_2 nano particles as dispersed phase in copper matrix on structure and properties of coatings was studied by the author. The second phase particle (TiO_2) of size 17 nm with various concentrations (5, 10 and 50 g/l) was added in electroplating bath. The codeposited TiO_2 in the layer verses current density was also analyzed (Fig.2.4). The microstructures and composition of layers were analyzed by optical and scanning electron microscopy (SEM) and EDX analysis. The deposition was carried out at different current densities (1, 2, 3 and 5 A/dm^2). After analyzing the result he observed that composite coating showed better hardness than pure copper and hardness increased with increasing amount of TiO_2 in the bath, which can be observed from the table 3.1. He also

reported about better surface roughness of composite coating than pure copper coating with lowest roughness at 10 g/l TiO_2 [82].

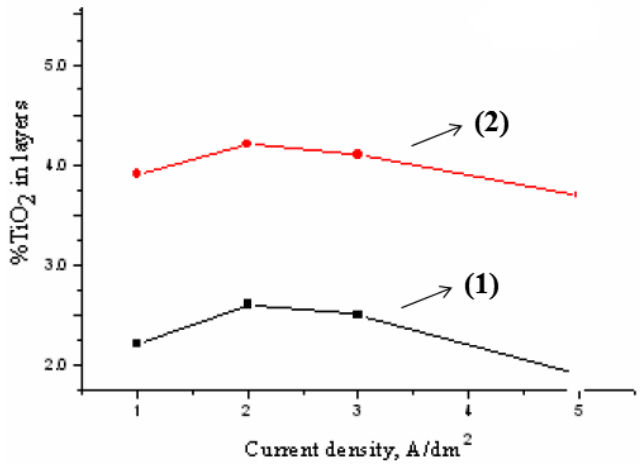

Fig. 2.4: nano-TiO_2 percentages in layers versus the electrolysis current density for two TiO_2 concentrations in electrolyte: 1) 10 g/l and 2) 50g/l [82].

Table.2.1 Microhardness of layers in copper matrix with and without nano-TiO_2 particles in electrolyte [82].

Dispersed phase (DP)	Concentration of DP in electrolyte, g/L	$HV_{0.025}$ Min. value	$HV_{0.025}$ Max. value	$HV_{0.025}$ Average value	Standard deviation
-	-	98	115	108	± 6.3
TiO_2	5	102	118	110	± 5.4
TiO_2	10	104	121	113	± 4.6
TiO_2	50	115	134	125	± 5.3

Ramalingam et al. was also reported about electrodeposited Cu-TiO_2 nano composite coating on copper substrate from copper sulfate bath and they have elaborated the effect of nano sized TiO_2 particles and different concentrations of the same on the wear and corrosion resistance of the developed coatings. He also observed that with increasing amount of TiO_2 in the bath, TiO_2 wt. % in the deposited matrix increases, which directly related to the increase in mechanical properties such as hardness and wear. The increased hardness and wear loss

verses wt.% TiO_2 presented ion the matrix was presented in Fig.2.5. Author more stressed on corrosion study rather than mechanical study of the material [83].

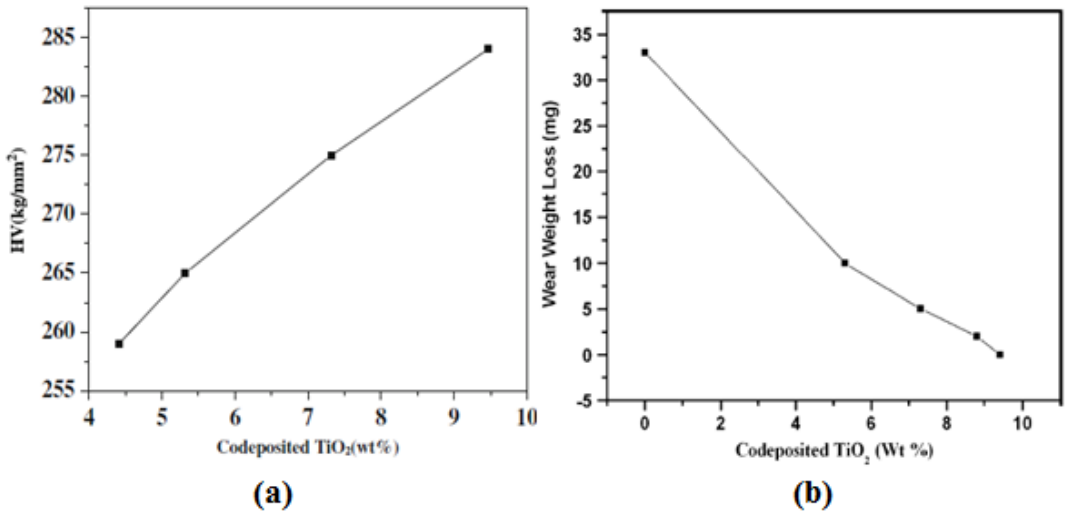

Fig.2.5: Effect of the amount of codeposited TiO_2 on the (a) microhardness and (b) wear loss of Cu-TiO_2 nanocomposite coatings [83].

Cu-Al_2O_3 thin films developed from three different types of baths such as an acidic copper sulfate, a neutral pyrophosphate, and an alkaline sorbitol based bath was reported by Andreas Bund et al. with variation of wide range of *pH*. Presences of Al_2O_3 in the matrix of the deposited specimens developed from different baths are presented in Fig. 2.6. From the figure it can be observed that the highest amount of incorporated Al_2O_3 particles (11 wt. %) was found in the deposited specimen prepared from pyrophosphate bath. Zeta potential of the second phase particles in diluted plating solutions was measured. Furthermore, the microstructure, microhardness and electric conductivity of the coating layers were characterized. By analyzing the obtained results he observed that deposits synthesized from neutral pyrophosphate bath shows better hardness (Fig. 2.7) than acidic copper sulfate bath and also reported higher electrical conductivity (Fig. 2.8) of the specimens deposited from neutral pyrophosphate electrolyte than acidic copper sulfate electrolyte at a particular current density (5 A/dm^2). The authors of the work emphasized more on the effect of *pH* and different type of bath on hardness and electrical conductivity rather than concentration of Al_2O_3, different process parameters, and other properties such as wear, surface roughness, etc. [80].

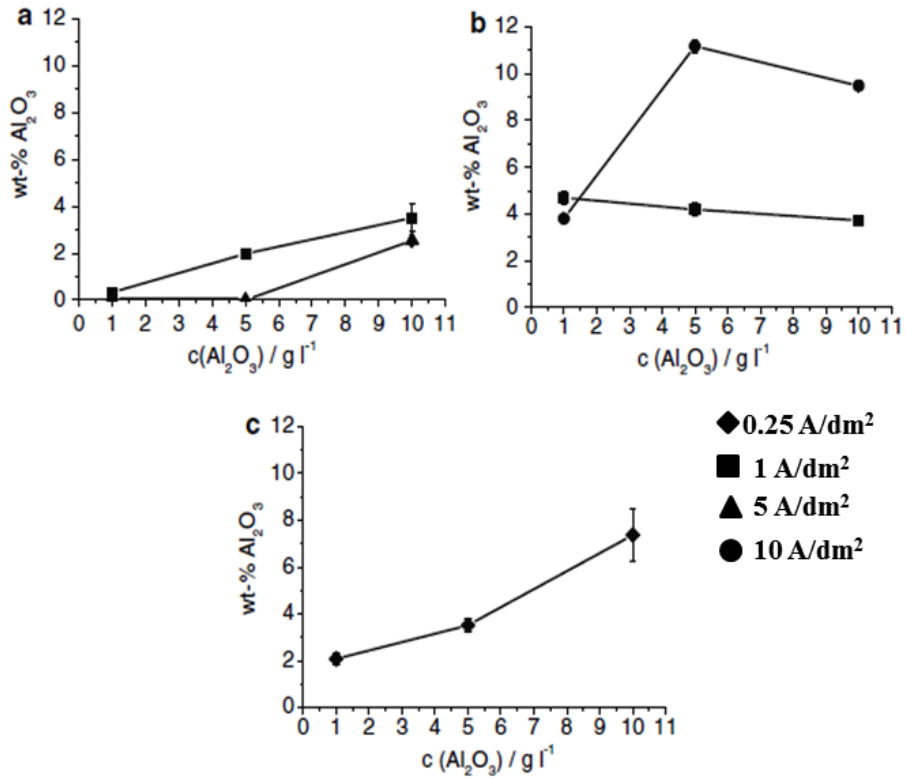

Fig. 2.6: Correlation between the Al_2O_3 content in the layer and the concentration of Al_2O_3 in the electrolyte for different current densities (a) acidic sulfate electrolyte; (b) neutral pyrophosphate electrolyte; (c) alkaline sorbitol electrolyte [80].

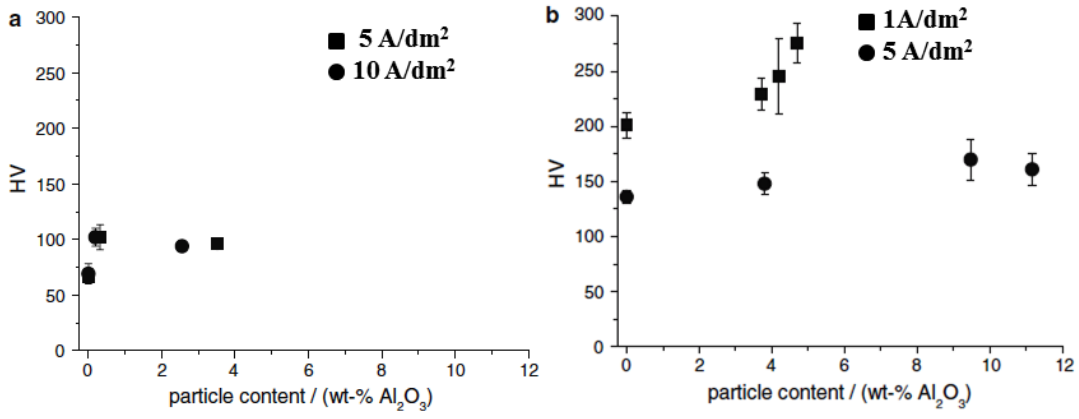

Fig. 2.7: Correlation between the Al_2O_3 content in the layer and the Vickers microhardness (a) acidic sulfate electrolyte, (b) neutral pyrophosphate electrolyte [80].

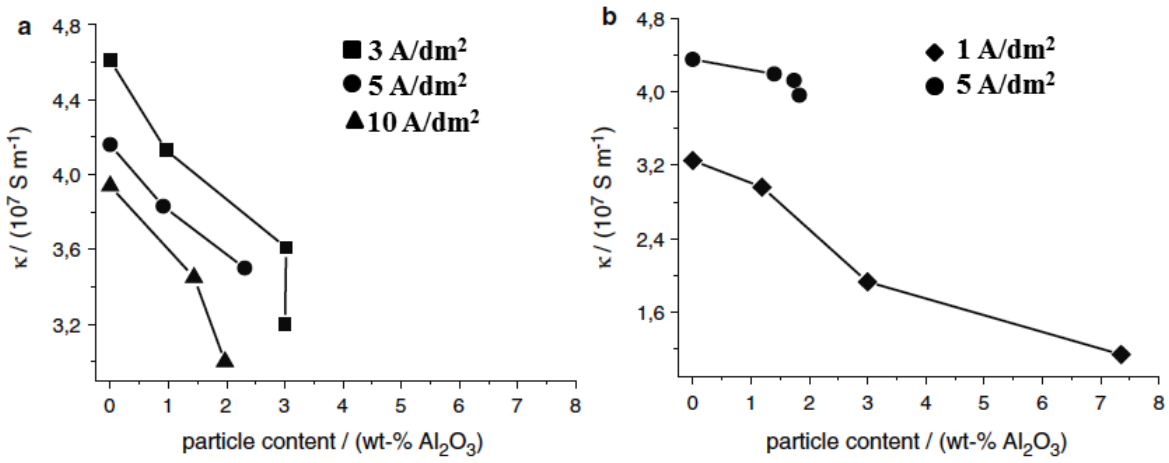

Fig. 2.8: Correlation between the Al_2O_3 content in the layer and the electrical conductivity of (a) acidic sulfate electrolyte, (b) neutral pyrophosphate electrolyte [80].

I. Zamblau et al. also prepared Cu-Al_2O_3 composite coatings on carbon steel by electrodeposition at *pH* level 3 and characterized by various characterization techniques. Polarization curves, microstructural study, electrochemical impedance spectroscopy, and the corrosion behavior of the Cu-Al_2O_3 nanocomposite coatings was examined by electrochemical methods such as open circuit potential measurements. He highlighted better corrosion resistance of Cu-Al_2O_3 compared to pure copper deposits [84].

The same composite coating as previous (Cu-Al_2O_3) was also prepared by J. R. Roos, et al. containing with either α-$A1_2O_3$ or γ-$A1_2O_3$ particles in copper sulfate baths and to which the additional thallium sulfate or aluminum sulfate were added as promoter for codeposition. The concentration of Al_2O_3 was varied from 5 to 35 g/l. They have studied the effect of thermomechanical processing on the microhardness of composite deposits. The as-deposited microhardness and the effect of annealing on the microhardness of the coating as well as the microstructure of cold-rolled and hot-rolled Cu-$A1_2O_3$ deposits were investigated. The effect of promoting agents on mechanical properties was also studied. The author also reported that in order to get optimum properties of the developed coatings a homogeneous dispersion of alumina particles in the matrix was necessary, which was not achieved by using aluminium sulfate as promoter for codeposition [85].

H. Li et.al reported about Cu-SiO_2 composite coating on carbon fiber reinforced epoxy composite. He has also studied by adding 0.6 and 3g/l concentrations of SiO_2 with 35 g/l glucose as surfactant. After comparing the microstructures of different developed composite coating, he confirmed that composite coating with 3 g/l SiO_2 without surfactant shows finer matrix with higher hardness followed by the same composite coating with 35 g/l glucose addition. He also reported minor decrease in electrical conductivity of the Cu-3g/l SiO_2 coating specimen without surfactant. [86]

I. Zamblau et al. also reported about the Cu-SiO_2 composite coating on steel substrate with cetyl trimethyl ammonium bromide (CTAB) as surfactant. The author strongly emphasized on corrosion behavior without any mechanical study. He also established that CTAB plays a key role in SiO_2 suspension stabilization, promotes the codeposition of second phase oxide in the copper matrix, which improves the morphology and structure of the deposit. Consequently, a higher corrosion resistance of Cu–SiO_2 deposits compared to pure copper was noticed in the presence of CTAB. Fig.2.9 shows the morphologies of the composite coating with variation of CTAB and SiO_2 concentrations. From the figure it can be observed that without CTAB assisted Cu–SiO_2 deposit was obtained consisting of irregular crystals. Composite coating with higher concentrations of SiO_2 shows finer matrix than lower SiO_2 concentration (Fig. 2.9a & b) due to the ability of SiO_2 to create more nucleation sites and prevent the crystal growth [87]. But, CTAB assisted Cu–SiO_2 deposits become more uniform, compact and fine grained than non-assisted Cu-SiO_2 coatings (Fig. 2.9c & d).

L. Benea et al. first and last reported about the Cu-ZrO_2 composite by electrodeposition method by adding 100 g/l ZrO_2 in the electrolyte. He studied the basics of the composite coating by varying the current density from 0 to 0.05 A/cm^2 and observed that at a current density of 0.02 A/cm^2 the wt. % of ZrO_2 in the deposited specimen was higher than other current density. After studying basic properties of the developed composite coating he observed that the electro-crystallization mechanism of copper does not change by zirconium oxide dispersed in the copper deposition electrolyte. He also observed that ZrO_2 plays an important role in the increasing rate of metal deposition and metal reducing overvoltage was lower in the presence of ZrO_2 in the electrolyte at same current density [88].

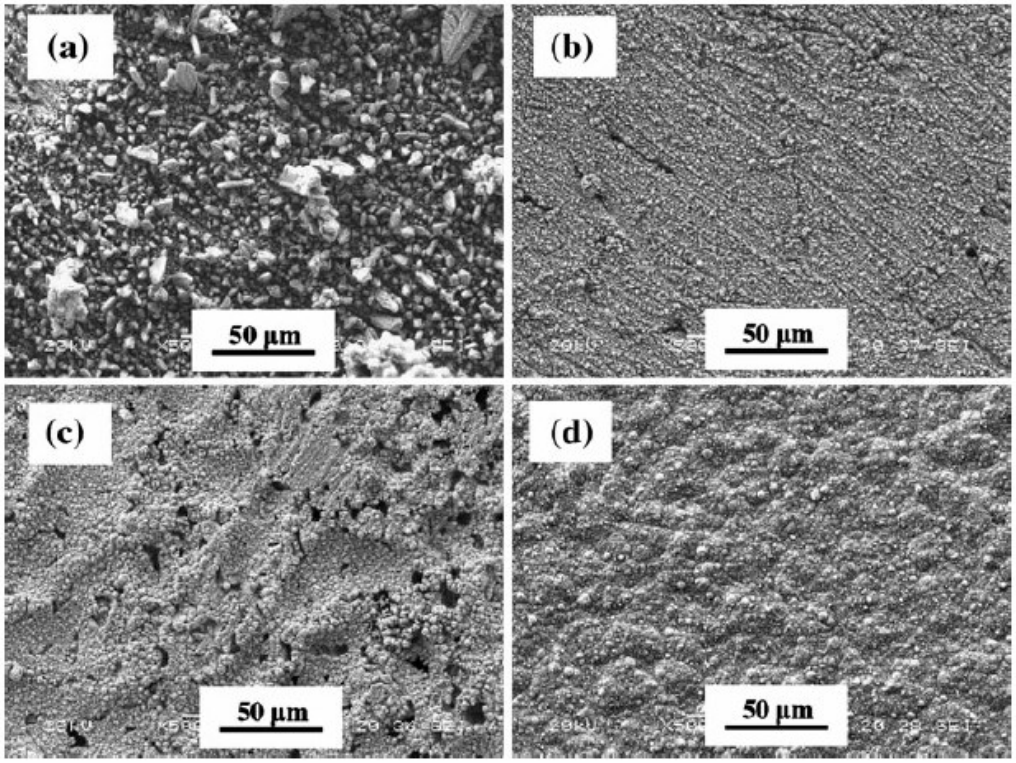

Fig. 2.9: SEM images of Cu–SiO_2 coatings obtained with different SiO_2 and CTAB concentrations in the plating baths: (a) 10 g/l SiO_2, (b) 20 g/l SiO_2, (c) 10 g/l SiO_2, and 10-3 M CTAB, (d) 20 g/l SiO_2, and 10^{-3} M CTAB [87].

Mangam et al. reported about Cu-CeO_2 composite coating by pulse electrodeposition. The author extensively study on wear and friction behavior of the developed composite coating and also reported hardness result. The reported hardness result ranges from 70-100 HV, which is quite low compared to other reported results. After analyzing the obtained results, he observed that composite coating showed better wear resistance than pure copper and also pointed out that Cu with 20 g/l CeO_2 shows best result in terms of wear resistance [89].

Recently Eslami et al. published on effect of various deposition conditions such as concentrations of Si_3N_4 and stirring rate in Cu-Si_3N_4 composite coating [17]. He also studied the composite coating with variation of SDS concentrations in bath as surfactant. From the result it was observed that, with increasing concentration of second phase particle the morphology of the matrix got finer. He also reported about and hardness results of the

developed coating, which suggested that with increasing concentration of Si_3N_4 better hardness and wear was observed (Fig. 2.10).

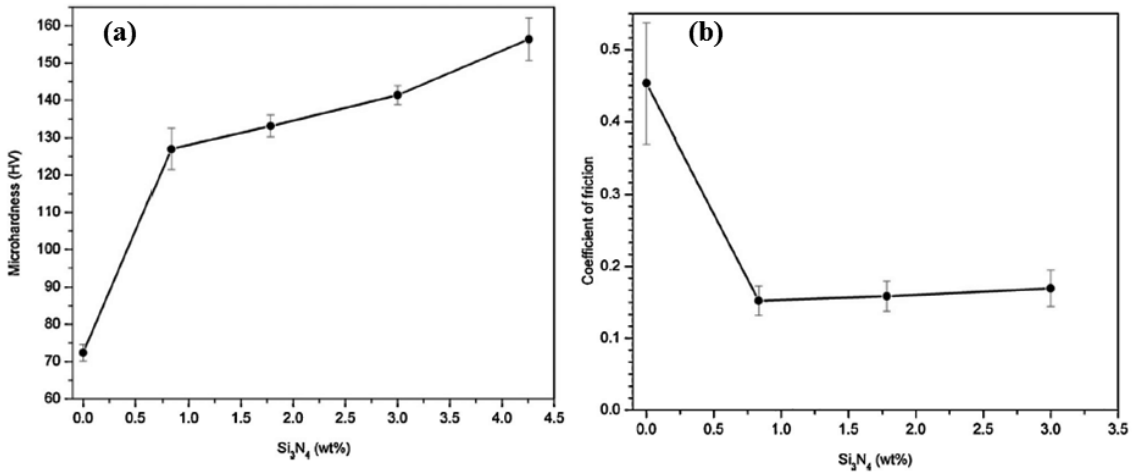

Fig. 2.10: Variations of (a) microhardness and (b) coefficient of friction of Cu–Si_3N_4 composite coatings as a function of the incorporated particle weight fraction [17]

Pradhan et al. also recently emphasized on SiC concentrations on the properties of Cu-SiC composite coating deposited by pulse reverse technique from the aqueous sulfate solution [90]. The author also studied the effect of cationic, anionic, and non-ionic surfactants' effect on the properties of the composite coatings. It was observed that incorporation of reinforcement in the composite matrix depend on the presence and nature of the surfactants. The most stable and capable surfactant for incorporating the SiC particles into the matrix was identified as cationic surfactant. Highest concentration of SiC particle concentration specimen shows best tensile stress. From the obtained hardness result it was observed that, the values are dependent on the combine effect of SiC incorporation and structure of the matrix. But in the presence of surfactants, best hardness value was observed in case of 5 g/l nano-Sic reinforced composite coating.

B. P. Singh et al. first reported the fabrication of a robust graphene reinforced copper based composite coating with excellent corrosion resistance by aqueous cathodic electrophoretic deposition (EPD) [91]. Composite coating exhibited a coating thickness of around 40 nm is obtained at 10 V and deposition time of 30 second at optimum deposition conditions. The

surface morphological characterization shows reduced graphene oxide (rGO) with sizes ranging from 1 to 2 μm uniformly deposited on the copper sheet. The composite coating showed significant increase in the resistance of the metal to electrochemical degradation. Tafel analysis confirmed that the corrosion rate displayed by composite coating is an order of magnitude lower than that of pure copper.

Pavithra et al. also reported about pulse reverse electrodeposition of Cu-Graphene composite foil on Ti substrate [92]. By optimizing the pulse parameter and current density, the composite foils with well dispersed graphene displayed best hardness of 2.5 GPa and and increased elastic modulus of 137 GPa was observed (Fig.2.11). But they also reported that the electrical conductivity of composite can be comparable to that of pure copper coating. They also reported that, annealing the composite foil at 300 ^{o}C neither caused grain growth of the Cu matrix nor deteriorated the mechanical properties, indicating graphene as an excellent reinforcement material for improvement of mechanical properties.

Xie et al. also reported about possible application of Cu based reduced graphene oxide (rGO) composite coating on copper foil by one step electro chemical reduction process for electrical contacts [93]. But the author emphasized more on surface characterization rather than mechanical characterizations. Though, he point out various weaknesses such as low hardness and wear resistance of Cu metal, which obstructs the material to be applicable in electrical contacts. Cyclic voltammetry (CV) was used to define the deposition conditions, and to confirm the chemical compositions, molecular structure of the composite, confocal Raman microscopy (CRM), X-ray photoelectron spectroscopy (XPS) and scanning electron microscopy (SEM) were used. Atomic force microscopy (AFM), conductive AFM (C-AFM) as well as impedance analysis were employed to evaluate the electroactive/electrical properties of the developed composite films, respectively.

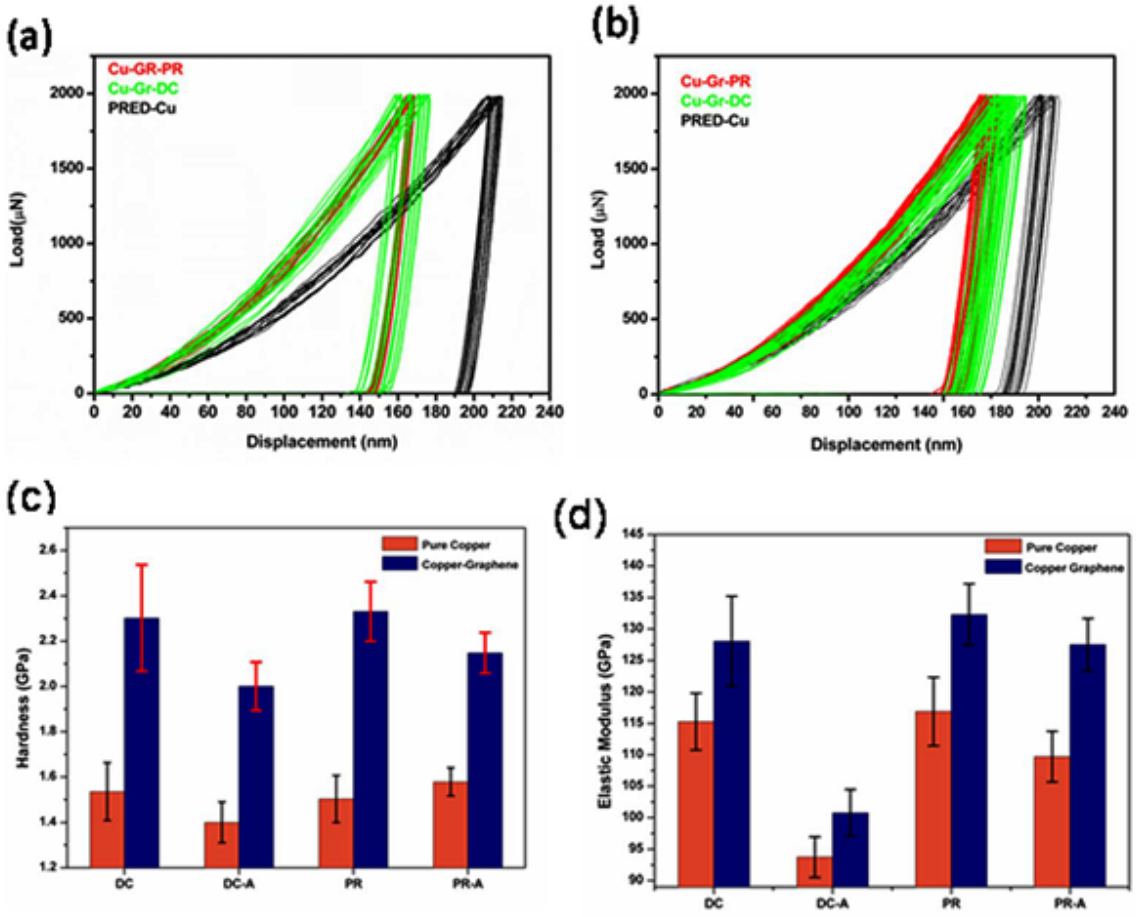

Fig. 2.11: Load displacement curves of (a) as deposited and (b) annealed PRED pure Cu, Cu-Gr composite foils (c) & (d) Plots exhibit the hardness and elastic modulus of as-deposited and annealed pure Cu and Cu-Gr composite foils prepared by DC and PRED [92].

The results obtained from CRM and XPS confirmed that the rGO/Cu composite films can be prepared through one-step electrochemical codeposition using suitable precursor solutions. They also observed electrical resistivity of the composite deposit was lower than the pure polished Cu foil and the electrodeposited Cu film. That means higher electrical conductivity of composite coating compared to pure copper coating and copper substrate was observed. Lower electrical resistivity of the composite coating may due to the higher conductivity (enhanced transfer of charge carriers) of the rGO present in the composite coating. Fig. 2.12 displays the SEM micrographs of the developed composite coating from the precursor

solution of Cu^{2+} 0.01 M/GO 0.5 mg/ml. Fig. 2.12(a-c) shows the morphology of the deposits with different time variations at a deposition potential of −1.2 V. After deposition for 10 min, many small spherical particles of diameter around 1μm were formed and uniformly distributed on the film surface (Fig. 2.12a). With increasing the deposition time to 30 minute the film surface displays pine-tree-leaf hierarchical nanostructures with 100 nm diameter trunks (Fig. 2.12b). Some branches with an average diameter of 50 nm and a length of 0.5−1 μm stretch out from the main trunk. Further increase in deposition time to 60 minute the nanostructures grow larger and denser (Fig. 2.12c). But with change in deposition potential from -12 V to -4 V, even after deposition of 3 hours the pine-tree-leaf nanostructures were not observed. Instead of pine tree many spherical particles with an average diameter of 2 μm were formed (Fig. 2.12d).

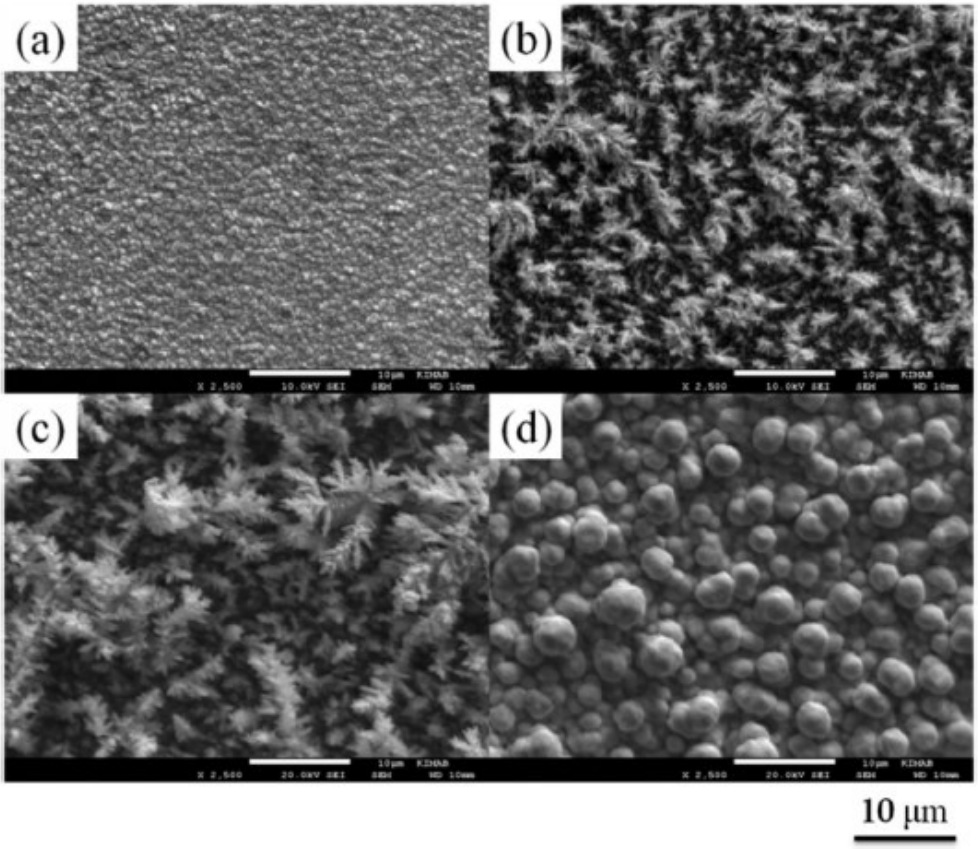

Fig. 2.12: SEM morphologies of Cu^{2+} 0.01 M/GO 0.5 mg·mL−1 solutions deposited under −1.2 V at different deposition times: (a) 10 min; (b) 30 min; (c) 60 min, and (d) under −0.4 V for 180 min [93].

It is reported that for copper based electrical applications, a highly (111) textured copper foil reveals better performance due to better hardness, electromigration resistance, oxidation resistance, and lower internal stress compared to those with other textured Cu deposits, and is required in improving the reliability of metal interconnections [92-96].

Lu et al. reported copper foils of high electrical conductivity with a preferred (101) texture containing a high density of coherent twin boundaries, exhibiting a hardness of 2.0–2.6 GPa [97, 98]. It was also documented that highly textured and twinned copper foils was prepared by pulse current (PC) deposition with a maximum hardness of 1.56 GPa only and the reason behind lower hardness was reported as the void formation due to hydrogen entrapment at higher applied current densities [99]. Some reports based on (111) oriented electrodeposited Cu films have also been published. Few years back fabrication of (111) oriented and nano-twinned Cu by DC electrodeposition from chloride bath at high current density with enhanced mechanical properties was reported. They also reported 40 ppm chloride concentration as critical concentration at serious agitation, above which (111) orientation was dominated [100]. But, Chen et al. [101] reported about formation of (110) texture from same chloride bath at DC and PC deposition. They have reported critical chloride concentration was about 40 ppm for DC electrodeposition without serious agitation and 60 ppm for pulse electrodeposition. But the effect of orientation on mechanical and electrical properties of composite coatings was not explored systematically before.

2.6 Scope of this study

Due to commercially applicable viability as electrical contacts of Cu to improve its surface-mechanical properties by composite electrodeposition was a worth trial. After extensive literature reviewing, the author of the dissertation came to know that, there were various reports available on electrodeposition of different systems (specifically Ni based composite coatings) with variations of different process parameters, but very few literatures are available on Cu based composite coatings by electrodeposition technique with no systematic surface-mechanical and electrical study, which could give an better understanding of the material properties in terms of applicability in electrical contacts.

Deficiency of systematic study on surface-mechanical and electrical properties of Cu based oxide composite coating by composite electrodeposition method as well as effect of different process parameters on the said properties for better understanding of the material properties for application viability in the existing literatures aspire the author of the current dissertation to carry out the desired work. In the current dissertation, the following coating systems (Cu-Al_2O_3, Cu-SiO_2, Cu-Y_2O_3, Cu-ZrO_2, and Cu-GO) were synthesized by composite electrodeposition and effect of various deposition parameters on surface-mechanical and electrical properties were also carefully examined.

- Each second phase powder was characterized by Zeta potential measurement for particle size analysis and isoelectric point measurement. Transmission electron microscopy was done for all the powders to confirm the size distribution.

- Effect of different current densities (5, 8, 11 and 14 A/dm^2) on surface-mechanical and electrical properties of Cu-Al_2O_3 composite coating was studied.

- Concentration of all the second phase powders such as Al_2O_3, SiO_2, Y_2O_3 (10 and 30 g/l), ZrO_2 (10 g/l) and GO/RGO/TRGO (0.1, 0.5 and 1 g/l) as reinforcements of Cu was studied.

- Effect of pulse frequency (1, 5, and 10 kHz) with 30% duty cycle for various coating systems was also studied.

- Different surfactants CTAB (cationic), SDS (anionic), PAA (polymeric) and glucose (non-ionic) assisted Cu-10 g/l ZrO2 composite coating with various concentrations at 5 kHz pulse frequency have been prepared and effect of surfactant concentrations on surface-mechanical and electrical properties of the developed composite coating was analyzed.

Final developed coatings of different composite systems were characterized by:

- X-ray diffraction (XRD) and Field emission scanning electron microscope (FESEM) for phase, microstructural analysis. Energy dispersive spectra (EDS) for composition analysis.
- Bulk texture by XRD for orientation dependent mechanism study.
- Surface profiler and atomic force microscopy (AFM) for roughness study of the coatings.
- Microhardness and wear study for mechanical properties analysis.
- Electrical conductivity for getting an idea about the conductivity of the developed coatings.

Chapter 3

Materials and method

3.1 Introduction

The present chapter deals with the detailed experimental procedures, materials used in the investigation and the equipment accessed to check the performance of developed materials by experimentation. All the equipment used for characterization purpose in the present investigations are discussed below with their specific utilization in the investigation along with their specifications and particulars in details.

The materials and chemicals required for the fabrication of developed composite coated specimens and bath electrolyte for deposition purposes are also provided in this chapter. Step wise procedures from substrate preparation to deposition process have been thoroughly elaborated.

3.2 Materials used

The chemicals utilized in the current dissertation work are provided in Table 3.1 with manufacturer name and purification percentage. All the chemicals used in the present investigations are in analytical grade without any further purification.

Table 3.1: Materials used with manufacturer name

Materials name	**Manufacturer and specifications**
Copper sulfate ($CuSO_4.5H_2O$)	98.5 (min. assay), Nice chemicals, India
Sulfuric acid (H_2SO_4)	97% concentrated, Fisher Scientific, India
SiO_2	99.5 (min. assay), Sigma Aldrich, china.
Y_2O_3	99.995% (min. assay), Alfa Aesar, USA
ZrO_2	99% (min. assay), Chempure private limited, India
Cetyl trimethyl ammonium bromide (CTAB)	99% (min. assay), Otto chemicals, India
Sodium dodecyl sulfate (SDS)	90% (min. assay), Merck specialties private

	limited, India
Poly acrylic acid (PAA)	Otto chemicals, India
D-Glucose	Fisher Scientific, India
Hydrochloric acid (HCl)	35-37% (min. assay), Fisher Scientific, India
Hydrazine Monohydrate	(64% Hydrazine), Acros Organics, USA
Graphite powder (Extra pure)	99.5% (min. assay), Loba chemie private limited, india
Potassium permanganate ($KMnO_4$)	99% (min. assay), Rankem, India
Sodium nitrate ($NaNO_3$)	84.99% (min. assay), Fisher Scientific, India
Hydrogen peroxide (H_2O_2)	30% (min. assay), Fisher Scientific, India

3.3 Synthesis of graphene oxide (GO)

Graphene oxide (GO) used for Cu based composite coating was synthesized by modified Hummers method [102] and details of the same is given in flowchart (figure 3.1). High purity graphite (2 g), H_2SO_4 (46 mL) and $NaNO_3$ (1 g) were mixed in an ice bath and the temperature kept below 5 ^oC followed by vigorous stirring for 30 minute. Then $KMnO_4$ (6 g) was slowly added as an oxidizing agent to the graphite solution and the temperature maintained below 15 ^oC. The whole mixture was stirred at 35 ^oC for 30 minute, and then the temperature was slowly raised to approximately 98 ^oC and stirred for 2 hour. Once the solution was homogenous, deionized water was added as the oxygen source and the stirring continued for another 15 minute. H_2O_2 (10 mL) was added slowly to remove Mn ions, the color of the solution changed to bright yellow. Finally, to remove the remaining residual, the mixture was centrifuged and washed with H_2O: HCl (10:1) volume percentage and the obtained powder dried at room temperature.

Synthesized graphene oxide was reduced by different methods. For reduction process 100 mg GO and 100 ml H_2O taken in a 250 ml round bottom flask followed by sonication till unnecessary particulates are out. Then 1ml hydrazine hydrate was added to it and the solution heated in an oil bath at 100^oC for 20-24 hour. The obtained powder after hydrazine hydrate treatment named as reduced graphene oxide (RGO). The RGO was further reduced by heating at 850^oC for 30 minutes in argon atmosphere was named as thermally treated reduced graphene oxide (TRGO).

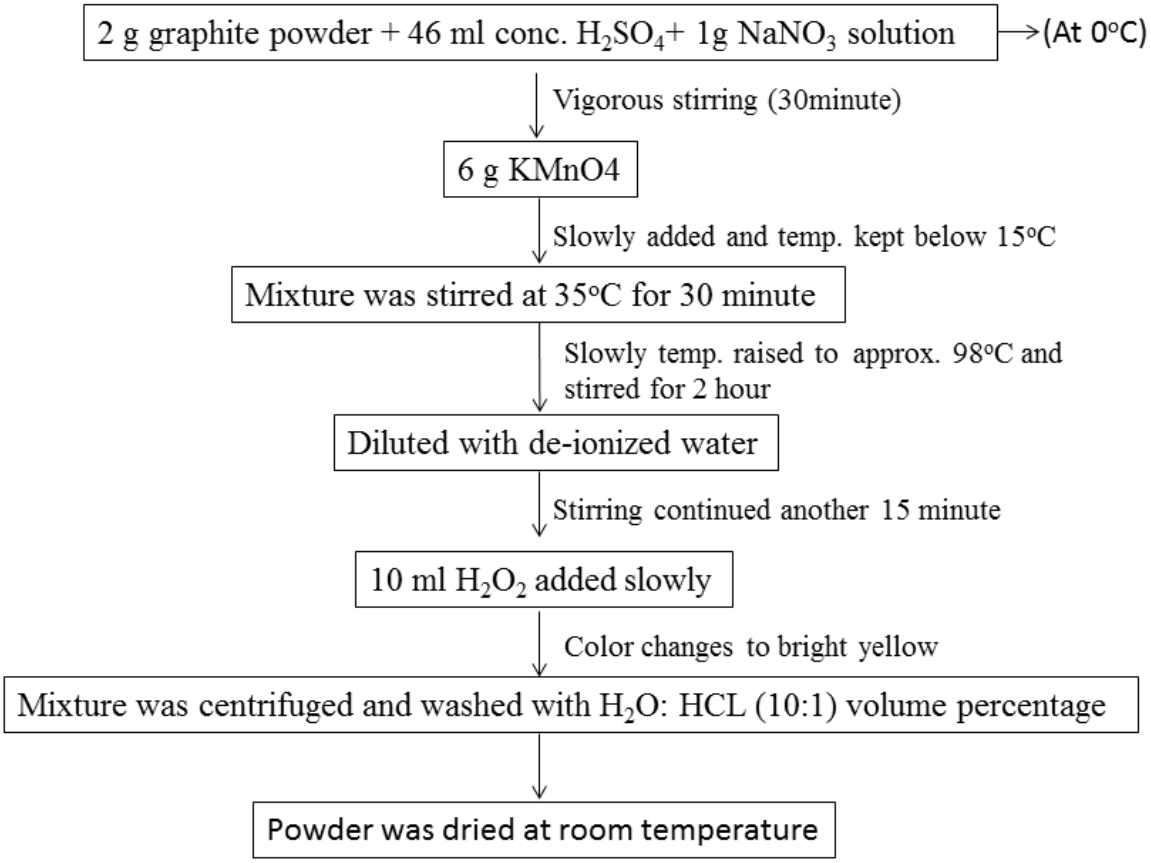

Fig.3.1: Schematic representation of synthesized graphene oxide

3.4 Substrate preparation

For the co-deposition of Cu based composite coatings, copper was selected as the substrate material. Hot rolled copper bus bar was procured from the market and was cut it into averagely 20 mm × 15 mm × 2 mm size pieces. These samples were metallographically polished by belt grinder, followed by different grade emery paper and cloth polishing with diamond paste. Later the substrates were cleaned with soap and then was washed with water and rinsed with acetone. Holes were made on the samples of 2 mm diameter to dip the samples in the electrolyte solution and to supply current by attaching copper wire to the hole.

3.5 Electrolytic bath preparation, deposition setup and process parameters

Parallel plate electrode configuration and surfactant free copper sulfate bath (for the co-deposition of SiO_2 and Y_2O_3) and with the addition of surfactants for ZrO_2 and graphene oxide deposition in the copper matrix was used. The pH of the electrolyte was maintained below the iso-electric point (IEP) of the second phase ultrafine particles used for codeposition so that the particles in the suspension acquire positive charge in the acid solution and get deposited on the cathode metal substrate. The pure copper strip was used as an anode and prepared copper substrates as cathodes for all deposition systems. Before deposition process, the solution was allowed for ultra-sonication (120 watts power and 34 kHz frequency) for 15 min and magnetic stirring for 30 min for homogeneous dispersion of the second phase powders and graphene oxide in the solution. A magnetic stirrer was used for stirring of the bath during entire deposition so that the sedimentation of powder particles in the solution is prevented and they can be homogeneously dispersed during a deposition in the copper matrix. Pure copper deposits were also made by using the same parameters for the comparison of the results. All the deposition developed by DC electrodeposition was controlled by a DC source (APLAB 7103), and a DC pulse-forming unit (FCIPT make) was attached to the DC source as an additional attachment for pulsed deposition. Deposition with a particular second phase material content was carried out with both pulse (at 30% duty cycle) and direct current modes. The variation of process parameters such as current densities (5, 8, 11 and 14 A/dm^2) and pulse frequencies (1, 5 and 10 kHz) were also employed to observe the effects on surface-mechanical and electrical properties of the coatings. The bath compositions and deposition parameters used for different composite coating systems tabulated in the respective chapters.

3.6 Characterizations

3.6.1 Particle size analysis

Particle size from nanometer to several microns was measured by Malvern Zetasizer series using dynamic light scattering. Zeta potential and electrophoretic mobility measurement by the same instrument require electrophoretic light scattering. Malvern Zetasizer can also measure molecular size using static light scattering [103]. In the current dissertation particle size distribution of second phase ceramic oxide particles such as, Al_2O_3, SiO_2, Y_2O_3 and ZrO_2 was measured by Malvern Zetasizer nano series Nano-ZS model. Iso electric point of the same second phase procured oxide powders was obtained by measuring zeta potential at different *pH* values after suspending them in de-ionized water with small amount of mild acid or base as required.

3.6.2 X-ray diffraction analysis

X-ray diffraction (XRD) is an analytical technique generally used for phase identification of a crystalline material and can also provide the information on unit cell dimensions. X-ray diffractometers consist of three basic elements: an x-ray tube, a sample holder, and an x-ray detector. X-rays are generated by heating a filament to produce electrons in a cathode ray tube, by applying a voltage the electrons are accelerated towards a target followed by bombarding the target material with electrons. Characteristic x-ray spectra are produced, when electrons are having sufficient energy dislodge the inner shell electrons of the target material. These characteristic spectra consist of several components, the most common radiations are, K_α and K_β. $K\alpha_1$ and $K\alpha_2$ radiations are a sub part of Kα and Kα1 has a slightly shorter wavelength and double the intensity as $K_{\alpha 2}$. The specific wavelengths are characteristic of the target materials (Cu, Fe, Mo, and Cr). Monochromatic x-rays produced filtering by crystal monochrometers is needed for diffraction. The weighted average of the both $K_{\alpha 1}$ and $K_{\alpha 2}$ is used due to sufficiently close in wavelength and are collimated and directed onto the sample. The intensity of the reflected x-ray is recorded with the rotation of detector and sample. When the geometry of the incident x-rays affects the sample satisfies the

Bragg Equation. Then constructive interference occurs followed by a peak in intensity. This x-ray signal recorded and processed by a detector and converts the signal to count rate verses 2θ value, which is then export to output devices such as a computer monitor or printer [104].

X-ray diffraction characterization of all the procured powders, substrate and deposited samples reported in the current dissertation has been done by multipurpose Rigaku Ultima-IV diffractometer by Bragg-Brentano ($\theta - 2\theta$) X-ray diffraction (XRD) using Cu K_α (α = 0.15406 nm) radiation. X-ray diffractometer geometry is such that, if the sample rotates in the path of the collimated x-ray beam at an angle θ, the x-ray detector collects the diffracted x-rays and rotates at an angle of 2θ. The instrument called goniometer present in XRD is used to maintain the angle and rotate the sample. For all electroplated samples of the current work, data is recorded in 2θ from ~10° to 100°.

3.6.3 SEM and FESEM with EDS characterization

An electron microscope is employed to produce an electronically magnified image of a specimen for finding its morphology. In an electron microscope, a beam of electrons illuminates the specimen and creates its magnified image. Unlike optical microscope, an electron microscope can achieve magnifications up to 1,000,000 times or more because the wavelength is about 100,000 times shorter compared to the visible light radiation; optical microscopes are limited to 2000 time magnification. Vaccume condition is required for scanning electron microscope (SEM) and field emission scanning electron microscope (FESEM) operation and it uses electrons to form an image that's why special preparations were made to the samples. The samples must be completely dry because the water would vaporize in the vacuum. The conductive metals require no preparation before being used. All other samples need to be made conductive by coating the specimen with a thin layer of conductive material and the deposition device to make the non conducting specimens to conducting called as sputter coater. Since the SEM relies on surface process rather than transmission, it is able to image bulk samples up to many centimeters in size and has a great depth of field, and so can produce images that are good representations of the three-dimensional shape of samples. FESEM has unlimited depth of field compared with

conventional scanning electron microscopy (SEM). FESEM produces clear and less electrostatically distorted images with spatial resolution down to 1.5 nanometers and three to six times better quality than conventional scanning electron microscope. Resulting improved spatial resolution and minimized sample charging and damage can be easily done by field-emission electron gun of a scanning electron microscope, which produces very narrower probing beams at both low as well as high electron energy [105, 106].

In the present study, the surface morphology of the samples was analyzed by Scanning electron microscope (SEM) of model JEOL JSM- 6480LV and NOVA nano SEM-450 field emission scanning electron microscope having a maximum accelerating voltage of 30 kV. The elemental analysis of the synthesized coating specimens was performed using an energy dispersive spectrometer (EDS) accessory of Oxford data-reference system.

3.6.4 Transmission electron microscopy

Transmission electron microscope (TEM) is an instrument, which uses electrons instead of light but operates on the same fundamental principles as the light microscope. The main difference between A light microscope and electron microscope is electron microscope uses electron as a light source with much lower wavelengths makes it possible to get a resolution thousand times better than the optical microscope, which is limited by the wavelength of light. Objects can be seen to the order of a few angstrom (10^{-10} m) by TEM. For example, small details in the cell or different materials down to near atomic levels can be easly studied by transmission electron micrographs. The possibility of use in high magnifications purpose has made the TEM a valuable tool in materials, medical, and biological research. Transmission electron microscope emits the electrons that travel through a vacuum in the column of the microscope. Electromagnetic lenses are used in TEM to focus the electrons into a very thin beam instead of glass lenses focusing the light of the optical microscope. Then, the electron beam travels through the specimen. Some of the electrons are scattered and disappear from the beam depending on the density of the materials. The unscattered electrons knocked a fluorescent screen at the lower part of the microscope, which produces a "shadow image" of the sample with its different parts revealed in varied darkness according to the density of the

specimen. Then, the image can be analyzed directly by the operator or photographed with a camera attached to the corresponding TEM [107, 108]. All second phase raw powders (Al_2O_3, SiO_2, Y_2O_3, and ZrO_2) are characterized by transmission electron microscopy (model:JEOL-2100) for particle size analysis purpose.

3.6.5 Surface profilometer

Stylus profiler is widely accepted for providing repeatable and accurate surface roughness and thin film thickness measurements on varied surfaces. It also provides traditional 2D surface roughness characterization and step height measurements along with advanced 3D mapping and film stress analysis [109]. All electrophoretic coating samples were characterized for measurement of surface roughness by a 2D stylus in a Veeco Dektak-150 stylus profilometer. All the roughness data reported in the current dissertation are average of minimum 3 data measured at different locations on the coating surfaces with 800 micron scan distance.

3.6.6 Microhardness measurement

Hardness is not a fundamental physical property but a characteristic of material. It is generally defined as the resistance to indentation and determined by measuring the permanent depth of the indentation. More simply, when using a fixed load and a given indenter, the smaller the indentation, the harder the material. The Vickers microhardness test method is commonly used for small parts, thin sections, coatings or case depth work. The Vickers microhardness method normally follows an optical measurement system. The microhardness test procedure specifies a range of light loads using a diamond indenter to make an indentation on the specimen which is measured and converted to vickers hardness (HV) value.Typically in microhardness case loads are lower compared to other hardness measurements, ranging from a few grams to one or several kilograms.Vickers microhardness test is very much useful for a variety of applications such as testing very thin materials like foils, measuring part of the surface, small parts or small areas, measuring hardness of individual microstructures, or measuring the depth of case hardening by sectioning a part and making a series of indentations to describe a profile of the change in hardness due to smaller test indentation. It is necessary to prepare the sample so that it can easily fit into the hardness tester and ensure

the sample can be held perpendicular to the indenter. The indentation of hardness tester should be clearly visible so that minimal error occour [110, 111].

Microhardness measurements of all the developed coatings were carried out on the coating surface using a Vickers indenter with a 10g load in a LECO microhardness tester with diamond indenter having a load range of minimum 1g to maximum 2kg. Each hardness value reported in this dissertation is an average of minimum 5 measurements in the same sample at identical locations.

3.6.7 Wear testing

Wear takes place either by a mechanical process or by a chemical process or by a combination of both and is accelerated by thermal processes (frictional heating). In different literatures, wear is classified into some categories based on the mechanism and severity of material removal. However, wear can be broadly classified mainly into 4 types

(a) Adhesive wear
(b) Abrasive wear
(c) Corrosive wear
(d) Fatigue wear

Generally adhesive wear takes place when two nominally flat solid surfaces are in sliding contact. At the interface asperities, contact and bonding occur due to adhesion. These contacts get sheared during sliding, resulting in detachment of a fragment from one surface and its attachment to the other surface or formation of loose wear particles. Some get fractured by a fatigue process during repeated loading and unloading process resulting in the formation of loose wear particles. However, abrasive wear includes two types of wear situation known as two body abrasion and three body abrasions. In both the cases, a soft surface is ploughed by a relatively hard material. In two body abrasion, a hard, rough surface slides against a relatively soft mating surface. In three body abrasion, rough, hard particles trapped between the two sliding surfaces cause one or both of them undergo abrasive wear. Corrosive wear takes place when sliding occurs in a corrosive environment. Corrosive wear in the air is called oxidative wear as the most dominant corrosive medium in the air is oxygen. In the case of fatigue wear

surface and sub, surface fatigue is observed during repeated sliding and rolling. Sometimes these are termed as microscopic and macroscopic fatigue wears [112,113].

Wear study of all developed coating specimens was carried out by a ball-on-plate-type wear-testing instrument (DUCOM TR-208-M1) having a hardened steel ball (SAE 52100) indenter of 4-mm diameter (Fig.3.2). All the specimens were tested in ambient temperature with 5N load and 10 rpm sliding speed. Sliding distance (in cm) or time in second versus wear depth (in micron) of all specimens was plotted and compared for the different samples.

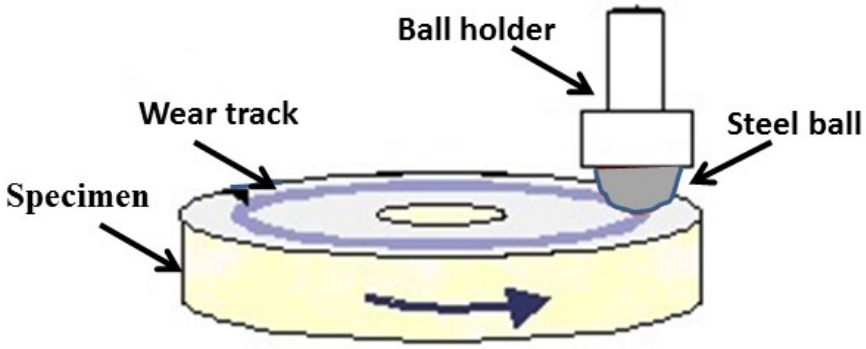

Fig.3.2: Schematic representation ball on plate wear.

3.6.8 Electrical conductivity

Electrical conductivity is an intrinsic property that quantifies how strongly in a given material, electric current flows. Electrical conductivity is the reciprocal of electrical resistivity and measures a material's ability to conduct an electric current. A low electrical conductivity indicates a material that strongly opposes the flow of electric current. Electrical conductivity is commonly represented by the letter sigma (σ).The SI unit of electrical conductivity is the S/m (Siemens per meter) [114-116] although another unit like Siemens/centimeter (S/cm) is also in use. For an example, if a solid cube of material (1m×1m×1m) has sheet contacts on two opposite faces, and the resistance between these contacts is 1 Ω, then the resistivity of the material is 1 Ω·m, and electrical conductivity of that material is 1 S/m.

The electrical conductivity of the coating specimens was measured at ambient temperature by four-probe method. The schematic representation of a common four-probe is shown in Fig.3.3. Linearly situated four contact points having 2-mm distance between neighboring

points on the coating surface were used for measuring electrical conductivity. Within the four points, outer two points were used for passing a known current, and the central two points were utilized for voltage measurement. For this purpose, a high-precision Keithley 6220 current source combined with 2182A nano-voltmeter was used. This conductivity test was repeated on randomly chosen locations on developed coating surfaces. The valued reported in the current thesis are the average value of minimum three measurements.

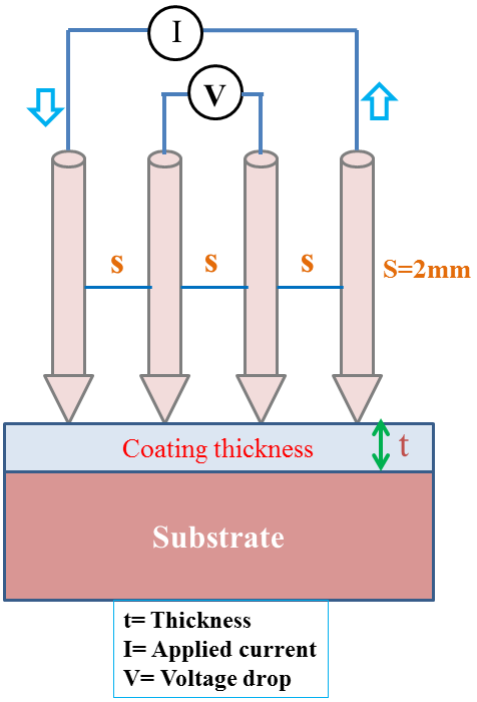

Fig.3.3: Schematic representation four probe technique.

3.6.9 Atomic force microscope (AFM)

The scanning probe microscope (SPM), which operates by measuring the force between a probe and the sample is called atomic force microscope (AFM). Normally, the AFM probe is a sharp tip of 3-6 um long pyramid shape with end radius ranges from 15-40 nm. Due to the convolution the horizontal resolution is low (~30nm), but the vertical resolution can be ranges up to 0.1nm. To obtain the image resolution, atomic force microscopes generally measures the lateral and vertical deflection of the cantilever by using the optical control. The operation of optical lever can be made by reflection of a laser beam off the cantilever. A position-sensitive photo-detector was strike by the reflected laser beam. The changes between the parts of

photodetector signals indicate the position of the laser spot on the detector and consequently the angular deflections of the cantilever [117].

Surface topography and roughness of some selected coating specimens were analyzed by Veeco di Innova atomic force microscope (AFM) with 20×20 square micron area at contact mode.

3.6.10 Raman spectroscopy

Raman spectroscopy tells the information about molecular vibrations, which is used for sample identification and quantification. The technique involves a monochromatic laser source on a sample and detecting the scattered light. The majority of the scattered light with frequency same as the excitation source is known as elastic scattering. Due to the interactions between the incident, electromagnetic waves, a small amount of the scattered light, i.e., 5-10% of the incident light intensity is shifted in energy from the laser frequency and the vibrational energy levels of the molecules in the sample [118]. Ramana spectroscopy plotting usually done between intensity as x-axis verses ramana shifts or in wavenumber(cm^{-1}) as the y-axis. Ramana specroscopy of graphene oxide, reduced graphene oxide and Cu-GO/RGO specimens are analyzed by Acton Spectra Pro SP-2500 instrument. All the spectra recorded in the range of 100 and 3000 cm^{-1}.

3.6.11 X-ray photoelectron spectroscopy (XPS)

X-ray Photoelectron Spectroscopy (XPS) is one of the most widely used surface analysis technique because it can provide valuable quantitative and chemical state information from the surface of the material and also applicable to a broad range of materials. It measures the elemental composition in the range of parts per thousand, chemical state, electronic state and an empirical formula of the elements that present in a material. XPS spectra produced by irradiating the material with x-ray beam analyze the kinetic energy and number of electrons escape from the suraface of the materials upto 10nm. High vacuum (P ~ 10−8 millibar) or ultra-high vacuum (UHV; P < 10−9 millibar) conditions are required for XPS measurements because electron counting detectors in XPS instruments are typically one meter long away from the material irradiated with X-rays. This long path length for detection requires such low

pressures. It analyzes the surface chemistry of material in its as-received state, or after some treatment [119]. XPS spectrum is usually a plot of the number of electrons detected (sometimes per unit time) or intensity in the arbitary unit (Y-axis) versus the binding energy of the electrons detected in X-axis. A unique set of XPS peaks at characteristic binding energy values produced by particular elements identifies each element that present in or on the surface of the material. These characteristic XPS peaks corresponding to the different electronic configuration can be written as 1s, 2s, 2p, 3s, *etc*. Each characteristic XPS spectra containing a number of detected electrons are related to the amount of element present in the XPS sampling volume. Each raw XPS spectra must correct by dividing its signal intensity (number of electrons detected) by a "relative sensitivity factor" (RSF) to generate atomic percentage value, and normalized over all of the detected elements. 5000 Versa Prob II (FEI Inc.) instrument was used to analyze x-ray photo electron specroscopy (XPS) of graphene oxide, reduced graphene oxide and Cu-GO/RGO specimens. All the spectra were recorded upto 1000 eV.

3.6.12 Oxidation study

Thermal oxidation behavior of as deposited Cu coating at 540 ^{o}C (approximately 60 percent melting temperature of pure copper in Kelvin) and Cu–30g/l Y_2O_3 composite coating at 540 ^{o}C and 675 ^{o}C (approximately 60 and 70 percent melting temperature of pure copper in Kelvin) for 20 hour was studied. The above said specimens were heated in an air furnace and the specimens were weighed before oxidation and during the process at various time intervals.

Chapter 4

Effects of current densities on surface-mechanical properties of Cu-Al_2O_3 composite coating

4.1 Introduction

In the present study, the effect of current density on the microstructure, hardness and wear resistance of DC electrodeposited Cu-Al_2O_3 composite coatings with different concentrations of alumina have been investigated. The purpose of this study is to improve the surface-mechanical properties of composite coating in comparison to pure copper without much deterioration of original electrical conductivity. The deposition parameters and bath composition details have been presented in table 4.1.

Table: 4.1 Plating bath composition and deposition parameters

Electrolyte (Acidic copper sulfate bath)	Copper Sulfate ($CuSO_4.5H_2O$): 200 g/l
	Sulfuric acid (H_2SO_4): 50 g/l
pH	2.17(±0.02)
Current density	5, 8, 11 and 14 A/dm^2
Temperature	Room temperature
Plating time	20 minutes
Dispersion	Al_2O_3: 0, 10 and 30 g/l

4.2 Isoelectric point measurement of Al_2O_3

To determine the iso-electric point of the as-received Al_2O_3 particles, zeta potentials of the same were measured at different pH values. Fig. 4.1 shows that the isoelectric point of Al_2O_3 powder was around 5.26 in pH. Subsequently, for co-deposition of Cu-Al_2O_3, the pH was

maintained at 2.17 (±0.02), so that the particles were positively charged in the suspension as well as the solution was acidic in nature.

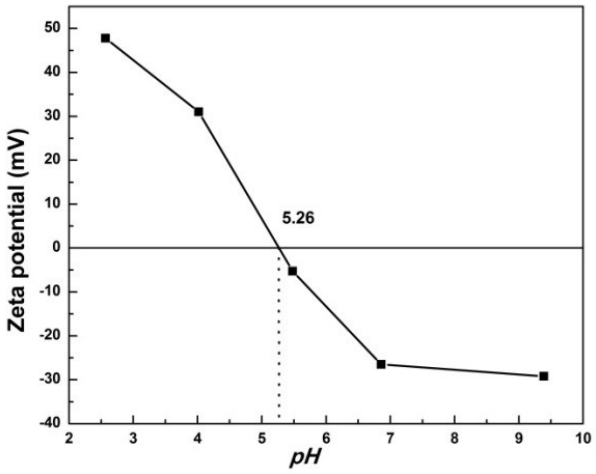

Fig. 4.1: *pH* Vs Zeta potential for isoelectric point determination of Al_2O_3 powder.

4.3 Al_2O_3 powder particle size analysis

Fig. 4.2(a) shows the particle size distribution of Al_2O_3 powders obtained from particle size analysis. In the figure, no sharp peak was observed; rather one broad peak was found centering approximately at 250 nm.

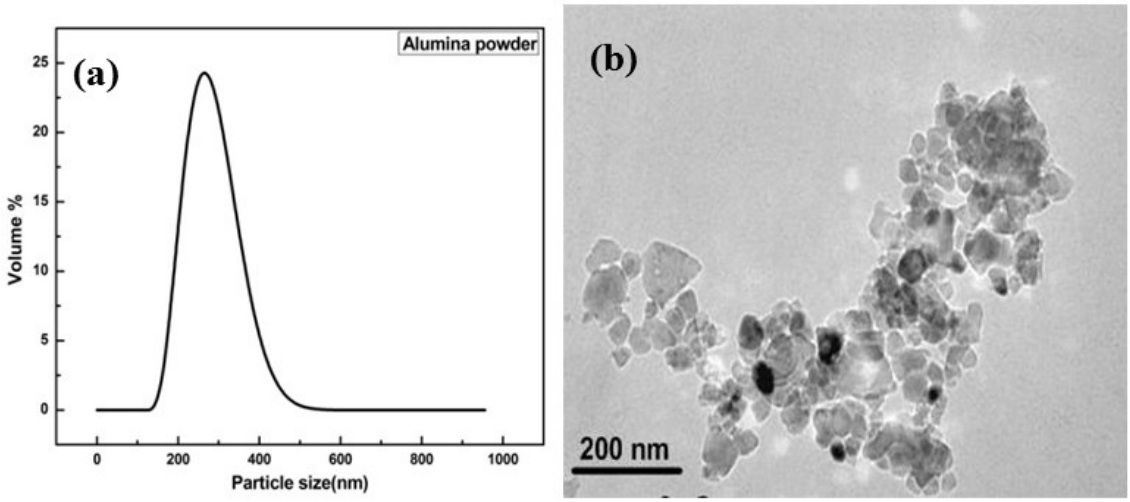

Fig. 4.2: (a) Particle size distribution and (b) TEM micrograph of Al_2O_3 powder.

Thus, normal distribution of particle size with a size range from 190 to 342 nm was recorded. However, higher volume percentage of particles was having sizes between 220 to 295 nm, and the mean size was at 287 nm. Transmission electron micrograph of procured Al_2O_3 powder is shown in Fig. 4.2(b). From the figure, it can be seen that particles are lower in size (20 to 70 nm) in comparison to zeta potential measurement. Moreover, particle size range obtained by TEM study is similar as claimed by the powder manufacturer. The reason behind the larger particle size reported by zeta potential measurement may be due to the agglomeration of powder particles in aqueous solution during the measurement.

4.4 XRD analysis

Fig. 4.3 shows the XRD profile of the received Al_2O_3 powder, which represents rhombohedral crystal structure. Fig. 4.4(a) and (b) show the XRD patterns of Cu-10 g/l Al_2O_3 and Cu-30 g/l Al_2O_3 composite coatings prepared with different current densities. From Fig. 4.4(a) and (b), it can be observed that all planes belong to pure Cu. Fig. 4.4(c) shows the enlarged XRD plot of Cu-30 g/l Al_2O_3 coating deposited with 11 A/dm^2 current density, and peaks of Al_2O_3 are visible in that. Such small intensity of these peaks is due to very low amount of deposited Al_2O_3 in the coating. In both Fig. 4.4(a) and (b), systematic change in relative intensity of a particular diffraction plane of Cu was observed. Effect of current density and Al_2O_3 content on such texturing could not be ruled out. To quantify this and as a basic study of crystallographic texture, RTC ($RTC_{(hkl)}$) of 4 Cu planes namely (111), (200), (220), and (311) of all coated samples were calculated, and the results are given in Table 4.2. The RTC [120] is defined as follows:

$$RTC_{(hkl)} = \frac{I_{(hkl)} / I_{0(hkl)}}{\Sigma I_{(hkl)} / I_{0(hkl)}} \times 100\% \qquad (4.1)$$

Where $I_{(hkl)}$ is the intensity obtained from textured sample and $I_{0(hkl)}$ is the intensity of the standard randomly oriented sample i.e., from JCPDS data.

Table.4.2: Relative Texture Coefficient ($RTC_{(hkl)}$) of different Cu-Al_2O_3 coatings and pure copper coating

Sample Type	Sample Details	$RTC_{(hkl)}$%				Crystallite size (nm)
		(111)	(200)	(220)	(311)	
Cu deposition	5 A/dm^2	20	10	40	30	41
	8 A/dm^2	16	9	45	30	56
	11 A/dm^2	16	9	52	23	53
	14 A/dm^2	10	8	64	18	64
Cu-Al_2O_3 coating	10 g/l, 5 A/dm^2	26	22	29	23	41
	10 g/l, 8 A/dm^2	18	21	36	25	45
	10 g/l, 11 A/dm^2	09	16	48	27	50
	10 g/l, 14 A/dm^2	07	12	57	24	62
	30 g/l, 5 A/dm^2	20	19	37	23	53
	30 g/l, 8 A/dm^2	14	19	41	26	45
	30 g/l, 11 A/dm^2	14	16	43	17	64
	30 g/l, 14 A/dm^2	16	11	49	24	64

From Table 4.2, it is clear that RTC of (220) was lower in case of composite coatings in comparison to pure copper coatings. (220) preferred orientation present in pure copper coating was changed to a mix ((220)+(311)) orientation in composite coatings.

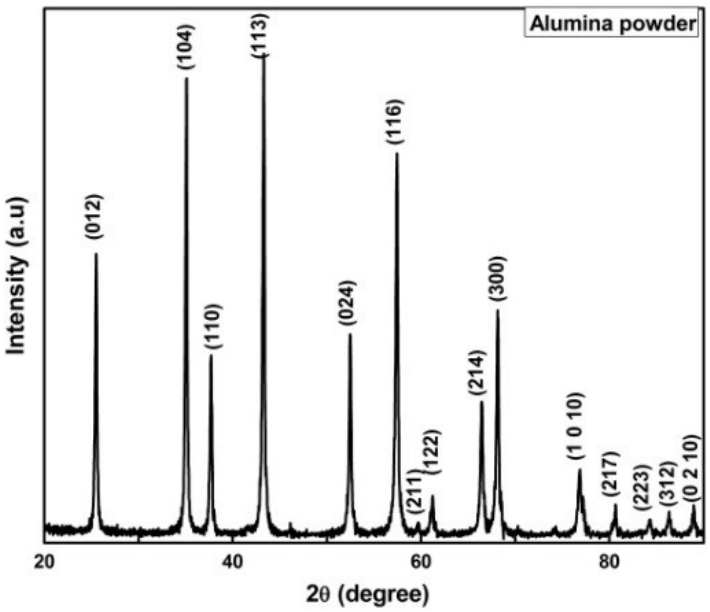

Fig. 4.3: XRD peaks of procured Al_2O_3 powder.

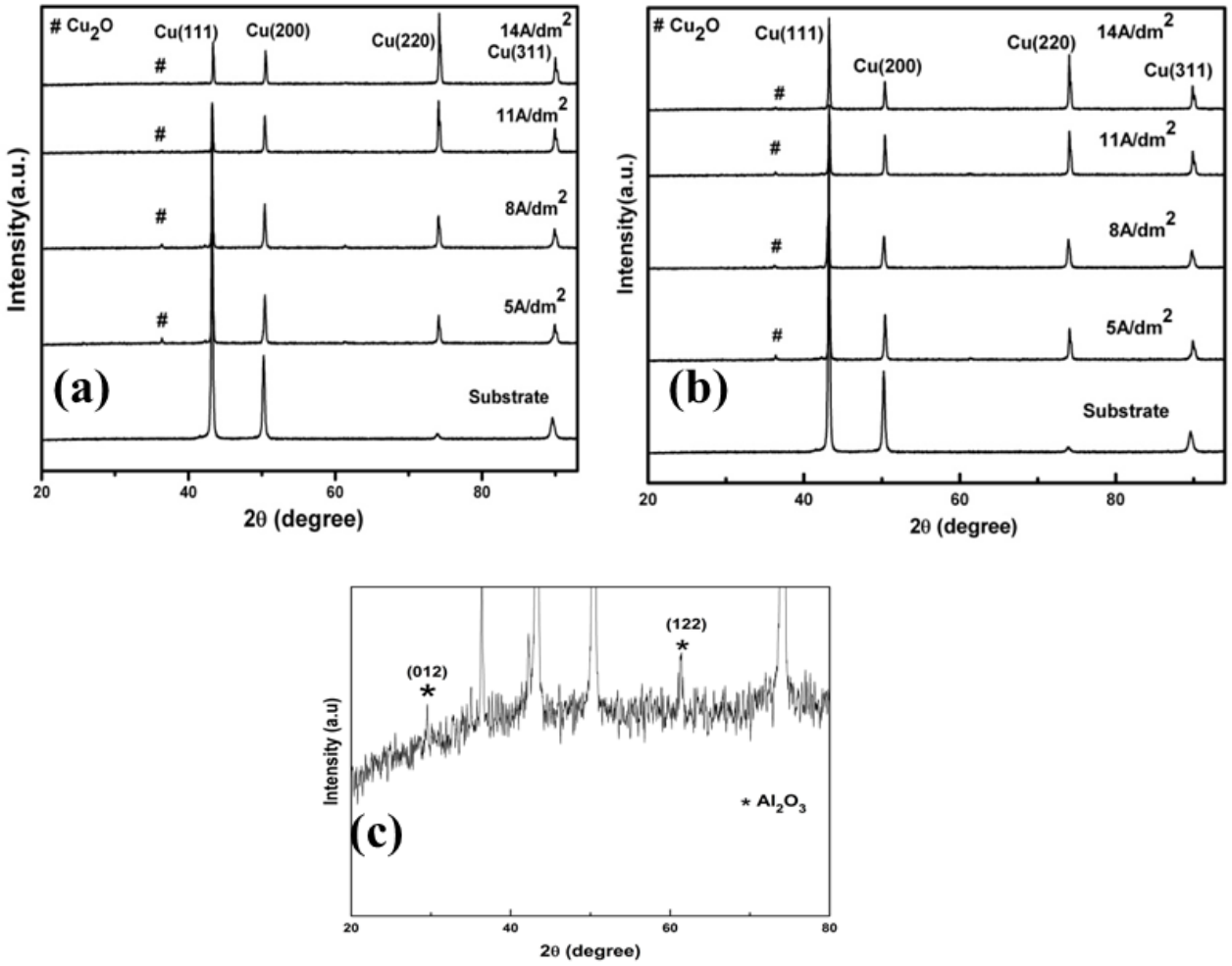

Fig. 4.4: XRD pattern of (a) Cu-10 g/l Al_2O_3 and (b) Cu-30 g/l Al_2O_3 coatings; (c) Enlarged XRD pattern of Cu-30 g/l Al_2O_3 coating deposited at 11A/dm^2.

Several theories about the preferred orientations in the electrodeposited metals, including ‘‘internal strain theory,’’ ‘‘the theories of geometrical selection,’’ and ‘‘two-dimensional nuclei theory’’ have been discussed in various literature [17]. In general, it can be concluded that the observed texture may be due to the influence of current density, embedded second-phase ceramic particles, and copper oxide formation in the composite coatings. Moreover, during electro-co-deposition, the formation of particular orientation may be due to interfacial energy-driven phenomena and subsequent alteration of interfacial energy in the presence of oxide particles.

The crystallite size of the Cu matrix of all the coated samples was calculated by using Scherrer formula [121] taking (111) as the reference plane, which is given by Eq. [4.2]

$$D = \frac{0.94\lambda}{\beta \cos\theta} \qquad (4.2)$$

Where D is the crystallite size, b is the full width at half maximum (FWHM) of the diffraction peak, k is the wavelength of the incidental X-ray (1.54 A˚), and h is the diffraction angle. All the calculated values are listed in Table II. It was observed that crystallite sizes of all developed coatings are within narrow range and at 10 g/ L addition of Al_2O_3 the values are little smaller than 30 g/l. It was also observed that the highest value was 64 nm which tells that the deposited coating was really fine in nature.

4.5 Microstructural studies

Fig. 4.5(a) through (d) show the SEM surface morphologies of Cu-10 g/l Al_2O_3 composite coatings developed at current densities of 5, 8, 11, and 14 A/dm^2, respectively. From the result, it can be observed that morphologies of the composite coatings changed with change in current density during the deposition. Surface of the composite coatings with current density 5 and 8 A/dm^2 looks porous, loosely compacted and rough (Fig. 4.5(a) and (b)) compared to the same deposited with higher current densities, such as 11 and 14 A/dm^2 (Fig. 4.5(c) and (d)). Moreover, in case of 8 A/dm^2 current density, the structure looks coarser due to its well-defined boundary evident in the microstructure. Otherwise, surface of the coating becomes denser and uniform as current density increases, as observed in other micrographs (Fig. 4.5(c) and (d)). Denser coating was mainly due to high nucleation rate which was created by higher current density. In case of 14 A/dm^2, part of the surface was found to have pyramidal (smaller grains are agglomerated and formed larger pyramid like) structure. As copper is a low over voltage material, at high current density (beyond certain limiting value), a larger number of smaller grains may have initiated resulting in finer structure.

Scanning electron micrographs of Fig. 4.6 show surface morphology of Cu-30 g/l Al_2O_3 composite coatings as a function of cathodic current density. It can be observed that with

increase in current density in general the structure becomes finer, but the effect is not so prominent as observed in Cu-10 g/l Al_2O_3 (Fig. 4.5). Moreover, like 10 g/l sample, here also, the morphology is coarser at 8 A/dm^2 current density, which may be due to higher growth rate of the deposit. In other words, at different current densities, nucleation and growth play competitive role to different extents, and at intermediate value of 8 A/dm^2, the growth is more pronounced. Analogy can be taken from simple case of nucleation and growth during solidification of polycrystalline materials where growth is best at intermediate super cooling value. In specific areas of microstructure of Fig. 4.6, the presence of void/pore and crack was also observed.

When Fig. 4.5 and 4.6 are compared, considering the magnification of the micrographs, it can be concluded that in case of 30 g/l samples, the structure is coarser. During co-deposition, Al_2O_3 may act adversely in nucleation by increasing the surface energy of Cu deposition. This may lead to less nucleation and more growth of Cu crystal, resulting in coarser structure in 30 g/l samples. This was also evident from first principle-based calculations that the formation of Cu-Cu cluster is more likely compared to Cu-Al_2O_3 cluster as the calculated formation energies (ΔE) for those are equal to -64,388 and -64,571 Cal/mol, respectively. Thus, nucleation was easier in copper compared to Cu-Al_2O_3 system. This in turn reduces the nucleation possibility of Cu in the presence of Al_2O_3 leading to coarse Cu structure. Such result has been reported earlier by Allahkaram et al. [122] but, interestingly, similar trend was observed in case of pulsed deposition.

To ascertain the coating thickness, cross-sectional micrograph of the coating was captured under SEM as shown in Fig. 4.7(a). The coating could not be easily distinguished from the substrate unless pulled up with excessive force during polishing as shown in left side of the figure, which was done deliberately. This figure represents coating thickness of Cu-30 g/l Al_2O_3 sample deposited with 11 A/dm^2. All such thickness data are compiled in Fig. 4.7(b), and from the plot, the trend can be observed that with increasing Al_2O_3 content, the thickness decreases, and with increase in current density, the thickness increases. Being a ceramic material, Al_2O_3 creates adherence and nucleation problem as mentioned in earlier section. This results in effective addition of deposited material on the substrate and thus with increasing amount of ceramic phase moving toward the substrate, the thickness increase is

hindered. With higher current density, the thickness increases due to the reason that, for a particular time scale of deposition, higher current density means higher number of ions being added in unit time.

It can also be observed that at 14 A/dm^2 current density, the thickness values are comparable. After a certain current density, the transportation/deposition of ceramic particle got sluggish as ceramic particle to Cu ion ratio in the bath is constant and the value is very small. At this condition, the charge is mainly carried by the Cu ion and actual deposition of Cu was not affected adversely by Al_2O_3 particle as was prevalent at lower current densities.

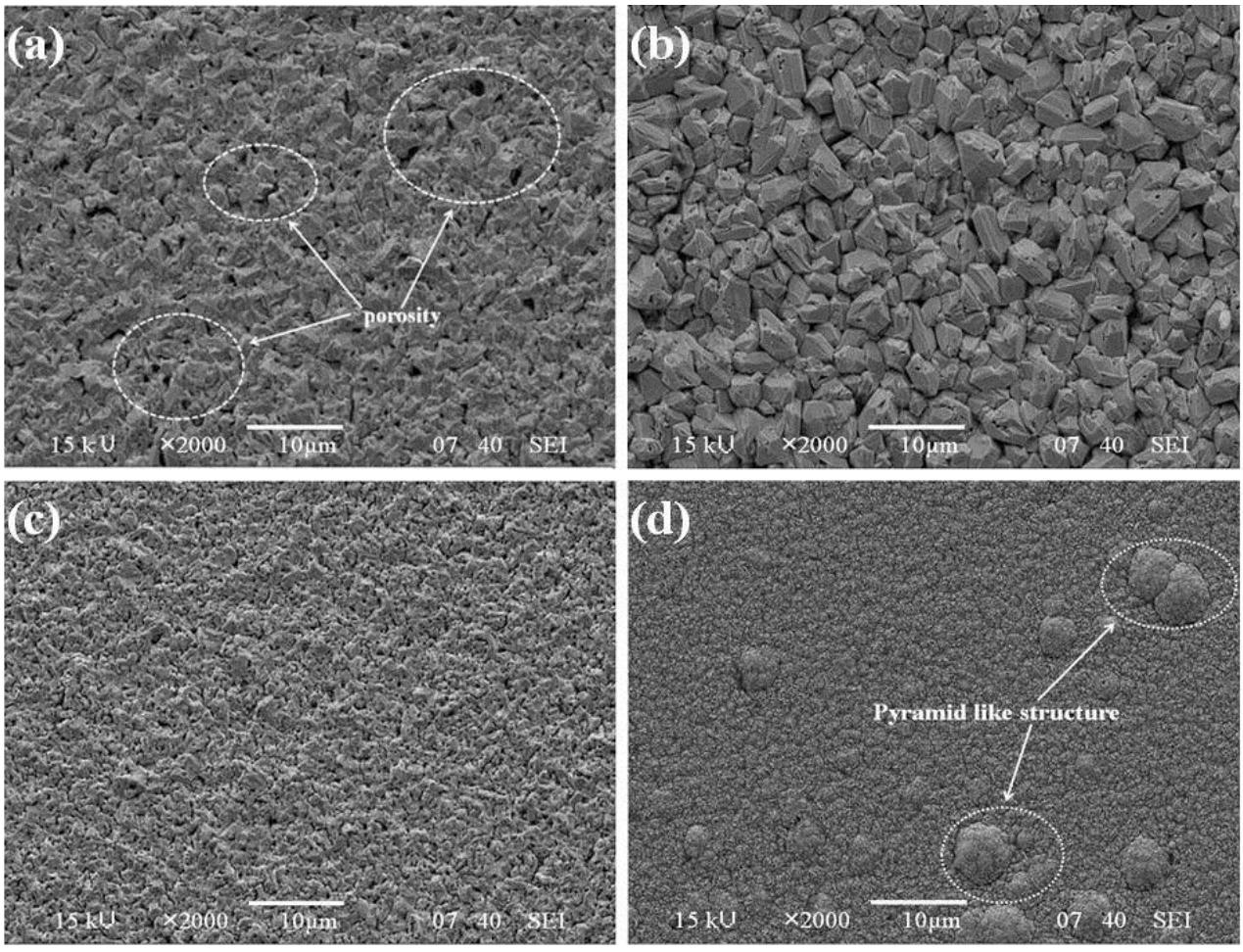

Fig. 4.5: Surface morphology of electrodeposited Cu-10g/l Al_2O_3 coatings at (a) 5, (b) 8, (c) 11 and (d) 14A/dm^2 respectively.

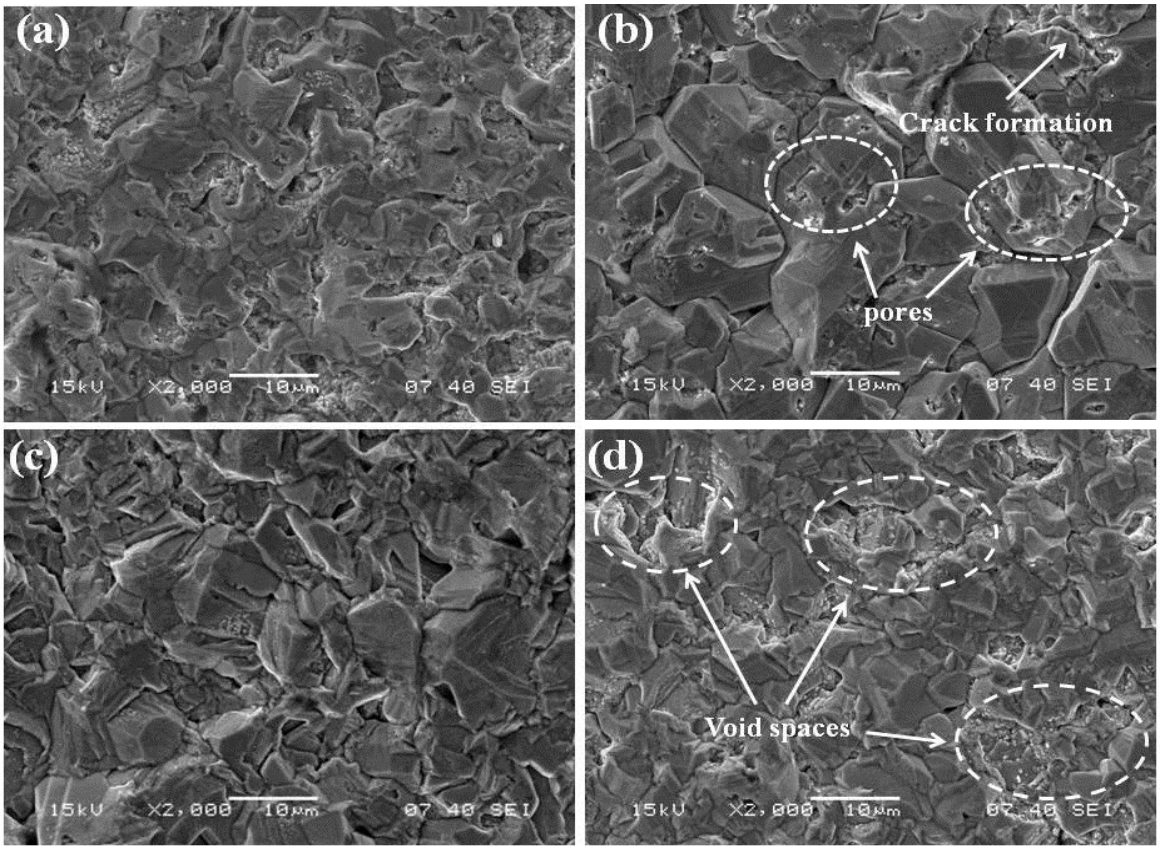

Fig. 4.6: Surface morphology of electrodeposited Cu-30g/l Al_2O_3 coatings at (a) 5, (b) 8, (c) 11 and (d) 14A/dm^2 respectively.

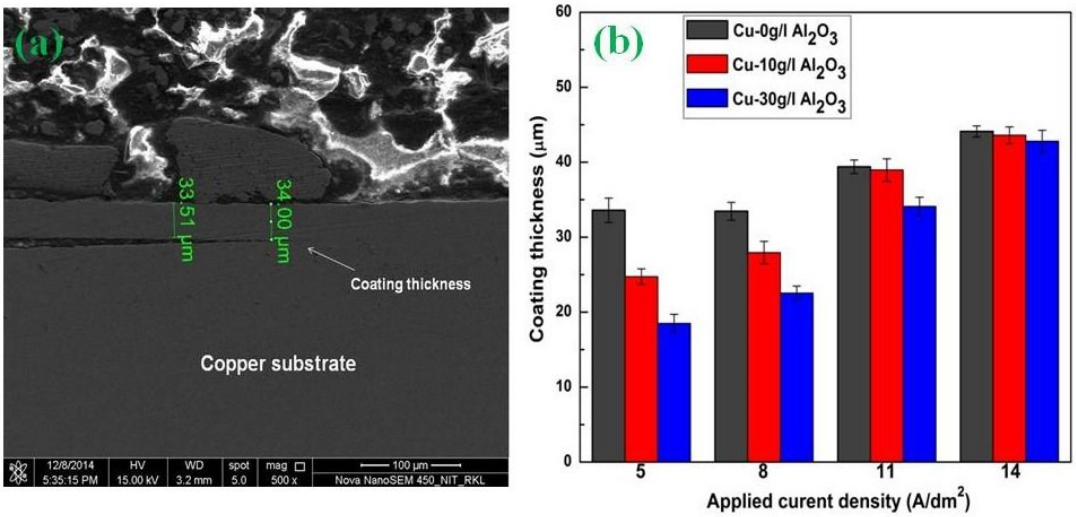

Fig. 4.7: Coating thickness of (a) Cu-30g/l Al_2O_3 with 11A/dm^2 and (b) all deposited samples with variation of current density.

4.6 EDS analysis

Fig. 4.8(a) shows EDS analysis of Cu-30 g/l Al_2O_3 coating prepared at 11 A/dm^2, which shows the presence of Al (4.69 wt%) along with oxygen (5.96 wt%) and copper (89.35 wt%). The relationship between the weight percent of codeposited second-phase particle content in the composite coatings and applied current density during the plating is presented in Fig. 4.8(b). From the figure, it can be concluded that the particle content in the composite coating depends on applied current density as well as the amount of suspended ultrafine particles in the electrolytic solution. The weight percentage of Al (as present in Al_2O_3 particles) in the deposit was increased with increasing amount of Al_2O_3 ultrafine particle in the bath at all current densities. This was due to higher amount of Al_2O_3 supply to the cathode region as the amount of Al_2O_3 increases in the plating bath. The variation of co-deposited Al_2O_3 content in the coating is not linearly proportional with the amount of particles charged to the electrolyte. The weight percentage of Al_2O_3 particles in the deposit increases with increasing current density and reaches its maximum value at 11 A/dm^2. This limiting content may correspond to the steady-state equilibrium, where the number of codeposition particles equals the number of second-phase particles approaching the cathode surface. At 14 A/dm^2, incorporation of second-phase particles is minimum, despite its higher loading level compared to other current density. Beyond the optimum value (11 A/dm^2) of current density, Al_2O_3 particles might be agglomerated in the bath and/or not adhered to the substrate after giving up the charge at the surface and consequently, a decreasing trend of co-deposition of Al_2O_3 particles was observed. This was also in agreement with previously reported result [123]. In case of possible agglomeration, the charge is mainly carried by the Cu ion; i.e., electrodeposition was prevalent over electrophoretic deposition. Thus, from the present study, it was observed that successful electrophoretic deposition of Al_2O_3 in the presence of Cu ion is best at intermediate range of current density due to availability of more non-agglomerated particle near the cathode and adherence to that at that condition.

Fig. 4.9 (a) displays the Cu-30 g/l Al_2O_3 composite coating deposited with 11 A/dm^2 current density and Fig. 4.9(b) through (d) show the corresponding X-ray mapping of Cu, Al, and O, respectively. From these figures, it can be clearly observed that Al and O are uniformly

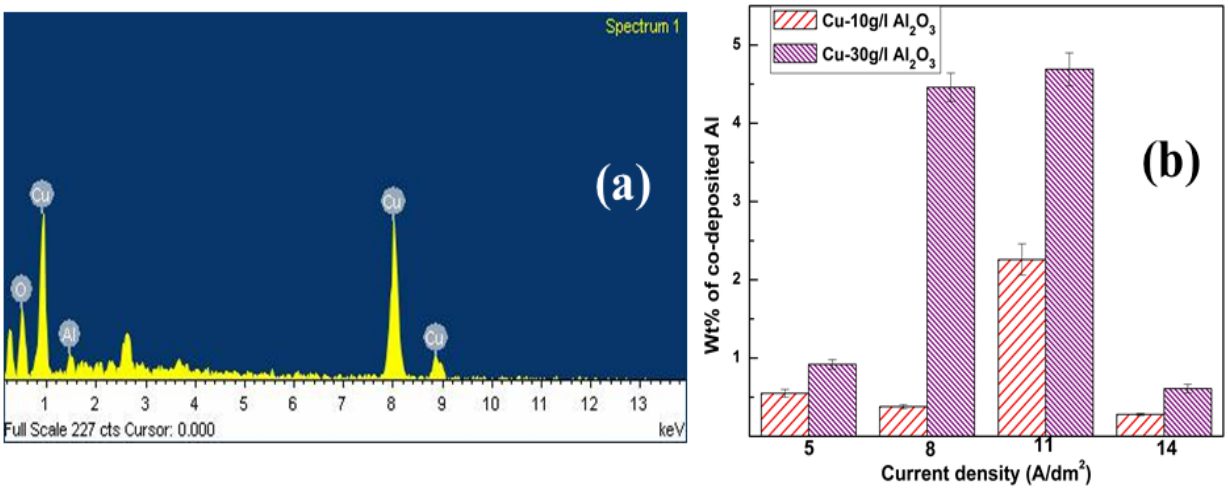

Fig. 4.8: (a) EDS of Cu-30g/l Al_2O_3 deposited at 11 A/dm^2 and (b) Co-deposited wt% of Al_2O_3 (in terms of Al) in Cu-Al_2O_3 composite coatings with 10 and 30 g/l bath and varying current density.

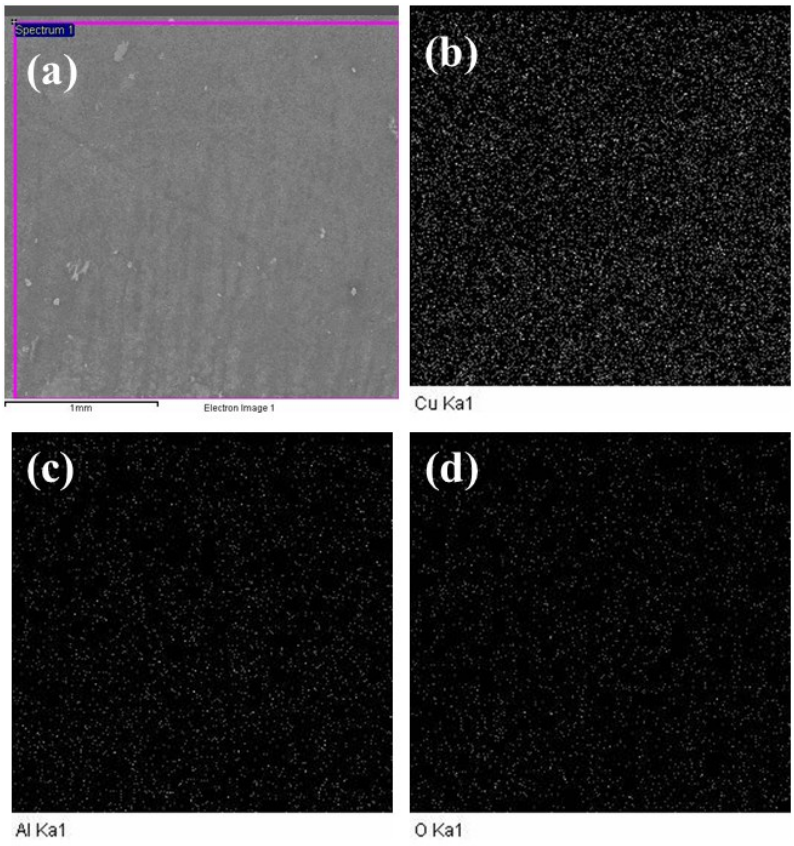

Fig. 4.9: (a) Cu-30 g/l Al_2O_3 composite coating deposited with 11 A/dm^2 current density; (b through d) corresponding X-ray mapping of Cu, Al, and O, respectively.

distributed on the coating which in turn reveals the homogeneity of Al_2O_3 throughout the coating. From the distribution and the distance between two consecutive Al spots in the mapping figure, it can be told that the particles are both inside grain and at grain boundary. As the process is co-deposition in nature, electrodeposition of Cu and electrophoretic deposition of the particle goes on simultaneously leading to deposition of Al_2O_3 both inside grain and at grain boundary of Cu.

4.7 Microhardness study

Microhardness of the composite coatings and pure copper coatings were measured by applying 10 gf load. Fig. 4.10 shows the effect of current density and ultrafine ceramic second-phase particle in bath solution on microhardness of Cu-Al_2O_3 composite coating surface. The hardness values obtained for the composite coatings (Cu-Al_2O_3) are higher than pure copper coating at all current densities. There are three main reasons which affect the hardness of the composite coating [124,125]: dispersion strengthening, grain refinement, and texturing of the matrix to some extent. Dispersion strengthening mechanism is associated with the incorporation of second-phase ultrafine particles (<1 lm) with a volume fraction lower than 15 percent. In this case, the matrix carries the load, and the fine particles hinder the dislocation motion. The second one (grain refinement) is generally related to the nucleation of small grains resulting in structural refinement. In case of grain refinement, the presence of smaller grains obstructs dislocation motion resulting in an increase in microhardness. Moreover, there may be an effect from crystallographic texture of matrix which is common in deposition kind of coating [126]. Trend observed in Fig. 4.10 is the effect of all these mechanisms in a complex way. In general, hardness increases with the increase of Al_2O_3 content, and the presence of Al_2O_3 in the coating can increase the hardness/strength of the same to high value and similar effect was observed in process like laser surface engineering also [127]. Grain size has a complex trend as discussed earlier, resulting in negative contribution of grain size effect in the hardness at higher Al_2O_3 concentration; i.e., structure is coarser in 30 g/l condition compared to 10 g/l sample. Thus, dispersion strengthening has mainly contributed toward the higher hardness value of 30 g/l samples.

When the current density was increased from 5 to 11 A/dm^2, the hardness values were also increased and it can be attributed mainly toward fine structure due to higher rate of nucleation. But beyond 11 A/dm^2 current density, a little decrease in hardness values was observed due to lower percentage of co-deposited ultrafine particle on the coating surface, which can be confirmed from EDS result reported in Fig. 4.8b.

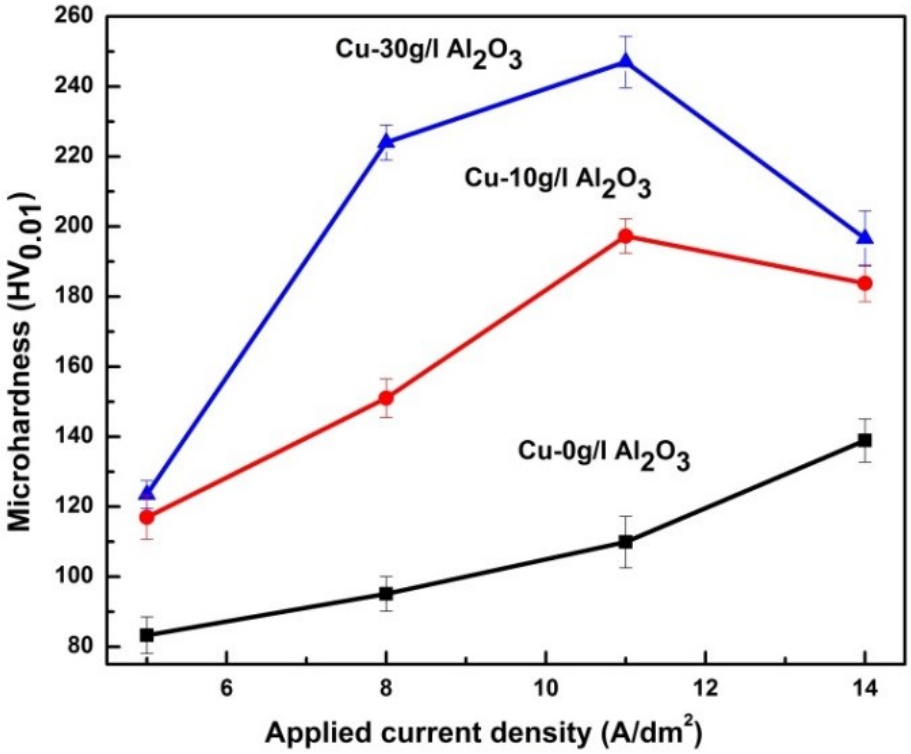

Fig. 4.10: Microhardness of Cu-Al_2O_3 coating samples at different current densities of 5, 8, 11 and 14 A/dm^2.

To study the effect of matrix texturing, when the hardness value is analyzed with Table 4.1, it was observed that hardness of pure copper deposition was different from codeposited samples mainly due to change of prominent (220) orientation in pure Cu to more random orientations in co-depositions. Planes having higher angle with (100) plane produces more strain, thus more hardness [128]. In the present study, due to conversion of (220) to ((111)+(220)+(311)) mixed orientation, the composite coatings showed higher hardness with little negative effect from (200) orientation. It can also be observed that in case of co-deposited samples, with

increase in current density, there is a decrease in RTC value of (200) plane and increase in (220). This has resulted in increase in hardness with current density in general.

Due to these combined effects, in the present range of study, with 30 g/l Al_2O_3 concentration and 11 A/dm^2 current density, the highest hardness value was observed (HV0.01 247) which was 3 times higher than that of pure Cu deposition (HV0.01 81). Moreover, the hardness value investigated here shows betterment over earlier reported work on the same system [122].

To analyze the variation of mechanical properties across the cross section, microhardness testing on the cross section, from surface to the substrate was carried out and it was observed that the hardness values are comparable at different depths of the coating. The values were same as that was mentioned in Fig. 4.10. But, when the hardness was measured on the substrate after crossing the interface, it records different values; i.e., hardness of the substrate. Thus, in the present study for a particular coating, across the depth, the mechanical property was found similar as there was no composition variation across the depth of the coating.

4.8 Adhesion and wear study

As a part of surface-mechanical testing, apart from microhardness test, adhesion tests and wear analysis were also carried out as coating performance depends on the interfacial strength of the coating. Peel tests carried out on all the coatings indicate no failure or peel off at the coating-substrate interface. This indicates good adhesion of the synthesized coatings.

Wear test on the surfaces of the pure Cu and composite coatings was carried out by ball-on-plate wear tester with applying 5 N load for 5 minutes with 10 rpm sliding speed on a 2-mm diameter track, and as the counter body hardened steel ball was used. Fig. 4.11 shows the comparable wear lose graphs (in terms of vertical penetration of the steel ball or wear depth) as a function of sliding distance of all coated samples at the current densities of 5, 8, 11 and 14 A/dm^2. From the figures, it can be observed that with addition of increased amount of Al_2O_3 in the coating, the wear resistance increases. The composite coating is thus successful in showing better surface-mechanical properties compared to the substrate as substrate wear

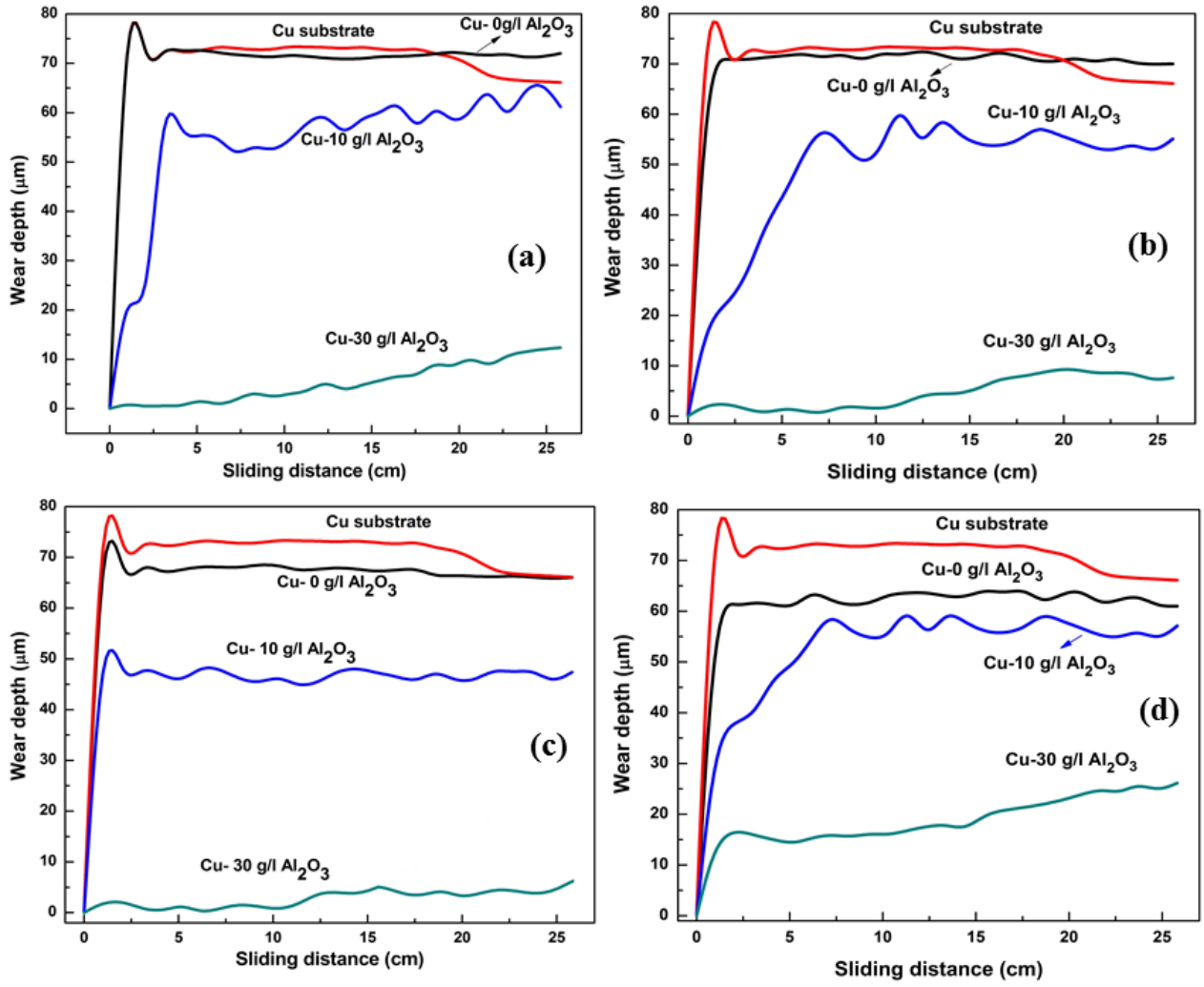

Fig. 4.11: Wear plots between wear depth and sliding distance of all coatings and substrate at (a) 5, (b) 8, (c) 11 and (b) 14 A/dm^2 respectively.

plot is having the maximum wear depth. Wear depth was more than the coating thickness for some specific samples and in those cases, the wear data are not truly independent of the substrate but comparative study can be made. Moreover, in such sample, there was no abrupt variation in wear plot, which is interpretive of good adherence or strong interface of the coating. Only in case of the coating with 30 g/l Al_2O_3 concentration, the wear depth is within the coating. The overall trend is similar to the hardness values as reported in Fig. 4.10. In case of some graphs, momentary negative slope could be observed which may due to temporary cold welding of soft Cu phase with the hardened steel ball resulting decrease in wear depth.

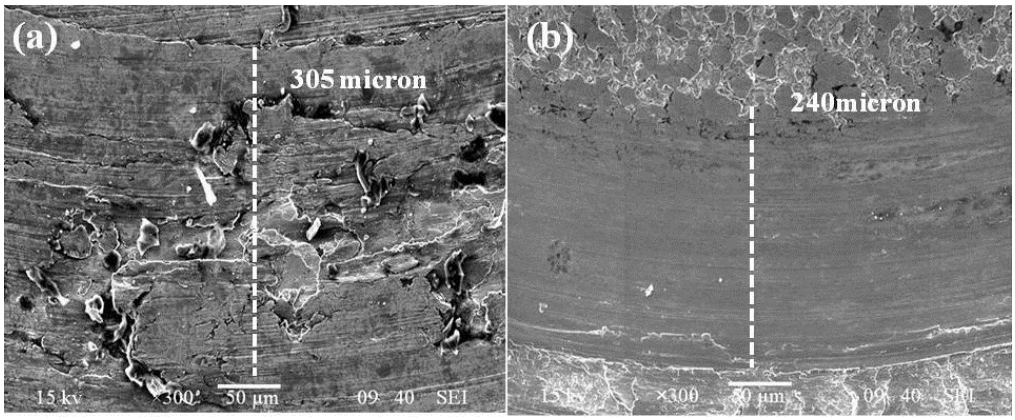

Fig. 4.12: SEM micrographs of worn wear track of (a) pure copper coating and (b) Cu-10 g/l Al_2O_3 coating at 11 A/dm^2 current density.

Fig. 4.12 shows worn wear track of pure copper and Cu-10 g/l Al_2O_3 coating at 11 A/dm^2. From the figure, it can be observed that wear track of pure copper coating is wider and rough in comparison to composite coating. The composite coating's wear track is smaller in width and shows only some fine lines in the track. This lines may be due the rubbing of worn out Al_2O_3 particles. In such case, it happens to be a three-body motion, and the ceramic particle creates an abrasive wear regime; whereas in case of pure Cu coating, it is mostly adhesive type of wear.

4.9 Electrical conductivity

Electrical conductivity of the deposited samples in percentage of International Annealed Copper Standard (IACS) with the variation of applied current density and alumina concentration in bath is reported in Fig. 4.13. In case of co-deposited sample, with increasing current density, the conductivity value increases till 8 A/dm^2 and then decreases which can directly be linked with the fineness of the structure at higher current density. It is due to the known fact that finer structure creates negative impact on electrical conductivity [129]. At a particular current density, 30 g/l concentration provides higher electrical conductivity in comparison to 10 g/l Al_2O_3 concentration. In earlier section, it was explained that with increase in Al_2O_3 content, the matrix becomes coarser. Moreover, these microstructures (Fig.

4.6) also show the presence of small crack and porosity. This provides two-opposing effect on electrical conductivity of the coating: decrease in conductivity due to more addition of non-conducting Al_2O_3 and the presence of porosity/crack and increase in conductivity due to formation of coarser matrix as grain size has strong effect on electrical properties of materials [129].

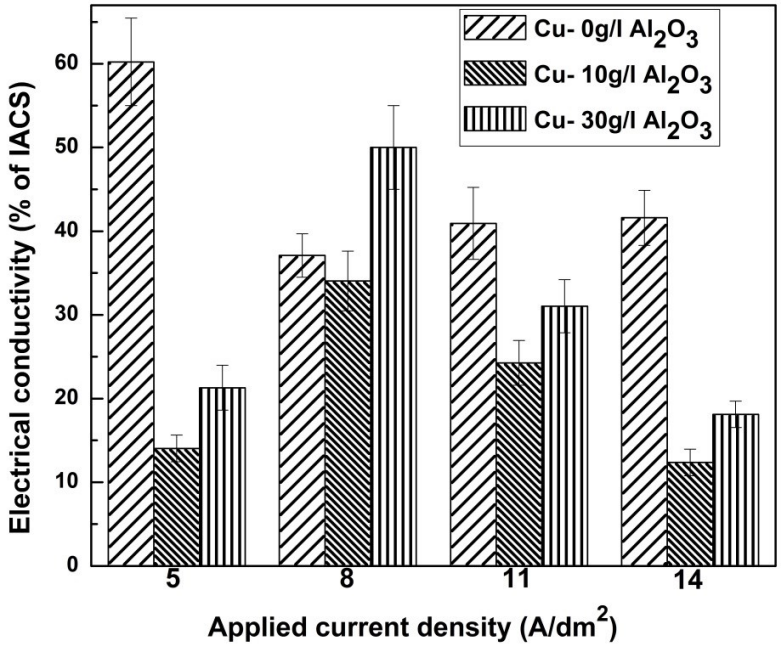

Fig. 4.13: Electrical conductivity of deposited samples with variation of current density and bath concentration.

Thus, the coarse matrix may have overcome the effect of non-conductive phase addition and pores in the coating. Crystallite size of Cu as mentioned in Table 4.1 gives a tentative idea about its effect on the conductivity. Moreover, there may still be the effect of crystallographic texture on conductivity which needs exploration.

The reported conductivity values of the coated samples were in the range from 10 to 50 % of IACS. As materials having conductivity values in this range can be used for commercial application as conductor, optimization of the present study can be considered fruitful for producing coating to be used as electrical contacts. It is worth mentioning that earlier studies of bulk modification of Cu-based alloys resulted in marginal lower conductivity value [130].

4.10 Summary

Cu-nano Al_2O_3 composite coatings were successfully prepared by DC electroplating using a modified acidic copper electrolyte with different concentrations of dispersed Al_2O_3 powder and the study revealed interesting outcomes.

- It was observed that except 8 A/dm^2, with increasing current density, the matrix become finer, and higher amount of Al_2O_3 leads to coarser matrix.
- Thickness of the coating was increasing in nature with higher current density, but was adversely affected by Al_2O_3 content.
- Composite coatings exhibit higher hardness, and the change in hardness was due to Cu matrix structure, second-phase concentration and minor effect from the matrix texture. Wear test result showed similar trend like hardness.
- The electrical conductivity shows that the values are in useable range and are affected mainly by the matrix grain size and second-phase concentration.

Chapter 5

Effects of pulse parameters on surface-mechanical properties of Cu-SiO_2 and Cu-Y_2O_3 composite coating

5.1 Introduction

The present study aims to enumerate the effect of ultrafine SiO_2 and Y_2O_3 dispersion in Cu matrix coating on Cu substrate with direct and pulsed electrodeposition. The effect of pulse parameters have also been studied in terms of surface-mechanical and electrical properties. The bath compositions and deposition parameters used for Cu-SiO_2 and Cu-Y_2O_3 systems are presented in table.5.1. Due to observation of overall better mechanical and electrical properties at 8 A/dm^2 in Cu-Al_2O_3 system, in this chapter 8 A/dm^2 was kept constant with variation of pulse frequencies.

Table 5.1: Plating bath composition and deposition parameter for Cu–SiO_2 and Cu–Y_2O_3 systems

Item	Parameters
Electrolyte (acidic copper sulfate bath)	Copper sulfate ($CuSO_4.5H_2O$): 200 g/l Sulfuric acid(H_2SO_4):50 g/l
pH	2.17 (±0.2)
Current density	8A/dm^2
Temperature	Room Temperature
Plating time	20 minutes
Dispersion	SiO_2 and Y_2O_3: 10 and 30 g/l
Pulse frequency	1, 5 and 10 kHz
Duty cycle (pulse on time)	30%

5.2 *Cu-SiO_2 System*

5.2.1 Isoelectric point measurement of SiO_2

Fig. 5.2.1 shows the isoelectric point (IEP) of SiO_2 powder, which was obtained by measuring zeta potential of procured powder at different *pH* values after suspending them in de-ionized water with mild acide/base.

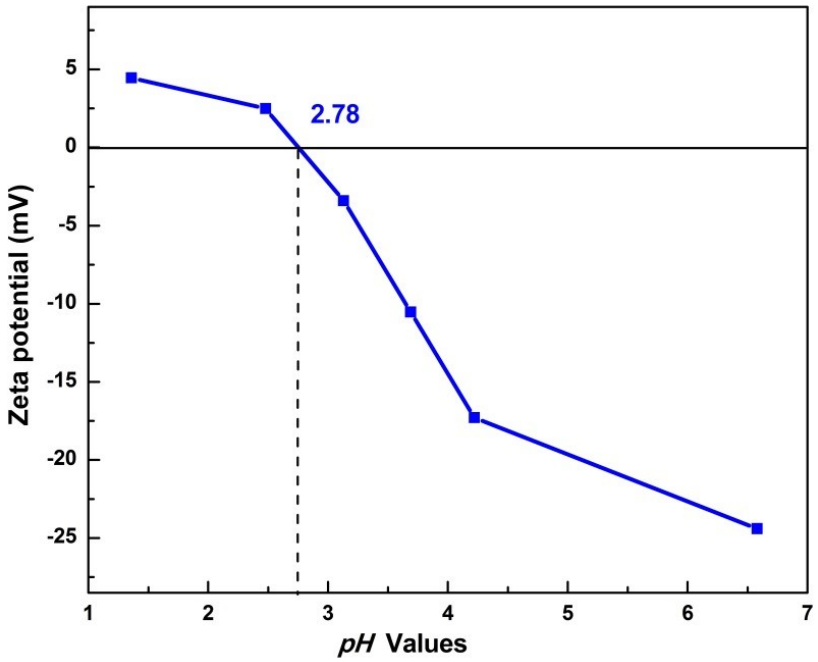

Fig. 5.2.1: Isoelectric point of SiO_2.

From the data, isoelectric point of SiO_2 particle was observed as 2.78. Thus, in all co-deposition process *pH* value of the electrolyte was maintained below the IEP value to ensure the uniform deposition of second phase ceramic powder on cathode (copper substrate).

5.2.2 Particle size analysis of SiO_2

Fig. 5.2.2(a) shows the particle size distribution of the procured SiO_2 powder which was measured by Malvern Zeta-sizer nano series Nano-ZS model. No sharp peak was found but only one broadened peak ranging approximately 200-700 nm was observed. The mean value was found to be around 400nm. Fig. 5.2.2(b) shows the transmission electron micrograph

(TEM) of the as-received SiO_2 powder. From the micrograph, it can be observed that the particles were in 9-36 nm range, and after statistical analysis, the average size was found to be 19 nm. The presence of fine-sized particle is important for better co-deposition and dispersion strengthening of the coating. Agglomeration of powder particles in aqueous solution during the zeta-sizer measurement can be explained as a reason behind the larger particle size reported by Zeta sizer study.

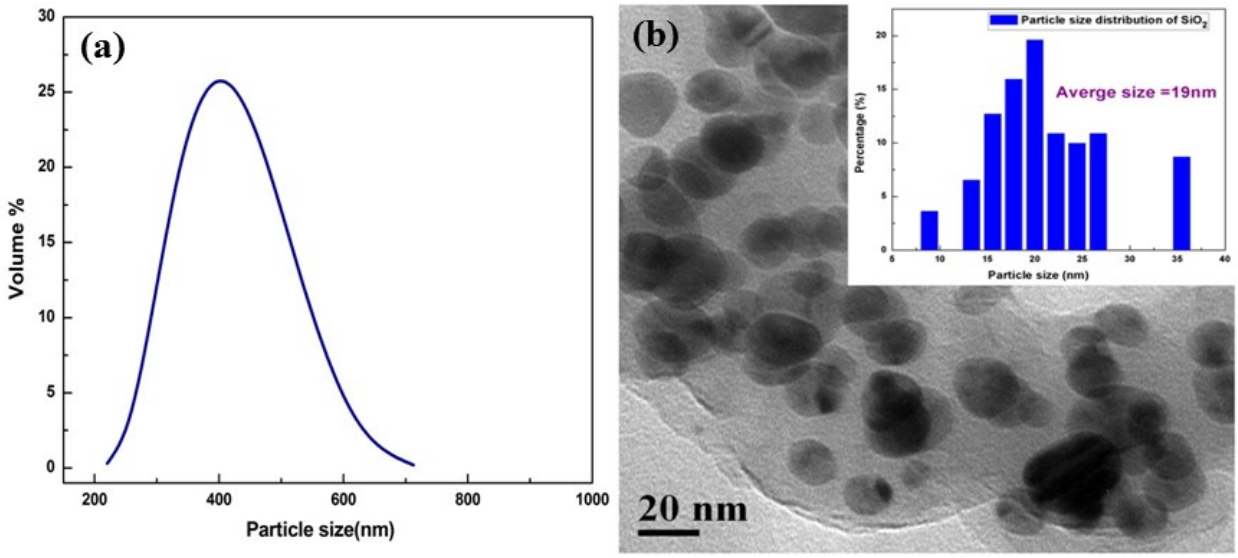

Fig. 5.2.2: (a) Particle size distribution and (b) TEM micrograph of procured SiO_2 powder.

5.2.3 XRD analysis

Fig. 5.2.3(a) shows the XRD pattern of the deposited samples with different concentrations of SiO_2 without pulsing, whereas Fig. 5.2.3(b) represents the XRD patterns of the samples deposited with pulsing (5 and 10 kHz frequencies) and at different concentrations (0, 10, and 30 g/l) of SiO_2. All the XRD peaks of the deposited samples were confirmed as pure Cu as assigned by JCPDS (card no. 04-0836) data. After co-deposition, no silica peaks was clearly observed due to the lower wt. % of SiO_2; though energy dispersive spectra confirmed the presence of the same.

Fig. 5.2.3 depicts change in relative intensities of Cu peaks at different coating conditions, which indicates formation of preferential crystallographic texture. To analyze the same, relative texture coefficient of each plane of all XRD patterns of the deposited samples were calculated by the formula of equation 4.1 (Refer to chapter 4) [120]:

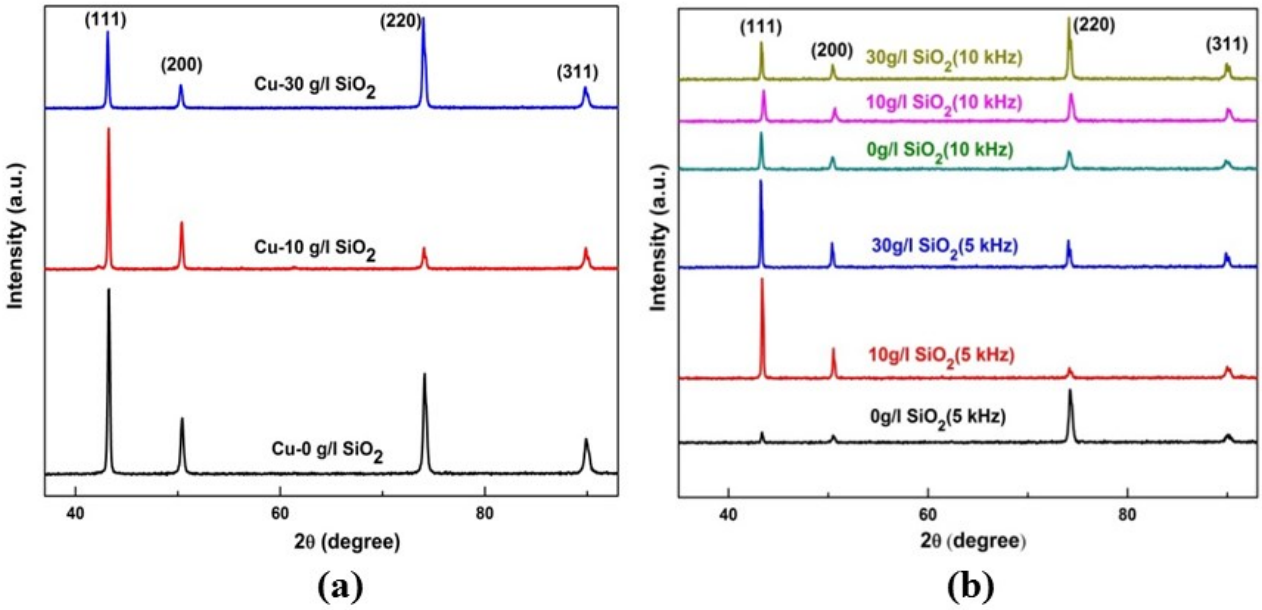

Fig. 5.2.3: XRD pattern of deposited samples with 0, 10 and 30g/l SiO_2 (a) without pulsing and (b) with pulsing rate 5 and 10 kHz.

Table 5.2.1 shows the variation of texture coefficients (TCs) of all the deposited samples under different deposition conditions. It can be observed in table. 5.2.1, that during pure Cu deposition (0% SiO_2), under all conditions of deposition (pulsing and without pulsing), TC_{220} was the most pronounced orientation followed by TC_{311}. However, addition of small amount of SiO_2 (10 g/l) to the plating bath decreases the TC_{220} value, and the same is compensated by the increase in the TC_{111} value (table 5.2.1). This effect is pronounced in case of coating deposited in DC mode and with 5-kHz frequency; whereas in 10-kHz frequency sample, such changes were not observed (table 5.2.1). 30 g/l SiO_2 coatings, carried out under different pulsing conditions show pronounced (220) orientation, which is similar to the coatings deposited without addition of SiO_2. Under pulsing conditions (table. 5.2.1), it is clear that (220) texture and its peak intensity became more pronounced when a higher pulse frequency

was applied, and meanwhile, the diffraction intensities of other crystallographic planes were reduced within the present scanned range. Thus, it can be inferred that at 10 g/l SiO_2 content the increase in TC_{111} value was compensated by the decrease in TC_{220} value. During electro-co-deposition, formation of particular orientation is observed maybe due to interfacial energy-driven phenomena and subsequent alteration of interfacial energy in the presence of oxide particles.

Table 5.2.1: Relative texture coefficient of all the samples

Sample Type	Sample Details	$RTC_{(hkl)}\%$			
		(111)	(200)	(220)	(311)
Cu deposition	DC	16	09	45	30
	PC(5 kHz)	03	04	81	12
	PC(10 kHz)	17	12	47	24
Cu-SiO_2 coating	10 g/l, DC	43	32	04	21
	10 g/l, PC(5 kHz)	32	25	21	22
	10 g/l, PC(10kHz)	11	09	54	26
	30 g/l, DC	13	10	52	25
	30 g/l, PC(5 kHz)	22	14	40	24
	30 g/l, PC(10kHz)	07	06	68	19

5.2.4 Microstructural and elemental studies

Fig. 5.2.4(a)-(c) shows SEM micrographs of Cu-10 g/l SiO_2 composite coatings in DC and pulsing (5 and 10 kHz frequency) conditions. Cu-10 g/l SiO_2 deposit obtained from DC deposition exhibits bulky morphology, as evident from Fig. 5.2.4(a). On the contrary, it was observed that, in the case of different pulsing rates (Fig. 5.2.4b and c); the structures are comparatively finer and more uniform than those for direct current deposition. Fig. 5.2.4 (d)-(f) shows Cu-30 g/l SiO_2 composite coatings, and here also the size trend is similar to that of Fig. 5.2.4(a)-(c). Image analysis of the micrographs was performed to understand the grain size variation, and the same is presented in Fig. 5.2.5.

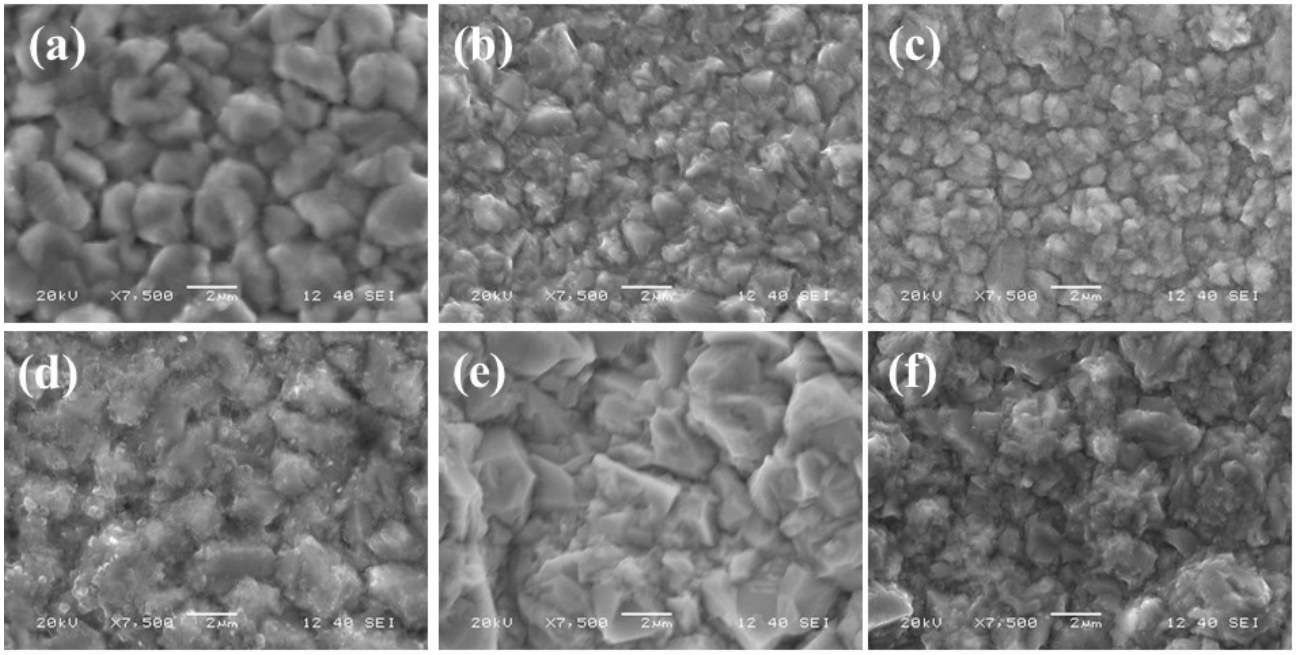

Fig. 5.2.4: SEM images of Cu-10g/l SiO_2 and Cu-30g/l SiO_2 coatings (a, d) without pulsing, (b, e) with pulsing rate 5 kHz and (c, f) with pulsing rate 10 kHz respectively.

Generally frequency (*f*) of the pulse is measured in Hz is given by:

$$f = \frac{1}{(T_{on} + T_{off})}$$

Where, T_{on} and T_{off} are the pulse on and off duration in second*s* respectively. In the present study the duty cycle is kept constant at 30%; i.e.

$$\frac{T_{on}}{(T_{on} + T_{off})} = 30\%$$

In case of higher pulse frequency, the pulses are shorter, i.e., both Ton and T_{off} are of short duration. This indicates that double layers do not get sufficient time to be fully charged during Ton and discharged during T_{off} time. As soon as one pulse cycle is completed, the next pulse arrives very quickly. These phenomena produce very thin pulse diffusion layer which causes hindrance to the transportation and diffusion of the migrating copper ions from the solution to the cathode surface (copper substrate). This leads to the enhanced nucleation with limited growth rate resulting in a finer microstructure. Thus, upon increasing the pulse frequency

from 5 to 10 kHz, the morphology looks more uniform, finer, and without porosity as shown in Fig. 5.2.4(b and c) and (e and f), and similar behavior was also reported in the literature [131, 132].

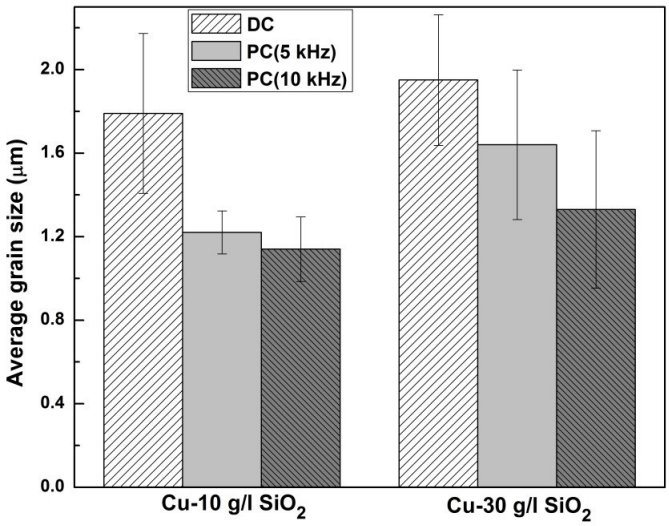

Fig. 5.2.5: Average grain size of Cu-10g/l SiO_2 and Cu-30g/l SiO_2 composite coatings.

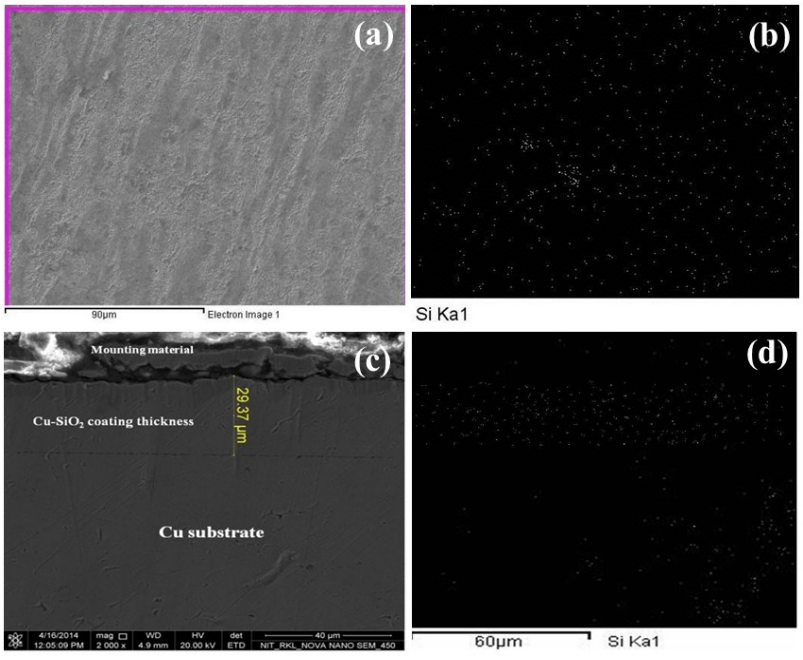

Fig. 5.2.6: Elemental X-ray mapping of Si (b and d) on (a) coated surface and (c) coating cross section, respectively for the samples deposited with Cu-30 g/l SiO_2 composition and 10 kHz pulsing rate.

To study the effect of SiO_2 content, when Fig. 5.2.4(a-c) and (d-f) were compared, it was seen that higher SiO_2 content produces coarser structure of the matrix, and the same is also confirmed by Fig. 5.2.5. Under each pulsing condition, Cu-30 g/l SiO_2 coating exhibits larger asperities compared to Cu-10 g/l SiO_2 coating. This was due to different deposition rates because of variation of nano-silica contents in plating bath. During co-deposition, the presence of SiO_2 may have adverse effect in nucleation by increasing the surface energy of Cu deposition. This may lead to less nucleation as well as extended growth of Cu crystals, resulting in coarser structure in 30 g/l samples. Similar results were also reported earlier by Allahkaram et al. [122]. It is also evident from the first-principle-based calculations that formation of Cu-Cu cluster is more likely compared to Cu-SiO_2 cluster as the calculated formation energies (ΔE) for those are equal to -56.10 and -67.37 kcal/mol, respectively. Therefore, nucleation is easier in pure copper compared to Cu-SiO_2 system. This in turn reduces the nucleation possibility of Cu in the presence of SiO_2 leading to coarse Cu grain as discussed earlier.

SEM micrograph of the cross-sectional view of the coating was also analyzed, and the thickness was found to be uniform in nature. Figure 5.2.6(c) shows such a micrograph obtained from Cu-30 g/l SiO_2 composite coating with the pulsing rate of 10 kHz. The figure indicates approximately 30 micron of coating thickness.

To enumerate the homogeneity of SiO_2 particles in deposition, elemental mapping (in EDS mode of SEM) of the coated surface was carried out. Fig. 5.2.6(a) shows the Cu-30 g/l SiO_2 composite coating surface prepared with the pulsing rate of 10 kHz, and Fig. 5.2.6(b) displays the corresponding x-ray mapping of Si. These represent uniform distribution of Si on the surface, and thus the homogeneity of SiO_2 in the deposition is confirmed. Similarly, Fig. 5.2.6(d) shows the x-ray mapping of Si in cross-sectional image as displayed in Fig. 5.2.6(c). Hence, along with the coated surface, the cross section was also homogeneously distributed with SiO_2 particles, although there were some Si particles distributed on the substrate due to dislodging of the same during metallographic sample preparation of the cross section by grinding and polishing.

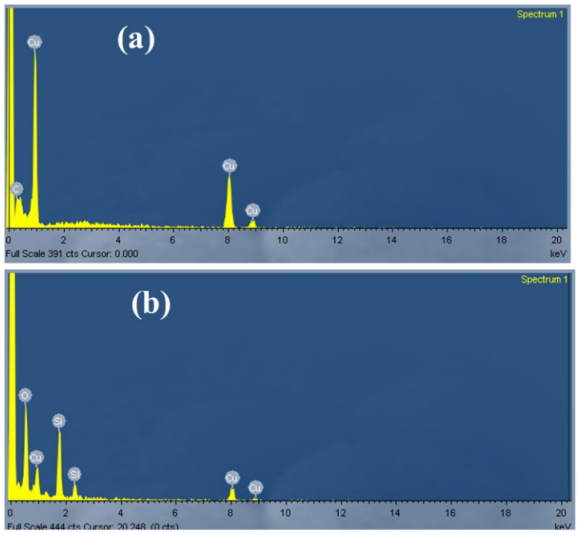

Fig. 5.2.7: EDS of deposited samples of (a) pure copper coating and (b) 30g/l SiO_2 with pulsing rate 10 kHz.

All the coated surfaces were subjected to compositional analysis by energy dispersive spectra (EDS). Fig. 5.2.7 shows such spectra of coated surface of pure copper coating without pulsing (Fig. 5.2.7a) and Cu-30 g/l SiO_2 composite coating with 10-kHz pulse (Fig. 5.2.7b). The Cu-SiO_2 composite coating exhibits the presence of Si due to the silica in the coating surface.

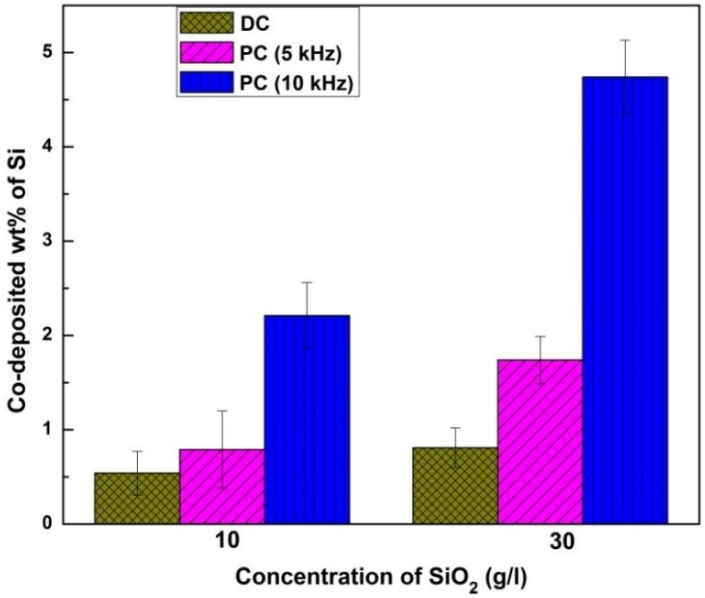

Fig. 5.2.8: Co-deposited wt% of SiO_2 (in terms of Si) in Cu-10g/l SiO_2 and Cu-30g/l SiO_2 deposited samples.

All the quantified EDS values have been summarized in Fig. 5.2.8. It shows the relationship between the wt.% of co-deposited Si in the coatings under different deposition conditions. From the figure, it can be observed that the particle content (in terms of Si wt.%) in the composite coating depends on the deposition condition (DC and PC) as well as on the amount of the suspended ultrafine particles in the bath. With the increasing SiO_2 ultrafine particle content in the bath, the weight percentage of SiO_2 (in terms of Si) in the deposits also increases irrespective of other deposition conditions. However, the increase in amount of co-deposited SiO_2 particles is not proportional with the amount of particles charged to the electrolyte. The weight percentage of SiO_2 particles in the deposit increases more in the case of pulsing condition compared to direct current deposition. With the increasing pulse frequency, the SiO_2 content of the deposit increases. Thus, from Fig. 5.2.8, it can be inferred that pulse deposition helps in electrophoretic deposition; but the effect is not linear with the pulse frequency.

5.2.5 Surface roughness analysis

All the deposited surfaces were characterized to calculate the average surface roughness (Ra), and Fig. 5.2.9 shows the Ra values of all the samples and its variations with deposition parameters. All the values were within the range of 0.14 to 1.2 lm, and it is reported that lower surface roughness is better for electrical contacts [133]. From the figure, it can be observed that under each pulsing condition (DC or PC with particular frequency), with the increasing SiO_2 content in the deposition bath, the surface roughness increases. This effect may be due to two possible reasons: incorporation of larger amount of ceramic particles in the matrix at higher SiO_2 content in the bath, and the coarser structure at higher SiO_2-containing coating matrix as discussed in SEM morphology section. However, the first mechanism would be logically less effective in increasing the surface roughness as the particles are very few in numbers and are nanometric in size. Coarser matrix at higher SiO_2 content leads to higher surface roughness value.

From Fig. 5.2.9, it can also be observed that for a particular bath composition, with the change in mode from DC to PC and with the increasing pulse frequency in PC mode, the Ra value decreases. This observation can be justified using SEM micrographs (Fig. 5.2.4) as it was

observed that at higher pulse frequency, the matrix structure becomes finer due to limited growth and more nucleation and finer structure leads to lower value of Ra. Thus, higher pulse frequency is better for smoother surface of deposition. Moreover, this effect was found to be negligible for pure Cu deposition, and it became more and more pronounced at higher amounts of SiO_2 content in the bath. This may be attributed to the role of second-phase particle which can trigger two mechanisms of higher roughness as discussed earlier.

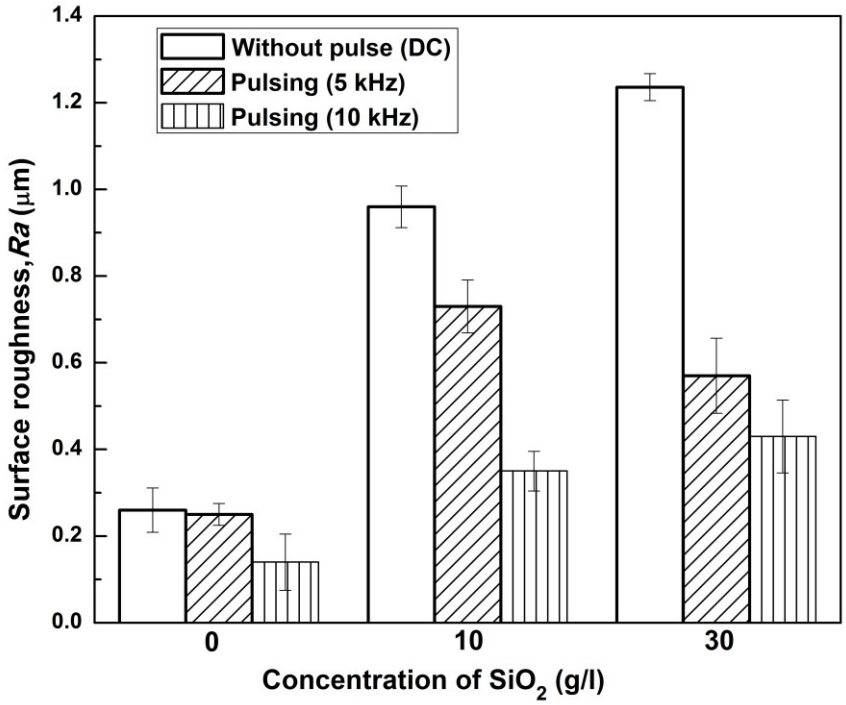

Fig. 5.2.9: Surface roughness of all Cu-SiO_2 deposited samples.

5.2.6 Microhardness study

Fig. 5.2.10 shows the microhardness values measured on the coated surfaces as a function of SiO_2 concentrations of the bath and pulsing values. Hardness values were measured with 10-g load confirming that the indentations were not affected by substrate hardness. From the figure, it is clear that with the addition of ultrafine ceramic (SiO_2) powder in the bath, the microhardness values increase. This can be attributed to the fact that more amounts of ceramic

nanoparticles got embedded with the increasing silica concentration in the deposition bath which could be confirmed from Fig. 5.2.8.

Thus, dispersion strengthening primarily helps in improving the strength of the coating. Dispersion strengthening is associated with the incorporation of ultrafine particles (<1 μm) which hinders dislocation motion resulting in better mechanical strength [18]. It can also be observed from the figure that the hardness of the deposited samples was increased with the increasing pulse frequencies, which confirms finer matrix and higher amount of SiO_2 incorporation in the deposits as discussed in EDS section. In case of higher frequency, growth restriction of existing nucleus and formation of fresh nucleus together causes finer structure. Apart from these mechanisms, the presence of crystallographic orientation can also play a vital role as was observed in Table 5.2.1. From Table 5.2.1, it is clear that at each SiO_2 concentration in the bath, with change in pulse condition, there were marginal changes between TC_{111} and TC_{220} values. As planes having higher angle with (100) produces more strain, higher hardness [134] will result due to higher TC_{111} value followed by TC_{220}. In the present study, TC_{311} values are less fluctuating followed by the softest one, i.e., TC_{200}. As TC_{111} and TC_{220} values are competitive with change in frequencies and their strain effects are not much differing, effects of these two are complex on the hardness value. In general, it can be commented that in the present study, the effect of the preferred orientation on hardness is less pronounced compared to that in earlier related studies [120].

From hardness study, it is evident that Cu-SiO_2 coatings can exhibit better mechanical properties than those of Cu-Al_2O_3 and Cu-SiC as reported earlier [122, 135]. Even with Cu-Si_3N_4 coating, the reported hardness was only 155 Hv [17].

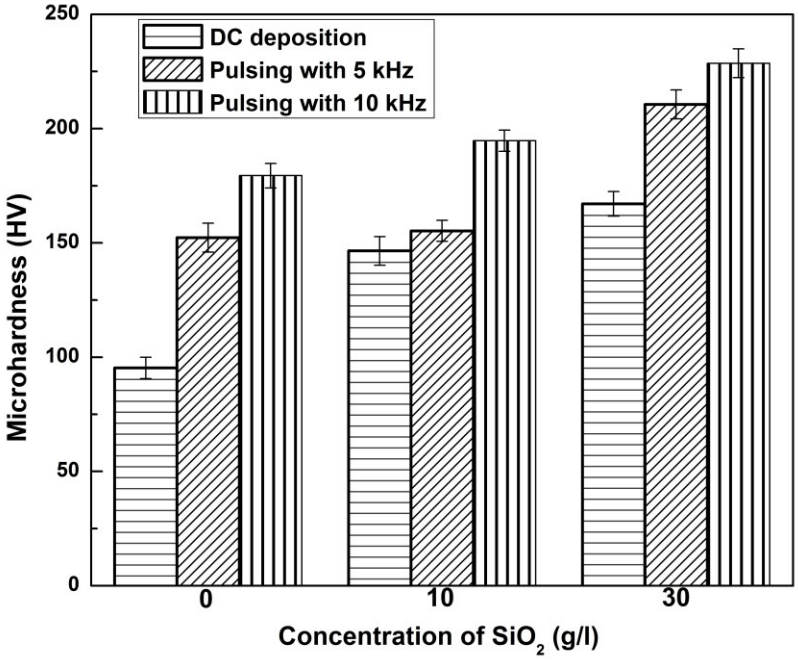

Fig. 5.2.10: Micro hardness of pure copper and Cu-SiO_2 deposited samples with different deposition parameters.

5.2.7 Wear study

Fig. 5.2.11 shows the variation of cumulative wear loss (in terms of vertical penetration of the indenter or wear depth) as a function of sliding distance considering different bath concentrations and pulsing conditions at an applied load of 5 N at 15-rpm speed (linear sliding speed 0.00314 m/s) on a 4-mm-diameter track for 5 min.

It is observed that pulsing condition decreases the wear loss and higher pulse frequency further reduces the wear depth. After comparing all the three plots of Fig. 5.2.11, it can also be concluded that wear loss decreases with the increasing SiO_2 contents on the bath/coatings, whereas copper coating without co-deposition of SiO_2 shows significant wear loss. The best wear resistance was found with 30 g/l SiO_2 content at 10-kHz pulse frequency. Thus, the trend of wear was similar to that of microhardness results as discussed in the previous section in the course of explaining Fig. 5.2.10. Another important observation was also made that in some specific samples, wear depth was more than the coating thickness. In those cases, the wear

result was not truly independent of the substrate, but inference based on comparative study can be made.

Fig. 5.2.12 shows the scanning electron micrographs of wear tracks on the coated surface. From the figure, it can be observed that the wear track of pure copper coating is wider than the Cu- SiO_2 composite coating obtained with 10 g/l SiO_2 and 5-kHz pulsing parameter. Similar trend was observed in other co-deposited samples. Moreover, at higher magnification, it can be observed that in case of pure copper, adhesive wear mechanism with sign of cold welding at the track is prevalent. However, in case of co-deposited sample, the track is clean with an appearance of cutting being present. This may be due to the rubbing effect of the third body (dislodged SiO_2 ceramic particle), which makes the mechanism to shift marginally toward abrasive wear.

To enumerate this effect more clearly, wear track roughness/profile was also studied. Stylus 2D surface profiles of different wear tracks are shown in Fig. 5.2.13. The obtained results show lower roughness values for wear tracks with the increasing pulse frequency and second-phase silica nanoparticles. This trend is not exactly the same as that was observed in the case of coating surfaces where surface roughness was proportional to silica content (Fig. 5.2.9), rather the wear tracks results showed the reverse. This means more extensive wear loss in case of low silica content samples due to low strength or hardness. In other words, due to higher wear loss and adhesive mechanism, Fig. 5.2.12(c) shows more roughness values than those in Fig. 5.2.12(d).

As an overall observation, it can be summarized that SiO_2 addition improves wear properties. Earlier reported wear study of Cu-CeO_2 coating revealed very high wear depth even with similar load [83].

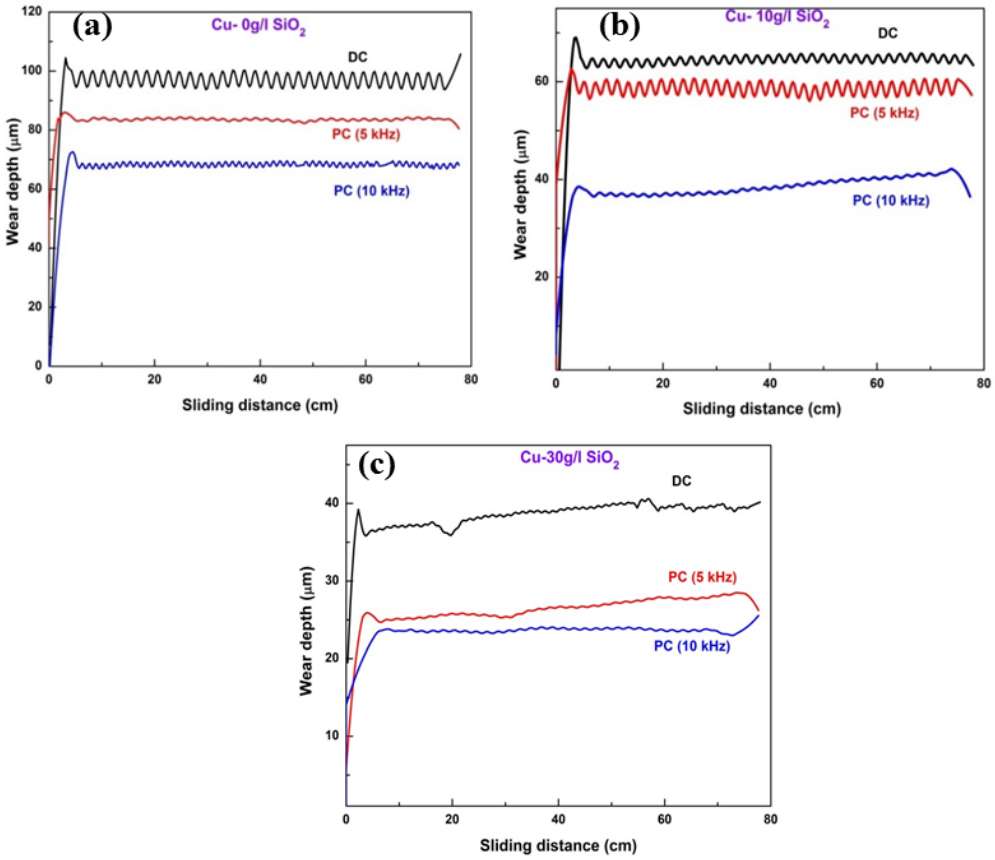

Fig. 5.2.11: Plot of sliding distance vs. cumulative wear depth obtained in samples: (a) Pure Cu, (b) Cu-10g/l SiO_2 and (c) Cu-30g/l SiO_2.

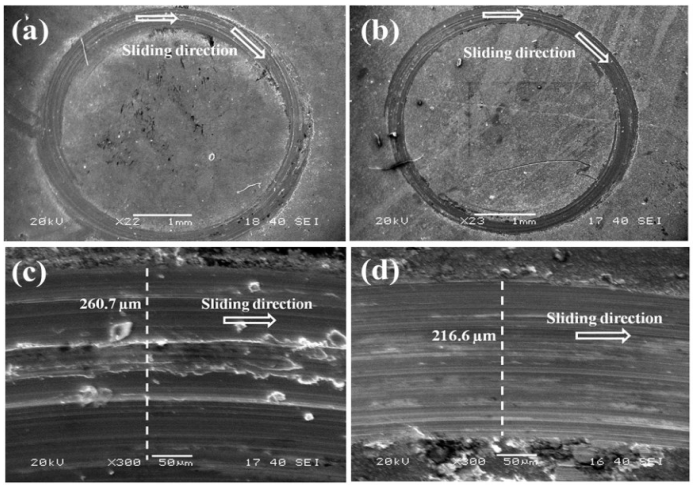

Fig. 5.2.12: Wear track of (a) pure copper coating (without pulse), (b) Cu-SiO_2 composite coating with 10g/l SiO_2 (5 kHz pulse), (c) and (d) are higher magnification photographs of (a) and (b) respectively.

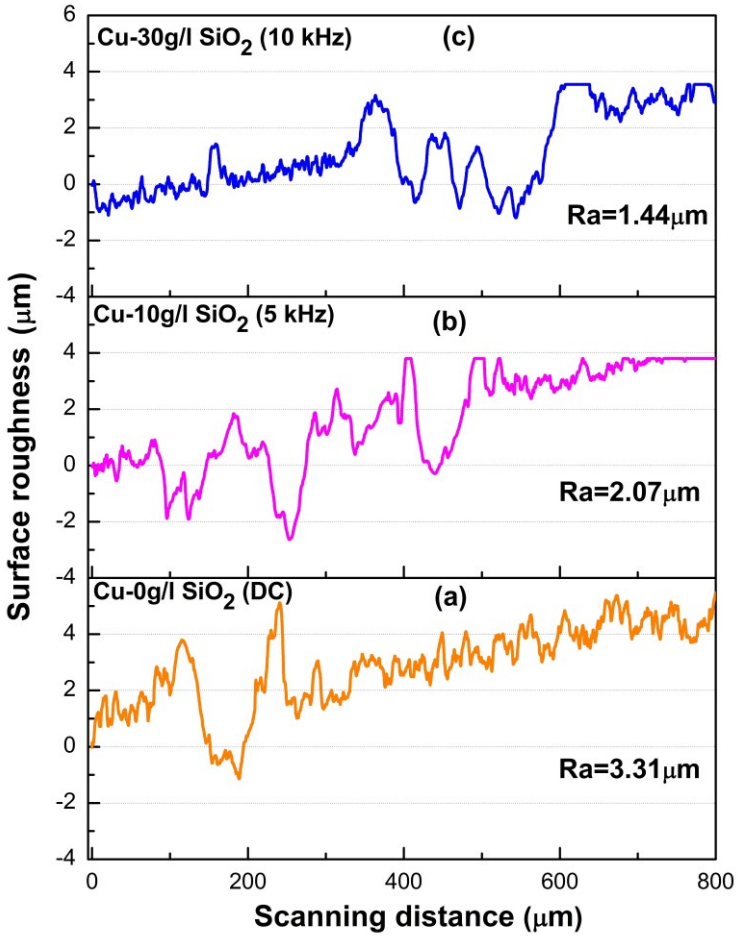

Fig. 5.2.13: Average surface roughness of (a) Cu-0g/l SiO_2 (DC), (b) Cu-10g/l SiO_2 with 5 kHz and (c) Cu-10g/l SiO_2 with 10 kHz wear tracks.

5.2.8 Electrical conductivity

Fig. 5.2.14 shows the results of electrical conductivity test in percentage of International Annealed Copper Standard (IACS) carried out on the coated surface by four-probe technique as a function of bath concentration and pulsing condition. From the figure, it can be observed that under every pulsing condition with the increasing SiO_2 content, the electrical conductivity of the co-deposited samples decreased. As SiO_2 is an insulating material having very high energy gap, it has led to the decrease in the conductivity value with its increasing concentration. Earlier it was discussed that the higher SiO_2 content increases the size of matrix asperities, which in turn can improve the electrical conductivity. Here, it seems that the

effect of higher non-conducting material is more prevalent than the influence of course-grained matrix structure.

From Fig. 5.2.14, it can also be observed that pulsing mode and higher pulse frequency decrease the electrical conductivity. This observation can be attributed to the fact that the higher pulse frequency results in finer structure with more SiO_2 deposition. Moreover, there may be an effect of crystallographic texture on electrical conductivity.

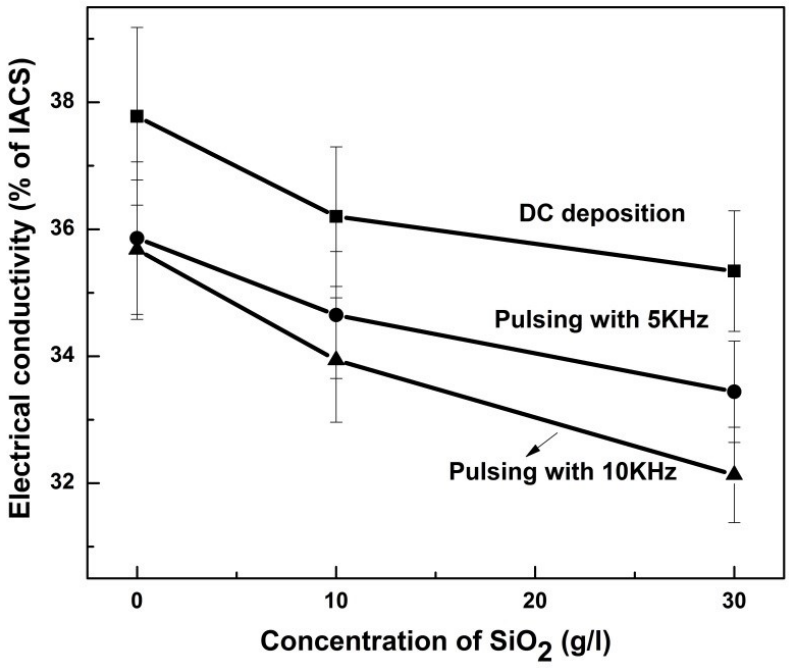

Fig. 5.2.14: Electrical conductivity with variation in bath concentration and pulsing conditions of deposited specimens.

Electrical conductivity values of the coated samples reported here were above the value of 32% of IACS. It is worth mentioning that materials having electrical conductivity values in this range can still be used for commercial application as conductor. Thus, optimization of electrical properties with better surface-mechanical properties is highly necessary while aiming for an effective end application.

5.2.9 Summary

In the present study, an attempt was made to co-deposit Cu-SiO_2 on copper substrate from ultrafine SiO_2-dispersed acidic copper sulfate bath with direct and pulsed direct current modes in different pulse conditions as well as bath concentrations. Morphologies and mechanical properties of Cu-SiO_2 deposition were studied experimentally in detail, and the relative nucleation possibility in pure copper compared to Cu-SiO_2 system is rationalized using first-principle-based calculations.

Conclusions, obtained from the detailed investigation as above, are summarized below:

- Higher SiO_2 content of the bath tends to increase SiO_2 content in the deposits, which results in better hardness and wear resistance of the coating. Pulsing mode and higher pulse frequency also result in better mechanical properties due to finer matrix of deposition
- SiO_2 distribution in the matrix was found to be homogeneous, and it was also observed that higher SiO_2 content increases the matrix grain size.
- Preferred crystallographic orientations of the deposited matrix were observed with the variation of pulse condition and SiO_2 content. Effects of these were not prominent on surface-mechanical properties due to complex effects of finer structure and dispersion strengthening.
- Electrical conductivity of coated samples decreases with the increasing SiO_2 content and pulse frequency mainly due to the increase in non-conducting Phase.

5.3 *Cu-Y_2O_3 System*

5.3.1 Isoelectric point measurement of Y_2O_3 powder

Fig. 5.3.1 shows the isoelectric point (IEP), Particle size distribution, TEM micrograph and XRD pattern of procured Y_2O_3 powder respectively. IEP of Y_2O_3 was obtained by measuring zeta potential of procured powder at different *pH* values. From the result, IEP of Y_2O_3 particle was observed as ~7.55. So, during the co-deposition process *pH* of the electrolyte was maintained sufficient below the IEP value (at ~2.17) to ensure uniform deposition of ultrafine ceramic powder on cathode (copper substrate) with minimum agglomeration.

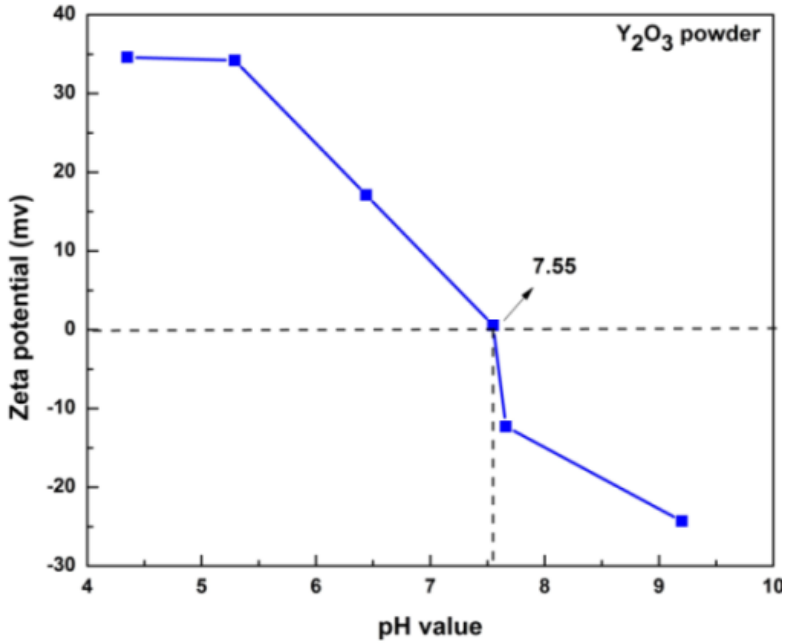

Fig. 5.3.1: Isoelectric point of Y_2O_3 powder.

5.3.2 Particle size analysis of Y_2O_3 powder

The particle size distribution of the procured Y_2O_3 powder, which was measured by particle size analyzer, is presented in Fig. 5.3.2 (a). Only one broadened peak ranging approximately 300-700 nm was observed and the mean value was found to be near 480 nm. However, from transmission electron micrograph (TEM), as shown in Fig. 5.3.2(b), smaller particle size

range (7-22 nm) was noticed with average size of 14 nm. Larger particle size reported by zeta-sizer measurement can be explained by agglomeration of powder particles in aqueous solution during the measurement.

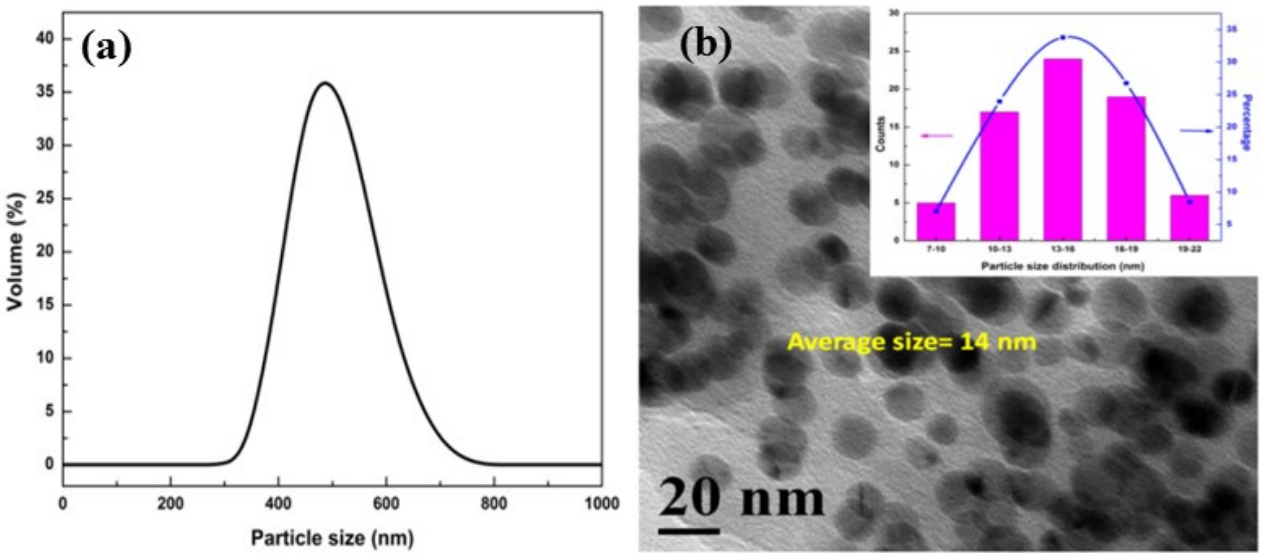

Fig. 5.3.2: (a) Particle size distribution and (b) TEM micrograph and of Y_2O_3 powder.

5.3.3 XRD analysis

XRD analysis of Y_2O_3 ultrafine particle (Fig. 5.3.3) shows BCC structure. Fig. 5.3.4 illustrates the XRD patterns of the pure copper and Cu–Y_2O_3 composite coatings with variation of Y_2O_3 (10 and 30g/l) at different pulsing rates. All the composite coatings exhibit single phase of copper matrix with face-centered cubic (FCC) crystal structure (JCPDS No: 04-0836). From the figure it can be observed that peak intensities of different planes of Cu are highly affected by deposition conditions. Similar effect was observed in other Cu based composite coatings also [136, 137]. Formation of particular orientation during electro-codeposition may be due to interfacial energy driven phenomena and subsequent alteration of interfacial energy in presence of oxide particles. To justify this, theoretical study of the same by first principle method is needed.

In Fig. 5.3.4(a-c), the peaks corresponding to Y_2O_3 phase are not found and this may be attributed towards the presence of minor amount of Y_2O_3 particles in the coatings. However,

enlarged XRD plot displays the peaks which correspond to Y_2O_3. Fig. 5.3.4(d) shows such peaks in Cu-30g/l Y_2O_3 coating deposited with 10 kHz frequency.

Fig. 5.3.3 shows change in relative intensities of Cu peaks at different coating conditions, which specifies formation of preferential crystallographic texture. To analyze the same, relative texture coefficient of each plane of all XRD patterns of the deposited samples were calculated by the formula of equation 4.1 (Refer to chapter 4) and presented in table 5.3.1. The result shows that in case of pure copper and Cu-10g/l Y_2O_3 coating (220) plane was most preferred orientation, but in case of Cu-30g/l Y_2O_3 the orientation shifted from (220) to (111) orientation except at 5 kHz pulse frequency.

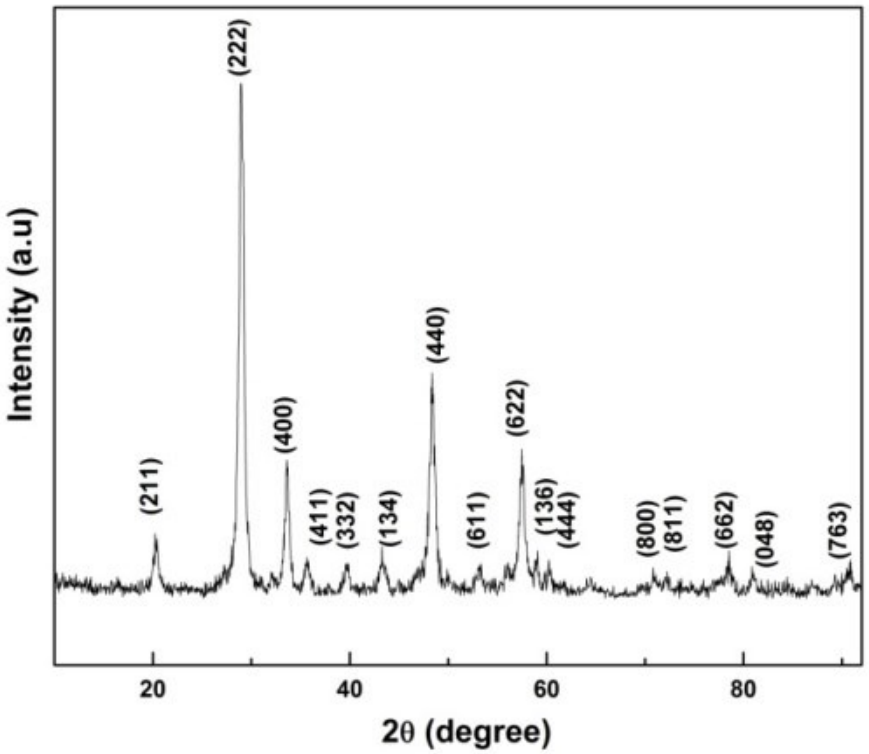

Fig. 5.3.3: XRD pattern of Y_2O_3 powder.

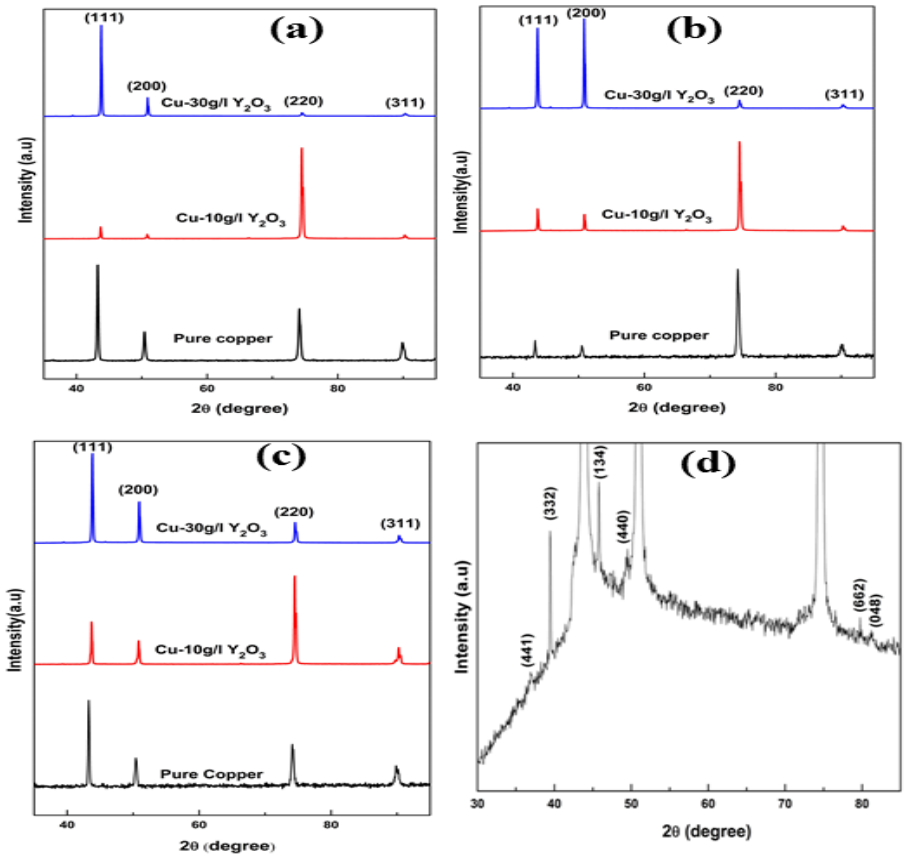

Fig. 5.3.4: XRD patterns of samples deposited with 10 and 30g/l Y_2O_3 in (a) DC and PC condition with (b) 5 and (c) 10 kHz frequency, (d) enlarged view of XRD plot of Cu-30g/l Y_2O_3 coating with 10 kHz.

Table 5.3.1: Relative Texture Coefficient ($RTC_{(hkl)}$) of different Cu-Y_2O_3 coatings and pure Cu coating

Sample Type	Sample Details	$RTC_{(hkl)}$%			
		(111)	(200)	(220)	(311)
Cu deposition	DC	16	09	45	30
	PC(1 kHz)	15	50	22	13
	PC(5 kHz)	03	04	81	12
	PC(10 kHz)	17	12	47	24
Cu-Y_2O_3 coating	10 g/l, DC	03	02	91	04
	10 g/l, PC(1 kHz)	27	06	54	13
	10 g/l, PC(5 kHz)	04	07	83	06
	10 g/l, PC(10kHz)	06	08	70	16
	30 g/l, DC	57	24	10	09
	30 g/l, PC(1 kHz)	36	19	27	18
	30 g/l, PC(5 kHz)	25	59	11	05
	30 g/l, PC(10kHz)	27	28	31	14

5.3.4 Microstructural and elemental studies

The surface morphologies of the Cu-Y_2O_3 composite coatings with variation of second phase Y_2O_3 particle and different process parameters were observed under a field emission scanning electron microscope (FESEM) and the images are displayed in Fig. 5.3.5. Fig. 5.3.5 (a-c) and (d-f) represent Cu-10g/l Y_2O_3 and Cu-30g/l Y_2O_3 coatings respectively, deposited with different pulsing conditions. It is clearly observed that the morphologies of the composite coatings are significantly influenced by pulse parameters and the addition of Y_2O_3 in the plating bath. From the figures it can be noticed that higher Y_2O_3 content tends to make the matrix marginally finer at higher pulse frequency. Oxide dispersion acts as heterogeneous nucleation site of Cu resulting in finer structure when Y_2O_3 is added. Thus, addition of ultrafine Y_2O_3 particles in deposits influences the competitive formation of copper nuclei and crystal growth. That means more nucleation sites are available for the copper ions and crystalline growth is less prevalent during electro-co-deposition.

At direct current and low pulse frequency (1 kHz) deposition both 10 and 30g/l Y_2O_3 coated specimens show large granular structure with well-defined grain boundaries. As pulse frequency was increased from 5 to 10 kHz the surface structure changed to colonies of fine granular features with dense structure. The coating deposited with highest pulse frequency (10kHz) exhibited well-refined granular structure with more uniform and finer matrix, which leads to better mechanical properties. Pulsing and higher pulse frequency possibly leads to formation of newer nuclei at each pulsing cycle that results in uniform fine structure.

Fig. 5.3.6 displays the average grain size vs. deposition conditions. The plot describes decrease in grain size with increase in second phase particle dispersion and pulse frequency as explained earlier.

Fig. 5.3.7(a) and (c) show SEM images of Cu-30g/l Y_2O_3 composite coating prepared with pulse frequency of 10 kHz and the corresponding X-ray mapping of Y respectively to confirm the presence of Y_2O_3 in the coating. Similarly Fig. 5.3.7(d) shows the X-ray mapping of Y on cross sectional view of the same specimen as displayed in Fig. 5.3.7(b). So, along with the coated surface, the cross section also shows homogeneity in distribution of Y_2O_3 particles.

Few Y spots were observed in other places of Fig. 5.3.7(d) due to dislodging of embedded of Y_2O_3 particles for grinding and polishing operation during cross sectional sample preparation.

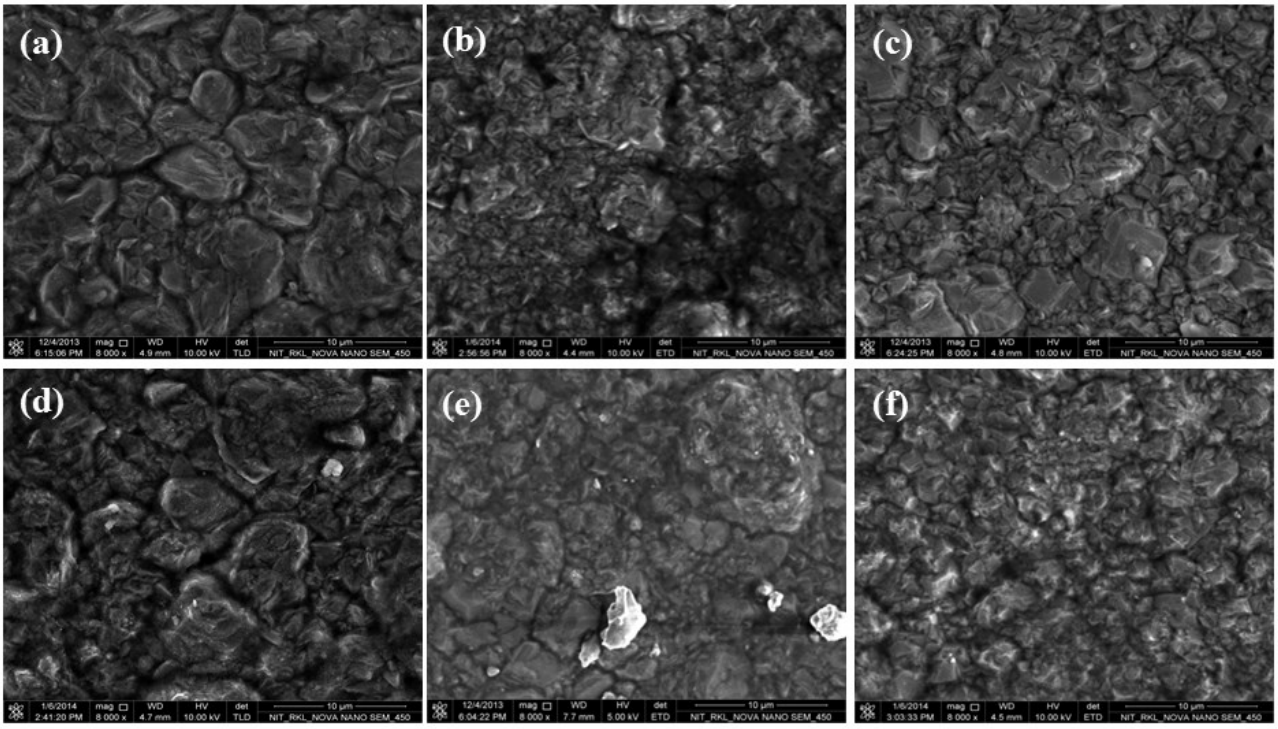

Fig. 5.3.5: FESEM images of Cu-10g/l Y_2O_3 (a, b and c) and Cu-30g/l Y_2O_3 (d, e and f) without pulsing, with pulsing rate of 5 and 10 kHz respectively.

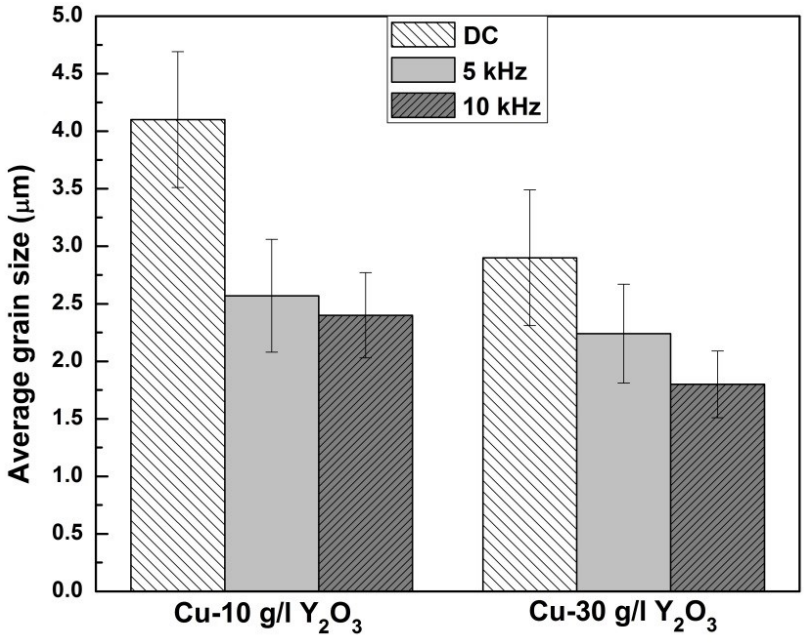

Fig. 5.3.6: Average grain size vs. deposition conditions of all deposited specimens.

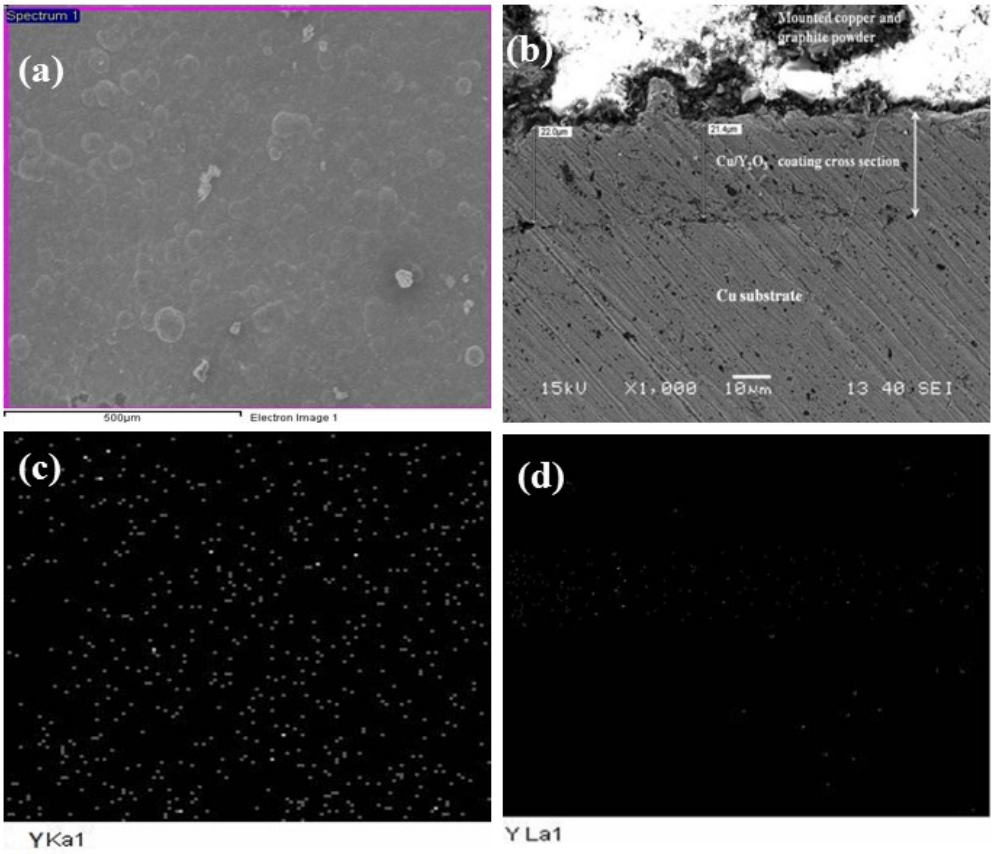

Fig. 5.3.7: SEM image of (a) Cu-30g/l Y_2O_3 deposited sample with 10 kHz pulsing rate and (b) its cross section; (c) and (d) show X-ray mapping of respective SEM images.

Fig. 5.3.8(a) shows the energy dispersive spectra (EDS) of Cu–Y_2O_3 composite coating deposited with 30 g/l Y_2O_3 particle loadings. The EDS result confirmed the detection of Cu, Y and O elements. Elemental analysis from such spectra was carried out for all the samples. The amount of Y was converted to equivalent amount of Y_2O_3 using the stoichiometric ratio of yttrium and oxygen as per chemical formula of Y_2O_3. The wt.% of Y_2O_3 present in the deposits as a function of Y_2O_3 particle loadings is plotted in Fig. 5.3.8(b). It was found that the Y_2O_3 particle content was increased with increasing loading level of Y_2O_3 particle in electrolyte. Moreover, it can also be observed that PC coatings contain more Y_2O_3 than DC and with increasing pulse frequency, it increases further. The trend is similar to the reports mentioned earlier by other researcher [132]. In case of DC deposition or PC deposition with lower frequency, the replenishment of the diffusion layer is less, which results in higher

amount of particle incorporation at higher pulse frequency. Thus, it is understood that higher content of Y_2O_3 can be obtained by increasing the powder concentration in the plating bath and pulse frequency in PC mode.

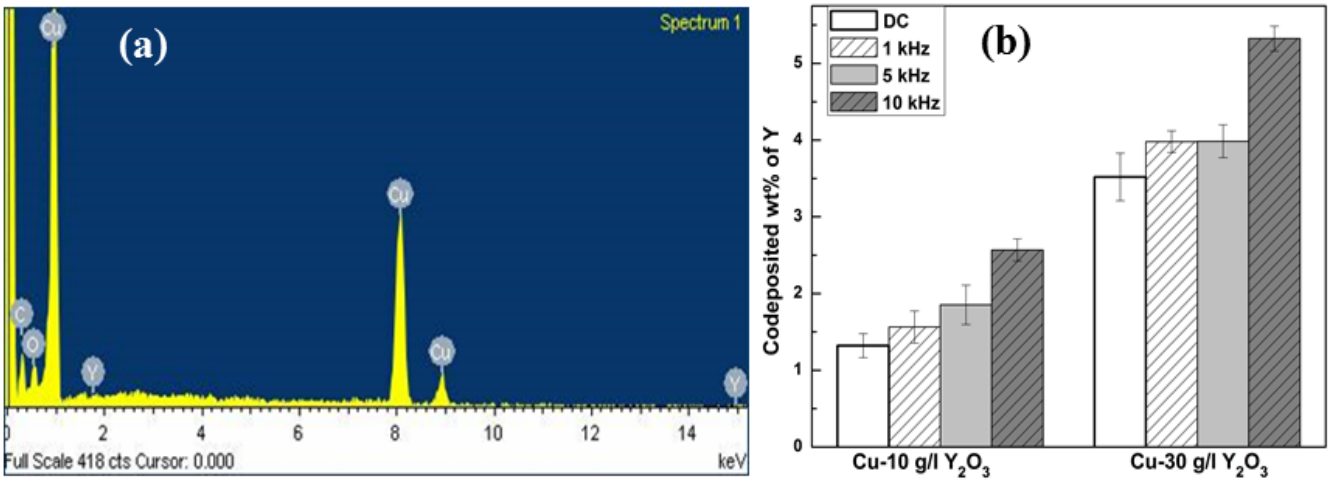

Fig. 5.3.8: (a) EDS of 30g/l Y_2O_3 coating surface with (pulsing rate 10 kHz) and (b) Co-deposited wt% of Y_2O_3 in Cu-10g/l Y_2O_3 and Cu-30g/l Y_2O_3 deposited samples.

Fig. 5.3.9 shows cross sectional view of Cu–30g/l Y_2O_3 composite coatings prepared in DC and PC mode. Coating thickness was found to be higher in direct current deposition than pulsed deposition. This is attributed to the fact that in pulsed deposition the actual time for ion and particle migration is less and is highly dependent on duty cycle compared to direct current (DC) deposition. Moreover, with increase in pulse frequency from 5 (Fig. 5.3.9(b)) to 10 kHz (Fig. 5.3.7(c)), the coating thickness was also decreased from approximately 25 to 22 µm. With increasing frequency the number of deposition cycle increases keeping total on time same as it is dependent on duty cycle only. And in each cycle the copper ion and oxide particles require fresh momentum for migration towards the cathode substrate. As a result lower thickness was observed in case of 10 kHz pulse frequency.

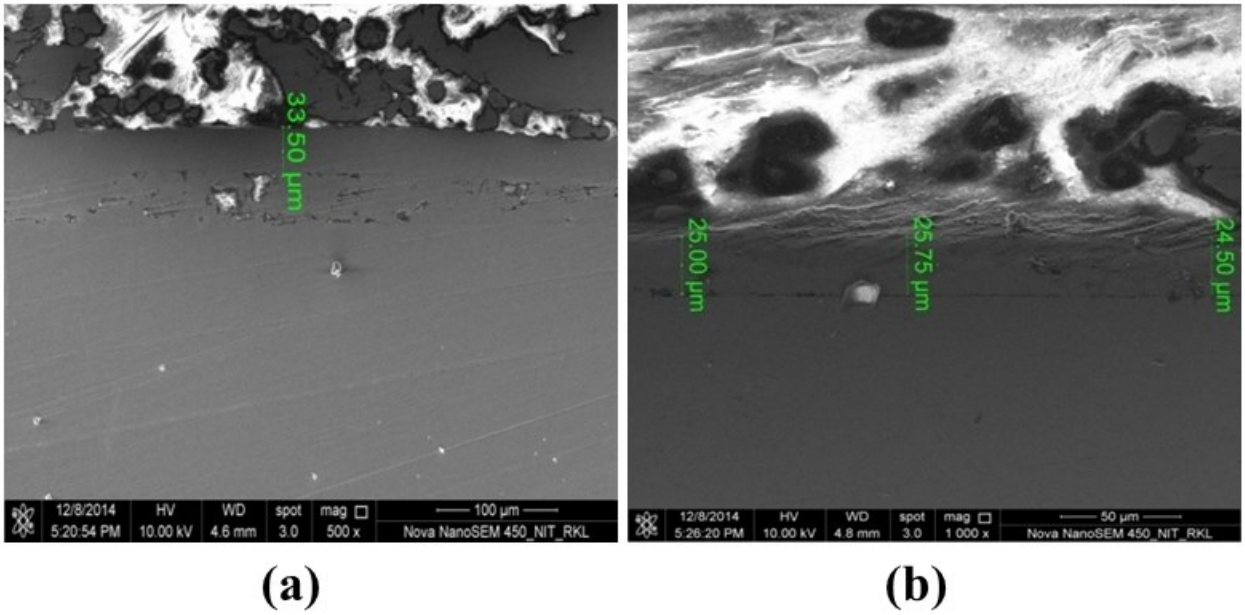

Fig. 5.3.9: Cross-sectional view of Cu-30g/l Y_2O_3 composite coating with (a) DC deposition, (b) 5 kHz pulsed deposition.

5.3.5 Surface roughness study

Conduction of electron through electrical contacts depends on their actual surface area in contact which in turn depends on their surface roughness. Higher roughness represents less contact surface leading to lower conductivity and temperature rise. In view of this, all the Cu-Y_2O_3 deposited surfaces were characterized to calculate the average surface roughness (*Ra*) of the same. The *Ra* values of all the deposited specimens with variations of second phase ultrafine Y_2O_3 and different pulsing parameters are presented in Fig. 5.3.10.

All the calculated values were within the range of 0.14 to 0.8µm, which is quite relevant for application purpose in electrical contacts. From the figure it can be observed that in each deposition condition (DC or PC with particular frequency) except 5 kHz, with increase in Y_2O_3 content in the deposition bath the surface roughness increases.

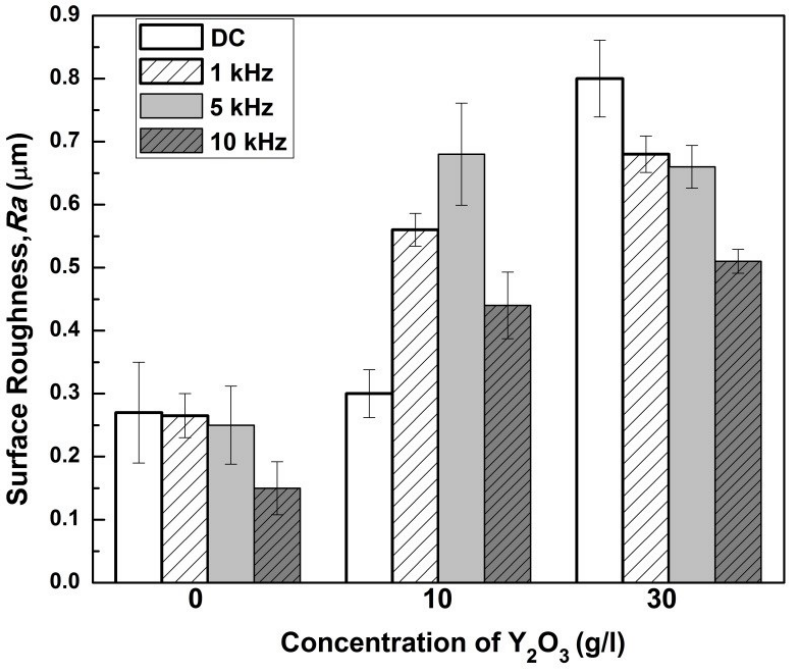

Fig. 5.3.10: Surface roughness of all Cu-Y_2O_3 deposited samples.

From Fig. 5.3.10 it can also be observed that compared to DC condition, all PC mode show lower roughness for 0 and 30g/l Y_2O_3 content; whereas, in case of 10g/l Y_2O_3, it shows higher roughness at intermediate range of frequencies. This can be explained by two possible reasons: (i) effect of Y_2O_3 content - incorporation more amount of ceramic particle in the matrix with more amount of dispersion in the bath (Fig. 5.3.8(b)) leads to roughness increase and (ii) effect of pulsing – pulsing and higher frequency of pulsing leads to finer matrix (Fig. 5.3.6(b)) resulting in lower roughness. Thus, change in bath composition and pulsing condition provides independent effects on roughness resulting in complex output without any generalized trend of roughness.

5.3.6 Microhardness study

Fig. 5.3.11 shows the effect of pulse frequency and ultrafine ceramic second phase particle content on microhardness of Cu-Y_2O_3 composite coatings. The hardness values obtained for the composite coatings (Cu-Y_2O_3) are higher than pure copper coating for all pulsing conditions. Moreover, pulsed deposition shows better hardness than DC deposition

irrespective of the compositions. Hardness increases with increasing value of Y_2O_3 amount and pulse frequency. The microhardness reaches its maximum value 222.3 HV at 30g/l Y_2O_3 content with 10 kHz pulse frequency. The strengthening mechanisms for the Cu–Y_2O_3 composite coating can be attributed to two factors: (1) grain refinement strengthening from finer Cu matrix with increase of pulse frequency and Y_2O_3 content and (2) dispersion strengthening caused by ultrafine Y_2O_3 particles. Moreover, it is worth mentioning that as seen from Fig. 5.3.7(b), the Y_2O_3 particles are well dispersed in the Cu matrix. In some cases formation of (111) orientation can be partially attributed to the improved hardness in Cu-30g/l Y_2O_3 composite coating.

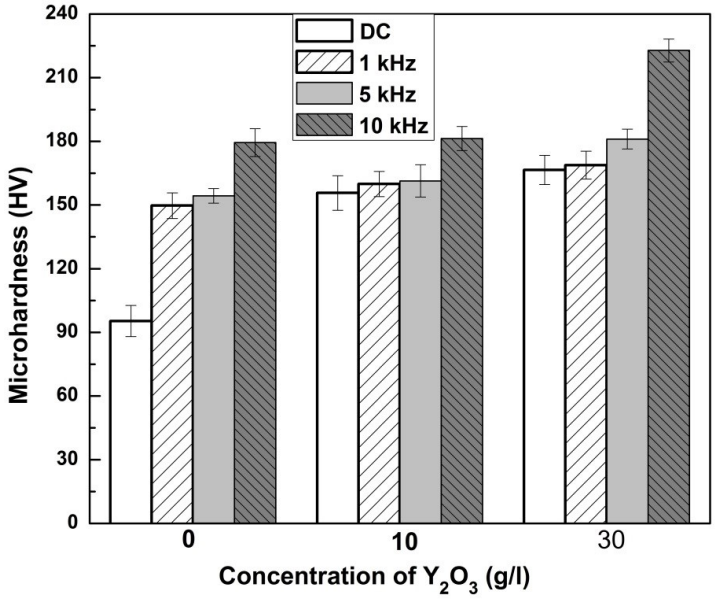

Fig. 5.3.11: Micro hardness of Cu-Y_2O_3deposited samples.

5.3.7 Wear study

Fig. 5.3.12(a) shows the comparable wear loss graphs (in terms of vertical penetration of the steel ball or wear depth) as a function of sliding distance of all composite coated samples, deposited with direct current and different pulse frequencies and penetration rate observed during the tests. From Fig. 5.3.12(a) it can be observed that pulsed coatings show less wear loss compared to DC coating. Moreover, wear resistance increases with addition of more amount of Y_2O_3 in the coating. The trend of wear plots is similar to that of hardness data.

Composite coating obtained by high frequency pulsed deposition is thus successful in showing better surface mechanical properties.

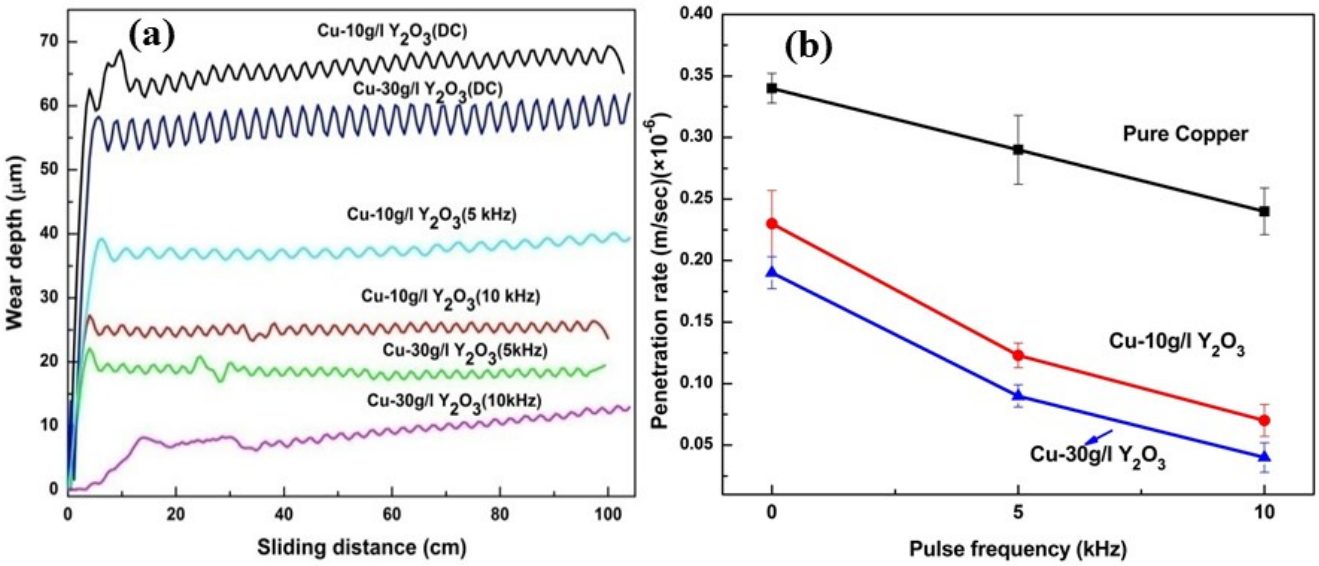

Fig. 5.3.12: Plot of sliding distance vs. cumulative wear depth obtained from (a) Cu-Y_2O_3 coated samples; (b) penetration rate of all deposited specimens measured during wear test.

Fig. 5.3.12(b) represents the variation of penetration rate (penetration depth/time) of Cu-Y_2O_3 composite deposits with different pulsing parameter as well as Y_2O_3 concentrations. This parameter can be considered equivalent to that of wear rate (weight loss/sliding distance or time) in standard ball on plate type wear test. The penetration rate shows highest value of 0.26 m/Sec (low wear resistance) in pure copper coating with DC deposition followed by Cu-10g/l Y_2O_3 and Cu-30g/l Y_2O_3 respectively at same deposition condition. Lower penetration rate was observed as 0.05 m/Sec in case of Cu-30g/l Y_2O_3 at 10 kHz pulse frequency. When pulse frequency was increased from 0 to 5 and 10 kHz, penetration rate showed decreasing trend. In other words, it can be explained as penetration rate is inversely proportional to pulse frequency as well as concentrations of Y_2O_3 particles added to the bath. The reason of lower penetration depth (higher wear resistance) with increasing amount of yitria concentration and pulse parameter can be attributed to dispersion hardening caused by dispersed second phase Y_2O_3 particles and nucleation mechanism due to pulsing.

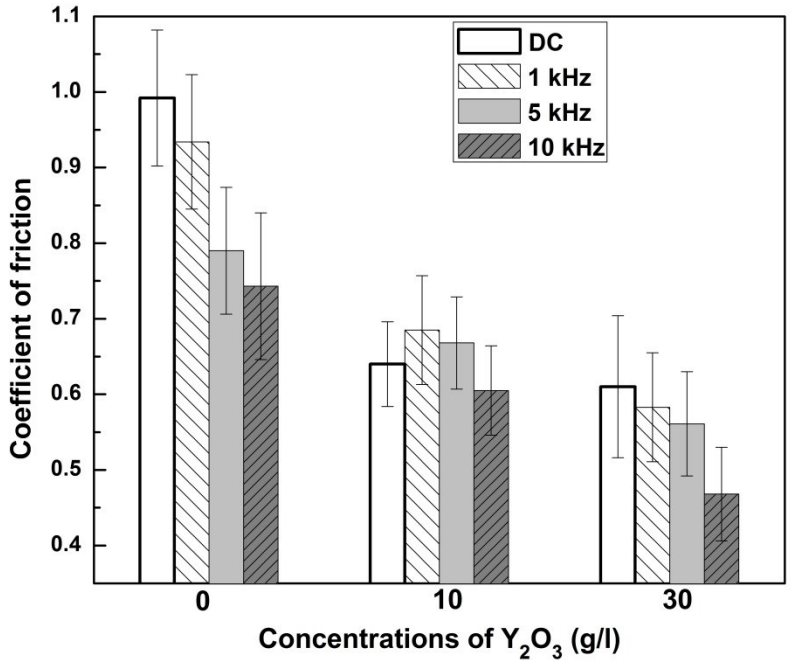

Fig. 5.3.13: Co-efficient of friction measured during wear test.

The friction coefficient of all the coatings as a function of deposition condtions are displayed in Fig. 5.3.13 . The figure depicts that friction coefficient merasured during wear test decreses with increasing amount of Y_2O_3 and pulse frequency for 0 and 30g/l Y_2O_3. The trend is attributed towards better surface mechanical property and finer grain size of the coating prepared with these specified conditions. It is also clear from the friction data that the friction coefficient and wear resistance of Cu–Y_2O_3 composite coatings are closely related with Y_2O_3 content in the deposited specimen as well as with pulse paramter. Moreover, though, ideally friction coefficiend and surface roughness can be correlated, in the present study the trends are not exactly same. Coefficient of friction depends on surface roughness and material property. Here, surface rougness is affected by mtrix grain size and incoporated particle amount. During wear testing the major fraction of dislodged Y_2O_3 particles can be displaced away resulting in lower value of roughness at run time which in turn lowers the steady state value of co-efficient of friction.. Thus, with increasing pulse frequency the friction co-efficient decreases in general. But in case of 10g/l Y_2O_3, the trend is not exactly same, which can be attributed by the complex effect as discussed in the surface roughness section. The SEM micrographs of worn out surfaces of the Cu, Cu–10g/l Y_2O_3 and Cu–30g/l Y_2O_3

composite coatings are shown in Fig. 5.3.14. In case of pure Cu coating (Fig. 5.3.14(a)), abrasive grooves can be observed on the worn surface with signifacntly wider track (424 µm) than composite coatings (Fig. 5.3.14 (b and c)). This reveals that wear resistance of the pure copper coating is rather weak. With addition of Y_2O_3 and higher Y_2O_3 content the wear track widtyh decreases resuting in better wear resistance. Similar trend was also observed in case of DC and 5 kHz deposition conditions.

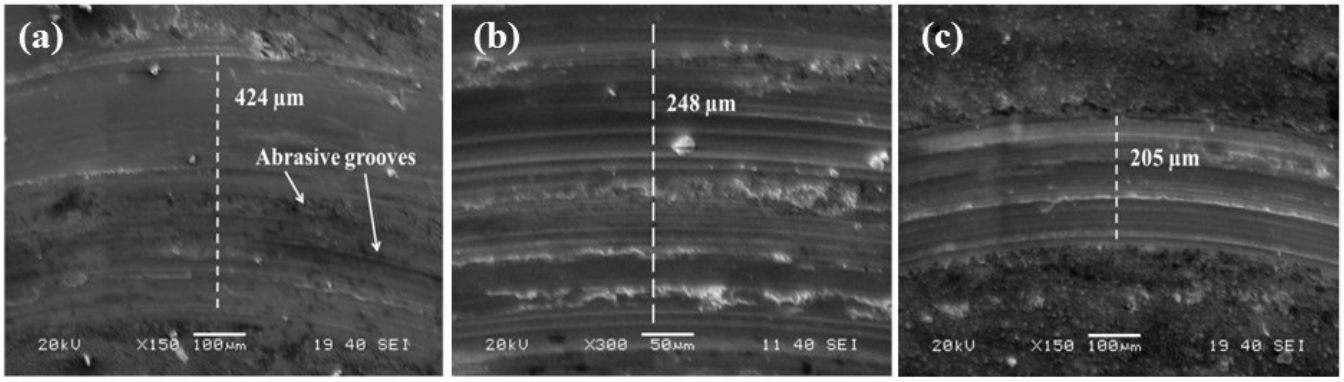

Fig. 5.3.14: SEM micrographs of worn wear track of (a) pure copper, (b) Cu-10 g/l Y_2O_3 and (c) Cu-30 g/l Y_2O_3 coating at 10 kHz pulse frequency.

5.3.8 Oxidation behavior

Isothermal oxidation study of Cu and Cu-30g/l Y_2O_3 coatings were carried out at 540^oC (approximately 60 percent of melting temperature of pure copper in Kelvin) to compare their oxidation properties. Moreover, Cu-30g/l Y_2O_3 coating was subjected to similar study at 675^oC (approximately 70 percent of melting temperature of pure copper in Kelvin) to compare the effect of oxidation temperature on this composite coating. All such tests were carried out for 20 h and mass gain results are shown in Fig. 5.3.15(a).The figure shows that Cu–Y_2O_3 composite coating exhibited better oxidation resistance than the as-deposited copper coating at 540^oC. Moreover, Fig. 5.3.15(a) also depicts that when the oxidation temperature was raised from 60% to 70% of melting point (540 to 675 ^oC), the change in mass gain during oxidation of Cu-30 g/l Y_2O_3 coating deposited with 10 kHz frequency was marginal. Better oxidation response of the composite coatings may be attributed towards the compact structure (Fig. 5.3.5) and presence of Y_2O_3 in the microstructure (Fig. 5.3.8). These lead to less oxygen diffusion during heating of the composite coatings in oxidizing atmosphere.

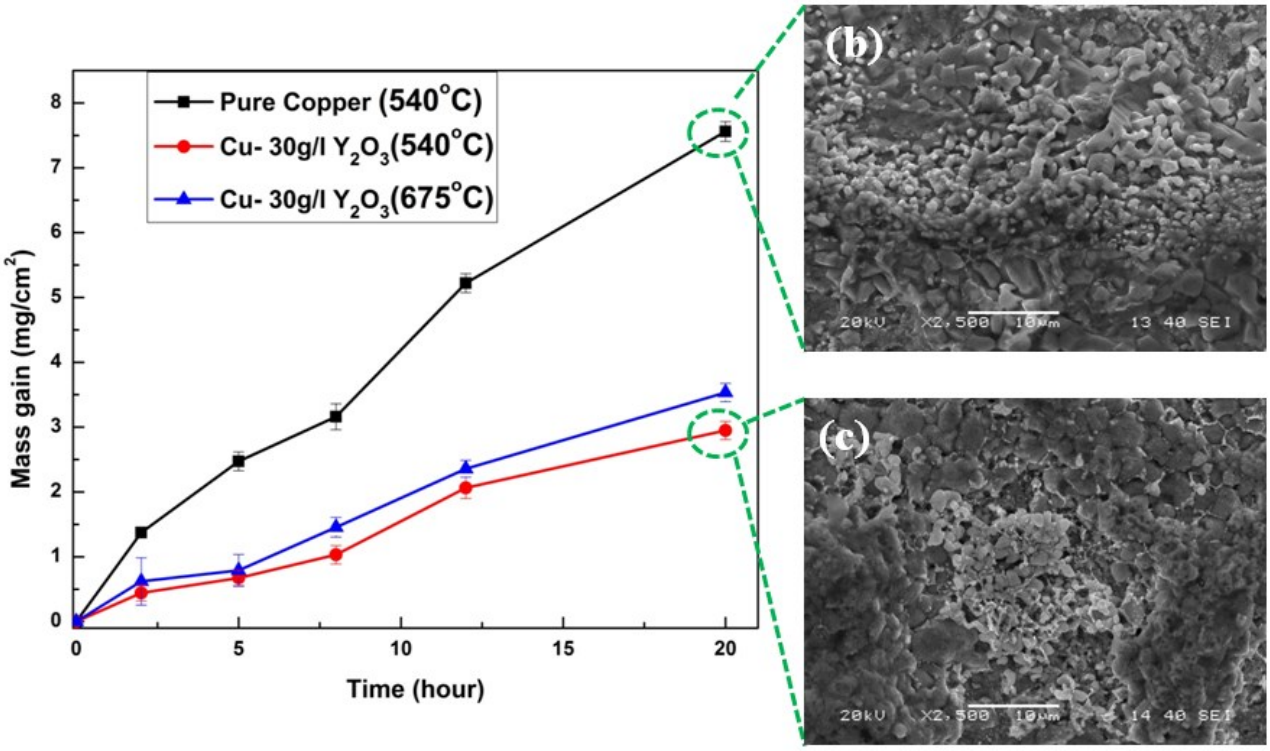

Fig. 5.3.15: (a) Isothermal oxidation behavior plots and (b, c) post oxidation surface micrographs of pure copper (at 540 ^{o}C) and Cu-30g/l Y_2O_3 (675 ^{o}C) deposited specimens prepared at 10 kHz.

Further, to clarify the difference in the oxidation performance of pure copper and Cu-30g/l Y_2O_3 composite coating, surface morphologies of the scales formed after 20 hours of oxidation were investigated and presented in Fig. 5.3.15(b) and (c). Both the figures comprise of common oxidized appearance but the growth of oxide layer is irregular due to faster kinetics in Fig. 5.3.15(b) (pure Cu coating) compared to Fig. 5.3.15(c) (composite coating).

5.3.9 Electrical conductivity

Electrical conductivity of the coatings in percentage of International Annealed Copper Standard (IACS) with variation of pulse frequency and Y_2O_3 concentration in bath is reported in Fig. 5.3.16. It was found that electrical conductivity value decreases with increasing pulse frequency and Y_2O_3 content. The decreasing trend in electrical conductivity can be attributed to the presence of higher Y_2O_3 content in the deposit and finer matrix of the composite specimens. It is worth mention that electrical conductivity of pure copper (used as substrate)

was 2.24×10^7 S/m, whereas, Cu-Y_2O_3 composite coating showing lowest conductivity amongst all the coatings in the in present study was 1.131×10^7 S/m. Thus, in spite of the drop in electrical conductivity, the values are in the same order. So, for actual applications, optimization of surface mechanical and electrical properties can be made as per the actual requirement by controlling the deposition parameters.

Oxidation/degradation of Cu based components even at room temperature is common phenomena. Thus, to judge the electrical property of the developed coatings after certain service live, the oxidized samples were tested for their electrical conductivity. Table 5.3.2 displays electrical conductivity values measured at different spots on coatings after thermal oxidation. Conductivity value mentioned at each spot is average of five readings. Due to uneven oxidation of the coating surface, conductivity values reported at different spots are widely varying which can be observed from table 5.3.2. As per the table, pure copper coating shows average 13-24% drop in IACS value of electrical conductivity after thermal oxidation at 540^{o}C, whereas, in case of Cu-30g/l Y_2O_3 coating, at same temperature, the average drop is approximately 1-7.5%. Cu-30g/l Y_2O_3 sample oxidized at 675^{o}C shows only 1.5-7.7 % drop, which is better than pure copper coating oxidized at 540^{o}C. From the obtained results, it is evident that composite coatings developed in the present study can retain their electrical property in a better way after thermal exposure of the same or even after a long service life.

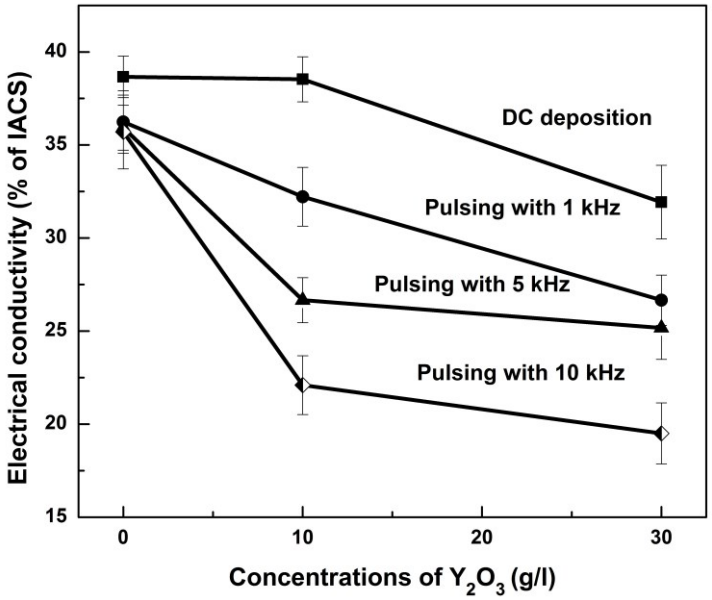

Fig. 5.3.16: Electrical conductivity of all deposited specimens.

Table 5.3.2: Electrical conductivity of pure copper coating and Cu-30g/l Y_2O_3 composite coating (10 kHz) after thermal oxidation

Average Electrical Conductivity (% of IACS)								
Before Oxidation (Refer Fig. 5.3.16)		After Oxidation						
			Spot-1	Spot-2	Spot-3	Spot-4	Spot-5	Spot-6
Pure Copper	35.85	Oxidation at 540 ^oC	22.8	17.6	15.7	11.79	13.5	14.9
Cu-30g/l Y_2O_3	19.62	Oxidation at 540 ^oC	18.64	13.2	15.45	12.1	14.8	16.5
		Oxidation at 675 ^oC	18.12	14.5	14.95	14.52	11.9	15.46

5.3.10 Summary

The current work is based on co-deposition of Cu-Y_2O_3 on copper substrate from acidic copper sulfate bath with incorporation of ultrafine Y_2O_3particles by direct and pulsed direct current mode in different pulse condition as well as bath concentrations. From the detailed investigated results, the following conclusions can be drawn:

- Cu-Y_2O_3 deposition was successfully developed on copper substrate.
- Higher Y_2O_3 content in electrolyte tends to increase Y_2O_3 content in the deposits, which results in better hardness and wear resistance.
- Higher hardness and better wear resistance properties of codeposited coatings were attributed to finer matrix and more amount of embedded Y_2O_3 particles resulted by pulsing mode with higher pulse frequency conditions as well as some texture effect.
- Better oxidation resistance was found in composite coatings due to better microstructure.
- Minor decrease in electrical conductivity of composite coatings was observed due to presence of Y_2O_3 and finer matrix.
- The present method can be considered as useful to improve surface properties of electrically used copper components.

Chapter 6

Effect of texture and microstructure on hardness and electrical conductivity of electrodeposited Cu-SiO_2 and Cu-Y_2O_3 coatings

6.1. Introduction

In this chapter detailed texture analysis of Cu-SiO_2 and Cu-Y_2O_3 coatings were carried out. In earlier chapters it was observed that coating parameters influence the texture of the coating matrix and the surface-mechanical properties of the obtained coating. So, aim of such a detailed crystallographic characterization was to determine the effect of DC and pulse parameters as well as second phase oxide nanoparticles (SiO_2 and Y_2O_3) on orientation development and their influence on mechanical and electrical behavior of the developed coatings. Detailed of bath composition and deposition parameters used in the present study are presented in table 6.1.

Table 6.1: Plating bath composition and deposition parameters

Electrolyte (Acidic copper sulfate bath)	Copper Sulfate ($CuSO_4.5H_2O$): 200 g/l Sulfuric acid (H_2SO_4): 50 g/l
pH	2.17(±0.02)
Current density	8A/dm^2
Pulse parameter/condition	No pulse (DC) and 5 and 10 kHz with 30% duty cycle
Temperature	Room temperature
Plating time	60 minutes
Dispersion	SiO_2 / Y_2O_3: 30 g/l

6.2 XRD analysis

Fig. 6.1(a-c) show the XRD spectra of the prepared pure copper, Cu-SiO_2 and Cu-Y_2O_3 coatings under various deposition conditions (DC, Pulsing 5 and 10 kHz) respectively. All Cu peaks were assigned in the deposits by JCPDS (card no. 04-0836) data. Some peaks are assigned as SiO_2 in Cu-SiO_2 composite coating due to the presence of silica at 5 and 10 kHz pulse frequency. In case of Cu-Y_2O_3 composite coating no Y_2O_3 peak was observed, but by enlarging the XRD profile of the composite coating small Y_2O_3 peaks were observed. Lattice strain of the developed coatings was calculated by the following formula [139] and the values were tabulated in table 6.2.

$$\delta\% = \frac{d_{substrate} - d_{coating}}{d_{substrate}} \times 100 \qquad (1)$$

Where $d_{substrate}$= d-spacing of the particular plane in the substrate (Cu), $d_{coating}$= d-spacing of the same plane in the coating specimen (Cu matrix).

Table 6.2: Lattice strain (%) of developed coatings

Samples	**Planes**			
	(111)	**(200)**	**(220)**	**(311)**
Pure Cu (DC)	0.484	0.562	0.506	0.505
Pure Cu (5 kHz)	1.650	1.630	1.014	0.855
Pure Cu (10 kHz)	1.278	1.195	0.811	0.685
Cu-SiO_2 (DC)	0.576	0.614	0.494	0.481
Cu-SiO_2 (5 kHz)	0.913	0.844	0.613	0.556
Cu-SiO_2 (10 kHz)	1.110	1.073	0.796	0.686
Cu-Y_2O_3 (DC)	1.205	1.218	0.863	0.743
Cu-Y_2O_3 (5 kHz)	1.435	1.307	0.912	0.735
Cu-Y_2O_3 (10 kHz)	1.862	1.632	1.044	0.843

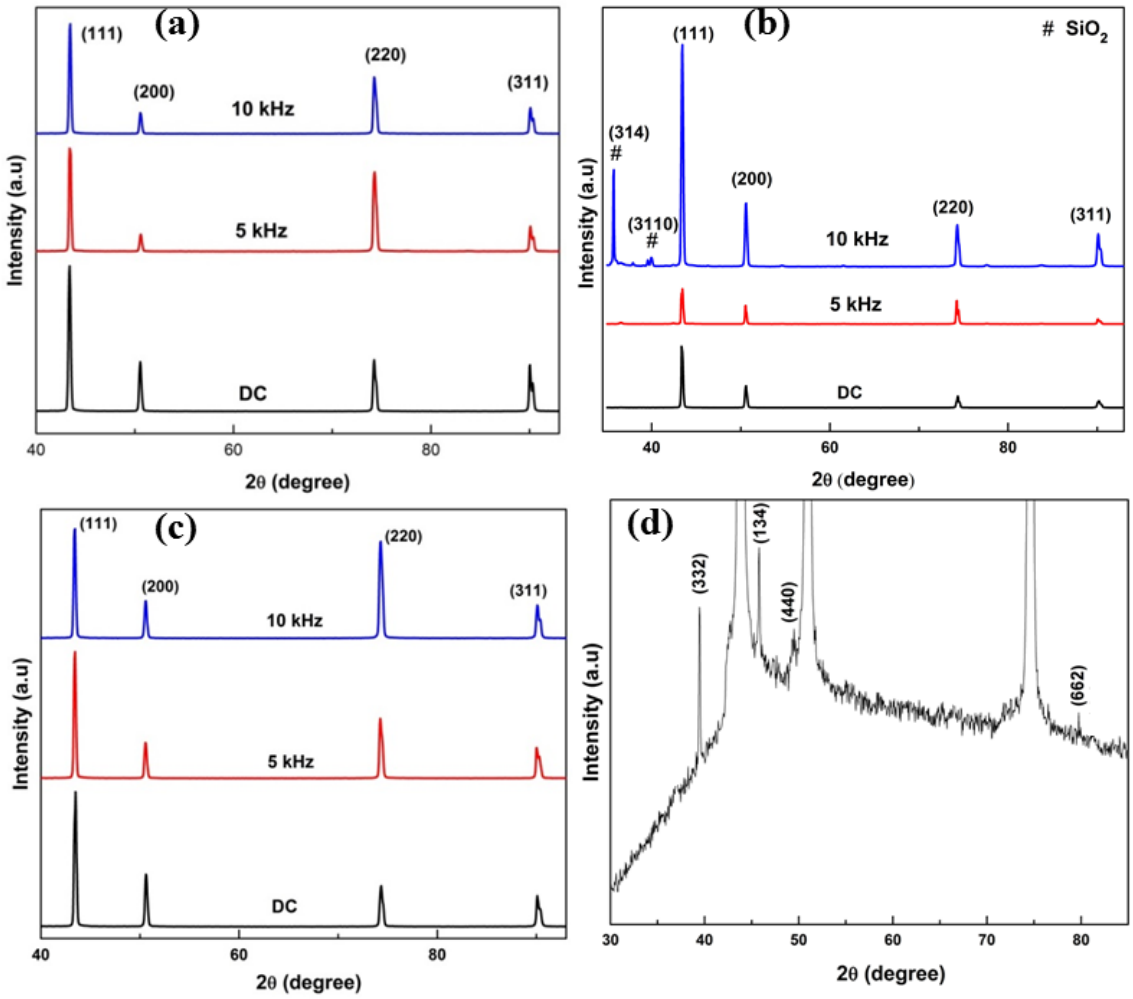

Fig. 6.1: XRD pattern of (a) pure copper (b) Cu-30 g/lSiO_2 and (c) Cu-30 g/lY_2O_3 coatings (d) enlarge view of Cu-Y_2O_3 composite coating.

From the table it was observed that lattice strain increased with changing of deposition conditions from DC to 5 kHz pulse frequency and further increased in 10 kHz pulsing in case composite coatings, but in pure copper coating strain is higher at 5 kHz pulse frequency followed by 10 kHz and DC deposition.

6.3 Texture study

Fig. 6.2 shows the texture development of electrodeposited copper coatings in terms of (111), (200) and (220) pole figures as a function of deposition conditions such as DC, 5 and 10 kHz pulse frequency. It can be clearly witnessed that [111] fibre texture was developed at the DC

electrodeposition. However, when the electrodeposition condition was changed to pulse frequency of 5 and 10 kHz, the initial intensity of [001], [110] and [111] orientations were decreased with the increase in pulse frequency, but the [111] orientation remained as preferred orientation.

The texture development in thin and thick coatings is largely depending upon the effect of the substrate and the influence of the surface energy on the growth rate [140]. During the deposition process strain energy, surface energy or a combination of both surface and strain energy and the energy arising from various interfaces are considered as controlling factors in the crystallographic texture formation of FCC metals [141]. In addition to this, the crystallographic texture of the coatings is also influenced by various process parameters such as *pH* of the electrolyte, surfactants, pulse frequency, applied current densities, the thickness of the deposits, and formation of stress/strain in the deposited specimens [142]. The change in crystallographic orientation from (111) to either (100) or (101) in most cases subject to the changes that happen during the deposition process [143, 144]. Besides this, the stability of the surface plane of the metal also has a great influence on evolution of crystallographic orientations [145, 146]. But, in general the stability of the individual surface plane of the FCC materials during texture formation follows the order (111) > (100) > (101) [147] due to the surface energies minimization in these metals follows the order $\gamma(101) > \gamma(100) > \gamma(111)$ [148]. Thus, due to minimization of energy, a dominant [111] fiber texture would be expected to develop during the electrodeposition process. This may be considered as the reason behind the development of [111] orientation in pure copper coating irrespective of deposition conditions or techniques used. The low surface energy of [111] orientation mainly driven by various factors such as the coordination number [149] and atomic density compared to (100) and (101) planes [150-152]. Low deposition temperatures and high current density are considered as another factors to minimize the surface and interfacial energies of the material, which favors growth of (111) orientation [153]. This can also be considered as partial explanation for formation of [111] orientation in pure Cu coating, because the current deposition process was carried out at high current density (8 A/dm^2) but not at low temperature. In the current study the temperature was maintained as room temp (30±5 ^oC) during the deposition process.

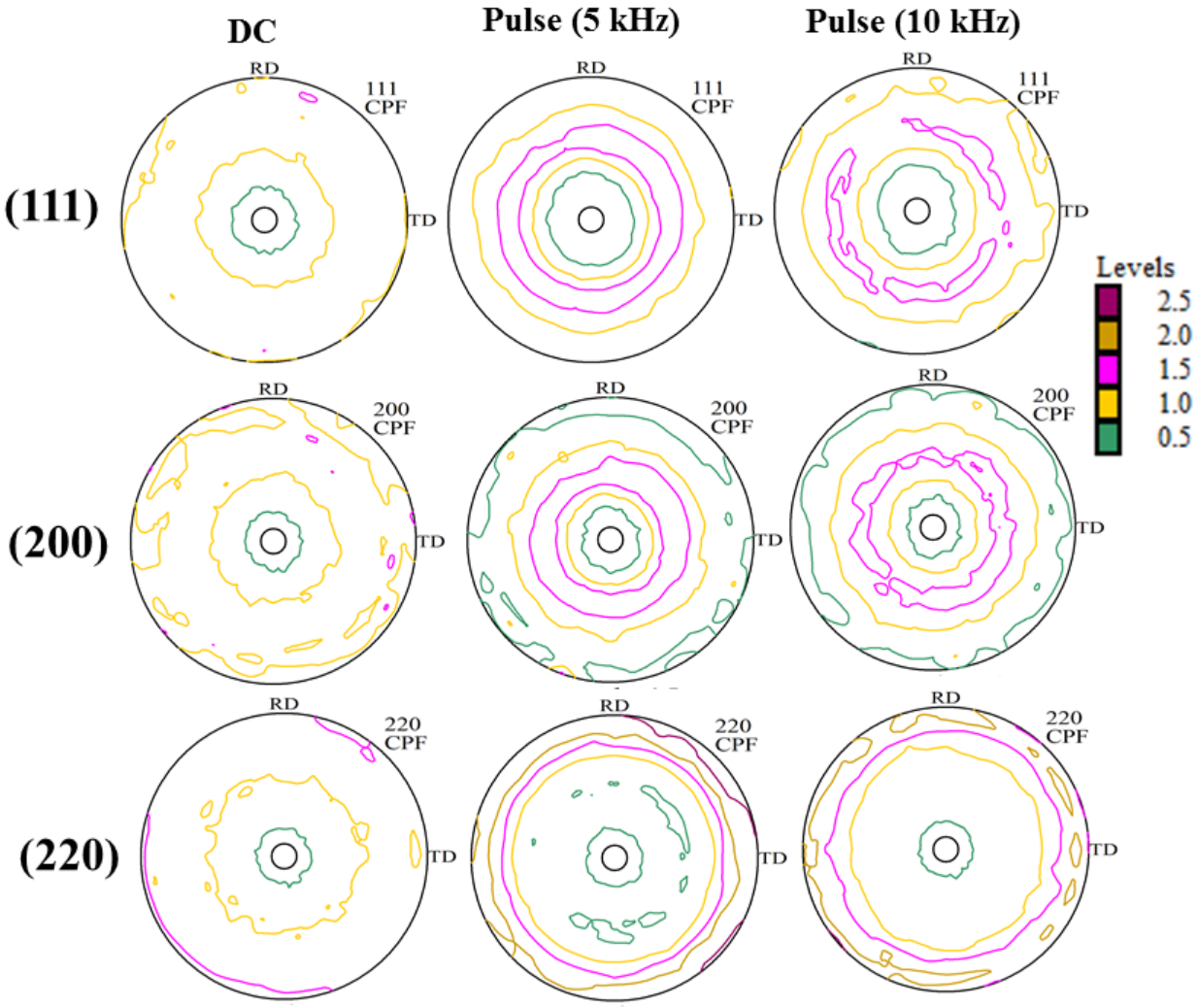

Fig. 6.2: (111), (200) and (220) pole figures of pure copper coatings with DC and pulse variation of 5 and 10 kHz.

Fig. 6.3 and 6.4 displays the (111), (200) and (220) pole figure of Cu/SiO_2 and $Cu\text{-}Y_2O_3$ composite coating respectively. From the pole figures (Fig. 6.3) development of random type texture was observed at DC deposition. However, with the change in deposition condition from DC to 5 kHz pulse the [111] fibre orientation was found to be increased whereas the other orientations ([001] and [110]) were decreased with the increase in pulse frequency. With further increase in pulse frequency to 10 kHz [111] fibre orientation was getting more preferred. Similar observations were also made in the case of $Cu\text{-}Y_2O_3$ composite coatings (Fig. 6.4).

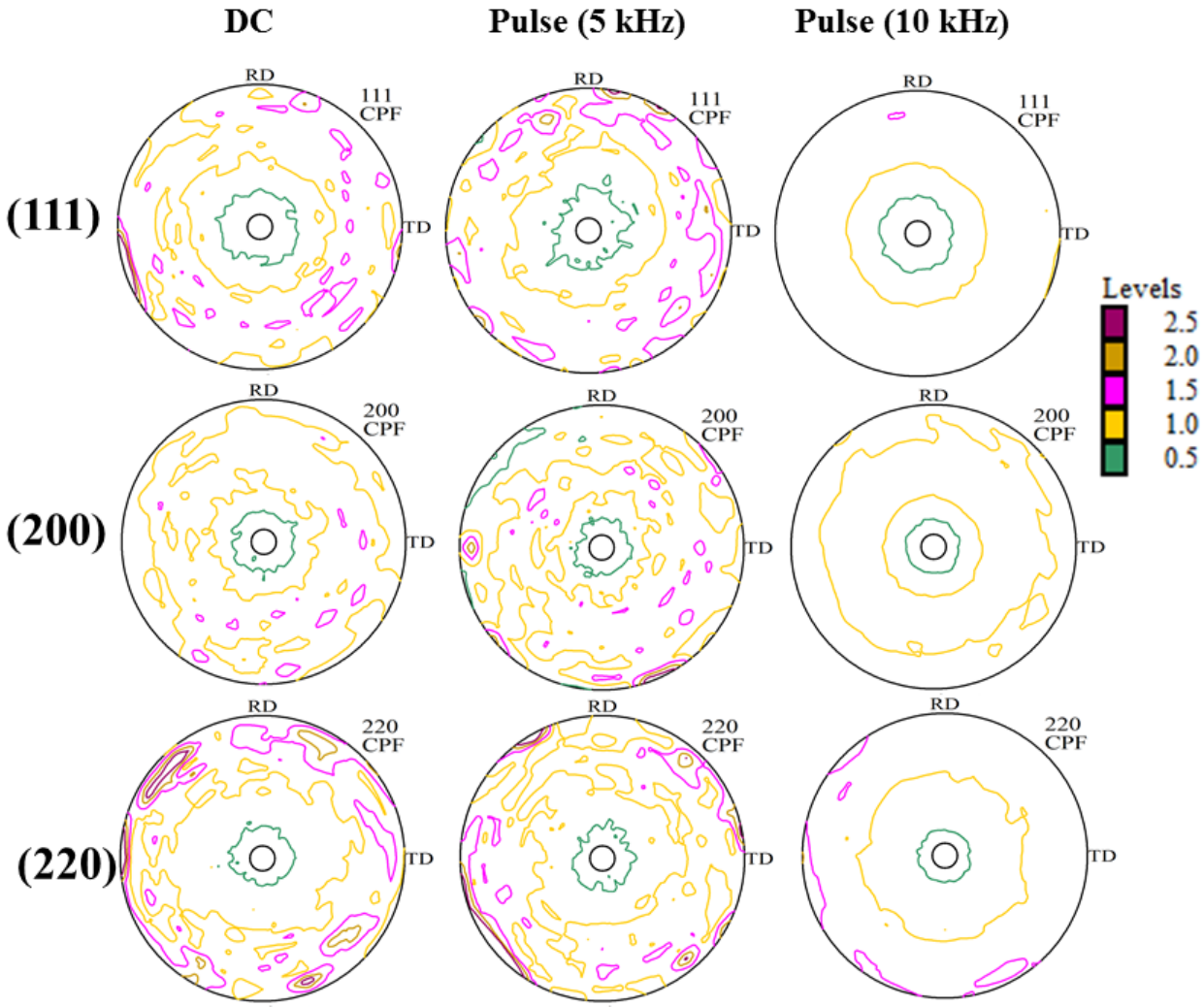

Fig. 6.3: (111), (200) and (220) pole figures of Cu-30g/l SiO_2 coatings with DC and pulse variation of 5 and 10 kHz.

Though, during deposition process, (100) orientation growth is favored slightly at larger off times [154] and (101) is known to be favored at very large off times [155]. This may be occurs by consuming the (111) grains resulting from the stress-driven recrystallization during pulse electrodeposition due to lower strain energies favored at high current densities [156].

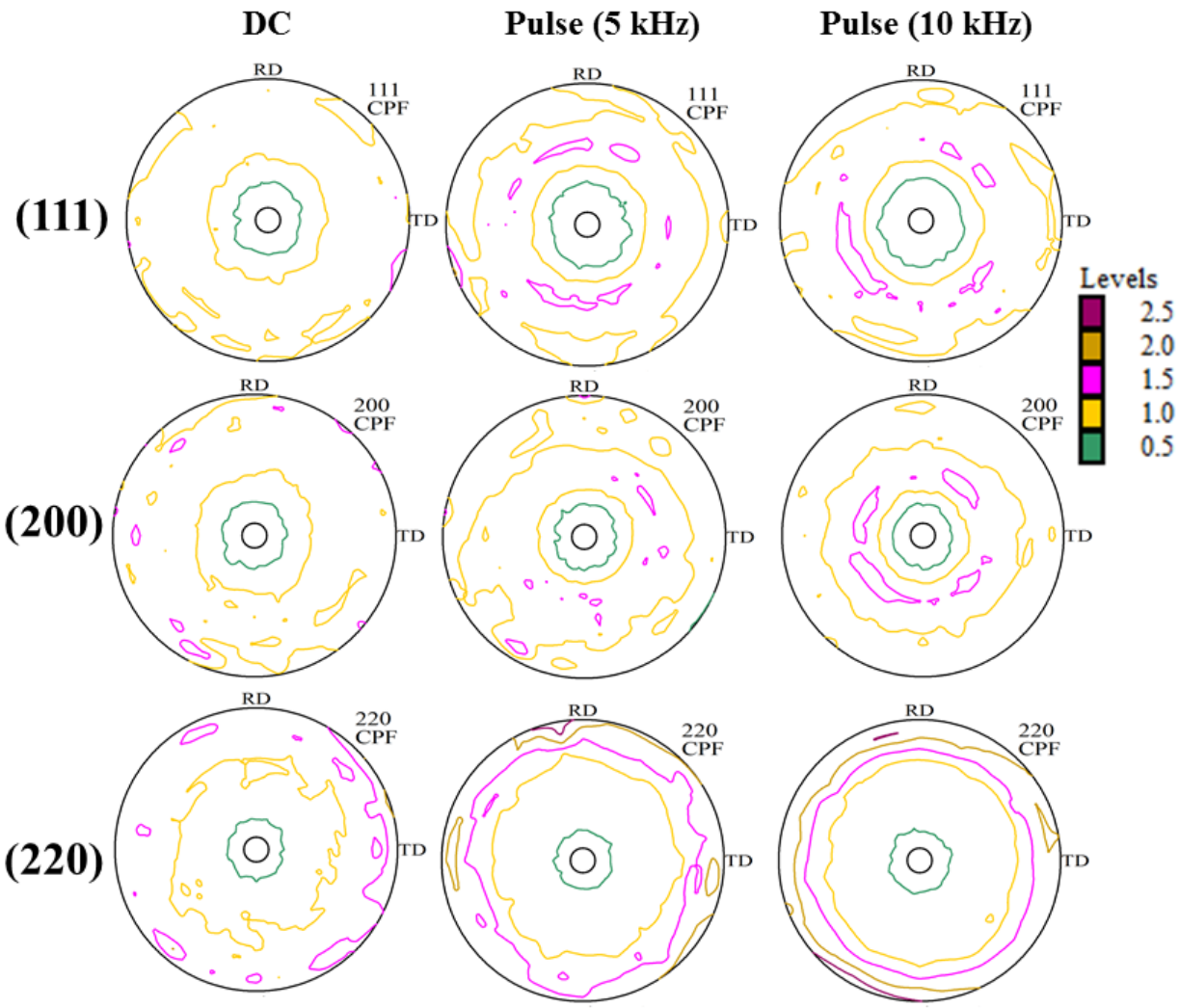

Fig. 6.4: (111), (200) and (220) pole figures of Cu-30g/l Y_2O_3 coatings with DC and pulse variation of 5 and 10 kHz.

High initial stresses caused by high applied current densities producing defects within the grains, which are directly associated with the strains leading to the development of texture. In addition, due to the lower atomic density in the plane and a large number of broken bonds, (101) texture is known to be more easily dissolved than (111) and (100) textures. Therefore, during PC deposition with longer off time formation of (101) texture is highly favorable [157]. But, in the current study depositions are carried out at high pulse frequency (5 kHz) means lower off time and further lower off time in case of 10 kHz creates higher strain

energy. The higher strain energy might be the cause of favoring [111] orientation at pulse electrodeposition in both (Cu-SiO_2 and Cu-Y_2O_3) composite coating systems.

To quantify the texture development in the deposited specimens, ODF figures of all the coatings are shown Fig. 6.5. The ODF figures are considered at $\phi_1 = 0^o$ and on ($\phi_2 - \phi$) plane. From the figure the development of [111] orientation along with [001] and [110] in pure copper coated specimens at DC electrodeposition was observed. The preferred [111] orientation was centered at $\phi_1 = 0^o$, $\phi_2 = 45^o$ and $\phi = 55^o$, whereas other two orientations [001] and [110] orientations centered at $\phi_1 = 0^o$, $\phi_2 = 3^o$ and $\phi = 5^o$ and $\phi_1 = 0^o$, $\phi_2 = 45^o$ and $\phi = 0^o$ respectively. Further, with increased pulse frequency, the [001] and [110] orientations became absent and the existence of only [111] orientation was observed. The higher intensity [111] fibre orientation was regarded as the final and main texture component in pure copper coated samples. From the ODF figure it was also observed that at DC deposition condition, the orientation distribution is more of a random in Cu/SiO_2 and Cu/Y_2O_3 composite coatings with [001] as the highest intensity. But after changing the deposition conditions from DC to 5 kHz pulse frequency the development of [111] fibre orientation was observed in all composite coated specimens and further intensification of [111] fibre orientation was also witnessed at the 10 kHz by consuming other [001] and [110] orientations.

To further quantify the texture development, volume fraction of the [111], [001] and [110] orientations presented with respect to the deposition parameter was measured and reported in Fig. 6.6. Fig. 6.6a shows the volume fraction of pure copper coatings. The obtained result shows higher volume fraction of [111] orientation at DC condition, which confirmed as strong [111] fibre. But, with the change in deposition condition from DC to pulse deposition of 5 and 10 kHz the volume fraction of [001] and [110] orientation decreased rapidly as compared to [111] fibre orientation. Though the volume fraction of the [111] fibre marginally decreased, it is the only orientation which exists after the pulse variation. Fig. 6.6b shows the volume fraction of Cu/SiO_2 composite coating. The figure clearly indicates the presence of random texture at the DC deposition with [001] orientation has higher volume fraction. This orientation was attributed may be due to the change in surface energy of the fibre orientations due to addition of second phase nano particles. And also addition of second phase particles

induced higher strain energy in case of both composite coatings compared to pure copper coating, which can be confirmed from the table 6.2, favors [001] and [110] orientations [158, 159]. This can be explained as the reason behind the higher volume fraction of [001] in case of both composite coatings. But when the process parameter changes from DC to pulse variation (5 and 10 kHz) the volume fraction of [001] and [110] suddenly decreases and at the same time the volume fraction of [111] orientation increases, which signifies that [111] fibre was the only preferable orientation developed. Similarly, Fig. 6.6c illustrates the change in volume fraction of [111], [001] and [110] fibre orientation with respect to the different process parameter in Cu/Y_2O_3 composite coating. The trends of different fibre textures were exactly similar to that of Cu/SiO_2 coatings. But the volume fraction of final and main [111] fibre was higher than Cu/SiO_2 specimen.

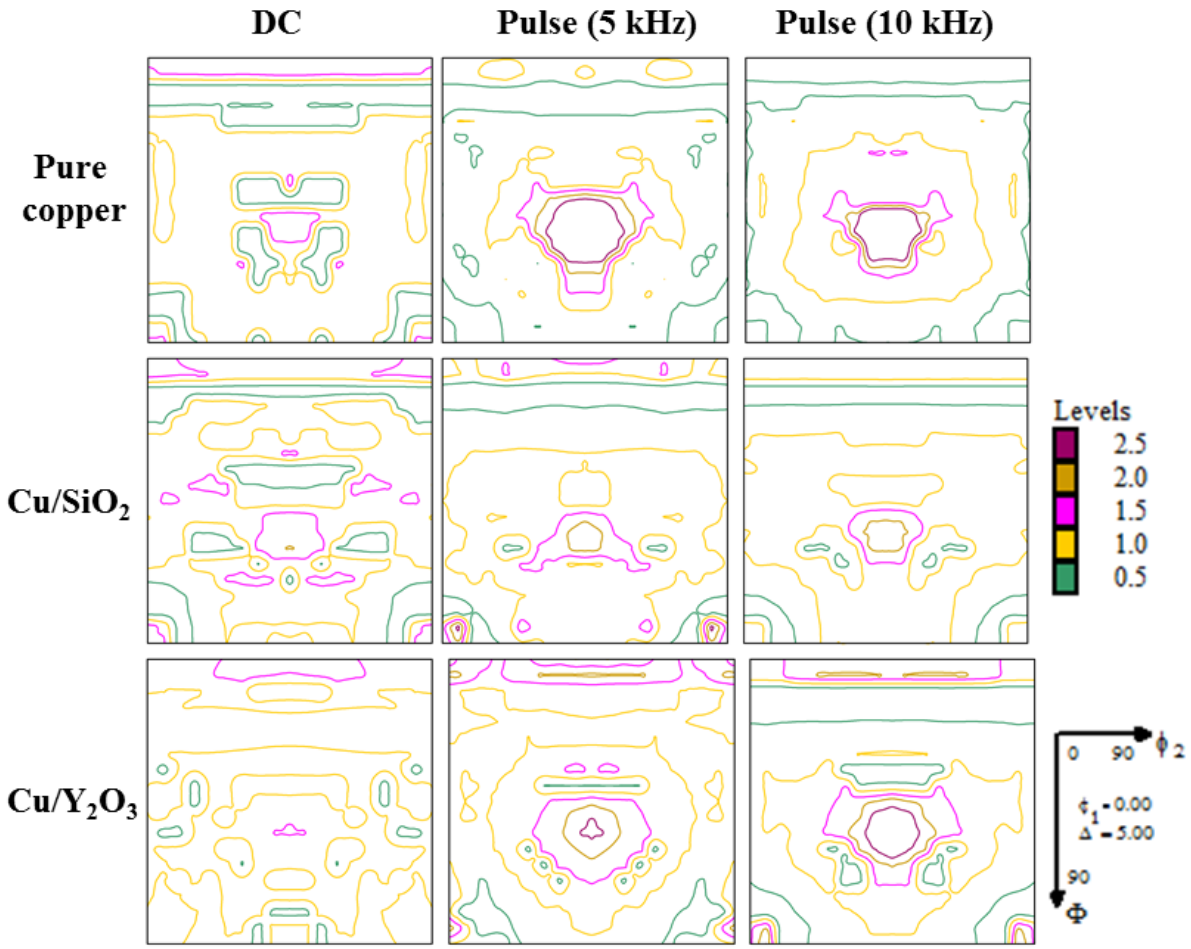

Fig. 6.5: ϕ_1= constant ODF figure of pure copper, Cu-30g/l SiO_2 and Cu-30g/l Y_2O_3 composite coatings with DC, pulse deposition of 5 and 10 kHz.

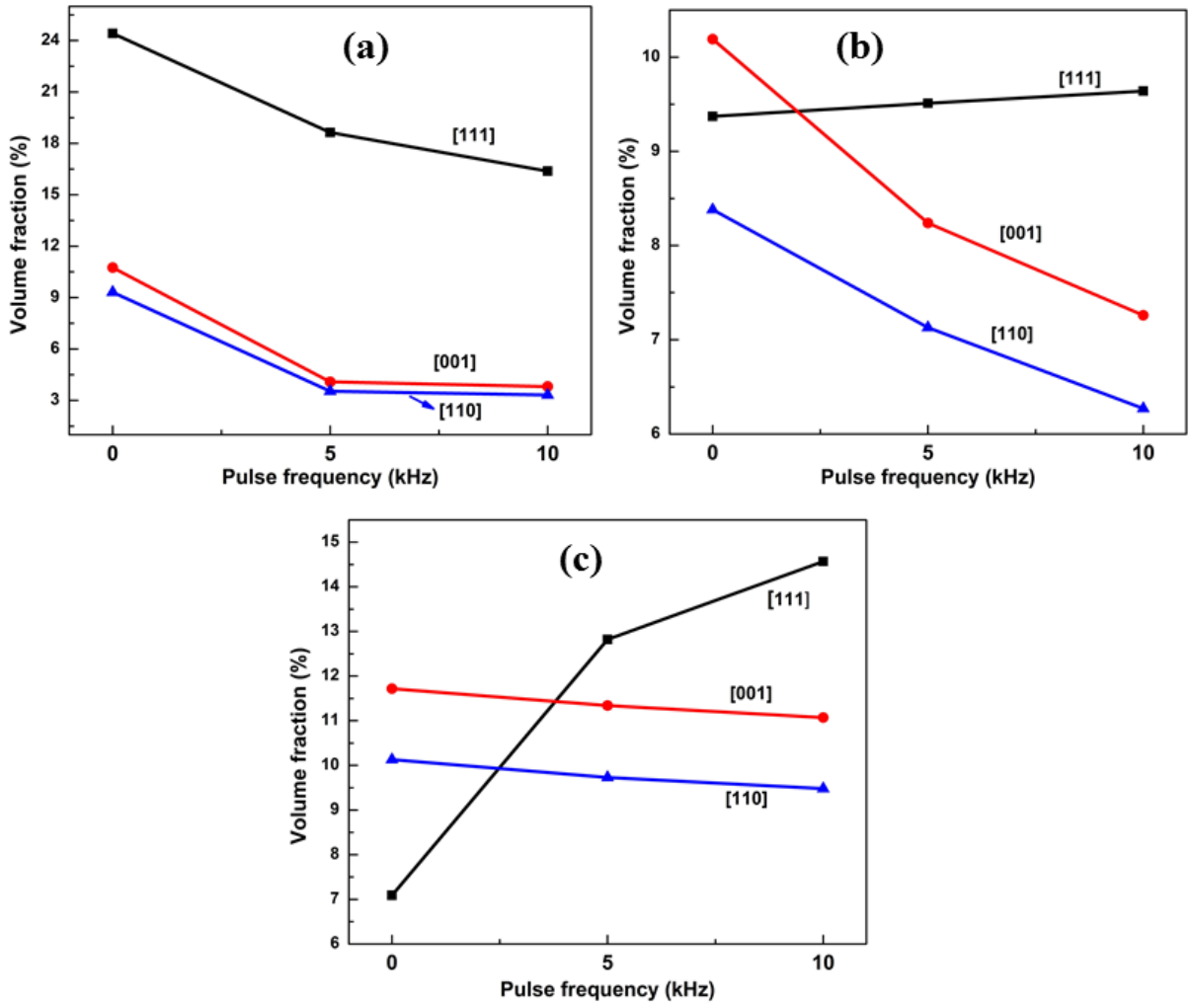

Fig. 6.6: Volume fraction of different orientations in(a) pure copper (b) Cu-30g/l SiO_2 and (c) Cu-30g/l Y_2O_3 coatings.

6.4 Microstructural characterization

The FESEM micrographs of all deposited specimen are presented Fig. 6.7(a-i). The obtained morphology of different samples gives comprehensive information about the grain structure with respect to deposition parameters and second phase oxide (SiO_2 and Y_2O_3) nanoparticle incorporation. Fig. 6.7(a-c) shows the morphology of pure copper coating at different deposition parameters (DC, 5 and 10 kHz) respectively. In case of different pulsing rates (Fig. 6.7b and c), reasonably finer and more uniform structures than that of direct current deposition was observed. Pure copper coating at DC deposition of 10.49 micron of average

grain size was reported in Table 6.3. Decreasing trend of average grain size with increasing pulse frequency was considered as obvious due to better nucleation mechanism. Basically higher pulse frequency means the pulses are shorter, i.e., both T_{on} and T_{off} are of short duration. This specifies that double layers do not get enough time to be fully charged and discharged during T_{on} and T_{off} time respectively. Due to shorter pulses the pulse arrives very quickly as soon as the previous pulse cycle is completed. Due to this mechanism a very thin pulse diffusion layer is produced, which obstruct the transportation and diffusion of the migrating copper ions from the electrolyte to the surface of the copper substrate. This leads to the superior nucleation with limited growth rate resulting finer matrix formation in all the coatings with increase of pulse frequency [160]. But, after addition of 30 g/l SiO_2 into the deposition bath the structure became coarser and the average grain size increases. The same was observed in each case of Cu-30g/l SiO_2 compare to pure copper coating under same deposition condtions. This may be explained as increaase in surface energy of the Cu deposition due to adverse nucleation effect by addition of SiO_2 in the electrolyte. This leads to excess growth of Cu crystals as well as less nucleation resulted bulkier grain size than pure copper coating. The formation of Cu-Cu cluster is more expected compared to Cu-SiO_2 cluster was evident from the first-principle calculations. The calculated formation energies (ΔE) for Cu-Cu and Cu-SiO_2 are equal to -56.10 and -67.37 kcal/ mol, respectively. Therefore, nucleation is more easier in case of pure copper compared to Cu-SiO_2 system. This can be considered as the reason behind the lesser nucleation possibility of Cu in the presence of SiO_2 leading to coarser grain. This kind of results also have been reported by current author for Cu-SiO_2 system for 20 minute deposition time [160]. But, in case of Cu-30g/l Y_2O_3 system (Fig. 6.7g-i), the structure looks more compact and finer than other coatings. The average grain size measured are 10.17, 8.84 and 7.9 microns for DC, 5 and 10 kHz respectively. The uniform codeposition of Y_2O_3 particles hinders the grain growth in the Cu matrix resulted smaller grain sizes, which is compeletily opposite to the Cu-SiO_2 coating.

In order to produce compact and finer structure, continuous nucleation of the crystals should occur and this can be realized by various ways, for example: (a) adding appropriate grain refining agents to the deposition bath, (b) adding a second phase reinforcement and/or (c) pulse current deposition. Addition of Y_2O_3 nano particles leads to inserting of second phase

particles in the Cu matrix changes the shape of copper crystallites to more compact and finer. Which in turn reduces their average grain sizes (Table 6.3).

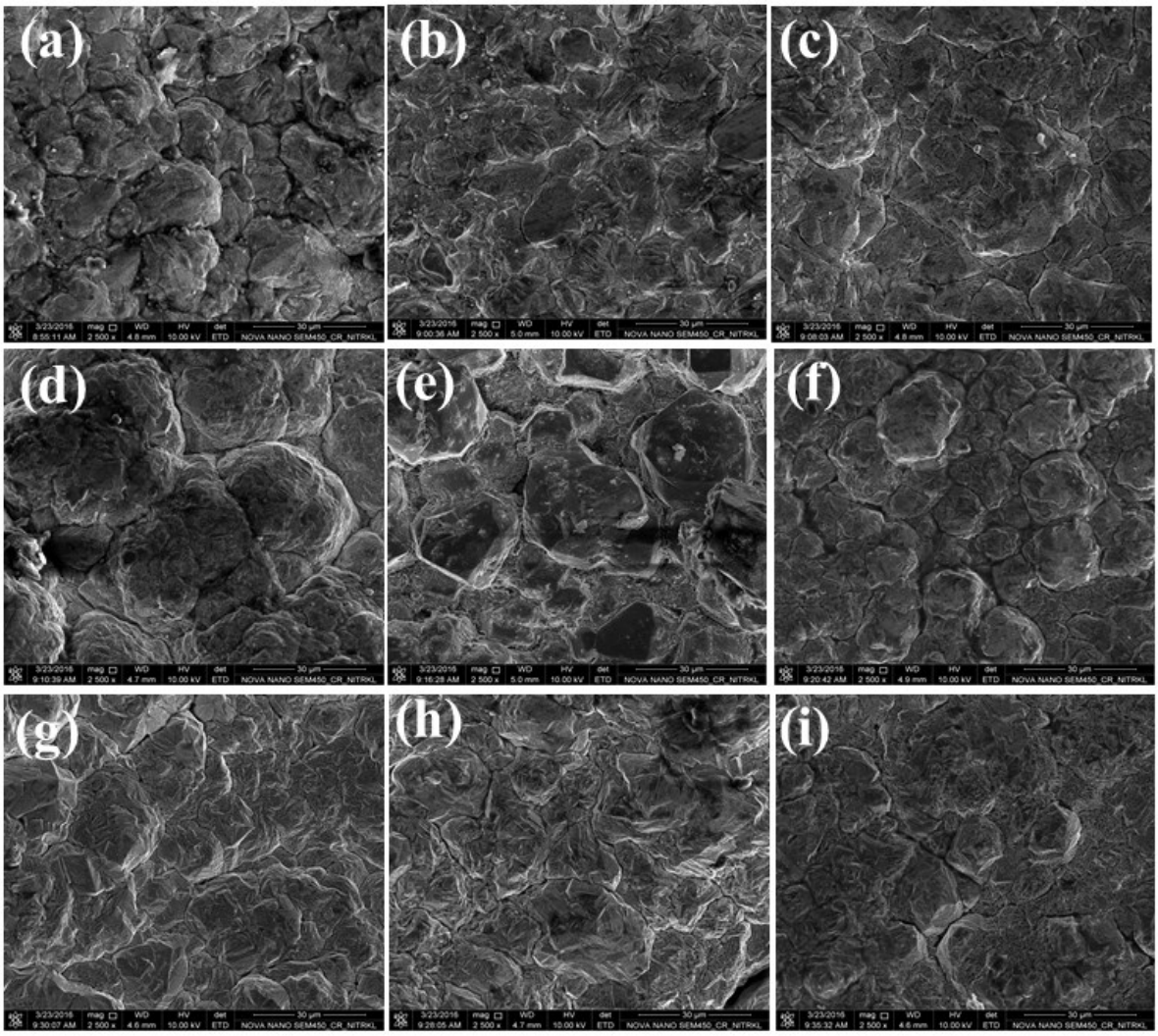

Fig. 6.7: SEM images of (a, b, and c) pure copper (d, e, and f) Cu-30g/l SiO_2 and (g, h, and i) Cu-30g/l Y_2O_3 coatings with DC, 5 kHz and 10 kHz respectively.

Table 6.3: Average grain sizes of all the deposits

	Average grain size (µm)		
Deposited specimens	DC deposition	Pulse deposition (5 kHz)	Pulse deposition (10 kHz)
Pure Copper	10.49	9.95	8.34
Cu-30g/l SiO_2	13.30	12.36	11.19
Cu-30g/l Y_2O_3	10.17	8.84	7.90

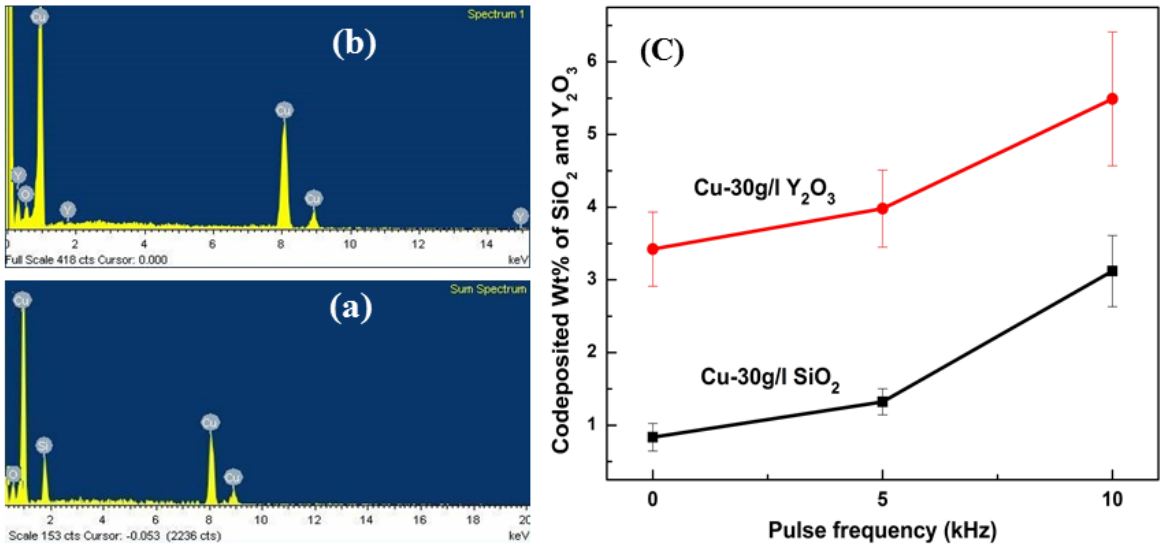

Fig. 6.8: (a and b) EDS spectra of Cu-SiO_2 and Cu-Y_2O_3 at 10 kHz pulse frequency, (c) Co-deposited Wt.% of SiO_2 and Y_2O_3 (in terms of Si and Y) verses pulse parameter.

Energy dispersive spectra of Cu-SiO_2 and Cu-Y_2O_3 composite coatings were displayed in Fig. 6.8a & b respectively. Fig. 6.8a confirmed the presence of Cu along with Si and O, whereas the presence of Cu, Y and O from Fig. 6.8b. Quantitative investigation of the spectra was carried out for all the Cu-SiO_2 and Cu-Y_2O_3 deposited specimens. The amount of Si was converted to equivalent amount of SiO_2 using the stoichiometric ratio of Si and O as per chemical formula of SiO_2. Similar calculation was also followed for conversion of amount of Y to Y_2O_3. Fig. 6.8(c) shows weight percentage of SiO_2 and Y_2O_3 in the deposited composite specimens at different deposition conditions. Each value reported in Fig. 6.8(c) was actually average of 5 EDS spectra. The amount of SiO_2 and Y_2O_3 wt.% in the composite coating increases with the increase in pulse frequency.

6.5 Microhardness and electrical conductivity study

Fig. 6.9(a) shows the hardness of copper, Cu-30 g/l SiO_2 and Cu-30 g/l Y_2O_3 coatings as a function of pulse frequency. The hardness values were found to be increasing by changing the deposition parameter from DC to 5 kHz and further changing to 10 kHz pulse frequency. For all the deposited specimens, the best hardness result was observed at 10 kHz pulse frequency.

In case of electrodeposited Cu and Cu-based composite coatings improvement of hardness can be attributed to various reasons such as (i) dispersion strengthening due to addition of second phase nano particles (SiO_2 and Y_2O_3), (ii) formation of finer matrix caused by nucleation mechanism due to altering the deposition parameters (pulse frequency, current density etc), (iii) development of specific crystallographic orientation with increase in pulse frequency, i.e [111] fibre orientation and (iv) lattice strain as observed in table 6.2. Development of [111] orientation is generally considered as harder orientation compared to other textures because when a load is applied on the (111) plane, it is less easy to activate the $\{111\}<01\bar{1}>$ slip systems of the material compared to other orientations [161]. Though, no second phase particle was added in the bath during the deposition in case of pure copper coating, the improvement in hardness at 10 kHz compared to 5 kHz and DC deposition can only be explained by the latter two mechanisms. But in case of both Cu-SiO_2 and Cu-Y_2O_3 composite coatings, the increased hardness with increasing pulse frequency can be attributed to all three mechanism i.e. increased amount of co-deposited SiO_2 and Y_2O_3 causing dispersion hardening, formation of finer matrix due to better nucleation and existence of [111] preferred orientation at higher pulse frequency. Moreover, it can be observed that in general with increasing lattice strain of the composite coatings, the hardness increases. Amongst all the coatings Cu-Y_2O_3 composite coating displayed better hardness compared to pure Cu and Cu-SiO_2 deposits. The higher hardness of Cu-Y_2O_3 coating can be explained by various factors such as; (i) higher amount of codeposited Y_2O_3 at all the deposition conditions than Cu-SiO_2 coating, (ii) lower average grain size in all cases than both pure Cu and Cu-SiO_2 coating, (iii) higher volume percentage of [111] orientation was observed in case of Cu-Y_2O_3 composite coating than Cu-SiO_2 coating.

Electrical conductivity of copper coating, Cu-30 g/l SiO_2 and Cu-30 g/l Y_2O_3 composite coating specimens are displayed in Fig. 6.9 (b). In case of pure Cu coating very minor decrease in electrical conductivity was observed with changing the deposition condition from DC to pulse. In other words it can be said that electrical conductivity of pure Cu coating shows very much stagnant behavior. It was previously well documented that in spite of finer matrix which directly related to the higher number of grain boundaries, formation of [111]

orientation favors the increase in electrical conductivity of the material [161, 162]. High electrical conductivity of (111) oriented coatings was reported due to the small angle grain boundaries, twin boundaries which exhibit one order lower electrical resistivity compared to that of high angle grain boundaries [163, 155], and the highly uniform orientation of the grains, which reduces the electron scattering. In addition, the absence of impurities due to the surfactant free sulfate bath might be contributing to the better electrical conductivity. This can be the reason behind the stagnant behavior in electrical conductivity values of pure copper coating in spite of decreasing grain size with increasing pulse frequency. But, this cannot be the reason for the case in Cu-SiO_2 and Cu-Y_2O_3 composite coatings, as decrease in electrical conductivity of all such deposits in spite of increase of [111] preferred orientation was observed. This can be explained by formation of finer matrix due to faster nucleation mechanism and addition of insulating oxides (SiO_2 and Y_2O_3) in the coatings. Comparing all the deposits, pure copper coating displayed best electrical conductivity followed by Cu-SiO_2 and Cu-Y_2O_3 composite coatings.

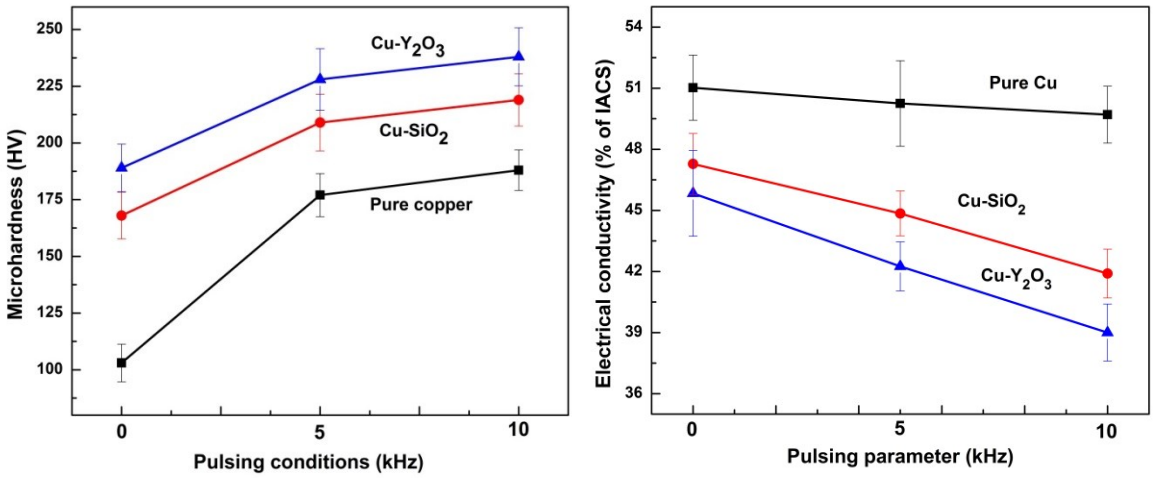

(a) (b)

Fig. 6.9: (a) Microhardness and (b) Electrical conductivity of all deposited specimens.

6.6. Summary

Pure copper, Cu-30g/l SiO_2 and Cu-30g/l Y_2O_3 composite coatings were developed by electro co-deposition process. The effect of texture, microstructure, grain morphology of the coating and incorporated second phase oxide nanoparticles on the microhardness and electrical conductivity were studied systematically. The key inferences are:

- Pure copper, Cu-SiO_2 and Cu-Y_2O_3 coatings were successfully prepared by DC, and pulsing mode with pulse frequency of 5 and 10 kHz.
- Improved of hardness result in case of 10 kHz pulse frequency followed by 5 kHz was observed of all the deposited specimens. This can be explained by development of (111) texture and higher amount of codeposited second phase particles in the matrix as well as formation of finer matrix at higher pulse frequency.
- Cu-Y_2O_3 composite coating displayed best hardness result compared to other deposits due to higher volume fraction of [111] orientation, finer grain size as well as more amount of codeposited Y_2O_3 particle than Cu-SiO_2 composite deposits.
- Formation of [111] preferred crystallographic orientations of the deposited matrix were observed with the variation of pulse condition of all deposited specimens. Development of (111) texture greatly affect the surface mechanical and electrical properties of the prepared coating.
- Though the existence of preferred [111] orientation favors better electrical conductivity of coated samples, but decrease in electrical conductivity with increasing pulse frequency of composite coated specimens was observed and can be attributed to the formation of finer matrix as well as addition of second phase insulating particles .

Chapter 7

Effects of surfactants on surface-mechanical properties of electro-codeposited Cu-ZrO_2 composite coating

7.1 Introduction

In the present chapter, electrodeposited Cu-10g/l ZrO_2 composite coating with different surfactants CTAB (cationic), SDS (anionic), PAA (polymeric) and glucose (non-ionic) with 5 kHz pulse frequency have been prepared and effect of surfactant concentrations on surface-mechanical and electrical properties of the developed composite coating was studied. Detailed electrolytic bath and deposition parameters presented in table.7.1. Specifically 5 kHz pulse frequency was considered for deposition in this system due to the observation of overall best mechanical and electrical properties for previous Cu-Y_2O_3 system at same pulse frequency.

Table 7.1: Plating bath composition and deposition parameter for Cu–ZrO_2

Electrolyte (Acidic copper sulfate bath)	Copper Sulfate ($CuSO_4.5H_2O$): 200 gm/l
	Sulfuric acid (H_2SO_4): 50 gm/l
Surfactants	CTAB (Cetrimonium bromide), SDS (Sodium dodecyl sulfate), PAA (Polyacrylic acid): 0.1, 0.5 and 1 g/l Glucose: 10, 20 and 40 g/l
pH	2.17 (±0.2)
Current density	8 A/dm^2
Temperature	Room temperature
Plating time	20 minutes
Dispersion	ZrO_2: 10 gm/l
Pulse frequency	5 kHz
Duty cycle (pulse on time)	30%

7.2 Isoelectric point measurement and particle size distribution

Zeta potential of ZrO_2 ultrafine powder was measured in de-ionized water with addition of mild acid at different *pH* values to determine the isoelectric point (IEP) of the powder. The obtained zeta potentials at different *pH* values were plotted and shown in Fig. 7.1(a). From the figure it can be observed that the isoelectric point of ZrO_2 was around 5.35 of *pH*. So, during deposition process the *pH* was maintained at a lower value than this (~2.17 *pH*) to avoid the agglomeration during the deposition process, so that homogeneous coating of Cu-ZrO_2 can be obtained on the cathode substrate.

Fig. 7.1(b) shows the cumulative size distribution of ZrO_2 particles obtained by transmission electron microscope (TEM). The inserted figure determined the statistical distribution as well as average particle size of the procured ZrO_2 particles. From the figure the average particle size of zirconia particle evidenced as 18nm and the particles ranges from 10-40nm.

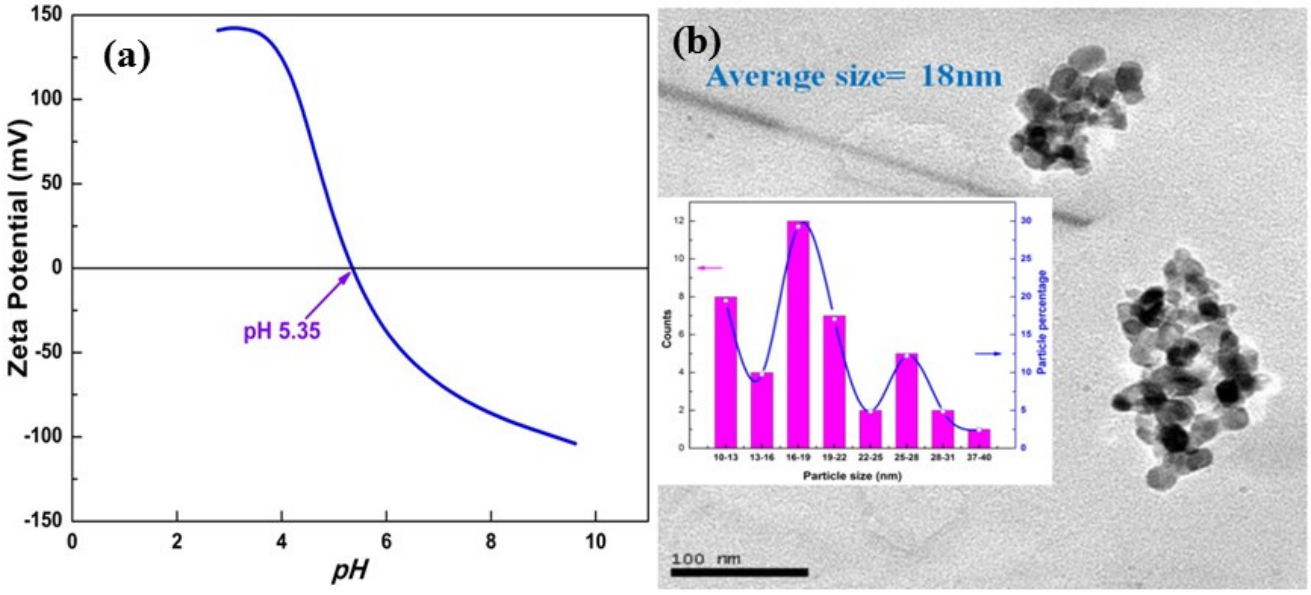

Fig. 7.1: (a) Isoelectric point of ZrO_2 and (b) TEM micrograph of procured ZrO_2 powder.

7.3 XRD analysis

Fig. 7.2 shows the XRD profile of procured ZrO_2 powder and by analyzing the peaks, it was confirmed that the structure of ZrO_2 is tetragonal. Fig. 7.3(a-d) shows the XRD patterns of Cu-ZrO_2 composite coatings with various surfactants (CTAB, SDS, PAA with concentrations of 0.1, 0.5 and 1 g/l) and Glucose with 10, 20 and 40 g/l concentrations synthesized by the pulse electrodeposition. The XRD pattern shows the presence of only copper peaks. The copper peaks corresponding to (111), (200), (220), and (311) reflections are observed by JCPDS data (card no. 04-0836). Though ZrO_2 peak was not found in the composite coating XRD profile due to very lower wt% codeposited Zr, but the same was observed by enlarging one of the developed coatings and shown in Fig.7.4. The enlarge XRD profile was assigned as ZrO_2. To observe the changes of peak intensities with respect to different surfactant concentrations, relative texture coefficient (RTC) of (111), (200), (220), and (311) planes were calculated by the equation 4.1(refer chapter 4) and displayed in table.7.2.

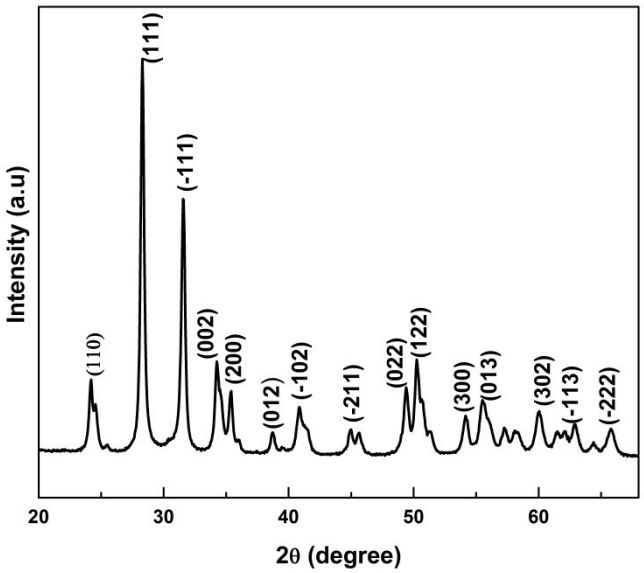

Fig. 7.2: XRD plot of ZrO_2 powder.

Table 7.2 shows the calculated texture coefficients of (111), (200), (220) and (311) copper planes. From the table it can be observed that with addition of CTAB, the preferred orientation of copper was changed from (220) to (111). Earlier Deng et al. also mentioned

<111> as preferred orientation during electrodeposition of pure copper using different electrolyte [20]. In case of SDS treated specimens TC_{220} was observed as preferred orientation. Similar results were also observed in case of Glucose assisted specimens. But PAA assisted specimens shows different trend of results, in which 0.1 g/l PAA treated coating shows (220) as most preferred orientation. By increase the amount of PAA from 0.1 to 0.5 g/l the orientation changes from (220) to (111) as preferred orientation. But further increment of PAA to 1 g/l, the coating shows random type texture. During electro-codeposition process, formation of particular orientation is observed maybe due to interfacial energy-driven phenomena and subsequent alteration of interfacial energy due to the addition of different surfactants as well as presence of oxide particles in the matrix.

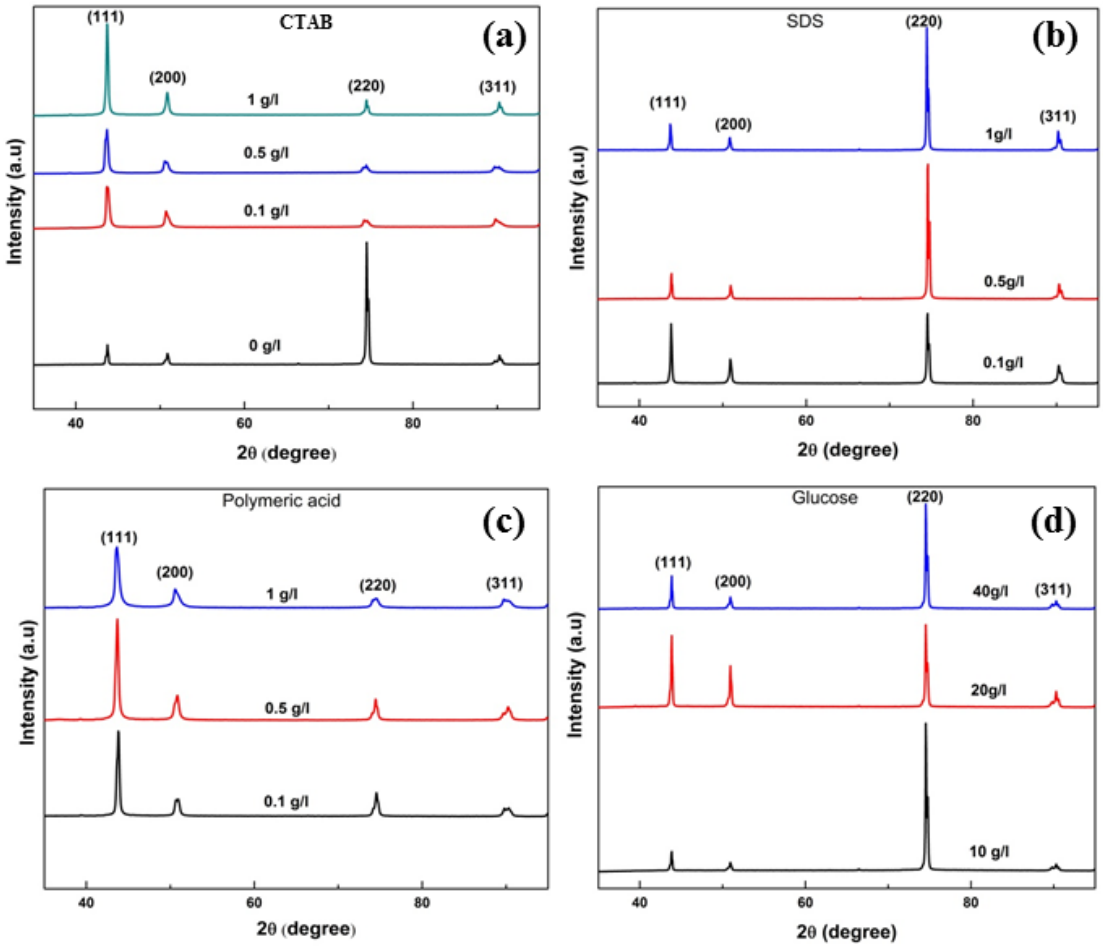

Fig. 7.3: XRD plot of Cu-10g/l ZrO_2 with various surfactant concentrations (a) with CTAB, (b) with SDS (c) with PAA and (d) with glucose.

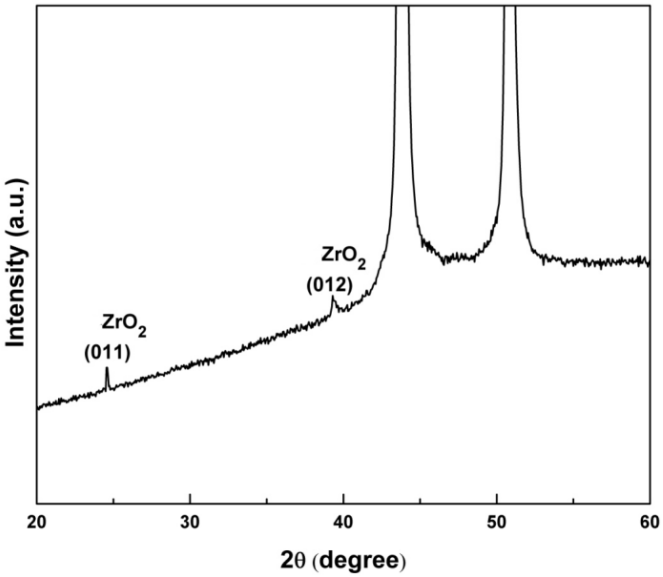

Fig. 7.4: Enlarge view of Cu-10g/l ZrO_2 with 0.5 g/l CTAB assisted XRD profile.

Table 7.2: Relative Texture Coefficient ($RTC_{(hkl)}$) of Cu-10g/l ZrO_2 coatings with different surfactant concentrations.

Sample Type	Sample Details	$RTC_{(hkl)}$%			
		(111)	(200)	(220)	(311)
Cu-10g/l ZrO_2 coating	Without surfactant	03	04	85	08
	0.1 g/l (CTAB)	28	24	22	26
	0.5 g/l (CTAB)	45	21	20	14
	1 g/l (CTAB)	34	19	30	17
	0.1 g/l (SDS)	11	10	60	19
	0.5 g/l (SDS)	03	03	84	10
	1 g/l (SDS)	03	03	82	12
	0.1 g/l (PAA)	28	14	45	13
	0.5 g/l (PAA)	36	17	26	21
	1 g/l (PAA)	27	24	26	23
	10 g/l (Glucose)	02	02	92	04
	20 g/l (Glucose)	10	14	62	14
	40 g/l (Glucose)	05	04	85	06

7.4 Microstructural and elemental analysis

The obtained microstructures of Cu-ZrO_2 composite coatings differ in each surfactant assisted deposits. Surface micrographs of the Cu-10g/l ZrO_2 composite coatings with different CTAB concentrations are displayed in Fig. 7.5 and other surfactants assisted Cu-10 g/l ZrO_2 coatings

are presented in Fig. 7.6. Cu-10g/l ZrO_2 coating prepared without CTAB addition, exhibits formation of non-uniform grain sizes with narrow voids as displayed in Fig. 7.5(a). But addition of CTAB makes the structure finer and the fineness increases with CTAB concentration. After addition of CTAB the appearance of structure became cone like. Cationic surfactant (CTAB) plays a significant role in controlling the formation of micro and nano structural architecture on the surface of the composite coating. The nucleation and growth of the matrix is associated with selective interaction with cationic surfactant on certain crystallographic facets to stimulate the crystal growth. This type of morphology has been reported by T. Hang *et al.* for cobalt nano-cone arrays on copper plate obtained by electrodeposition technique with addition of crystallization modifier (inorganic salt with NH_4^+ ion) [164]. Y. Deng *et al.* also reported electrodeposited single phased pure copper nano-cone arrays without exploring much about surface mechanical characterizations [165]. Formation of ultrafine matrix in CTAB assisted coating can be explained by the adsorption of CTAB molecules on the cathode (substrate) surface that helps better nucleation and prevent growth of the copper grains. Similar effect was also reported in previously published results on different systems [166, 167]. It was observed that cones are very fine and sharp when CTAB concentration is 0.5g/l. This CTAB assisted composite coating reveals unique duplex structures; one with uniform arrays of nano-cones named as 'B' and another is spherical colony like structure (approximately 12 μm diameter) with highly dense and sharp nano-cone arrays named as 'A' in the figure. The structure shows vertically aligned nano-cone arrays with size of the base in the range of 200-500nm and height of 0.5-1.5 μm. 1.0g/l CTAB addition shows relatively coarse/inhomogeneous morphology with flowery structure. It can also be commented that 0.1g/l CTAB shows most homogeneous structure, 0.5g/l displays duplex structure and 1.0g/l shows little inhomogeneous size of cones. CTAB assists better nucleation but higher addition of CTAB may lead to uncontrolled excessive nucleation leading to duplex structure as observed in 0.5g/l CTAB structure and further addition of it (1.0g/l CTAB) promotes growth phenomena. Formation of coarser structure at higher CTAB concentration was reported earlier by Aref *et al.* [168].

But in case of SDS assisted Cu-ZrO_2 composite shows reverse trend nucleation of Cu grains and increasing trend of grain sizes were observed with increasing concentration of SDS in the

electrolyte. From the Fig.7.6 (a-c), it can be observed that at 0.1g/l SDS concentration the morphology looks fine, uniform and loosely packed. There was a clear evidence of crack formation in the matrix. But when the concentration was increased to 0.5 g/l the matrix became more compact than 0.1 g/l SDS assisted coating and the morphology looks further compacted with granular shaped grains with increased SDS concentration to 1 g/l.

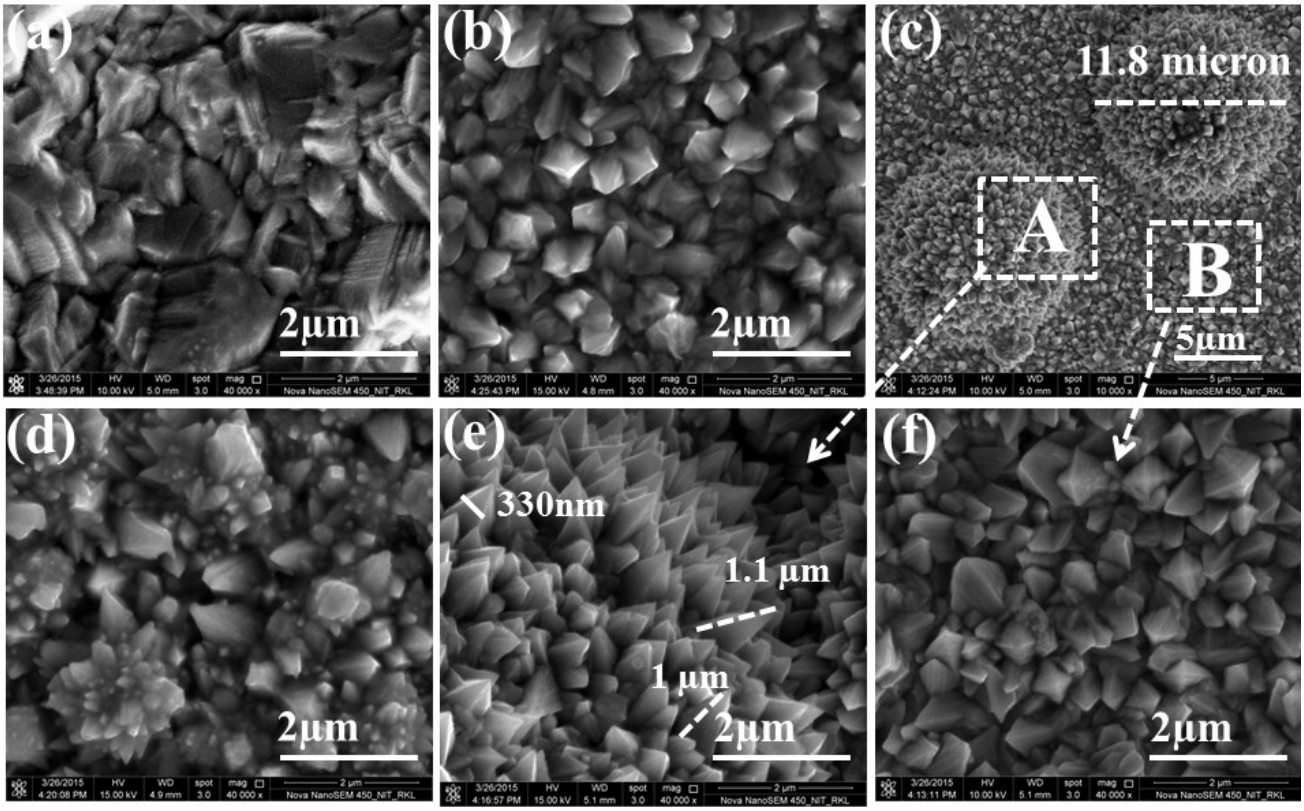

Fig. 7.5: Surface morphology of electrodeposited Cu-10g/l ZrO_2coatings (a) without, (b) with 0.1g/l, (c) 0.5g/l and (d) 1.0g/l of CTAB; (e) and (f) are enlarged views of (c).

In case of PAA assisting composite coated specimen, the microstructure shows completely different trend. 0.1 g/l PAA assisted specimen looks highly dense, fine and uniform whisker like structure. Increment of PAA concentration from 0.1 to 0.5 g/l in the electrolyte, morphology changes to highly bulky globular structure with densely packed grains. But further increment in concentration of PAA to 1 g/l the structure changes to very fine, uniform, compacted spherical structure. Cu-ZrO_2 composite coating with 10g/l assisted Glucose shows fine, highly dense and uniform matrix and further increase in glucose concentration to 20 g/l

the structure looked finer and well compacted as well as uniform grain sizes than previous one. But increment of glucose concentration to 40 g/l changes the structure to coarse dense granular morphology.

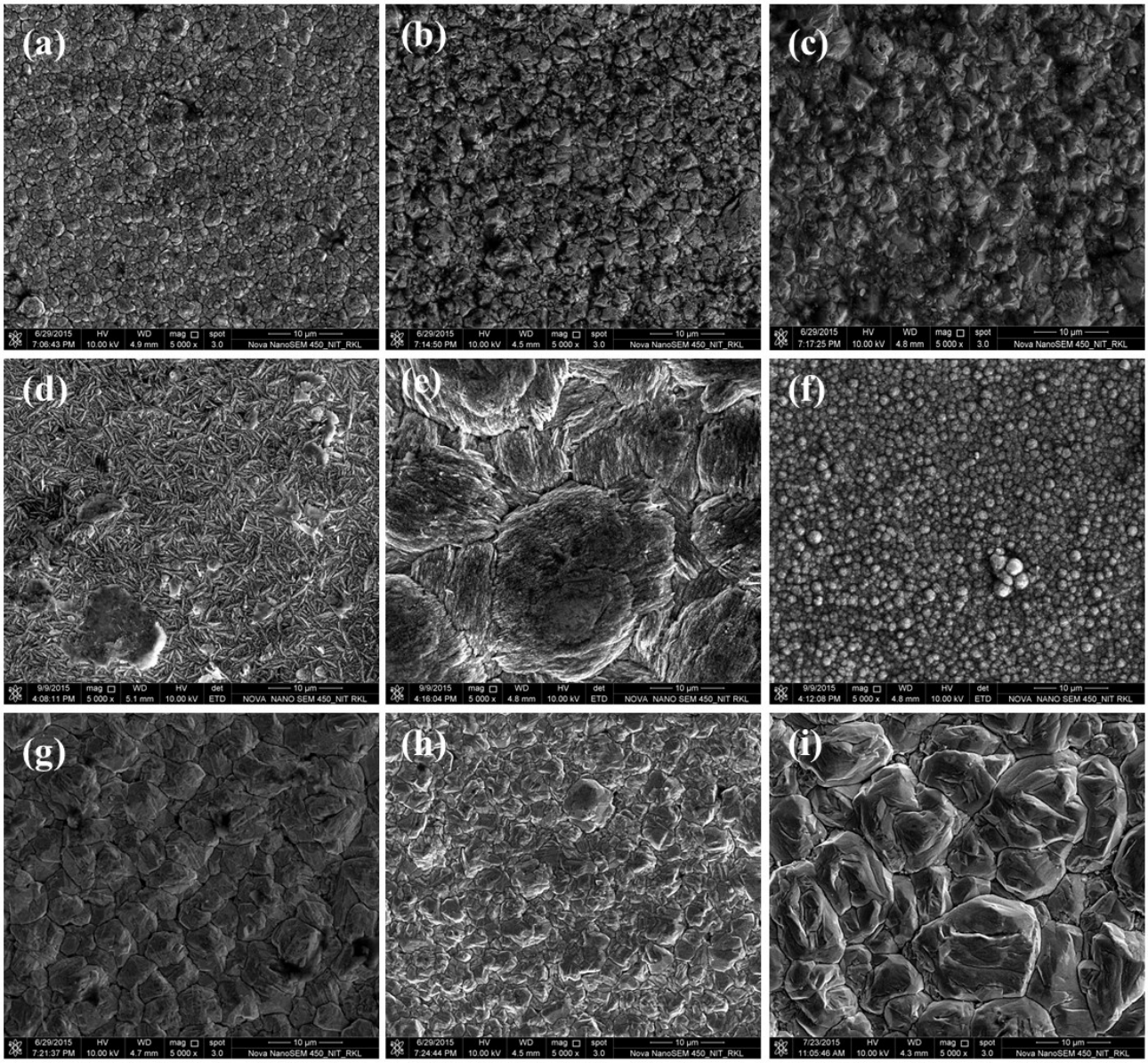

Fig. 7.6: FESEM images of Cu-10g/l ZrO_2 (a-c) with SDS (0.1, 0.5 and 1 g/l) (d-f) with PAA (0.1, 0.5 and 1 g/l) and (g-i) with Glucose (10, 20 and 40 g/l).

Fig. 7.7(a and b) shows the energy-dispersive spectrum of Cu–10 g/l ZrO_2-coated surface developed at 5 kHz pulse frequency with 0.1 g/l CTAB and SDS treated coating. It is evident from the figure that Zr was present in the composite coating along with copper and oxygen. Similar confirmation was also observed in cases of other surfactant treated specimens. Fig. 7.7(c) shows the codeposited wt.% of Zr (ZrO_2) particle in the matrix verses surfactant concentrations. From the figure it can be observed that higher amount Zr particle codeposited in the matrix at medium range surfactant concentration except SDS assisted composite coating.

Addition of CTAB and PAA increases the incorporation of ZrO_2 in the coatings up to 0.5g/l and in case of 1.0g/l CTAB and PAA, drop in Zr% (or ZrO_2) was observed. Similar trend was also observed in case of glucose assisted composite coating. 20 g/l glucose treated specimen shows highest incorporation of ZrO_2 particles followed by 10 and 40 g/l glucose addition specimens. But in case of SDS treated specimens codeposition of Zr wt.% (ZrO_2) increased with increase of SDS concentrations. Enhancement in incorporation of second phase particles in the composite matrix is considered to be associated with the manipulation of particle's surface charge by the adsorbed ions or surfactant molecules. This can promote electrophoretic migration of the second phase particles towards cathode substrate. At higher surfactant concentrations decrease in particle addition was earlier reported by Rudnik et al. [169]. Incorporation of less ZrO_2 can also result in coarser matrix as ZrO_2 causes enhanced nucleation of Cu matrix, but this is not the case in all deposited coatings. Specifically in case of cationic and nonionic treated composite coating, the finer matrix formation can be relate to the higher amount of codeposited ZrO_2 in the matrix and same can be observed from Fig.7.5 and Fig. 7.6(g-i).

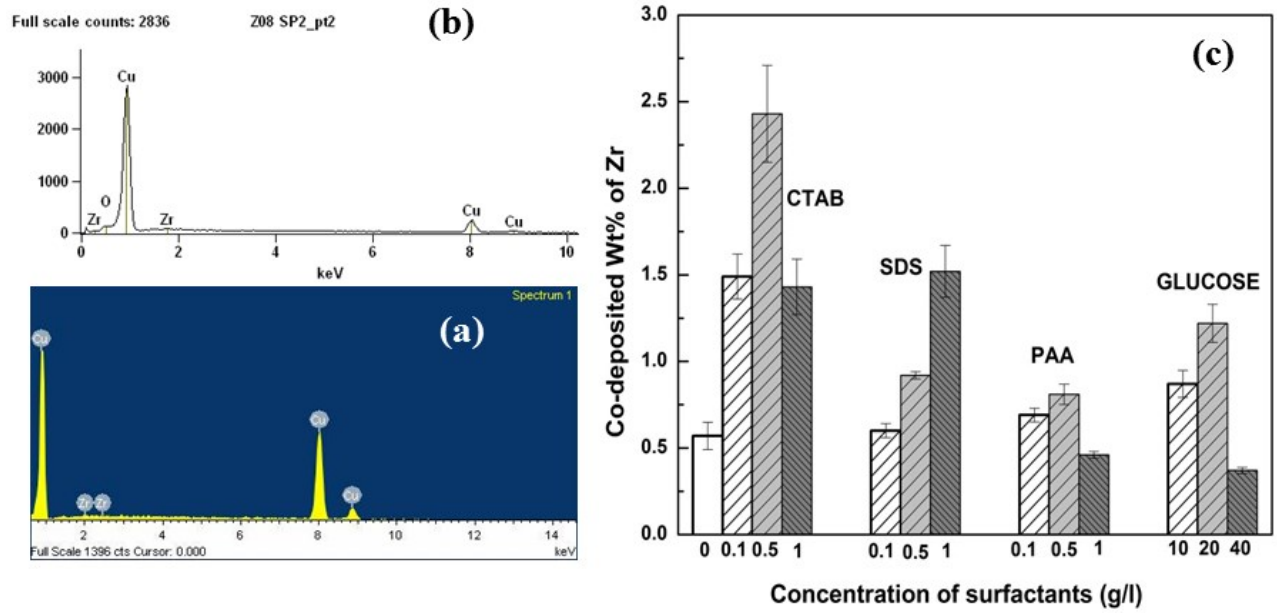

Fig. 7.7: EDS spectra of 0.1 g/l (a) CTAB and (b) SDS treated Cu-ZrO_2 deposited specimen (c) codeposited wt.% of Zr in all Cu-ZrO_2 deposited specimens.

Fig.7.8 (a and b) displays the x-ray mapping of Cu, Zr, and O in Cu-10 g/L ZrO_2 composite coating deposited with 5 kHz pulse frequency assisted with 0.5 g/l CTAB and SDS respectively. From these figures, it can be clearly observed that Zr and O are uniformly distributed on the coating which confirms the homogeneity of ZrO_2 throughout the coating. From the distribution and the distance between two consecutive Zr spots in the mapping figure, it can be told that the particles are both inside grain and at grain boundary of the coating surfaces.

SEM micrograph of the cross-sectional view of Cu-ZrO_2 coating assisted by 0.5 g/l CTAB was also analyzed to confirm the uniformity of thickness, and the thickness was found to be irregular shape and very slight gap between the coating and substrate was observed in Fig. 7.9(a). This may be due to belt grinding of the cross-sectional mounted specimen against the coating direction accidentally. The coating thickness of the said specimen was measured to be 30-40 µm Fig. 7.9(a). To enumerate the homogeneity of ZrO_2 particles in deposition, elemental mapping (in EDS mode of SEM) of the cross-sectional surface was carried out. Fig. 7.9(b) displays the corresponding x-ray mapping of Zr and the figure represent uniform

distribution of Zr on the cross-sectional surface, and thus the homogeneity of ZrO_2 in the deposition is confirmed.

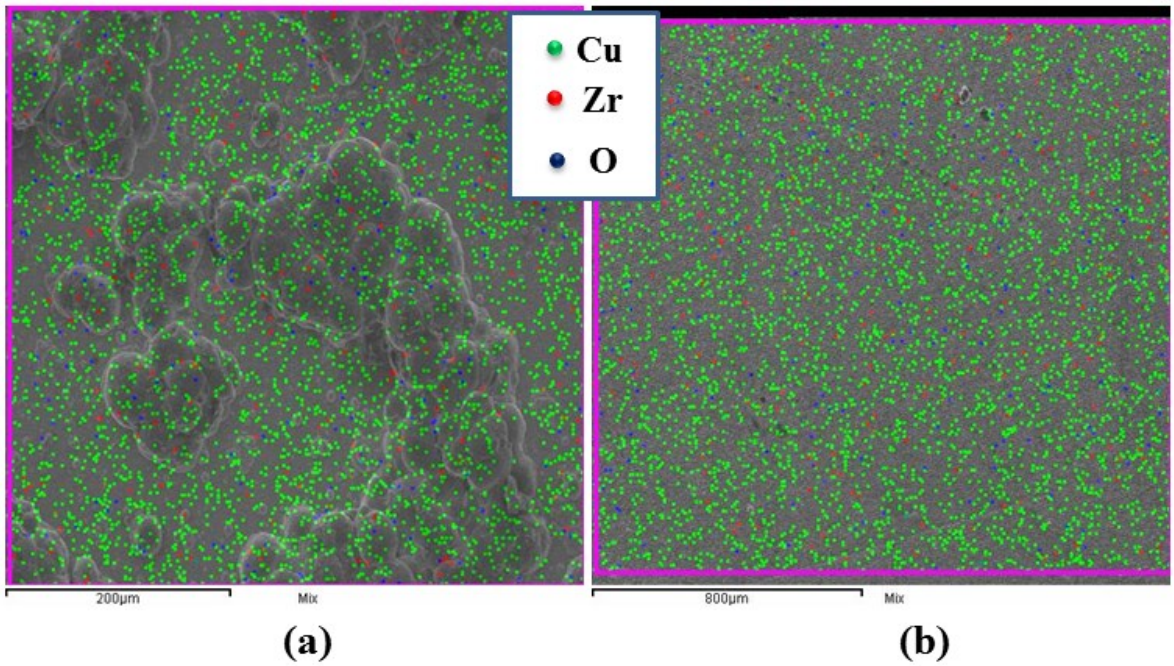

Fig. 7.8: X-ray mapping of Cu, Zr, and O in Cu-10 g/l ZrO_2 composite coating deposited with 5 kHz pulse frequency assisted with (a) 0.5 g/l CTAB (b) 0.5 g/l SDS.

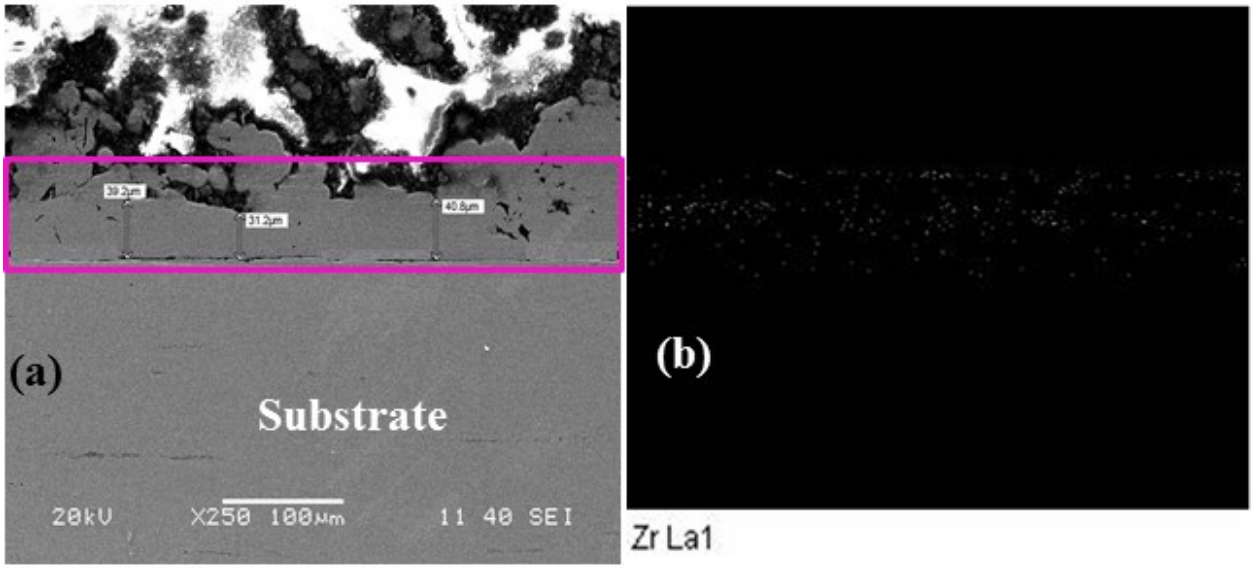

Fig. 7.9: X-ray mapping of Zr in Cu-10 g/l ZrO_2 composite coating deposited with 5 kHz pulse frequency assisted with 0.5 g/l CTAB.

7.5 Surface roughness study

Surface roughness of composite coatings could be an important factor for applications of such materials, especially in electrical contacts, because electron conduction through electrical contacts depends on their actual surface area in contact which in turn depends on their surface roughness. Higher roughness represents less contact surface leading to lower conductivity of the material. Roughness of all the Cu-ZrO_2 deposited specimens with various surfactant concentrations was presented in Fig. 7.10. Most of the calculated roughness value was observed below 1μm, which is quite relevant for application purpose. But in some cases, for example 0.5 g/l CTAB assisted composite deposit shows an average roughness of 5.6 micron, which is quite high for electrodeposition cases. The observation of high roughness of the said coating was obvious due to formation of duplex structure of nano cone arrays. Slightly higher roughness (~1μm) was also observed in 1g/l CTAB assisted coating due to the formation of coarser structure with flower shape nanocone arrays.

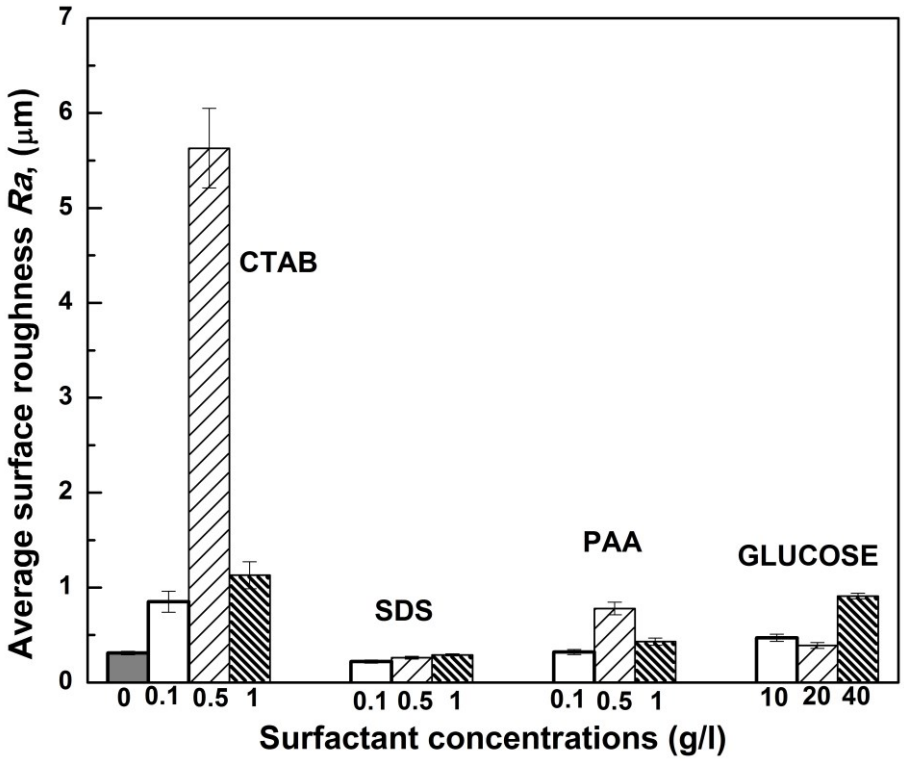

Fig. 7.10: Surface roughness of all Cu-ZrO_2 deposited specimens.

7.6 Microhardness study

The evolution of microhardness of Cu–ZrO_2 composite coatings with various surfactants (CTAB, SDS, PAA and glucose) concentrations is shown in Fig. 7.11. Results of the microhardness characterization reveal hardness value of 181.25 HV for Cu-10g/l ZrO_2 deposit without CTAB addition. 0.5g/l CTAB addition shows highest hardness value (339.38 HV, in region 'B'), which is ~87% higher compared to non CTAB assisted coating. But 'A' region of same coating shows extraordinarily high hardness of 1150 HV, which is approximately 3.4 times higher hardness than region 'B' and 6.3 times better than non-assisted CTAB Cu-10g/l ZrO_2 composite coating. So high hardness in region 'B' can be attributed towards the compressive stress originated from the formation and growth of numerous nano-cones at the region due to excessive nucleation phenomena. 1.0g/l CTAB coating shows drop in hardness value compared to 0.5g/l coating. Better hardness observed in CTAB assisted Cu-ZrO_2 coating can be explained by dispersion hardening, fine matrix configuration and formation of (111) [170]. With this same reason, 1.0g/l CTAB coating shows drop in hardness due to comparatively coarser matrix compared to 0.5g/l, smaller value of RTC_{111} (table 7.2) and lower value of ZrO_2 content in the coating (Fig. 7.7). Moreover it can also be mentioned that compared to without CTAB added coating, 1.0g/l CTAB added coating shows more randomized orientation (table 7.2) leading to least hardness value in the same.

In SDS assisted composite coatings, the hardness of the specimens increased with increasing concentrations of SDS in the electrolyte. 1g/l SDS assisted specimen shows highest hardness of 253.9 HV and the lowest hardness of 182.56 HV was observed in case of 0.1 g/l SDS concentration. Generally planes having higher angle with (100) plane produces more strain, thus resulted more hardness. (220) plane considered as second hardest plane followed by (111) plane due to the same reason. Better hardness in higher concentration of SDS was attributed to formation of highly dense microstructure and TC_{220} preferred orientation. Higher amount of codeposited ZrO_2 particle with increase in SDS concentration can be considered as another reason for increase in hardness with increase in SDS concentration.

In case of PAA assisting coated specimens highest hardness was observed at mid-range of 0.5 g/l PAA, which is slightly higher than the 0.1g/l assisted coating, but further increment of

PAA concentration to 1g/l, hardness of the coating was decreased to 191.76 HV. The reason behind witnessing of highest hardness in case of 0.5 g/l PAA assisted composite coating can be explained as the formation of TC_{111} orientation, which is similar to CTAB treated coatings.

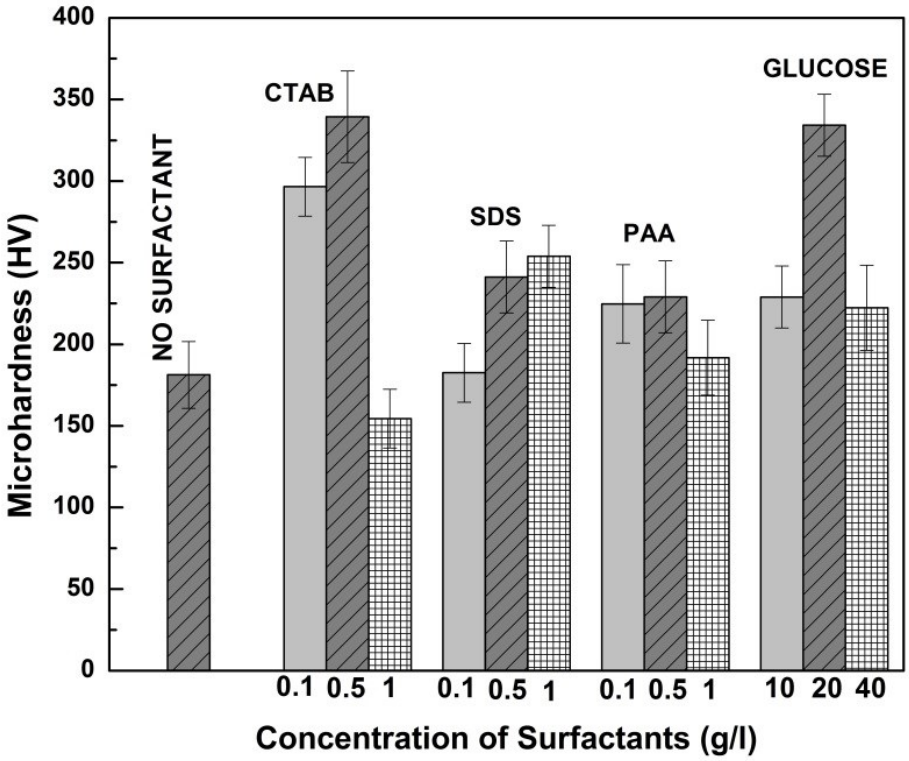

Fig. 7.11: Microhardness of all Cu-ZrO_2 deposited specimens.

The trend of observing highest hardness value at medium range of glucose (20 g/l) assisted coating was quite similar to CTAB and PAA assisted coatings. The value observed in case of 20 g/l assisted specimen was 334.24 HV, which is slightly lower than of 0.5 g/l CTAB assisted sample. The observation of highest hardness value in 20 g/l glucose assisted coating followed by 10 and 40 g/l assisted coating samples can be explained by the formation finer matrix as well as codeposited ZrO_2 percentage in the coating. In 20 g/l glucose assisted coating, TC_{111} value is marginally higher than that of 10 and 40 g/l treated coatings, which may result in higher hardness at 20 g/l glucose.

7.7 Wear study

Wear loss (in terms of wear depth) profile of without and with different surfactants (CTAB, SDS, PAA and Glucose) assisted Cu-10g/l ZrO_2 composite coatings are presented in Fig. 7.12(a-d). The results show higher wear loss of without surfactant assisted composite deposit compared to 0.5g/l CTAB assisted deposit (Fig.7.9a), which is also in agreement with hardness result (Fig. 7.11). Similar result was also observed in case of PAA assisted composite coatings, in which 0.5 g/l assisted deposit shows best wear resistant result followed by 0.1 and 1 g/l PAA treated coatings. But in other cases of specific surfactant concentrations, higher wear loss was observed compared to the composite deposit without assisting any surfactant in spite of lower hardness of the without surfactant assisted deposit. Higher wear loss observed in case of 0.5 g/l SDS treated deposit compared to non-treated deposit can be attributed to the stick-slip behavior of the steel ball indenter on the surface of the deposit. Due to the formation of pores and cracks on the surface of the 0.5 g/l SDS assisted composite coating (Fig. 7.6 b) might initiate easy sticking and penetration of the indenter on the surface, which in turn create higher wear depth. Similar kind of result was also observed in case of 40 g/l glucose assisted composite coating in spite of densely packed grains with almost no porosity. In this case higher wear loss in spite of higher hardness compared to surfactant free deposit only attributed to non-uniform coarser microstructure with accumulation of globular shape grains, which can also be confirmed from the roughness result (Fig. 7.10). But in other two cases (10 and 20 g/l) wear depth verses time plot follows the hardness result. From the obtained wear resistant results it was clearly observed that the wear depth verses time results not entirely follow the hardness results, but also depend on the microstructure and roughness data.

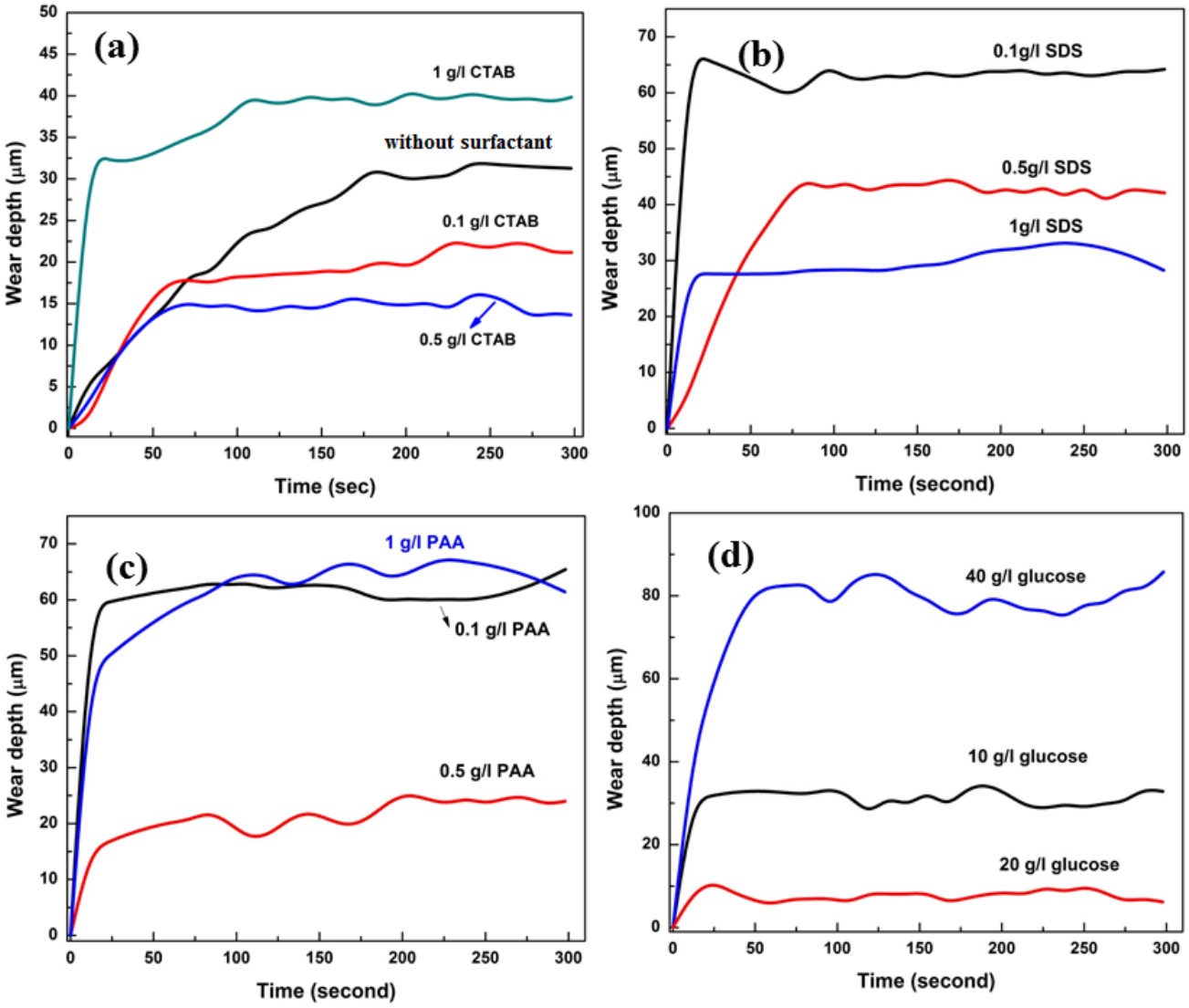

Fig. 7.12: Wear depth vs time plot of Cu-ZrO_2 deposited specimens at different surfactant variations.

7.8 Electrical conductivity

Fig. 7.13 shows the electrical conductivity values of the coatings prepared with different surfactant concentrations in terms of international annealed copper standards (IACS). Obtained result reveals that sample obtained without surfactant treated has 50% of IACS conductivity, but CTAB assisted specimen shows marginally lower electrical conductivity (~46% of IACS for 0.1g/l CTAB added coating). Though formation of preferred (111) orientation favors higher electrical conductivity [161], the reasons behind minor decrease in

conductivity with CTAB addition can be attributed towards finer grain size and presence of higher amount of ZrO_2 in the deposit compared to without CTAB assisted composite coating. In case of 0.5 and 1 g/l SDS assisted coatings; marginal decrease in conductivity value compared to 0.1 g/l SDS treated specimen can be attributed to incorporation of higher amount ZrO_2 insulating particle in the matrix. But in case of 0.5g/l PAA assisted coating; higher electrical conductivity compared to other PAA coatings was only explained by formation of coarser matrix in spite of higher amount of ZrO_2 deposition in the matrix. Similar results were also observed in case of glucose treated composite. In this present work, though depositions of ZrO_2 in all deposits have minor effect on electrical conductivity, but observed conductivity value signifies that it is more dependent on structure of the matrix rather than the deposited amount of ZrO_2 particles. Thus, fine structure and dispersion adversely affect the conductivity but helps in surface mechanical property improvement. Still the conductivity values obtained in some cases are in the range of acceptable scale of commercial use.

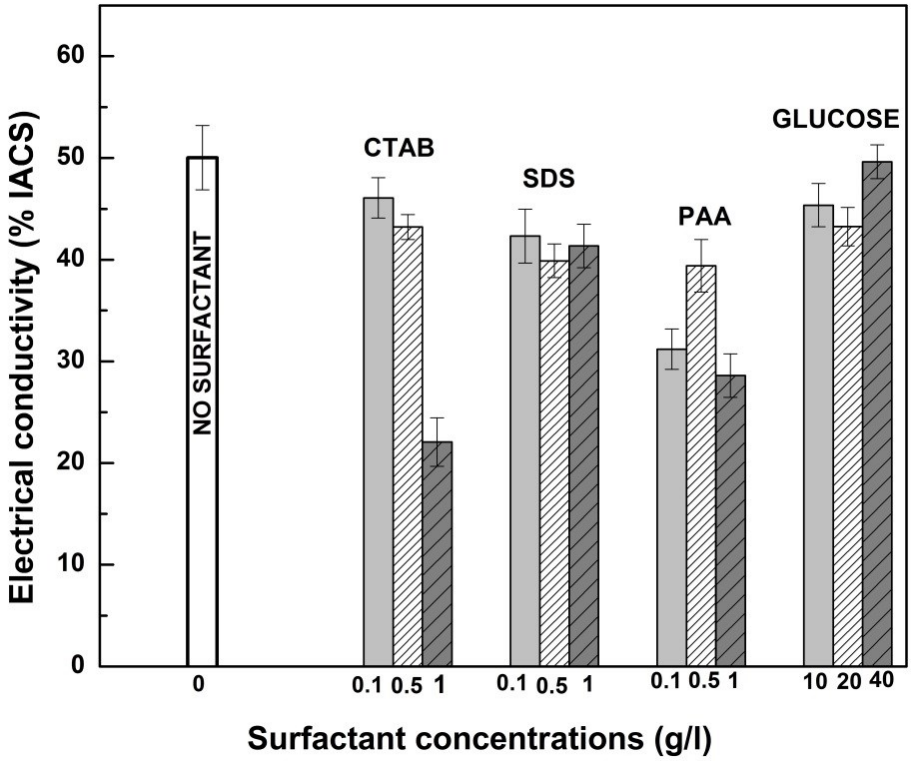

Fig. 7.13: Electrical conductivity of Cu-ZrO_2 composite coatings with different surfactant concentrations.

7.9 Summary

The present work deals with various surfactants (CTAB, SDS, PAA, and Glucose) assisted Cu-ZrO_2 composite coatings from copper sulfate electrolyte and its effect on various mechanical and electrical properties. Conclusions drawn from detailed investigation of the obtained results are summarized below:

- Higher ZrO_2 content in the deposits, leads to better hardness and wear resistance of the coating.
- Surfactants type and concentration greatly affects the microstructure as well as various properties of the developed coatings.
- Crystallographic orientation also played an important role in increasing and decreasing the mechanical and electrical properties.
- Electrical conductivity of coated samples affected not only by incorporation of ZrO_2 content in the deposits, but also the morphological and crystallographic structure of the composite matrix.

Chapter 8

Effects of graphene oxide concentrations on surface-mechanical properties of electrodeposited Cu-GO composite coating

8.1 Introduction

In the present communication, Cu/GO, Cu/RGO and Cu/thermally reduced graphene oxide (TRGO) composite films were prepared on polished copper substrate by pulsed electrodeposition method. Effects of GO, RGO and TRGO concentrations on the surface-mechanical and electrical properties were studied elaborately for possible application in electrical contacts. The chemical compositions of the electrolyte and the plating parameters are presented in Table 8.1.

Table 8.1: Plating bath composition and deposition parameters of Cu-graphene oxide composite coating

Item	Details
Electrolyte (Acidic copper sulfate bath)	Copper Sulfate ($CuSO_4.5H_2O$): 200 g/l, Sulfuric acid (H_2SO_4): 50 g/l
pH	1(±0.02)
Current density	8A/dm^2
Pulse parameter	5 kHz with 30% duty cycle
Poly acrylic acid (PAA)	25ppm
Temperature	Room temperature
Plating time	20 minutes
Dispersion	GO, RGO, TRGO: 0.1, 0.5 and 1 g/l each

8.2 Isoelectric point measurement

Zeta potential measurement is considered as an important factor for characterizing the stability of the dispersion and measurement of isoelectric point (IEP) of dispersed second phase particle. To determine the isoelectric point of the synthesized GO and RGO and TRGO, zeta potentials of the same were measured at different pH values. Fig. 8.1 displays the isoelectric point of GO, RGO and TRGO. Generally, particles with high positive or negative values of zeta potentials are considered to form stable dispersions due to inter particle electrostatic repulsion [171, 172]. IEP of RGO and TRGO are measured as 2.94 and 4.15 respectively.

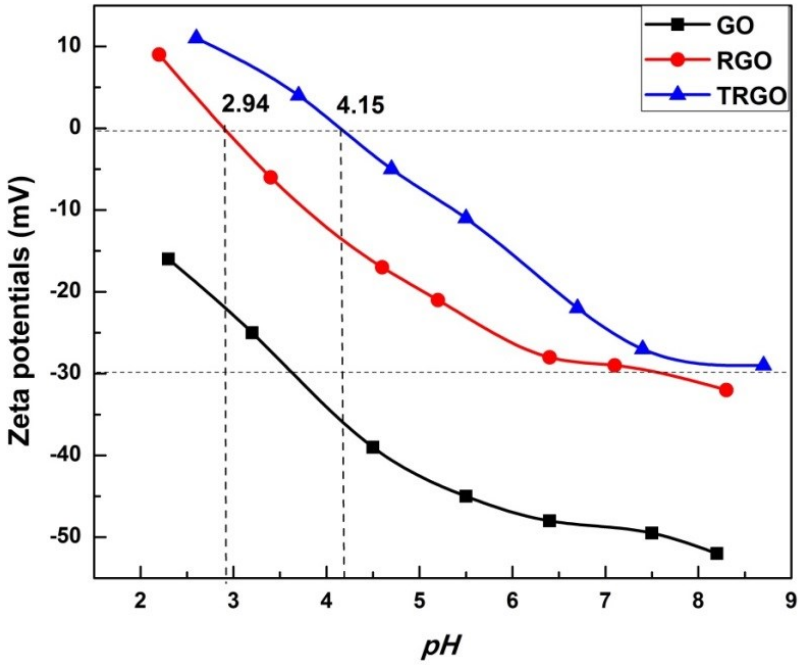

Fig. 8.1: Isoelectric point measurement of GO, RGO and TRGO in aqueous dispersion as a function of *pH*.

The pH of the copper sulfate electrolyte has been adjusted around 1±0.02, which is sufficiently lower than the obtained IEP values for second phase GO, RGO and TRGO. Hence, the GO particles are positively charged in the suspension. Therefore, the positively charged Cu^{2+} ions would not easily interact electrostatically with the negatively charged groups on the GO surface. This has resulted lower chance of agglomeration between copper

ions and GO in the suspension during the deposition process. In other words, it can be said that copper ions and GO are attracted to the cathode (negatively charged) substrate and get deposited on it.

8.3 XRD analysis

Fig. 8.2 represents the XRD pattern of GO, RGO and TRGO. The figure depicts comparatively very sharp peak at 2θ around 26° for TRGO compared to RGO which is attributed to the diffraction of the (002) plane. A typical oxidation reaction during the synthesis of GO leads to the appearance of a diffraction peak at 2θ around 12.5° as (001) without the visibility of (002) peak compared to RGO and TRGO due to the introduction of oxygen-containing groups to the GO surface [173]. In the case of RGO, only a broad peak at 2θ = 24.4° can be observed can be attributed breakage of the GO sheets as well as higher interlayer distance between the RGO sheets. The existence of (002) peak in RGO and TRGO indicates sufficient reduction process of the GO.

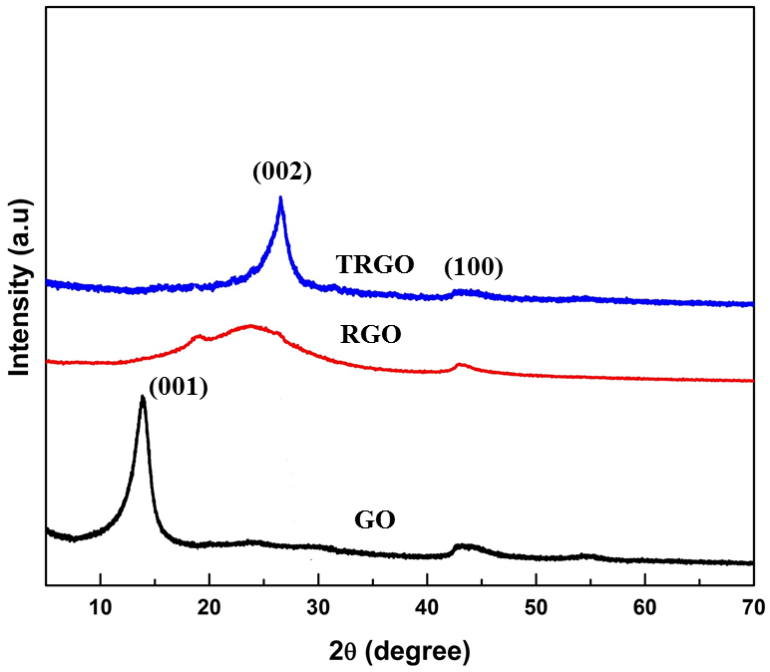

Fig. 8.2: XRD pattern of GO, RGO and TRGO.

Fig. 8.3(a-c) shows the XRD pattern of the Cu-GO, Cu-RGO and Cu-TRGO deposited specimens with different concentrations of GO, RGO and TRGO at 5 kHz pulse frequency, All the XRD peaks of the composite coating specimens were confirmed as pure Cu assigned by JCPDS (card no. 04-0836) data. After co-deposition, no graphene oxide peak was clearly observed as small amount of GO/RGO (up to maximum 1 g/l) was added in the electrolyte. But the presence of the same was confirmed from other characterization, such as FESEM and Raman spectra.

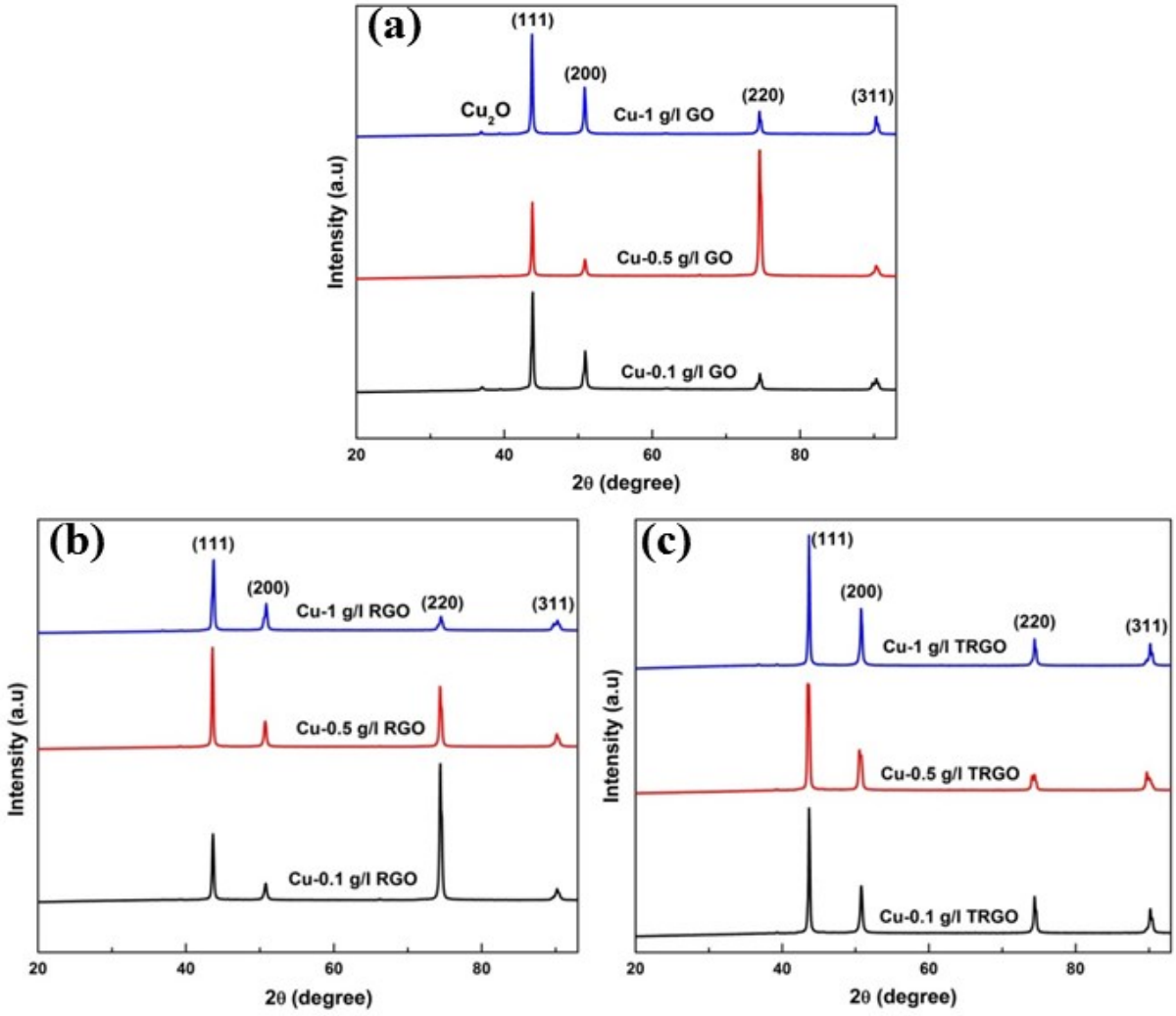

Fig. 8.3: XRD pattern of (a) Cu-GO (b) Cu-RGO and (c) Cu-TRGO composite coating with 5 kHz pulse frequency.

In Fig. 8.3(a) small intensity peaks of Cu_2O was observed and the same was absent in Fig. 8.3(b) and (c), which was formed during deposition process. In Fig. 8.3, changes in the relative intensities of different peaks of Cu were noticed and the same was found to be dependent on the deposition parameters. To identify the effect mathematically, relative texture coefficient (RTC) of each copper plane ((111), (200), (220), and (311)) of all XRD pattern of the deposited specimens were calculated by formula presented in equation 4.1 (refer chapter 4) and the same was reported in table 8.2.

Table 8.2: Texture coefficients of all deposited specimens

Sample Type	Sample Details	$RTC_{(hkl)}\%$			
		(111)	(200)	(220)	(311)
Cu-GO	0.1 g/l	25	25	27	23
	0.5 g/l	09	04	81	06
	1 g/l	23	25	29	23
Cu-RGO	0.1 g/l	08	04	82	06
	0.5 g/l	29	24	22	25
	1 g/l	30	25	26	19
Cu-TRGO	0.1 g/l	22	19	34	25
	0.5 g/l	19	10	57	16
	1 g/l	26	25	25	24

Table 8.2 reveals that Cu-GO composite coating with 0.1 g/l GO reinforcement leads to nearly random orientations (each value is near to 25), but addition of increased amount of GO (0.5 g/l) displayed (220) as preferred orientation and further increment in GO (1g/l) showed again random orientation. In case of Cu-RGO coating, reinforced with 0.1 g/l RGO displayed (220) as preferred orientation and addition of more RGO (0.5 and 1g/l) into the plating solution helped in forming relatively random orientation. In case of Cu-TRGO, 0.5g/l dispersion of TRGO leads to prominent (220) peak, whereas, in other concentrations orientations are nearly random. During composite electrodeposition, formation of particular orientation may be due to interfacial energy driven phenomena and subsequent alteration of interfacial energy in presence of dispersed particle. This may be investigated theoretically by first principle method. Effect of such orientation change can affect the surface mechanical properties to a great extent.

8.4 Morphology study

Fig. 8.4 displays the SEM image of few layers (more than three) of graphene oxide synthesized by modified Hummer's method. From the figure it can also be observed that the layers are extremely fine in nature.

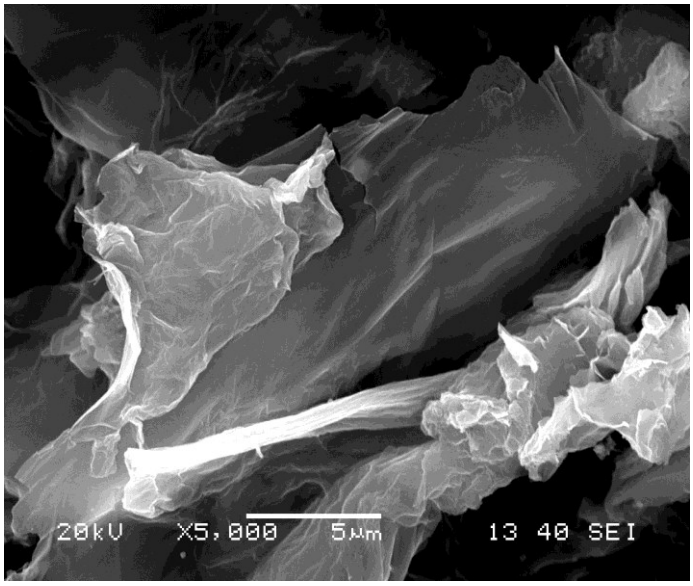

Fig. 8.4: Scanning electron micrograph of GO.

Fig. 8.5(a-i) shows the field emission scanning electron microscopic (FESEM) images of the Cu-GO, Cu-RGO and Cu-TRGO with different concentrations of graphene oxides at different magnifications. The FESEM images of developed composite coating by electrodeposition on copper substrate confirm the presence of GO in the Cu matrix mainly as needle like structures. Morphology of Cu-0.1 g/l GO shows ply-form laminae or platelets are vertically aligned and perpendicular to the substrate. The composite nano platelets (approximate thickness of less than 80 nm) are intersecting with each other in various longitudinal directions (Fig. 8.5a) and loosely packed with each other. But in case of Cu-RGO and Cu-TRGO with same loading level morphology looks denser than Cu-GO coating (Fig. 8.5d, g). All the composite coatings with 0.1 g/l loading level showed almost similar structures. When loading level of GO, RGO and TRGO was increased from 0.1 to 0.5 g/l, morphology of the same became denser, compact and uniform than 0.1 g/l loading level. Beyond 0.5g/l loading, microstructures show coarse structure with possible agglomerated graphene oxide.

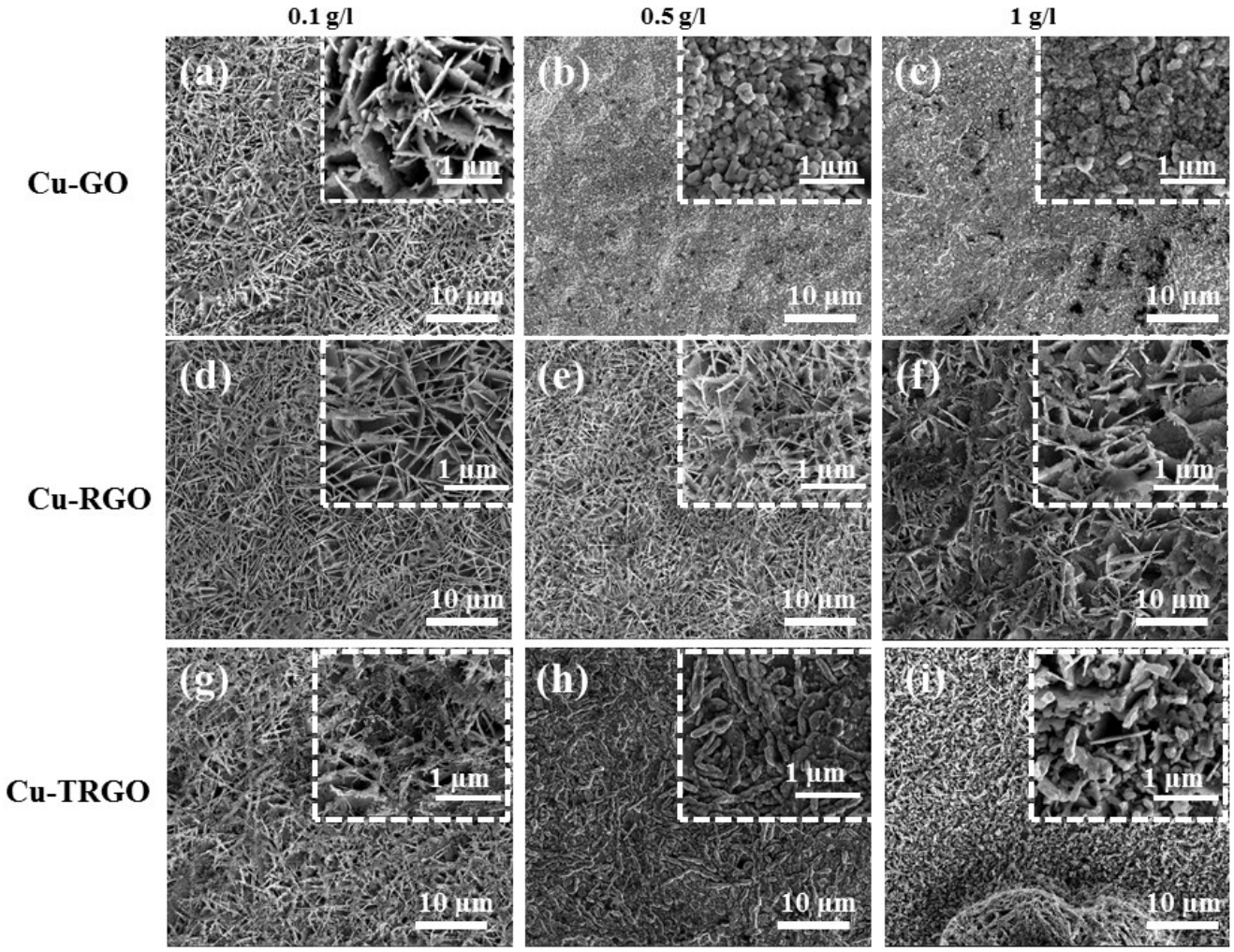

Fig. 8.5: FESEM images of Cu-GO, Cu-RGO and Cu-TRGO composite coatings.

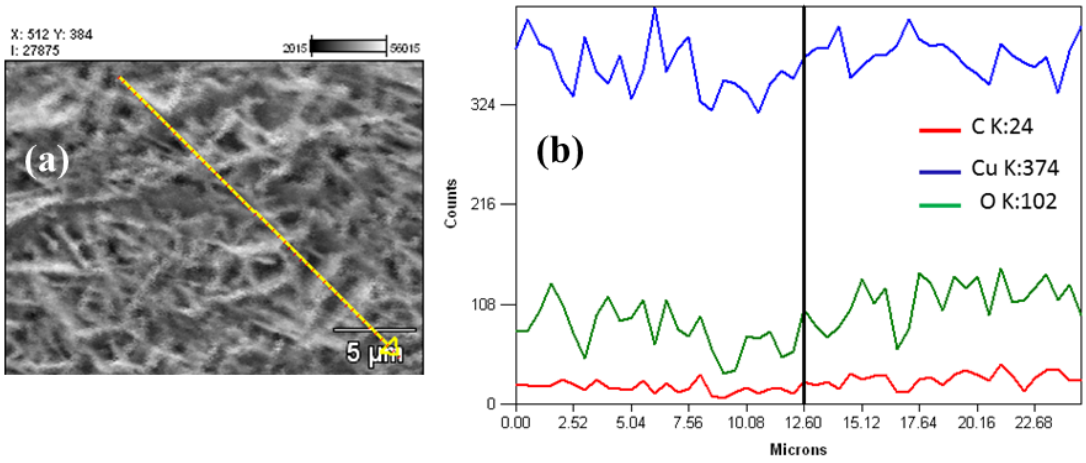

Fig. 8.6: X-ray line mapping of Cu-0.1 g/l GO composite coating.

Fig. 8.6 shows the x-ray line mapping as Cu-0.1 g/l GO composite coating. From the obtained result, the presence of Cu, C and O was confirmed. The result displayed the maximum intensity of copper (Cu) followed by oxygen (O) and carbon (C). The lower intensity in case of C compare O was obvious due to the presence of excess oxygen containing groups in GO.

8.5 Raman spectroscopy

Structural changes arising due to the chemical and thermal processing from GO to reduced GO and then to TRGO, are reflected in their Raman spectra (Fig. 8.7(a-c)). Spectra of Cu-0.5g/l TRGO coating is also displayed in Fig. 8.7(d). The Raman spectrum of the GO contains both D and G bands (at 1343 and 1594 cm^{-1}, respectively). But, in case of RGO, D and G band are slightly shifted to 1349 and 1596 cm^{-1} respectively. However, an increased D/G intensity ratio of RGO (0.94) as compared to that of GO (0.91) suggests a decrease in the average size of the sp^2 domains upon reduction of the exfoliated GO by chemical treatment due to the generation of strains and/or topological defects upon the quick removal of oxygen [174]. The sudden decrease in I_D/I_G ratio to 0.66 in case of TRGO was observed.

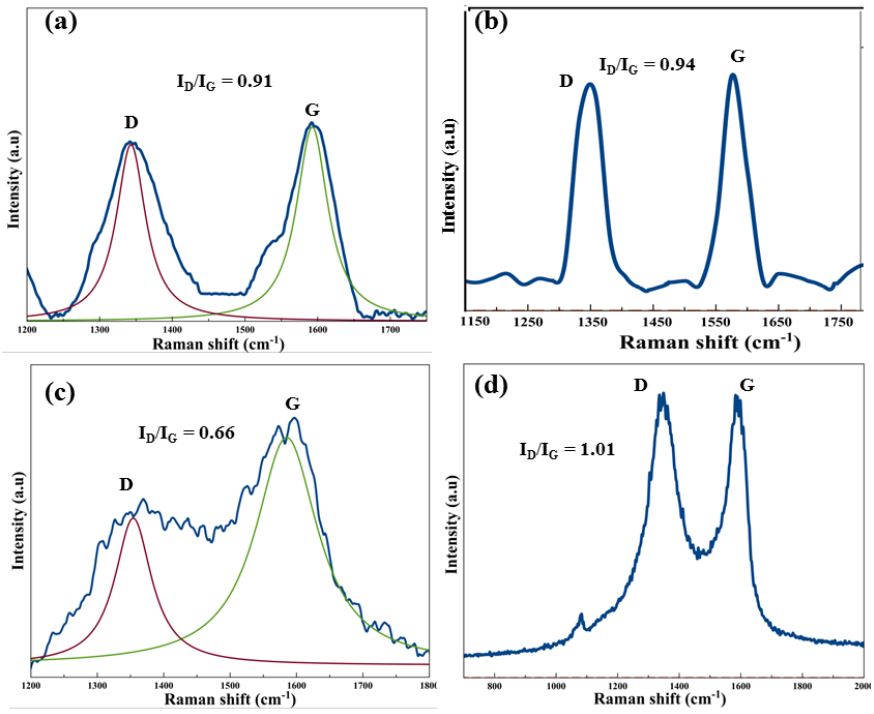

Fig. 8.7: Raman spectra of (a) GO, (b) RGO, (c) TRGO and (d) Cu- 0.5 g/l TRGO specimens.

This can be explained by slow rise in temperature (5^{o}C/min) in the furnace, which may allow the removal of the functional groups with less structural strain. This leads to recovered high surface area due to expansion and exfoliation of graphene oxides without breakage [175]. In the Raman spectra (Fig. 8.7d), Cu-0.5g/l TRGO composite coating showed the D-Band at a wave number of 1346 cm^{-1}, and the G-band at a wave number of 1592 cm^{-1}. A minor increase in the intensity of the D-band than the G-band is observed in the composite coating. The intensity ratio of D to G band (1.01) was also increased in case of composite coating compared to pure GO, RGO and TRGO, which may be due to the stresses of formation in TRGO and crumpling/folding of TRGO in the matrix during co-deposition with Cu on copper substrate [86].

8.6 XPS spectra

Fig. 8.8 shows XPS spectra of RGO and TRGO and Cu-0.5 g/l TRGO coating which confirmed C/O ratio of 4, 8.25 and 6.3 respectively. In case of RGO and TRGO, TRGO obtained better C/O ratio, means better reduction of oxygen containing groups during thermal reduction process was successful.

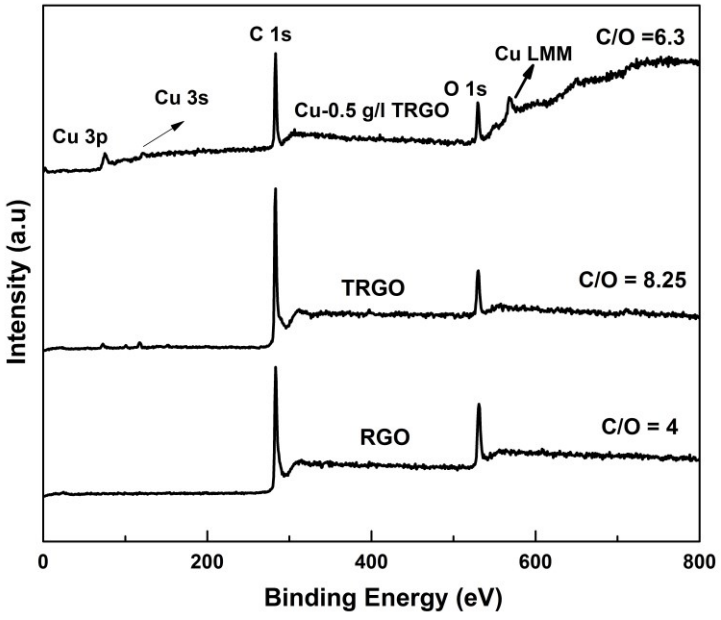

Fig. 8.8: XPS spectra of RGO and TRGO and Cu-0.5 g/l TRGO coating.

Further, the chemical states of different elements present in Cu-TRGO composite coating were analyzed by using high-resolution XPS. Fig. 8.9 shows the detailed XPS spectra of the Cu/TRGO composite coating deposited from the sulfate bath of 0.5 g/l TRGO concentration for 20 minute. Fig. 8.9(a) depicts the C1s spectrum of the composite film, where the main peak at 283.8 eV corresponds to the sp^2 bonded carbon, and the small deconvoluted peaks at 285.4, 287.3, and 288.1 eV represent the C−O, C=O and O−C=O bonds, respectively [86]. Similarly Fig. 8.9(b) correspond to the O1s spectrum and was deconvoluted into four peaks: the two peaks with 533.6 and 531.8 eV of binding energy can be assigned to the C−O and C=O/O−C=O bonds [176, 177] and other two peaks of binding energies at 530.2 and 530.9 eV corresponds to Cu_2O and $Cu(OH)_2$, [178, 179] respectively. The main peaks in the Cu 2p spectrum (Fig. 8.9(c)) of the composite coating at 931.9 eV (Cu $2p_{3/2}$) and 951.7 eV (Cu $2p_{1/2}$) are assigned to the spectral overlapping of metallic Cu−Cu bond and Cu_2O, and the peak at 934.3 eV of binding energy related with $Cu(OH)_2$ [178, 179].

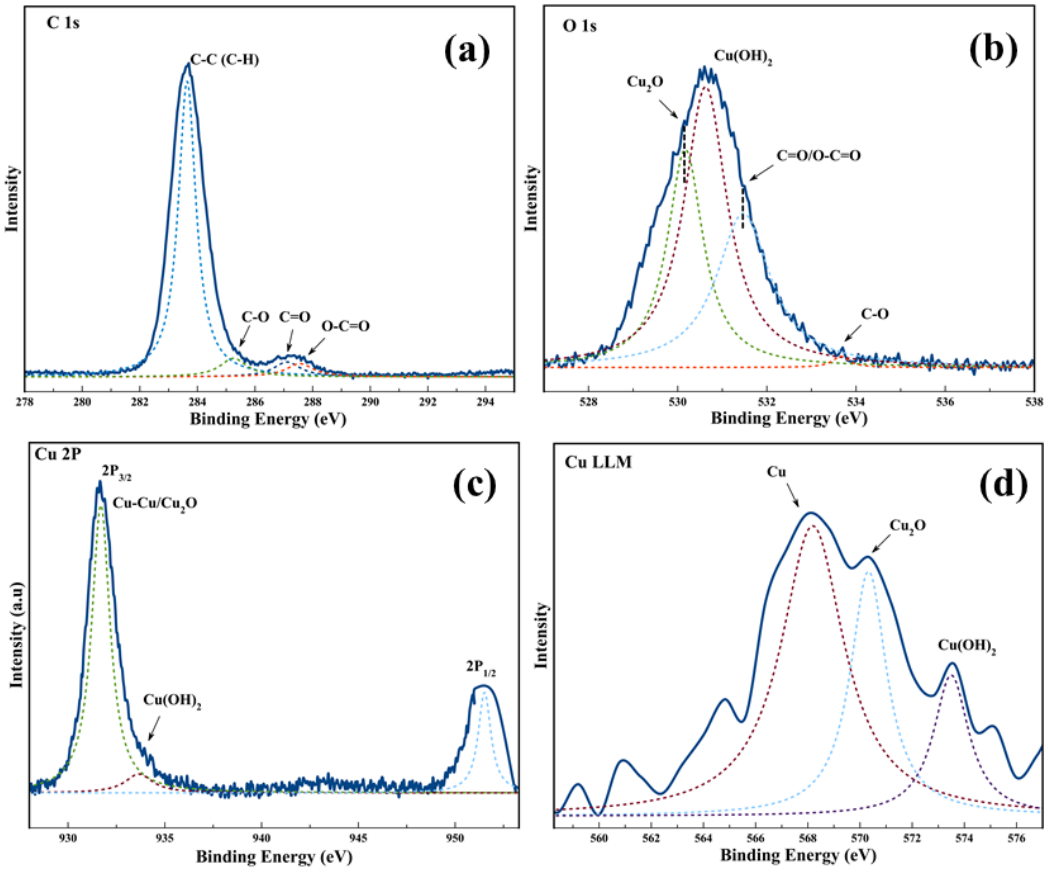

Fig. 8.9: XPS spectrum of Cu-0.5 g/l TRGO specimen.

In the Cu LMM spectrum (Fig. 8.9(d)), the strong peak at 568.2 eV confirms the main copper peak and another less prominent peak at 570.3 eV further confirms the presence of Cu_2O on the top surface layer of the composite film [178]. The formation of Cu_2O is mainly attributed to the interaction between copper ions and oxygen attached TRGO surfaces. From the Fig.8.8, it can be confirmed that atomic percentage of C/O ratio of TRGO is greater than 8, whereas in case of RGO it is around 4, which is much higher than synthesized GO. The very high C/O ratio indicates that majority of oxygen containing groups, e.g., carboxyl and hydroxyl groups, on the GO sheet surfaces have been successfully reduced during chemically and themally reduction process, which leads to better elelctrical conductivity of the same. Slightly decrease in C/O ratio (6.3) in case of Cu-TRGO composite coating can be explained by formation of copper oxide due to interaction between copper and oxygen presence in TRGO.

8.7 Microhardness study

Fig. 8.10 displays the hardness values measured on the coated surfaces of all the specimens as a function of GO, RGO and TRGO concentrations. Addition of 0.5 g/l of GO/RGO/TRGO displayed highest hardness values compared to other reinforcement concentrations. This is worth mentioning that, hardness value for pure copper coating obtained with 5 kHz pulse frequency is 154 HV, as reported earlier [160]. Such earlier analysis shows that surface hardness is highly dependent on reinforcement, matrix structure and crystallographic orientation. In the present study, most of the samples shows higher hardness compared to this value. The maximum hardness value was observed as 215 HV for Cu-0.5g/l GO followed by Cu-0.5g/l TRGO (207 HV) composite coatings, which were approximately 40 and 34 percent higher than pure copper coating deposited at same processing parameter. This can be attributed to GO reinforcement, which hinders the dislocation motion of the grains caused by dispersion hardening mechanism. In case 0.1 g/l GO reinforced copper based composite coatings show lower hardness values, which was consider to be obvious due to inadequate amount of GO deposited in the matrix. But in case of RGO and TRGO reinforced composite coating with same loading level (0.1g/l), the hardness was higher, which can be explained by reduction of average size of RGO during chemical treatment of the same which in turns forms

uniform distribution of RGO throughout the matrix and decrease the inter particle distances between RGO in the coating. This caused better dispersion hardening than 0.1 g/l GO reinforced composite coating. But, Cu-0.1g/l TRGO showed further better hardness value due to high surface area of TRGO recovered during slow heating in furnace. Cu-0.5g/l GO shows best hardness followed by Cu-0.5g/l TRGO.

Compared to 0.1 g/l GO coating, presence of excess amount of functional groups in 0.5g/l GO has better binding capability to divalent Cu^{2+} ions [180], which leads to better hardness than 0.5 g/l RGO and TRGO reinforced composite coating. Formation of dense granular structure can be considered as another reason for highest value of hardness (Fig. 8.3b) of 0.5g/l GO coating. Cu-0.5g/l TRGO shows minor decrease in hardness value, but hold better hardness than Cu-0.5g/l RGO due to the compact microstructure formation. Beyond 0.5 g/l reinforcement, sudden decrease in hardness value was observed for all 1g/l reinforced composite coatings. This can be explained as the probability of agglomeration and clustering of GO in the copper matrix, which is due to the difficulty of evenly dispersing such amount of GO by stirring. Thus the non-uniformity of distribution of GO in the developed composite will weaken the effects of GO on the strength and toughness of the Cu matrix composite, which is responsible for the deterioration in hardness of 1g/l GO/RGO/TRGO reinforced composite coating.

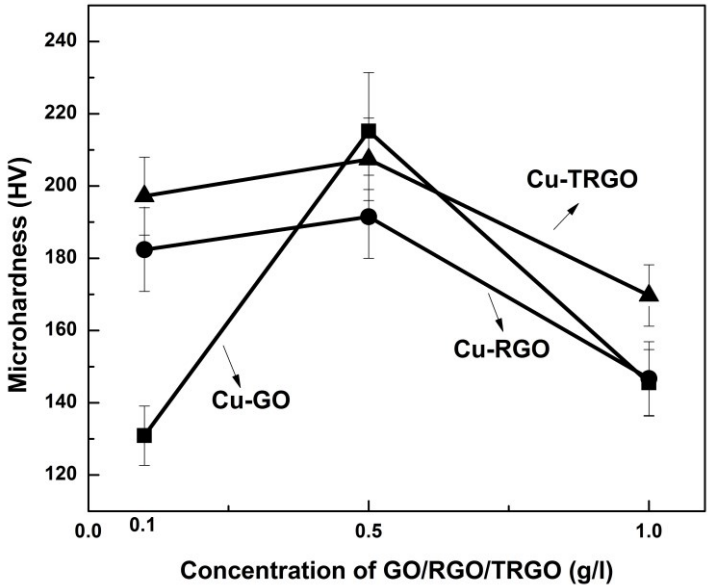

Fig. 8.10: Microhardness of all deposited specimens.

Further, if table 8.2 is considered, it can be observed that 0.5g/l GO coating has high value of $RTC_{(220)}$ followed by 0.5g/l TRGO. Prominent (220) peak can produce more strain energy [137] compared to random orientation which leads to better surface mechanical properties. Similarly, lower hardness values of coatings deposited with 1g/l dispersion can also be explained by the RTC value as all such coatings displays nearly random orientations.

8.8 Wear study

Fig. 8.11 (a-c) represents the influence of GO, RGO and TRGO content on the wear performance of Cu-GO, Cu-RGO and Cu-TRGO composite coatings respectively. As seen from the result, wear performance of Cu-TRGO composite coatings are better than Cu-GO and Cu-RGO composite coatings. Best wear resistance result was obtained for all composite films in medium value of dispersion concentration i.e. 0.5 g/l GO/RGO/TRGO followed by 0.1 and 1 g/l loading level. This trend is quite similar to that of hardness trend (Fig. 8.10). The hardness of the developed composite coating played an important role to explain the wear loss behavior of composite coatings. Generally, the materials with lower hardness have higher wear loss compared to the materials with higher hardness. Further, as per Archard equation it is well established fact that there is a direct relation between wear resistance and hardness of the materials [181, 182]. For this reason, 1 g/l reinforced GO, RGO and TRGO showed lower wear resistance compared to other specimens. With increase in reinforcement loading level form 0.1 to 0.5 g/l, the improvement in wear resistance can be attributed to the strengthening and lubricating effect of GO to the copper matrix, which restricts the removal of material during the dry sliding process. However, with further increasing the volume fraction of GO (beyond 0.5g/l) in copper matrix, an increase in wear loss was observed. The degradation of anti-wear ability of 1 g/l GO, RGO, TRGO reinforced copper composite coating may be attributed to the deterioration of mechanical properties as observed in the hardness result. But, if wear properties or wear depth at particular concentrations of GO, RGO or TRGO are compared then it can be found that wear depth is least for TRGO coating followed by GO and RGO. In this aspect, the trend is not exactly same with hardness. Static loading during hardness testing and dry sliding wear test may display different results due to frictional

condition of the surface and surface roughness. It is worth mentioning that graphene has been reported as one of the novel solid lubricant due to its excellent tribological performance [183]. Thus all wear result cannot be explained by simple hardness trend.

The coefficient of friction (CoF) for each developed coating was found to be varying with GO, RGO and TRGO concentrations as presented in Fig. 8.11(d). From the figure, it can be observed that friction coefficient was increased with increasing concentrations of GO, RGO and TRGO, which is opposite to the previously reported results [183]. But in some cases, it was reported that CoF decreases with increasing amount of graphene due to interlayer sliding usually concentrates on single or double layer. But, when the sliding occurs on multiple interfaces (more than 3 layers) like the current work, CoF was increased due to stick-slip behavior [184]. According to Prandtl–Tomlinson model (PT model) [185, 186], in the shear sliding of GO sheets with multiple layers (more than three), stick–slip behavior cannot be avoidable, because the lateral stiffness of the sliding body, which is significantly reduced by the existence of multiple weak interlayer interfaces and is always lower than the lateral contact stiffness at the sliding interface. Stick–slip behavior is usually not so evident due to smaller number of interfaces of graphene sheets (lesser than three). The CoF of the present work was observed minimum as 0.04 and maximum as 0.17 composite coating. Cu-TRGO coatings showed lower CoF than Cu-GO and Cu-RGO coatings. The coefficient of friction reduction to a greater extent in case of Cu-TRGO owed to formation of extremely adherent and continuous graphene layer at the sliding surfaces as evident from Fig. 8.5(g-i). Another reason can be considered for low CoF of TRGO reinforced coating as high surface area of TRGO due to expansion and exfoliation of RGO during slow heating at high temperature. It was worth to mention that the reported CoF values in the current study is far better than previously reported copper based composite coatings [160, 83, and 17]. From Fig. 11(d) it can also be observed that at all concentrations, GO based coatings show higher CoF than TRGO based coatings and further RGO based coatings display maximum CoF values. Reason of showing best CoF values of TRGO coatings has already been discussed; moreover, it is worth mentioning that Cu-GO coating may be better in comparison to Cu-RGO coatings in terms of CoF due to breakage of GO layers during the chemical treatment which is required to

synthesize RGO. Thus, in the present study the tribological properties of Cu-GO coatings show intermediate properties compared to others.

Fig. 8.12(a-c) shows worn wear track of Cu-0.5 g/l GO, Cu-0.5 g/l RGO and Cu-0.5 g/l TRGO, respectively. The obtained result shows Cu-0.5 g/l RGO has wider and rough wear track compared to both 0.5 g/l GO and TRGO reinforced specimens, which is also in agreement with the wear depth verses time result (Fig. 8.11(a-c)).

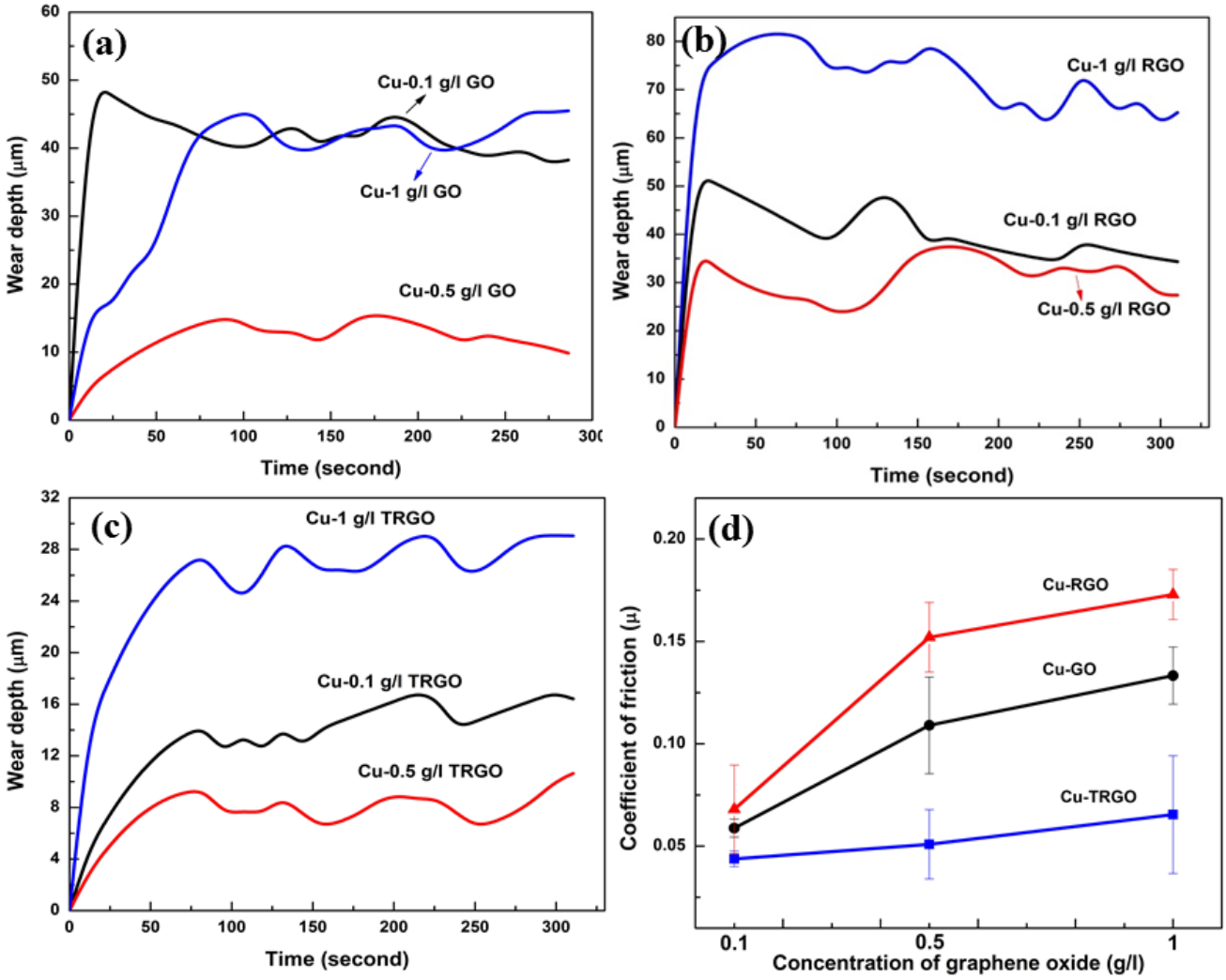

Fig. 8.11: Wear depth vs Time plot of (a) Cu-GO (b) Cu-RGO, (C) Cu-TRGO composite coatings with 5 kHz pulsing condition and (d) Coefficient of friction of all deposited specimens.

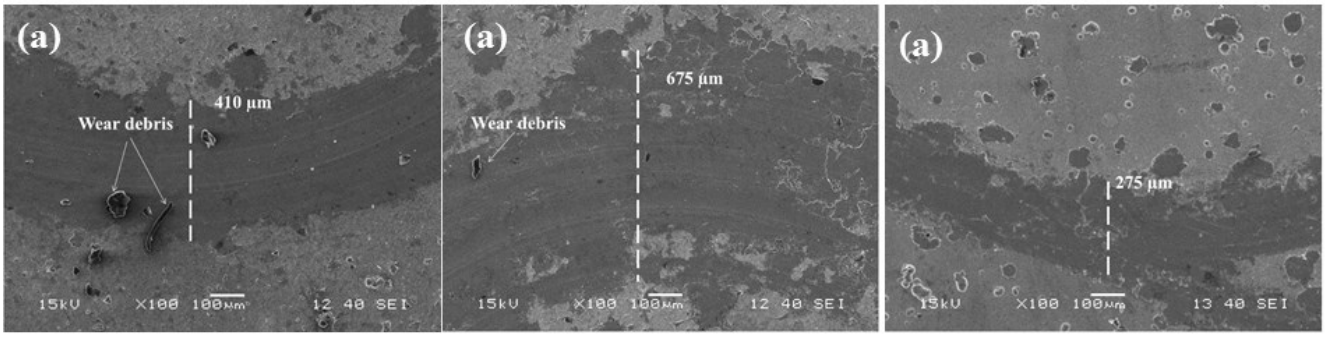

Fig. 8.12: SEM images of worn wear tracks (a) Cu-0.5 g/l GO (b) Cu-0.5 g/l RGO, (C) Cu-0.5 g/l TRGO composite coating.

8.9 AFM study

Fig. 8.13 displays the representative AFM images of some selected coatings on the surface area of 20 µm×20 µm. Fig. 8.13(a-c) shows surface after deposition with 0.5 g/l reinforced Cu based GO, RGO, and TRGO composite coatings. To investigate the surface roughness (Ra) of the above said specimens, AFM data was used and it was observed that Cu-0.5g/l TRGO specimen exhibited lowest surface roughness (0.23 µm) followed by 0.5 g/l GO and RGO reinforced (0.35 and 0.67 µm) composite coatings respectively. This observation is well in agreement with the wear depth vs time and CoF plot (Fig.8.11). This can also be revealed that the *Ra* values observed from the AFM measurements are well in the range of acceptable limits of Cu-based electrical components.

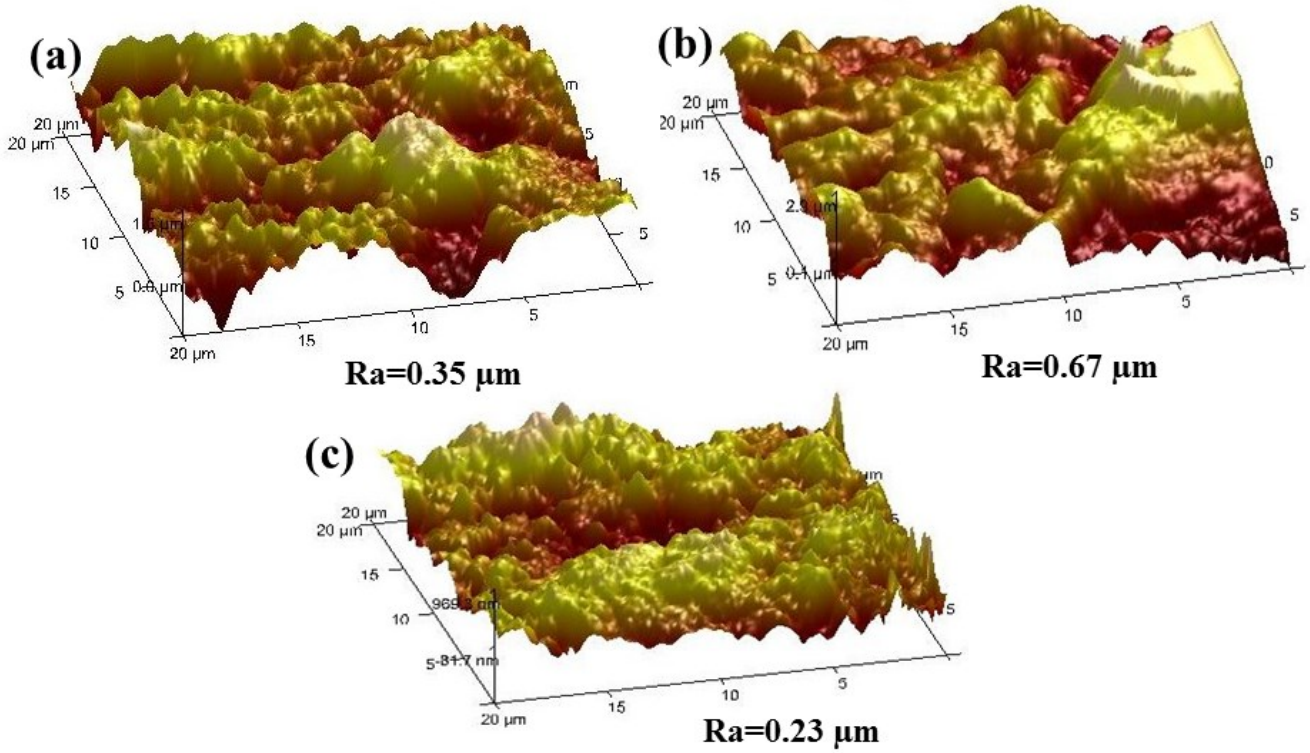

Fig. 8.13: AFM images of (a) Cu-0.5g/l GO, (b) Cu-0.5g/l RGO and (c) Cu-0.5g/l TRGO deposited specimens.

8.10 Electrical conductivity

Electrical conductivity of synthesized GO, RGO and TRGO is presented in Fig. 8.14(a). As this conductivity test was carried out on green pellet, these data cannot be considered as standard. But, comparative trend showed that TRGO had best electrical conductivity (in order of 10^3) compared to both GO and RGO, whereas, RGO shows 10^1 and GO shows 10^{-3} order. Thus, the conductivity result of TRGO is 6 orders higher than GO and 2 order higher than RGO. Increased electrical conductivity of TRGO in comparison to GO and RGO was attributed to the reduction of major oxygen containing functional groups during the thermal reduction process, which is also in complete agreement with C/O ratio of the XPS result presented in Fig. 8.8. Fig. 8.14(b) displayed the result of electrical conductivity values in terms of percentage of International Annealed Copper Standard (IACS) of all coated

specimens. The reported result is based on different copper based GO, RGO and TRGO composite coatings as a function GO/RGO/TRGO concentrations. From the obtained result, it can be observed that Cu-GO composite coating show lower electrical conductivity compare to Cu-RGO and Cu-TRGO composite coating, which is obvious due to insulating nature of GO as well as excess Cu_2O formation due to presence of higher amount of oxygen. This result can also be supported by information given in Fig. 8.14(a). Cu-TRGO coatings showed excellent electrical conductivity result due to better conductivity of TRGO followed by Cu-RGO coatings. Minor decrease in conductivity value in case of Cu-RGO was directly affected by the lower conductivity of value of RGO obtained in Fig. 8.14(a).

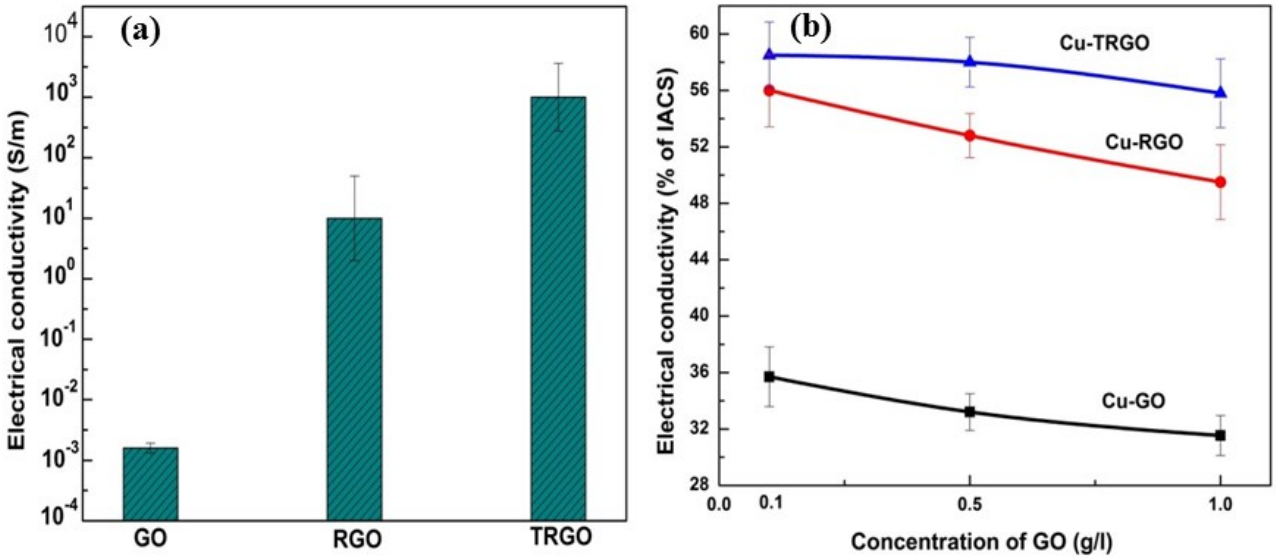

Fig. 8.14: Electrical conductivity of (a) GO, RGO, TRGO and (b) Cu-GO, Cu-RGO and Cu-TRGO deposited specimens.

8.11 Summary

The present work is based on electro-codeposition of Cu-GO, Cu-RGO, and Cu-TRGO on copper substrate from acidic copper sulfate bath with incorporation of these dispersions at different concentrations by pulsed electrodeposition method. From the detailed investigated results, the following inferences can be drawn.

- Different concentrations (0.1, 0.5 and 1 g/l) of GO, RGO and TRGO reinforced Cu based composite coatings were successfully developed.

- Composite deposits from 0.5 g/l GO/RGO/TRGO dispersed electrolyte results in better hardness and wear resistance than 0.1 and 1 g/l reinforced composite coating.
- Excellent electrical conductivity of Cu-TRGO and Cu-RGO coatings was observed.
- Overall, Cu-0.5 g/l TRGO exhibited optimum mechanical and electrical properties compared to other composite coatings.
- The present work can be considered as a potential way to improve surface-mechanical and electrical properties for electrically used copper components.

Chapter 9

Conclusions

9.1 Essence of the Dissertation

In the present dissertation, an attempt was made to codeposit different oxide ultrafine particles (Al_2O_3, SiO_2, Y_2O_3, ZrO_2 and GO) with copper on copper substrate from acidic copper sulfate bath with direct and pulsed direct current modes in different current densities (5, 8, 11 and 14 A/dm^2) as well as pulse conditions (1, 5 and 10 kHz) with dispersion of various concentrations of second phase particles. Effect of various surfactants (cationic, anionic, non-ionic and polymeric) on different properties was also studied. Microstructural, mechanical and electrical properties of all deposited specimens were studied experimentally.

Conclusions, obtained on the basis of detailed investigation as in the current dissertation, are summarized below:

- Various Cu-based composite coatings (Cu-Al_2O_3, Cu-SiO_2, Cu-Y_2O_3, Cu-ZrO_2 and Cu-GO) were successfully developed by electrodeposition technique and distribution of second phase particles in the matrix was confirmed.
- Effect of different current densities (5, 8, 11 and 14 A/dm^2) on surface-mechanical behavior of Cu-Al_2O_3 coating was studied and Cu-30 g/l Al_2O_3 at 8 A/dm^2 current density shows overall the best mechanical and electrical properties on the basis of experimental findings.
- Cu-SiO_2 and Cu-Y_2O_3 deposited by pulse electrodeposition shows better surface-mechanical properties compared to DC deposition technique due to formation of finer matrix.
- In case of Cu-SiO_2 system, Cu- 30 g/l SiO_2 developed at 10 kHz pulse shows overall better mechanical and electrical properties compared to other deposited specimens can be explained as higher amount of codeposited SiO_2 in the matrix, formation of finer matrix caused by nucleation, and crystallographic orientation.

- Considering all the mechanical and electrical properties of Cu-Y_2O_3 coating specimens for possible applicability proposes, Cu-30 g/l Y_2O_3 deposited with 5 kHz pulse frequency can be considered as best material.
- Though Cu is known for easy oxidation even in normal atmosphere, high temperature (575 and 640 ^oC) thermal oxidation behavior of pure Cu and Cu-Y_2O_3 composite coatings was studied. From the obtained results, Cu-Y_2O_3 composite coating confirmed better thermal oxidation resistance behavior compared to pure Cu coating.
- Crystallographic texture characterization studies of both Cu-SiO_2 and Cu-Y_2O_3 composite coatings as well as pure copper coating were briefly elaborated. It was observed that formation of [111] fibre orientation favors better hardness and electrical conductivity compared to other orientation in spite of lower grain size in case of pure copper coating. In case of composite coatings hardness value increased with development of [111] fibre, but decrease in electrical conductivity in spite of the formation of [111] orientation was attributed to higher amount of codeposited second phase insulating particles.
- Different surfactants (cationic, anionic, non-ionic and polymeric) treated Cu-ZrO_2 composite coating at 5 kHz pulse frequency was synthesized and the effects of surfactants concentrations on surface-mechanical and electrical properties were elucidated. Surfactants concentrations greatly affect the microstructure, which in turn influence the mechanical and electrical properties. Evolution of nano-cone arrays of Cu-ZrO_2 composite coating at 5 kHz pulse frequency with CTAB assisted was observed. 0.5 g/l CTAB assisted Cu-ZrO_2 coating shows duplex structure of nano-cone arrays with ultrahigh hardness. Beyond 0.5 g/l CTAB assisted composite coating becomes coarser and flower like structure was observed.
- After analyzing all the mechanical and electrical results of different surfactant assisted composite coatings, it was observed that 0.1 g/l CTAB and 20 g/l glucose shows overall better results compared to their counterparts. But, among the two best result showing coatings 20g/l glucose assisted coating can be considered as best in terms of mechanical and electrical properties.

- Elaborate study on GO/RGO/TRGO reinforced Cu based composite coating was carried out at 5 kHz pulse frequency with different concentrations (0.1, 0.5 and 1 g/l) of GO/RGO/TRGO. Among all the coated specimens 0.5 g/l reinforced GO/RGO/TRGO composite coating showed better mechanical and electrical properties. But, Cu-0.5g/l TRGO was considered as best among all coated specimens in terms of mechanical and electrical properties for possible application in electrical contacts.

9.2 Future scope of the work

- Due to time constrain, effect of various process parameters such as pH, stirring rate, and duty cycles *etc*. on surface-mechanical study was not explored. This can be explored in future may not be with same composite coating systems, but with other coating systems.
- In the current dissertation, detailed optimization of second phase oxide particle concentrations, current densities as well as pulse parameters were not studied due to time and complicacy of the dissertation, which is important to understand the different material properties for its end use. The optimization of process parameters can be explored in future.
- In the present thesis, deposition systems were based on composites, basically Cu with one second phase particles on copper substrate for specific property improvement. The addition of second phase insulating oxide particle into the matrix might have increased the mechanical properties, but deterioration in original electrical conductivity of Cu was observed, which is a major concern over applicability in copper based electrical components. To improve the electrical conductivity further and adhesiveness between metal and second phase oxide particles simultaneous metal coating with other primary metal and second phase ceramic oxide particle can be a scope for future. This also indirectly resists the oxidation diffusion and help to retain its conductivity for longer period of time.
- Previously crystallographic orientation dependent properties of various coating material have been explored. In future, texture characterization of the current coated

specimens by Energy back scattered diffraction study (EBSD) will be interesting to study the effect of different crystallographic orientation on mechanical and electrical properties of the material.

- Cu is commonly considered as oxidation prone material in ambient temperature, whereas graphene is regarded as good oxidation resistance material. Though, in the current dissertation Cu-0.5g/l TRGO was observed to be the best material in terms of surface-mechanical and electrical properties. But further high temperature thermal oxidation study of the material will be a fruitful trial.

References

[1] L. Jun, W. Yiyong, W. Dianlong, and H. Xinguo, *Journal of Material Science*, 35 (2000) 1751–1758.

[2] L. J. Durney, *Electroplating engineering handbook,*Van Nostrand Reinhold Company, 1985.

[3] Y. Boonyongmaneerat, K. Saengkiettiyut, S. Saenapitak and S. Sangsuk, *Surface & Coatings Technology,* 203 (2009) 3590-3594.

[4] I. Gurrappa and L. Binder, *Science and Technology of Advanced Materials,* 9 (2008) 043001.

[5] C. T. J. Low, R. G. A. Wills and F. C. Walsh, *Surface & Coatings Technology* 201 (2006) 371-383.

[6] H. K. Lee, H. Y. Lee and J. M. Jeon, *Surface & Coatings Technology* 201 (2007) 4711-4717.

[7] H. Gul, F. Kilic, S. Aslan, A. Alp and H. Akbulut, *Wear*, 267 (2009) 976-990.

[8] L. Wang, Y. Gao, Q. Xue, H. Liu, and T. Xu, *Materials Science and Engineering: A*, 390 (2005) 313–318.

[9] Z. A. Hamid and I.M. Ghayad, *Materials Letters*, 53 (2002) 238–43.

[10] Z. Guo and X. Zhu, *Materials Science and Engineering: A*, 363 (2003) 325–329.

[11] L. Shi, C.F. Sun, F. Zhou, and W.M. Liu, *Materials Science and Engineering: A*, 397 (2005) 190–194.

[12] Q. Li, W. Fu, Y. Mu, W. Zhang, P. Lv, L. Zhou, H. Yang, K. Chia and L. Yanga, *Crystal Engineering Communication*, 16 (2014) 5227-5233.

[13] R. D. Srivastava and S. K. Nigam, *Surface Technology*, 10 (1980) 343 – 348.

[14] Z. A. Hamid, *Materials Letters*, 57 (2003) 2558–2564.

[15] A. Gomes and M.I. da Silva Pereira, *Electrochimica Acta*, 51 (2006) 1342–1350.

[16] H. Ogihara, H. Wang, T. Saji, *Applied Surface Science*, 296 (2014) 108–113.

[17] M. Eslami, H. Saghafian, F. Golestani-fard, and A. Robin, *Applied Surface Science*, 300 (2014) 129–140.

[18] G. E. Dieter, *Mechanical metallurgy*, McGraw Hill, Singapore, 1988.

[19] L. S. Raju and A. Kumar, *Defense Technology*, 10 (2014) 375–383.

[20] Carl H. Samans, *Engineering Metals and their Alloys*, MacMillan, 1949.

[21] J. R. Davis, *Copper and Copper Alloys*, ASM International, 2001.

[22] J. W. Kaczmar, K. Pietrzak, W. Wlosinsi, *Journal of Materials Processing Technology*, 106 (2000) 58-67.

[23] E. R. I. Mahmoud, A. M. A. Al-qozaim, *Arabian Journal for Science and Engineering*, 41(2016)1757-1769.

[24] J. Pelleg, *Mechanical Properties of Materials,* Springer, New York, 2013.

[25] W.D. Callister, *Fundamentals of Materials Science and Engineering*, Wiley & Sons, 2004.

[26] P. M. Unterweiser (ed.), *Source Book on Copper and Copper Alloys*, ASM, Metals Park, Ohio, 1979.

[27] E. G. West (ed.), *Copper and its Alloys*, Ellis Horwood, Chichester, 1982.

[28] M. Bauccio (ed.), *ASM Metals Reference Book*, Third Edition, Materials Park, Ohio, 1999.

[29] R. Chattopadhyay, *Advanced Thermally Assisted Surface Engineering Processes*, Kluwer Academic Publishers, MA, USA (now Springer, New York), 2004.

[30] R. H. Todd, Dell K. Allen, L. Alting, "*Surface Coating*", Manufacturing Processes Reference Guide. Industrial Press Inc, 1994.

[31] A. Brenner, and G. Riddell, *Deposition from Aqueous solution: An overview*, J. Res. Natl. Bureau of Standards, 1947.

[32] A. Andre (ed.), *Handbook of Plasma Immersion Ion Implantation and Deposition*, Wiley-Interscience, New York, 2000.

[33] J. E. Mahan, *Physical Vapor Deposition of Thin Films*, John Wiley & Sons, New York, 2000.

[34] M. L. Hitchman, and K. F. Jensen, *Chemical Vapor Deposition-Principles and Applications*, Academic Press, London, 1993.

[35] A. Sherman, *Chemical Vapor Deposition For Microelectronics—Principles, Technology and Applications*, Noyes Publications, New Jersey, 1987.

[36] S. Paulussen, R. Rego, O. Goossens, D. Vangeneugden, K. Rose, *Surface & Coatings Technology*, 200 (2005) 672 – 675.

[37] R. G. Ehl, A. Ihde, *Journal of Chemical Education* 31 (1954) 226–232.

[38] "*Electrocoating*"; The Electrocoat Association; Cincinnati, OH; 2002.

[39] L. Besra, M. Liu, *Progress in Materials Science*, 52 (2007) 1–61.

[40] K. Hasegawa, S. Kunugi, M. Tatsumisago, T. Minami, *Journal of Sol-Gel Science and Technology*, 15 (1999) 243–249.

[41] W. Shan, Y. Zhang, W. Yang, C. Ke, Z. Gao, Y. Ke, *Microporous and Mesoporous Materials*, 69 (2004) 35–42.

[42] M. Wei, A.J. Ruys, B.K. Milthorpe, C.C. Sorrell, J.H. Evans, *Journal of Sol-Gel Science and Technology*, 21 (2001) 39–48.

[43] T.M. Sridhar, U.K. Mudali, *Transactions of the Indian Institute of Metals*, 56(3) (2003), 221–230.

[44] M. J. Shane, J. B. Talbot, B. G. Kinney, E. Sluzky, H. R. Hesse. *Journal of Colloid and Interface Science,* 165 (1994) 334–340.

[45] M. J. Shane, J. B. Talbot, R. G. Schreiber, C. L. Ross, E. Sluzky, K. R. Hesse, *Journal of Colloid and Interface Science*, 165 (1994) 325–333.

[46] H. Zhang, Z. Jiang, and Y. Qiang, *Materials Science and Engineering: A*, 517 (2009) 316–320.

[47] C. Shanthi, S. Barathan, J. Rajasrisen, R.M. Arunachalam, S. Mohan, *Materials Letters*, 62, (2008) 4519–4521.

[48] X. Zhang, K. N. Tu, Z. Chen, Y. K. Tan, C. C. Wong, *Journal of Nanoscience and Nanotechnology*, 8 (2008) 2568–2574.

[49] W. Kim and R. Well, *Surface and Coatings Technology*, 38 (1989) 289 – 298.

[50] M. S. Chandrasekar, M. Pushpavanam, *Electrochimica Acta,* 53 (2008) 3313–3322.

[51] A. K. Pradhan and S. Das, *Journal of Alloys and Compounds,* 590 (2014), 294–302.

[52] J. Zhu, L. Liu , G. Hu , B. Shen , W. Hu and W. Ding, *Materials Letters*, 58 (2004) 1634-1637.

[53] P. Gyftou, E.A. Pavlatou, N. Spyrellis, *Applied Surface Science*, 254 (2008) 5910–5916.

[54] Bin Wu, Bin-shi Xu, Bin Zhang, Yao-hui Lü, *Surface & Coatings Technology*, 201 (2007) 6933–6939.

[55] C. Cai, X.B. Zhu, G.Q. Zheng, Y.N. Yuan, X.Q. Huang, F.H. Cao, J.F. Yang, Z. Zhang, *Surface & Coatings Technology*, 205 (2011) 3448–3454

[56] A. Lozano-Morales, and E.J Podlaha, *Journal of The Electrochemical Society*, 151 (2004) 478- 483.

[57] V. Medelien, *Surface and Coatings Technology*, 154 (2002) 104-111.

[58] L. Chen, L. Wang, Z. Zeng, J. Zhang, *Materials Science and Engineering: A,* 434 (2006) 319–325.

[59] S. Mohammadi H, M. A. Apoorva, R. Ravishankar, *International Journal of Technical Research and Applications*, 3 (2015) 398-406.

[60] P. Narasimman, M. Pushpavanama, V. M. Periasamy, Portugaliae, *Electrochimica Acta,* 30 (2012) 1-14.

[61] S. J. Osborne, W.S. Sweet, K.S. Vecchio, and Jan B. Talbot, *Journal of The Electrochemical Society*, 154, (2007) D394-D399.

[62] D. Thiemig, A. Bund, *Surface & Coatings Technology* 202 (2008) 2976–2984.

[63] J. L. Stojak, J. Fransaer and J. B. Talbot, Review of Electrocodeposition, *Advances in Electrochemical Science and Engineering*, Wiley-VCH Verlag GmbH, 2001.

[64] K. H. Hou, M. D. Ger, L. M. Wang, S. T. Ke, *Wear,* 253 (9-10) (2002) 994-1003.

[65] I. Garcia, J. Fransaer, J. P. Celis, *Surface and Coatings Technology*, 148 (2001) 171-178.

[66] M. R. Vaezi, S. K. Sadrnezhaad, L. Nikzad. *Colloids and Surfaces A: Physicochemical and Engineering, 315* (2008) 176-182.

[67] M. Srivastava, V.K. William Grips, K.S. Rajam, *Applied Surface Science,* 253 (2007) 3814-3824.

[68] C. Zanella, M. Lekka, P. L. Bonora, *Journal of Applied Electrochemistry,* 39 (2009) 31-38.

[69] L. Benea, P.L. Bonora, A. Borello, S. Martelli, F. Wenger, P. Ponthiaux, J. Galland, *Solid State Ionics*, 151 (2002) 89-95.

[70] G. Maurin, A. Lavanant, *Journal of Applied Electrochemistry,* 25 (1995) 1113-1121.

[71] S.Y. Park, R.H. Kim, J.S. Kim, C.K. Kim, *Journal of the Korean institute of surface engineering,* 25 (1992) 73-81.

[72] S.C. Wang, W. C. J. Wei, *Materials Chemistry and Physics,* 78 (2003) 574-581.

[73] A.W. Adamson, A. P. Gast, "*Physical Chemistry of Surfaces*", John Wiley and Sons, 1997.

[74] X. Wang, H. Bai, and G. Shi, *Journal of the American Chemical Society,* 133 (2011) 6338–6342.

[75] A. Bund and D. Thiemig, *Journal of Applied Electrochemistry*, 37 (2007) 345–351.

[76] P. Atkins, P. de, *Physical Chemistry*, Oxford University Press, 2006.

[77] K. Helle, F. C. Walsh, *Transactions of the Institute of Metal Finishing*, 75 (1997) 53-58.

[78] C. Kerr, B. D. Barker, F. C. Walsh, J. Archer, *Transactions of the Institute of Metal Finishing*, 78 (2000) 171-178.

[79] F. C. Walsh & C. Ponce de Leon, *Transactions of the Institute of Metal Finishing*, 92 (2014) 83-98.

[80] F. C. Walsh, C. Ponce de León, D. V. Bavykin, C. T. J. Low, S. C. Wang & C. Larson, *Transactions of the Institute of Metal Finishing*, 93 (2015) 209-234.

[81] F. C. Walsh, C. Ponce de León, D. V. Bavykin, C. T. J. Low, S. C. Wang & C. Larson, *Transactions of the Institute of Metal Finishing*, 93 (2015) 241-247.

[82] C. Iticescu, G. Carac, O. Mitoseriu and T. Lampkt, *Revue Roumaine de Chimie*, 53(1) (2008) 43–47.

[83] S. Ramalingam, V.S. Muralidharan, & A. Subramania, *Journal of Solid State Electrochemistry*, 13 (2009) 1777–1783.

[84] I. Zamblau, *Chemical and Biochemical Engineering Quarterly,* 23 (1), (2009) 43–52,

[85] J.R Roos, J.P Celis, and H. Kelchtermans, *Thin Solid Films*, 54 (1978) 173-182.

[86] H. Li, Y. Wan, H. Liang, X. Li, Y. Huang, and F. He, *Applied Surface Science,* 256 (2009) 1614–1616.

[87] I. Zamblau, S. Varvara, L. M. Muresan, *Journal of Materials Science,* 46 (2011) 6484–6490.

[88] Lidia Benea, *Materials and Manufacturing Processes*, 14 (1999) 231-242.

[89] V. Mangam, S. Bhattacharya, K. Das, S. Das, *Surface & Coatings Technology*, 205 (2010) 801–805.

[90] A. K. Pradhan and S. Das, *Journal of Alloys and Compounds,* 590 (2014), 294–302.

[91] B. P. Singh, S. Nayak, K. K. Nanda, B. K. Jena, S. Bhattacharjee, L. Besra, *Carbon*, 61 (2013) 47 –56.

[92] C. L. P. Pavithra, B. V. Sarada, K. V. Rajulapati, T. N. Rao, G. Sundararajan, *Scientific Report*, 4 (2014) 1-7.

[93] G. Xie, M. Forslund, and J. Pan, *ACS Applied Materials & Interfaces*, 6 (2014) 7444−7455.

[94] D. Y. Li, Q. Chen, and X. Y. Wang, *Journal of Applied Physics,* 99 (2006) 044305.

[95] T. Himuro, and S.Takayama, *Journal of the Japan Institute of Metals,* 67 (2003) 342-347.

[96] C. Ryu, K. W. Kwon, A. L. S. Loke, H. Lee, T. Nogami, V. M. Dubin, R. A. Kavari, G. W. Ray, and S. S. Wong, *IEEE Transactions on Electron Devices*, 46 (1999) 1113-1120.

[97] L. Lu, Y. Shen, X. Chen, L. Qian, and K. Lu, *Science*, 304 (2004) 422-426.

[98] L. Lu, R. Schwaiger, Z. W. Shan, M. Dao, K. Lu, and S. Suresh, *Acta Materialia*, 53 (2005) 2169-2179.

[99] B. Z. Cui, K. Han, Y. Xin, D. R. Waryoba, and A. L. Mbaruku, *Acta Materialia*, 55 (2007) 4429-4438.

[100] T. C. Liu, C. M. Liu, H. Y. Hsiao, J. L. Lu, Y. S. Huang, and C. Chen, *Crystal Growth & Design,* 12 (2012) 5012−5016.

[101] T. C. Chan, Y. L. Chueh, C. N. Liao, *Crystal Growth & Design,* 11 (2011) 4970-4974.

[102] J. Hu, H. Li, Q. Wu, Y. Zhao, Q. Jiao, *Chemical engineering Journal* 263 (2015) 144-150.

[103] W. B. Russel, D. A. Saville, and W. R. Schowalter, "*Colloidal Dispersions*", Cambridge University Press, 1992.

[104] B. D. Cullity, *Elements of X-ray diffraction*, Addison-Wesley, 1978.

[105] D. McMullan, *Scanning*, 17 (2006) 175–185.

[106] D. McMullan, V. Ardenne, *The scanning electron microscope*, *Proceedings of the Royal Society*, 23 (1988) 283–288

[107] B. Fultz, and J. Howe, *Transmission Electron Microscopy and Diffractometry of Materials*, Springer, 2007.

[108] D. Williams and C. B. Carter, *Transmission Electron Microscopy: 1 – Basics*, Plenum Press, 1996.

[109] J. M. Bennett, L. Mattsson, *Introduction to Surface Roughness and Scattering,* Optical Society of America, Washington, D.C.

[110] Meyers and Chawla, *Mechanical Behavior of Materials*, 1999, 162–168.

[111] E.J. Pavlina and C.J. Van Tyne, *Journal of Materials Engineering and Performance*, 17 (2008) 888-893.

[112] E. Rabinowicz, *Friction and Wear of Materials*, John Wiley and Sons, New York, 1995.

[113] J. R. Davis (ed.), *Metals Handbook*: Desk Edition. ASM International, 1998.

[114] N. Kumar, *Comprehensive Physics XII*, Laxmi Publications. 2003, pp. 282.

[115] E. Bogatin, *Signal Integrity: Simplified*, Prentice Hall Professional, 2004, pp. 114.

[116] Y. Pauleau, Péter B. Barna, P. B. Barna, *Protective coatings and thin films: synthesis, characterization, and applications*, Springer, 1997.

[117] G. Binnig, C. F. Quate, C. Gerber, *Physical Review Letters*, 56 (1986) 930–933.

[118] D. J. Gardiner, *Practical Raman spectroscopy*, Springer-Verlag, 1989.

[119] S. Ray, and A.G. Shard, *Analytical Chemistry*, 83 (2011) 8659-8666.

[120] S. A. Lajevardi and T. Shahrabi, *Applied Surface Science,* 256 (2010) 6775–6781.

[121] A. Abdel Aal and H.B. Hassan, *Journal of Alloys and Compounds*, 477 (2009) 652–656.

[122] S. R. Allahkaram, S. Golroh, and M. Mohammadalipou, *Materials & Design*, 32 (2011) 4478–4484.

[123] A. Abdel Aal, K.M. Ibrahim, and Z. Abdel Hamid, *Wear*, 260 (2006) 1070–1075.

[124] Q. Feng, T. Li, H. Yue, K. Qi, F. Bai, and J. Jin, *Applied Surface Science*, 254 (2008) 2262–2268.

[125] A. Robin and R.Q. Fratari, *Journal of Applied Electrochemistry*, 37 (2007) 805–812.

[126] G. Parida, D. Chaira, M. Chopkar, and A. Basu, *Surface and Coatings Technology,* 205 (2011) 4871–4879.

[127] J. D. Majumdar, B. Ramesh Chandra, B.L. Mordike, R. Galun, and I. Manna, *Surface and Coatings Technology,* 179 (2004) 297–305.

[128] J.M. Zhang, Y. Zhang, and K.W. Xu, *Journal of Crystal Growth*, 285 (2005) 427–435.

[129] A. Kumar, D. Singh, and D. Kaur, *Surface and Coatings Technology,* 203 (2009)1596–1603.

[130] S. Bera and I. Manna, *Materials Chemistry and Physics*, 132 (2012) 109–118.

[131] M. S. Chandrasekar and M. Pushpavanam, *Electrochimica Acta*, 53 (2008) 3313–3322

[132] N. Ibl, J. C. Puippe, and H. Angerer, *Surface and Coatings Technology*, 6 (1978) 287–300.

[133] M. Braunovic, V. V. Konchits, and N. K. Myshkin, *Electrical Contacts.* CRS Press, USA, 2006.

[134] J. M. Zhang, Y. Zhang, and K.W. Xu, *Journal of Crystal Growth*, 285 (2005) 427–435.

[135] A. K. Pradhan and S. Das, *Journal of Alloys and Compounds,* 590 (2014) 294–302.

[136] A. Ashok, H. S. Maharana and A Basu, *Bulletin of Materials Science,* 38 (2015) 335–342.

[137] H. S. Maharana, A. Ashok, S. Pal, and A. Basu, *Metallurgical and Materials Transactions A*, 47A (2016) 388-399.

[138] R. Bose, G. P. Kalaignan, *Ionics,* 17 (2011) 495–501.

[139] S. Dhar, *Analytical Mobility Modeling for Strained Silicon-Based Devices*, PhD. dissertation, de 1979.

[140] A. K. N. Reddy, *Journal of Electroanalytical Chemistry,* 6 (1963) 141−152.

[141] D. P. Field, *Textured Structures. In ASM Handbook: Metallography and Microstructures*, ASM International, Materials Park, OH, 9 (2004) 215−226.

[142] B. Hong, C.H. Jiang, X. J. Wang, *Materials Transactions,* 47 (2006) 2299−2301.

[143] C. V. Thompson, *Acta Metallurgica,* 36 (1988) 2929−2934.

[144] M. McLean, B. Gale, *Philosophical Magazine,* 20 (1969) 1033−1045.

[145] V. M. Kozlov, L. Peraldo Bicelli, *Materials Chemistry and Physics,* 77 (2003) 289−293.

[146] C. B. Nielsen, A. Horsewell, M. Østergard, *Journal of Applied Electrochemistry,* 27 (1997) 839−845.

[147] S. G. Wang, E. K. Tian, C. W. Lung, *Journal of Physics and Chemistry of Solids*, 61 (2000) 1295−1300.

[148] R. J. Stokes, D. F. Evans, *Fundamentals of interfacial engineering*, John Wiley & Sons, New York, 1997.

[149] E. M. Zielinski, R. P. Vinci, J. C. Bravman, *MRS Online Proceeding Library* 391(1995) 103.

[150] C.V. Thompson, *Scripta Metallurgica et Materialia,* 28 (1993) 167−172.

[151] V. M. Dubin, S. Lopatin, S. Chen, R. Cheung, C. Ryu, S. S Wong, *MRS Online Proceeding Library,* (514) 1998 null.

[152] M. Schlesinger, M. Paunovic, *Modern electroplating*; John Wiley & Sons, New York, 2011.

[153] H. Lee, S. S. Wong, S. D. Lopatin, *Journal of Applied Physics*, 93 (2003) 3796-3804.

[154] Y. W. Lin, J. C. Kuo, K. T. Lui, D. Chen, *Material Science Forum,* 638−642 (2010) 2841−2845.

[155] L. Lu, Y. Shen, X. Chen, L. Qian, and K. Lu, *Science*, 304 (2004) 422-426.

[156] F. Maurer, J. Brotz, S. Karim, M. E. T. Molares, C. Trautmann, H. Fuess, *Nanotechnology,* 18 (2007) 135709.

[157] M. Georgiadou, D. Veyret, *Journal of The Electrochemical Society*, 149 (6) (2002) C324−C330.

[158] H. L. Wei, H. Huang, C. H. Woo, R. K. Zheng, G. H. Wen, X. X. Zhang, *Applied Physics Letters,* 80 (2002) 2290−2292.

[159] H. Huang, H. L. Wei, C. H. Woo, X. X. Zhang, *Applied Physics Letters,* 82 (2003) 4265−4267.

[160] H.S. Maharana, S. Lakra, S. Pal, and A. Basu, *Journal of Materials Engineering and Performance*, 25(1) (2016) 327-337.

[161] C. L. P. Pavithra, B. V. Sarada, K. V. Rajulapati, M. Ramakrishna, R. C. Gundakaram, T. N. Rao, and G. Sundararajan, *Crystal Growth & Design,* 15 (2015) 4448−4458.

[162] S. J. Skrzypek, W. Ratuszek, A. Bunsch, M. Witkowska, J. Kowalska, M. Goły, K. Chruściel, *Journal of Achievements in Materials and Manufacturing Engineering*, 43 (2010) 264-268.

[163] W. Q. Cao, C. F. Gu, E. V. Pereloma, and C. H. J. Davies, *Materials Science and Engineering: A*, 492 (2008) 74-79.

[164] T. Hang, A. Hu, M. Li and D. Mao, *Crystal Engineering Communication*, 12 (2010) 2799–2802.

[165] Y. Deng, H. Ling, X. Feng, T. Hang and M. Li, *Crystal Engineering Communication,* 17 (2015) 868–876.

[166] E. Rudnik, L. Burzynska, L. Dolasinski, M. Misiak, *Applied Surface Science*, 256 (2010), 7414–7420.

[167] Y.C. Chen, S.L. Kuo, J.L. Lee, S.T. Ke, C.H. Wong, M.D. Ger, *Key Engineering Materials,* 364–366 (2008) 346–350.

[168] A. A. Aref, L. Xiong, N. Yan, A.M. Abdulkarem, Y. Yu, *Materials Chemistry and Physics,* 127 (2011) 433–439.

[169] E. Rudnik, L. Burzynska, M. Gut, *Materials Chemistry and Physics,* 126 (2011) 573–579

[170] T. C. Chan, Y. L. Chueh, C. N. Liao, *Crystal Growth & Design,* 11 (2011) 4970–4974.

[171] B. Konkena and S. Vasudevan, *The Journal of Physical Chemistry Letters,* 3 (2012) 867−872.

[172] X. Wang, H. Bai, and G. Shi, *Journal of the American Chemical Society,* 133 (2011) 6338–6342.

[173] Y. Wu, M. Huang, N. Song, W. Hu, *Analytical Methods,* 6 (2014) 2729–2735.

[174] S. Stankovich,, D. A. Dikin, R. D. Piner, K. A. Kohlhaas, A. Kleinhammes, Y. Jia, Y. Wu, S. T. Nguyen, R. S. Ruoff, *Carbon,* 45 (2007) 1558–1565.

[175] X. Chen, D. Meng, B. Wang, B. W. Li, W. Li, C. W. Bielawski, R. S. Ruoff, *Carbon,* 101 (2016) 71-76.

[176] M. Hilder, B. Winther-Jensen, D. Li, M. Forsyth, D. R. MacFarlane, *Physical Chemistry Chemical Physics,* 13 (2011) 9187−9193.

[177] G. Jo, M. Choe, C. Cho, J. H. Kim, W. Park, S. Lee, W. Hong, T. Kim, S. Park, B. H. Hong, Y. H. Kahng, T. Lee, *Nanotechnology,*21 (2010) 175201.

[178] B. L. Hurley, S. Qiu, R. G. Buchheit, *Journal of The Electrochemical Society,* 158 (2011) C125−C131.

[179] E. Cano, C. L. Torres, J. M. Bastidas, *Materials and Corrosion,* 52 (2011) 667−676.

[180] I. Chowdhury, N. D. Mansukhani, L. M. Guiney, M. C. Hersam, and D. Bouchard, *Environmental Science & Technology,* 49 (2015) 10886−10893.

[181] J. F. Archard, *Journal of Applied Physics,* 24 (1953) 981–988.

[182] J. F. Archard, W. Hirst, *Proceedings of the Royal Society*, 236A (1956) 397–410.

[183] M. Tabandeh-Khorshid, E. Omrani, P. L. Menezes, P. K. Rohatgi, *Engineering Science and Technology, an International Journal*, 19 (2016) 463–469.

[184] L. Xu, T. B. Ma, Y. Z. Hu, H. Wang, *Carbon*, 50 (2012)1025-1032.

[185] G. A. Tomlinson, *Philosophical Magazine*, 7(46) (1929) 905–939.

[186] L. Xu, T. B. Ma, Y. Z. Hu, H. Wang, *Nanotechnology*, 22 (2011) 285708.

Disseminations

Publications in Journals

1. **H. S. Maharana** and A. Basu, Evolution and of structure property correlation of electrodeposited Cu-ZrO_2 nano-cone arrays, *Surface and Coatings Technology* (**Revision submitted**).
2. **H. S. Maharana**, P. K. Rai and A. Basu, Surface-mechanical and electrical properties of pulse electrodeposited Cu-graphene oxide composite coating for electrical contacts, *Journal of Material Science,* 52 (2017) 1089-1105.
3. **H. S. Maharana** and A. Basu, Surface-mechanical and oxidation behavior of electro-codeposited Cu-Y_2O_3 composite coating, *Surface and Coatings Technology,* 304 (2016) 348-358.
4. **H. S. Maharana**, Suprabha Lakra, S. Pal, and A. Basu, Electrophoretic Deposition of Cu-SiO_2 Coatings by DC and Pulsed DC for Enhanced Surface-Mechanical Properties, *Journal of Materials Engineering and Performance*, 25 (2016) 327-337.
5. **H. S. Maharana**, Akarapu Ashok, S. Pal, and A. Basu, Surface-Mechanical Properties of Electrodeposited Cu-Al_2O_3 Composite Coating and Effects of Processing Parameters, *Metallurgical and Materials Transactions A*, 47A (2016) 388-399.
6. **H. S. Maharana**, S. Panda and A. Basu, Effect of texture and microstructure on hardness and electrical conductivity of electrodeposited Cu-SiO_2 and Cu-Y_2O_3 coatings, ***(Communicated)***
7. Akarapu Ashok, **H. S. Maharana** and A Basu, Effect of electro-co-deposition parameters on surface mechanical properties of Cu–TiO_2 composite coating, *Bulletin of Material Science*, 38 (2015) 335-342.
8. Suprabha Lakra, **H. S. Maharana** & A. Basu, Synthesis and Characterization of Cr-ZrO_2 Composite Coating Formed by DC and Pulse Electrodeposition, *Materials and Manufacturing Process,* 31 (2016) 1447-1453.
9. **H. S. Maharana** and A. Basu, Effect of different surfactants on surface-mechanical properties of electrodeposited Cu-ZrO_2 composite coating. (Under Preparation).

10. **H. S. Maharana**, S. Panda and A. Basu, Micro-texture characterization of electrodeposited Cu and Cu-Y_2O_3 coatings, (Under Preparation).

Conferences/Workshops

1. Workshop on Surface Engineering of Metals and Alloys, SEMA-2012, BESU, SHIBPUR, 1-2 MARCH 2012.
2. Electrophoretic deposition and characterization of Cu-SiO_2 nanocomposite coating, NCPCM-2012, NIT ROURKELA, 7-8 DECEMBER 2012.
3. Synthesis of Cu-SiO_2 nanocomposite coating on Cu substrate by direct and pulse direct current electro-co-deposition, ICONEST-2014, IISC BENGALURU, 7-9 AUGUST 2014.
4. DC and pulsed electrodeposition of Cu-Y_2O_3 composite coating: A study of process and surface-mechanical properties, NMD ATM-2014, COLLEGE OF ENGINEERING PUNE, 12-15 NOVEMBER 2014.
5. Synthesis of Cu- Al_2O_3 composite coating by electro-co-deposition and optimization of processing parameters, ISRS-2014, IIT MADRAS, 11-13 DECEMBER 2014.